University of Alberta

Alkyne Complexes of the Group 8 Metals:
Reactivity of the $M(CO)_4(\eta^2\text{-alkyne})$ (M = Fe, Os) Compounds

by

Quinn Major ©

A thesis submitted to the Faculty of Graduate Studies and Research
in partial fulfillment of the requirements for the degree of Doctor of Philosophy

Department of Chemistry

Edmonton, Alberta

Spring 2003

National Library
of Canada

Acquisitions and
Bibliographic Services

395 Wellington Street
Ottawa ON K1A 0N4
Canada

Bibliothèque nationale
du Canada

Acquisisitons et
services bibliographiques

395, rue Wellington
Ottawa ON K1A 0N4
Canada

Your file Votre référence
ISBN: 0-612-82136-6
Our file Notre référence
ISBN: 0-612-82136-6

The author has granted a non-exclusive licence allowing the National Library of Canada to reproduce, loan, distribute or sell copies of this thesis in microform, paper or electronic formats.

L'auteur a accordé une licence non exclusive permettant à la Bibliothèque nationale du Canada de reproduire, prêter, distribuer ou vendre des copies de cette thèse sous la forme de microfiche/film, de reproduction sur papier ou sur format électronique.

The author retains ownership of the copyright in this thesis. Neither the thesis nor substantial extracts from it may be printed or otherwise reproduced without the author's permission.

L'auteur conserve la propriété du droit d'auteur qui protège cette thèse. Ni la thèse ni des extraits substantiels de celle-ci ne doivent être imprimés ou aturement reproduits sans son autorisation.

Canada

University of Alberta

Library Release Form

Name of Author: Quinn Major

Title of Thesis: Alkyne Complexes of the Group 8 Metals: Reactivity of the $M(CO)_4(\eta^2\text{-alkyne})$ (M = Fe, Os) Compounds

Degree: Doctor of Philosophy

Year this Degree Granted: 2003

Permission is hereby granted to the University of Alberta Library to reproduce single copies of this thesis and to lend or sell such copies for private, scholarly or scientific research purposes only.

The author reserves all other publication and other rights in association with the copyright in the thesis, and except as herein before provided, neither the thesis nor any substantial portion thereof may be printed or otherwise reproduced in any material form whatever without the author's prior written permission.

Quinn Major

Quinn Major

79 Sibbald Crescent
Regina, Saskatchewan
S4T 7L6
Canada

Date: January 30, 2003

University of Alberta

Faculty of Graduate Studies and Research

The undersigned certify that they have read, and recommend to the Faculty of Graduate Studies and Research for acceptance, a thesis entitled Alkyne Complexes of the Group 8 Metals: Reactivity of the $M(CO)_4(\eta^2\text{-alkyne})$ (M = Fe, Os) Compounds submitted by Quinn Major in partial fulfillment of the requirements for the degree of Doctor of Philosophy.

Josef Takats.
J. Takats (Supervisor)

Steven Bergens
S. H. Bergens

Arthur Mar.
A. Mar

J. M. Stryker

R. E. Hayes

D Zargarian
D. Zargarian (External Examiner)

January 29, 2003
Date

Abstract

The reactivity of $M(CO)_4(\eta^2\text{-alkyne})$ (M = Fe, Os) compounds toward two electron donor ligands has been investigated. These compounds were found to undergo both ligand substitution and reactions that involve coupling of the alkyne and selected unsaturated organic ligands.

Reaction of $Fe(CO)_4(\eta^2\text{-}C_2(CF_3)_2)$ with two or more equivalents of bulky phosphine ligands (P^tBu_2Me, P^iPr_3, PCy_3) proceeded with the substitution of two carbonyl ligands. The structure of the products $Fe(CO)_2(PR_2R')_2(\eta^2\text{-}C_2(CF_3)_2)$ is trigonal bipyramidal with the phosphine ligands occupying mutually *trans* axial coordination sites. Reaction of $Fe(CO)_4(\eta^2\text{-}C_2(CF_3)_2)$ with one equivalent of bulky phosphine ligand (P^tBu_2Me, P^iPr_3, PCy_3, P^tBu_3) yielded isolable $Fe(CO)_2(PR_2R')(\eta^2\text{-}C_2(CF_3)_2)$ compounds. The geometry around the iron atom is best described as distorted tetrahedral or square pyramidal. The ^{13}C NMR chemical shift of the alkyne carbons and the $Fe\text{–}C_{alkyne}$ separations are indicative of a four electron donor alkyne ligand. Therefore, stabilization of these coordinatively unsaturated compounds stems from additional electron donation from the $\pi_\perp$ orbital of the alkyne ligand. Reaction of $Os(CO)_4(\eta^2\text{-}C_2(CF_3)_2)$ with one equivalent of either cyclohexylisocyanide or *trans*-cyclooctene proceeded by single carbonyl substitution and yielded $Os(CO)_3(CNCy)(\eta^2\text{-}C_2(CF_3)_2)$ or $Os(CO)_3(\eta^2\text{-}trans\text{-cyclooctene})(\eta^2\text{-}C_2(CF_3)_2)$,

respectively. Ligand substitution in $M(CO)_4(\eta^2\text{-alkyne})$ (M = Fe, Os) compounds is not limited to carbonyl ligands. Reaction between $M(CO)_4(\eta^2\text{-}C_2H_2)$ and the pseudo-alkyne complex $(\eta^5\text{–}C_5H_5)(CO)_2W{\equiv}CC_6H_5$ proceeds by loss of the alkyne ligand and formation of the carbyne bridged heterobimetallic complex $FeW(\mu\text{–}CC_6H_5)(CO)_6(\eta^5\text{-}C_5H_5)$.

Both $Fe(CO)_2(PR_2R')(\eta^2\text{-}C_2(CF_3)_2)$ and $Os(CO)_4(\eta^2\text{-}C_2(CF_3)_2)$ compounds were found to promote coupling of coordinated $F_3CC{\equiv}CCF_3$ and selected unsaturated organic ligands. Reaction of $Fe(CO)_2(PR_2R')(\eta^2\text{-}C_2(CF_3)_2)$ with allenes yielded $Fe(CO)_2(PR_2R')(\eta^1,\eta^3\text{-}(F_3C)C{=}C(CF_3)C(CH_2)CR''_2)$ (R'' = H, Me), which contained a chelating 2-vinylallyl ligand. This ligand resulted from the coupling of the alkyne and allene ligands *via* C-C bond formation between a ligating carbon of the alkyne and the central carbon of the allene. The products exist as geometric isomers and were characterized by both NMR spectroscopy and X-ray structure determination. The reaction of $Os(CO)_4(\eta^2\text{-}C_2(CF_3)_2)$ with excess *trans*-cyclooctene affords *fac-/mer-* $Os(CO)_3(\eta^2\text{-}\textit{trans}\text{-cyclooctene})(\eta^1,\eta^1\text{-}(F_3C)C{=}C(CF_3)\overline{CH(CH_2)_6CH})$, compounds with a metallacyclopentene unit formed *via* $F_3CC{\equiv}CCF_3$ and *trans*-cyclooctene coupling. Both geometric isomers exhibit stererochemical isomerism. The solid state molecular structures and solution NMR characteristics of the compounds are presented.

Acknowledgements

Many members, both past and present, of the Takats research group have helped me during my stay at the University of Alberta and they deserve many thanks. Most importantly, I want to thank professor Takats for his guidance and professionalism, and for the chance to learn from him. I would also like to thank Jason Cooke for teaching me that God-awful preparation of those God-awful $Fe(CO)_4(\eta^2$-alkyne) compounds. Also, Guanyang Lin and Greg Ferrence, two dedicated and hard working PDF's, thank you for demonstrating both good and bad laboratory techniques. I wish to thank Joanne Gainsforth and John Washington for their help and advice.

I would also like to thank the support staff of the Chemistry Department, University of Alberta, for their assistance and help. Most notably I would like to thank members of the NMR spectroscopy, X-ray crystallography, elemental analysis and Mass spectroscopy laboratories. In addition, members of the administration and the electronic, machine and glass shops and the chemical stores have also helped in the progress of my research. Also, many thanks to the staff of the University of Alberta libraries for their assistance in obtaining some of the more obscure references.

I wish to thank the Max-Planck-Gesellschaft and professor Takats for the funding which allowed me to travel to Germany and work with some very talented and dedicated chemists. I want to thank Dr. Grevels of the Max-Planck-Institut für Strahlenchemie for being a delightful host and teaching me the finer points of carbonyl chemistry. I would also like to extend my gratitude to the other members of the Grevels research group; Herren Bayer, Kerpen and Frauen Schrader and Merkel. In addition, the support staff of both the Max-Planck-Institut für Strahlenchemie and Max-Planck-Institut für Kohlenforschung helped greatly in the collection of data for part of this thesis.

Finally, I would like to thank my family for their unwavering support and encouragement.

Table of Contents

Chapter 1 Introduction

1.1 A Brief Introduction to Transition Metal Carbonyl Chemistry 1

1.2 The Group 8 Metal Carbonyls 9

  1.2.1 Synthesis and Characterization of Group 8 Metal Carbonyls 9

  1.2.2 Substitution Reactions of $M(CO)_5$ (M = Fe, Ru, Os) Complexes 14

1.3 $M(CO)_4(\eta^2\text{-alkyne})$ (M = Fe, Ru, Os) Complexes 16

  1.3.1 Synthesis of $M(CO)_4(\eta^2\text{-alkyne})$ (M = Fe, Ru, Os) Complexes 16

  1.3.2 Bonding Between an Alkyne Ligand and a Transition Metal 20

  1.3.3 Substitution Reactions of $M(CO)_4(\eta^2\text{-alkyne})$ (M = Fe, Ru, Os) Complexes 30

1.4 Carbon to Carbon Bond Formation Promoted by Group 8 Carbonyls 31

1.5 Scope of Thesis 33

1.6 References 36

Chapter 2 Reactions of $Fe(CO)_4(\eta^2\text{-HFB})$ with Bulky Phosphines: Synthesis and Structures of $Fe(CO)_2(PR_2R')_n(\eta^2\text{-HFB})$ (n = 1, 2) Complexes

2.1 Introduction 48

2.2 Synthetic Aspects and Characterization of $Fe(CO)_2(PR_2R')_n(\eta^2\text{-HFB})$(n = 1, 2) Complexes 53

  2.2.1 $Fe(CO)_2(PR_2R')_2(\eta^2\text{-HFB})$ Complexes (**1a-c**) 53

  2.2.2 $Fe(CO)_2(PR_2R')(\eta^2\text{-HFB})$ Complexes (**2a-d**) 62

2.3 Molecular Structures of $Fe(CO)_2(PR_2R')_n(\eta^2\text{-HFB})$ (n = 1, 2) Complexes 70

2.3.1 $Fe(CO)_2(PR_2R')_2(\eta^2$-HFB) Complexes (**1a-c**) 70

2.3.2 $Fe(CO)_2(PR_2R')(\eta^2$-HFB) Complexes (**2a**, **c**, **d**) 78

2.4 Conclusions 87

2.5 Experimental 89

2.5.1 Solvents, Techniques and Physical Measurements 89

2.5.2 Reagents 90

2.5.3 Synthetic Procedures 90

2.5.4 X-ray Crystal Structure Determination of $Fe(CO)_2(PR_2R')_2(\eta^2$-HFB) (**1a**, **b**) 95

2.5.5 X-ray Crystal Structure Determination of $Fe(CO)_2(PR_2R')(\eta^2$-HFB) (**2a**, **d**) 99

2.6 References 102

Chapter 3 Reactions of Four Electron Donor Alkyne $Fe(CO)_2(PR_2R')(\eta^2$-HFB) Complexes with Allenes: The Serendipitous Discovery of Metal Mediated Alkyne-Allene Coupling

3.1 Introduction 106

3.2 Experimental Aspects 107

3.2.1 Initial Attempts 107

3.2.2 Reaction of $Fe(CO)_2(PR_2R')(\eta^2$-HFB) with Allenes; Experimental Observations 109

3.3 Characterization of $Fe(CO)_2(PR_2R')(\eta^1,\eta^3$-$\{F_3CC=C(CF_3)C(CH_2)_2\})$ (**4a-c**) 110

3.3.1 X-ray Crystal Structure Analysis of $Fe(CO)_2(PR_2R')(\eta^1,\eta^3\text{-}\{F_3CC=C(CF_3)C(CH_2)_2\})$ (**4a-c**) 112

3.3.2 Initial NMR Spectroscopic Analysis of $Fe(CO)_2(P^tBu_2Me)(\eta^1,\eta^3\text{-}\{F_3CC=C(CF_3)C(CH_2)_2\})$ (**4a**) 120

3.3.3 Low Temperature and Variable Temperature NMR Studies of $Fe(CO)_2(P^tBu_2Me)(\eta^1,\eta^3\text{-}\{F_3CC=C(CF_3)C(CH_2)_2\})$ (**4a**) 129

3.3.4 NMR Spectroscopic Analysis of $Fe(CO)_2(PR_2R')(\eta^1,\eta^3\text{-}\{F_3CC=C(CF_3)C(CH_2)_2\})$ (**4b,c**) 144

3.3.5 Low Temperature and Variable Temperature NMR Studies of $Fe(CO)_2(PCy_3)(\eta^1,\eta^3\text{-}\{F_3CC=C(CF_3)C(CH_2)_2\})$ (**4c**) 153

3.4 Characterization of $Fe(CO)_2(PR_2R')(\eta^1,\eta^3\text{-}\{F_3CC=C(CF_3)C(CH_2)CHMe\})$ (**5a-c**) 156

3.4.1 X-ray Crystal Structure Analysis of $Fe(CO)_2(P^iPr_3)(\eta^1,\eta^3\text{-}\{F_3CC=C(CF_3)C(CH_2)CHMe\})$ (**5b**) 157

3.4.2 NMR Spectroscopic Analysis of $Fe(CO)_2(PR_2R')(\eta^1,\eta^3\text{-}\{F_3CC=C(CF_3)C(CH_2)CHMe\})$ (**5a-c**) 164

3.5 Characterization of $Fe(CO)_2(PR_2R')(\eta^1,\eta^3\text{-}\{F_3CC=C(CF_3)C(CH_2)CMe_2\})$ (**6a-c**) 184

3.5.1 X-ray Crystal Structure Analysis of $Fe(CO)_2(PR_2R')(\eta^1,\eta^3\text{-}\{F_3CC=C(CF_3)C(CH_2)CMe_2\})$ (**6aI, 6bI**) 185

3.5.2 NMR Spectroscopic Analysis of $Fe(CO)_2(PR_2R')(\eta^1,\eta^3\text{-}\{F_3CC=C(CF_3)C(CH_2)CMe_2\})$ (**6aI-6cI**) 189

3.5.3 Variable Temperature NMR Studies of $Fe(CO)_2(PCy_3)(\eta^1,\eta^3\text{-}\{F_3CC=C(CF_3)C(CH_2)CMe_2\})$ (**6c**) 196

3.5.4 X-ray Crystal Structure Analysis of the Kinetic Product

$Fe(CO)_2(P^iPr_3)(\eta^1,\eta^3\text{-}\{F_3CC{=}C(CF_3)C(CH_2)CMe_2\})$ **(6bII)** 206

3.6 Conclusions 214

3.7 Experimental 217

3.7.1 Solvents, Techniques and Physical Measurements 217

3.7.2 Reagents 217

3.7.3 Synthetic Procedures 217

3.7.4 X-ray Crystal Structure Determination of

$Fe(CO)_2(PR_2R')(\eta^1,\eta^3\text{-}\{F_3CC{=}C(CF_3)C(CH_2)_2\})$ **(4a-c)** 232

3.7.5 X-ray Crystal Structure Determination of

$Fe(CO)_2(P^iPr_3)(\eta^1,\eta^3\text{-}\{F_3CC{=}C(CF_3)C(CH_2)CHMe\})$ **(5b)** 236

3.7.6 X-ray Crystal Structure Determination of

$Fe(CO)_2(PR_2R')(\eta^1,\eta^3\text{-}\{F_3CC{=}C(CF_3)C(CH_2)CMe_2\})$ **(6aI, 6bI, 6bII)** 238

3.8 References 242

Chapter 4 Reaction of $M(CO)_4(\eta^2\text{-}C_2H_2)$ (M = Fe, Os) with $(\eta^5\text{–}C_5H_5)(CO)_2W{\equiv}CC_6H_5$: Unexpected Substitution of Acetylene and Formation of $MW(\mu\text{-}CC_6H_5)(CO)_6(\eta^5\text{-}C_5H_5)$

4.1 Introduction 249

4.2 Experimental Observations 250

4.3 Spectroscopic Characterization 250

4.4 Molecular Structures of $MW(\mu\text{-}CC_6H_5)(CO)_6(\eta^5\text{-}C_5H_5)$ **(7, 8)** 254

4.5 Carbonyl Exchange Processes in **7** and **8** 259

4.6 Conclusions 260

4.7 Experimental 261

4.7.1 Solvents, Techniques, Physical Measurements and Reagents 261

4.7.2 Synthetic Procedures 261

4.7.3 X-ray Crystal Structure Determination of $MW(\mu\text{-}CC_6H_5)(CO)_6(\eta^5\text{-}C_5H_5)$ (**7, 8**) 263

4.8 References 266

Chapter 5 Reactions of $Os(CO)_4(\eta^2\text{-HFB})$ with Cyclohexylisocyanide and *Trans*–Cyclooctene: A Further Demonstration of the Reactivity of $M(CO)_4(\eta^2\text{-alkyne})$ Complexes Toward Two Electron Donor Ligands

5.1 Introduction 269

5.2 Reaction of $Os(CO)_4(\eta^2\text{-HFB})$ with Cyclohexylisocyanide 272

5.2.1 Experimental Observations 272

5.2.2 Spectroscopic Characterization of **11** 273

5.2.3 X-ray Crystal Structure Analysis of $Os(CO)_3(CNCy)(\eta^2\text{-HFB})$ (**11**) 276

5.3 Reaction of $Os(CO)_4(\eta^2\text{-HFB})$ with *Trans*-Cyclooctene 279

5.3.1 Experimental Observations 279

5.3.2 Spectroscopic Characterization of **12** 279

5.3.3 X-ray Crystal Structure Analysis of $Os(CO)_3(\eta^2\text{-}eco)(\eta^2\text{-HFB})$ (**12**) 284

5.4 Reaction of $Os(CO)_4(\eta^2\text{-HFB})$ with Excess *Trans*-Cyclooctene: Discovery of Alkyne-Olefin Coupling 288

5.4.1 Experimental Observations 288

5.4.2 X-ray Crystal Structure Analysis of **13**: *fac*-$Os(CO)_3(\eta^2\text{-}eco)(\eta^1,\eta^1\text{-}(F_3C)C{=}C(CF_3)\overline{CH(CH_2)_6CH})$ 289

5.4.3 Synthesis and NMR Spectroscopic Characterization of *fac*-Os(CO)$_3$(η^2-*eco*)(η^1,η^1-(F$_3$C)C=C(CF$_3$)$\overline{\text{CH(CH}_2)_6\text{C}}$H) **(13)** 292

5.5 The Discovery of *mer*-Os(CO)$_3$(η^2-*eco*)(η^1,η^1-(F$_3$C)C=C(CF$_3$)$\overline{\text{CH(CH}_2)_6\text{C}}$H) **(14)** 297

5.5.1 Experimental Observations 297

5.5.2 X-ray Crystal Structure Analysis of *mer*-Os(CO)$_3$(η^2-*eco*)(η^1,η^1-(F$_3$C)C=C(CF$_3$)$\overline{\text{CH(CH}_2)_6\text{C}}$H) **(14)** 298

5.5.3 Synthesis and NMR Spectroscopic Characterization of *mer*-Os(CO)$_3$(η^2-*eco*)(η^1,η^1-(F$_3$C)C=C(CF$_3$)$\overline{\text{CH(CH}_2)_6\text{C}}$H) **(14)** 304

5.6 Conclusions 307

5.7 Experimental 308

5.7.1 Solvents, Techniques and Physical Measurements 308

5.7.2 Reagents 309

5.7.3 Synthetic Procedures 309

5.7.4 X-ray Crystal Structure Determination of Compounds **11-14** 314

5.8 References 319

Chapter 6 Conclusions

6.1 Conclusions 322

6.2 References 326

List of Tables

Chapter 1

Table 1-1 Physical and Spectroscopic Properties of the Group 8 Carbonyls 10

Chapter 2

Table 2-1 Low Temperature FT-IR Data in the Carbonyl Region, $^{31}P\{^1H\}$, ^{19}F and ^{13}C NMR Data of Compounds **1a-c** 58

Table 2-2 FT-IR Data in the Carbonyl Region, $^{31}P\{^1H\}$, ^1H and $^{13}C\{^1H\}$ NMR Data of Compounds **2a-d** 65

Table 2-3 FT-IR Data in the Carbonyl Region of Compounds **3a-c** 67

Table 2-4 Selected Interatomic Distances and Angles in **1a-c** 72

Table 2-5 Interatomic Distances and Angles in $Fe(CO)_2(PR_3)_2(\eta^2\text{-}C_2R'R'')$ 74

Table 2-6 Selected Interatomic Distances and Angles in **2a-c** 79

Table 2-7 Selected Interatomic Distances and Angles in $Fe(CO)_3\{\eta^2\text{-}C_2(NMe_2)_2\}$ 86

Table 2-8 Crystallographic Experimental Details for Compound **1a** 97

Table 2-9 Crystallographic Experimental Details for Compound **1b** 98

Table 2-10 Crystallographic Experimental Details for Compound **2a** 100

Table 2-11 Crystallographic Experimental Details for Compound **2d** 101

Chapter 3

Table 3-1 $Fe(CO)_2(PR_2R')(\eta^1,\eta^3\text{-}\{F_3CC{=}C(CF_3)C(CH_2)CR^1R^2\})$ Compounds 110

Table 3-2 FT-IR Data in the Carbonyl Region of **4a-c** 111

Table 3-3 Selected Interatomic Distances and Angles in **4a** 113

Table 3-4 Selected Interatomic Distances and Angles in **4b** 115

Table 3-5 The $^{31}P\{^1H\}$, ^{19}F, ^1H and $^{13}C\{^{19}F\}$ NMR Data of **4aI** and **4aII** 121

Table 3-6 The $^{31}P\{^1H\}$, ^{19}F, ^1H and $^{13}C\{^1H\}$ of **4aII**, **4aII′** and **4aII″** 131

Table 3-7 The $^{31}P\{^1H\}$, ^{19}F, ^1H and $^{13}C\{^1H\}$ of **4aI** and **4aII** 132

Table 3-8 The $^{31}P\{^1H\}$, ^{19}F, ^1H and $^{13}C\{^{19}F\}$ NMR Data of **4bI** and **4bII** 145

Table 3-9 The $^{31}P\{^1H\}$, ^{19}F, ^1H and $^{13}C\{^{19}F\}$ NMR Data of **4cI** and **4cII** 146

Table 3-10 FT-IR Data in the Carbonyl Region of **5a-c** 156

Table 3-11 Selected Interatomic Distances and Angles in **5b** 158

Table 3-12 Selected Interatomic Distances and Angles in

$[NEt_4][Cr(CO)_3(P(OMe)_3(\eta^3$-*anti*-1-methylallyl)]

and $Mn(CO)_3(PMe_3)(\eta^3$-*anti*-1-ethenylallyl) 162

Table 3-13 The $^{31}P\{^1H\}$, ^{19}F, ^1H and $^{13}C\{^1H\}$ NMR Data of **5bI** and **5bII** 165

Table 3-14 The $^{31}P\{^1H\}$, ^{19}F, ^1H and $^{13}C\{^1H\}$ NMR Data of **5cI** and **5cII** 166

Table 3-15 The $^{31}P\{^1H\}$, ^{19}F, ^1H and $^{13}C\{^1H\}$ NMR Data of **5aI** and **5aII** 167

Table 3-16 FT-IR Data in the Carbonyl Region of **6a-c** 184

Table 3-17 Selected Interatomic Distance and Angles in **6bI** and **6aI** 187

Table 3-18 The $^{31}P\{^1H\}$, ^{19}F, ^1H and $^{13}C\{^1H\}$ NMR Data of **6bI** 190

Table 3-19 The $^{31}P\{^1H\}$, ^{19}F, ^1H and $^{13}C\{^1H\}$ NMR Data of **6cI** 191

Table 3-20 The $^{31}P\{^1H\}$, ^{19}F, ^1H and $^{13}C\{^1H\}$ NMR Data of **6aI** 192

Table 3-21 The $^{31}P\{^1H\}$, ^{19}F, ^1H and $^{13}C\{^1H\}$APT NMR Data of **6cII** 200

Table 3-22 Selected Interatomic Distances and Angles in **6bII** 207

Table 3-23 Crystallographic Experimental Details for Compound **4a** 233

Table 3-24 Crystallographic Experimental Details for Compound **4b** 234

Table 3-25 Crystallographic Experimental Details for Compound **4c** 235

Table 3-26 Crystallographic Experimental Details for Compound **5b** 237

Table 3-27 Crystallographic Experimental Details for Compound **6aI** 239

Table 3-28 Crystallographic Experimental Details for Compound **6bI** 240

Table 3-29 Crystallographic Experimental Details for Compound **6bII** 241

Chapter 4

Table 4-1 The FT-IR Data in the Carbonyl Region, ^{1}H, and ^{13}C{^{1}H} NMR Data of MW(μ-CC$_6$H$_5$)(CO)$_6$(η^5-C$_5$H$_5$) (M = Fe, **7**; M = Os, **8**) 251

Table 4-2 Selected Interatomic Separations and Angles for **7** and **8**. 256

Table 4-3 Crystallographic Experimental Details for Compound **7** 264

Table 4-4 Crystallographic Experimental Details for Compound **8** 265

Chapter 5

Table 5-1 The FT-IR (carbonyl region), ^{19}F, ^{1}H and ^{13}C{^{1}H} NMR Data of **11** 275

Table 5-2 Selected Interatomic Distances and Angles in **11** 277

Table 5-3 The FT-IR (carbonyl region), ^{19}F, ^{1}H and ^{13}C{^{1}H} NMR Data of **12** 281

Table 5-4 Selected Interatomic Distances and Angles in **12** 285

Table 5-5 Selected Interatomic Distances and Angles in **13** 290

Table 5-6 The ^{19}F and ^{13}C{^{1}H} NMR Data of **13** and **13′** 294

Table 5-7 Selected Interatomic Distances and Angles in **14** 299

Table 5-8 The ^{19}F and ^{13}C{^{1}H} NMR Data of **14** and **14′** 305

Table 5-9 Crystallographic Experimental Details for Compound **11** 315

Table 5-10 Crystallographic Experimental Details for Compound **12** 316

Table 5-11 Crystallographic Experimental Details for Compound **13** 317

Table 5-12 Crystallographic Experimental Details for Compound **14** 318

List of Figures

Chapter 1

Figure 1-1 Tetrahedral, Trigonal Bipyramidal and Octahedral Geometries of Simple Binary Carbonyls 4

Figure 1-2 An Example of a Cluster Carbide Compound $[Ru_6C(CO)_{17}]$ 4

Figure 1-3 Structures of $M_2(CO)_9$ (M = Fe, Os) 13

Figure 1-4 Structures of $M_3(CO)_{12}$ (M = Fe, Ru, Os) 14

Figure 1-5 Archetypical Structure of $M(CO)_4(\eta^2\text{-alkene})$ (M = Fe, Ru, Os) 16

Figure 1-6 Solid State Molecular Structure of $Fe_2(CO)_8(\eta^2\text{-}Ph_2C{\equiv}C^tBu)$ 18

Figure 1-7 Molecular Structure of $Os(CO)_4(\eta^2\text{-}C_2(SiMe_3)_2)$ 19

Chapter 2

Figure 2-1 Structure of $Fe(CO)_3(PPh_3)(\eta^2$-*cis*-RCH=CHR) and $Fe(CO)_3(PPh_3)(\eta^2$-*trans*-RCH=CHR) (R = CO_2Et) 52

Figure 2-2 Low Temperature FT-IR Spectra of Compound **1a** 57

Figure 2-3 Two Possible Structures of $Fe(CO)_3(PR_2R')(\eta^2\text{-HFB})$ 59

Figure 2-4 The $^{13}C\{^1H\}$ NMR Spectrum of **1b**; 100-225 ppm Region 61

Figure 2-5 The $^{13}C\{^1H\}$ NMR Spectra of **1b** and **2b**; 100-225 ppm Region 69

Figure 2-6 Solid State Molecular Structure of **1a** and **1b** 71

Figure 2-7 Space Filling Model of the Molecular Structure of **1a** 75

Figure 2-8 Solid State Molecular Structure of **2a** and **2d** 78

Figure 2-9 Structure of $Fe(CO)_3(\eta^2\text{-}C_2H_2)$ 81

Figure 2-10 Solid State Molecular Structure of $Fe(CO)_3\{\eta^2\text{-}C_2(NMe_2)_2\}$ 86

Figure 2-11 Intermediate [$Fe(CO)_3(\eta^2$-alkyne)] 88

Chapter 3

Figure 3-1 FT-IR Solution Spectrum of **4a** 111

Figure 3-2 Solid State Molecular Structure of **4a** 113

Figure 3-3 Solid State Molecular Structure of **4b** 115

Figure 3-4 Iron Carbonyl Compounds with Chelating Allyl Ligands 118

Figure 3-5 Iron Carbonyl Compound with a Cyclohexadienyl Chelating Ligand 119

Figure 3-6 ^1H NMR Spectrum of **4a** 122

Figure 3-7 Structures of the Major isomer **4aI** and Minor Isomer **4aII** 124

Figure 3-8 The $^{13}C\{^{19}F\}$ NMR Spectrum of **4a** 125

Figure 3-9 The Variable-Temperature $^{31}P\{^1H\}$ NMR Spectra of the Reaction of **2a** with Allene 133

Figure 3-10 The Variable-Temperature $^{13}C\{^1H\}$ NMR Spectra of the Reaction of **2a** with Allene 136

Figure 3-11 The Variable-Temperature ^1H NMR Spectra of the Reaction of **2a** with Allene 138

Figure 3-12 The ^1H NMR Spectrum of **4b** 147

Figure 3-13 The $^{13}C\{^1H\}$APT NMR Spectrum of **4b** 151

Figure 3-14 The Variable-Temperature ^1H NMR Spectra of the Reaction of **2c** with Allene 155

Figure 3-15 Solid State Molecular Structure of **5b** 158

Figure 3-16 Structure of $[NEt_4][Cr(CO)_3(P(OMe)_3(\eta^3$-*anti*-1-methylallyl)] and $Mn(CO)_3(PMe_3)(\eta^3$-*anti*-1-ethenylallyl) 161

Figure 3-17 The ^{1}H NMR Spectrum of **5b** 168

Figure 3-18 The $^{13}C\{^1H\}$ NMR Spectra of the α-Carbon and β-Carbon Region of **5b** and **5c** 173

Figure 3-19 Reconstruction of the α-Carbon Signal in the $^{13}C\{^1H\}$ NMR Spectra of **5c** 174

Figure 3-20 Reconstruction of the β-Carbon Signal in the $^{13}C\{^1H\}$ NMR Spectra of **5c** 176

Figure 3-21 Possible Geometric Isomers of **5nI** and **5nII** (n = a, b, c) 181

Figure 3-22 Solid State Molecular Structure of **6bI** 186

Figure 3-23 Solution and Solid State Structure of **6nI** (n = a, b, c) 196

Figure 3-24 The Variable-Temperature $^{31}P\{^1H\}$NMR Spectra of the Reaction of **2c** with 1,1-Dimethylallene 198

Figure 3-25 The Variable-Temperature ^{1}H NMR Spectra of the Reaction of **2c** with 1,1-Dimethylallene 201

Figure 3-26 The $^{13}C\{^1H\}$NMR Spectrum of **6cII** 203

Figure 3-27 Possible Geometric Isomers of **6nII** (n = a, b, c) 205

Figure 3-28 Solid State Molecular Structure of **6bII** 207

Figure 3-29 Structure of μ-(o-$C_6H_4CH_2NN{=}CHPh)Fe_2(CO)_6$ 209

Figure 3-30 The Pictorial Representation of $Cp_2Zr(\mu\text{-}C_4H_6)(\mu\text{-}Cl)AlCl_2$ 210

Figure 3-31 The η^1,η^2-Allyl Bonding Mode in **6bII** 210

Figure 3-32 The Kinetic Product **6nII** and Thermodynamic Product **6nI** (n = a, b, c) 211

Figure 3-33 A Possible Rearrangement of **6nII** to **6nI** (n = a, b, c) 213

Chapter 4

Figure 4-1 Solid State Molecular Structures of **7** and **8** 255

Chapter 5

Figure 5-1 The Enantiomers of *Trans*-Cyclooctene (*eco*) 272

Figure 5-2 FT-IR Spectrum (carbonyl region) of **11**. 273

Figure 5-3 Structure of **11** 274

Figure 5-4 Solid State Molecular Structure of **11** 277

Figure 5-5 FT-IR Spectra (carbonyl region) of **12** 280

Figure 5-6 The $^{13}C\{^{1}H\}$ NMR Spectrum of **12** 282

Figure 5-7 Possible Structures of **12** 284

Figure 5-8 Solid State Molecular Structure of **12** 285

Figure 5-9 Structure of $Fe(CO)_3(\eta^2\text{-}eco)_2$ 286

Figure 5-10 *Trans*-2-Cyclooctene-1-yl-3,5-Dinitrobenzoate 287

Figure 5-11 The Two Enantiomers of **12** 288

Figure 5-12 FT-IR Spectrum (carbonyl region) of **13** 289

Figure 5-13 Solid State Molecular Structure of **13** 290

Figure 5-14 Enantiomeric Forms of **13** Containing Both Enantiomers of *Trans*-Cyclooctene 292

Figure 5-15 The $^{13}C\{^{1}H\}$ NMR Spectrum of **13** 295

Figure 5-16 Enantiomeric Forms of **13** Containing a Single Enantiomer of *Trans*-Cyclooctene 297

Figure 5-17 FT-IR Spectrum (carbonyl region) of **14** 298

Figure 5-18 Solid State Molecular Structure of **14** 299

Figure 5-19 Possible Diastereomers in the Crystal of **14** 302

Figure 5-20 Enantiomeric Forms of **14** Containing a Single Enantiomer of *Trans*-Cyclooctene 303

Figure 5-21 Enantiomeric Forms of **14** Containing Both Enantiomers of *Trans*-Cyclooctene 303

List of Schemes

Chapter 1

Scheme 1-1 Valence Bond Representation of Metal-Carbonyl Bonding 3

Scheme 1-2 Reaction of $Ru_3(CO)_{12}$ with Alkynes 5

Scheme 1-3 The Berry Pseudorotation Mechanism for $Fe(CO)_5$ 11

Scheme 1-4 Metal-Alkyne In-Plane Bonding 20

Scheme 1-5 Valence Bond Representation of Metal-Alkyne Bonding; Two Electron Donor Alkyne 22

Scheme 1-6 Metal-Alkyne Perpendicular Bonding 23

Scheme 1-7 Valence Bond Representation of Metal-Alkyne Bonding; Four Electron Donor Alkyne 24

Scheme 1-8 Interaction Diagram for a C_{3v} $M(CO)_4$ Fragment with a Perturbed Alkyne Ligand 27

Scheme 1-9 Interaction Diagram for a C_{2v} $M(CO)_4$ Fragment with an In-Plane Orientated Perturbed Alkyne Ligand 29

Scheme 1-10 Replacement of Axial Carbonyls with Phosphine Ligands 31

Chapter 2

Scheme 2-1 η^2-Alkyne as a Two Electron Donor or a Four Electron Donor 48

Chapter 4

Scheme 4-1 Equilibrium Between $MW(\mu\text{-}CR)(CO)_6L$ and $MW(\mu\text{-}CR)(CO)_5L$ 253

Chapter 5

Scheme 5-1 Valence Bond Representation of MCNR Bonding 279

Chapter 6

Scheme 6-1 Formation of $Fe(CO)_2(PR_2R')(\eta^1,\eta^3\text{-}(F_3C)C{=}C(CF_3)C(CH_2)R^1R^2)$ 324

List of Abbreviations and Symbols

Å	angstrom
acac	acetylacetonate ion $(CH_3C(O)CHC(O)CH_3)^-$
APT	attached proton test
atm	atmosphere(s)
ave.	statistical mean
ax	axial
br	broad (NMR spectra)
C_{alkyne}	alkyne carbons (≡C)
cm^{-1}	wave number (IR spectra)
CMIA	carbonylmetalloimmunoassay
COSY	correlation spectroscopy
Cy	cyclohexyl, C_6H_{11}—
d	doublet (NMR spectra)
δ	chemical shift in ppm (NMR spectra)
Δ	heat or coordination shift
deg.	degrees
DEPT	distortionless enhancement by polarization transfer
DMAD	dimethylacetylenedicarboxylate $(MeO_2CC_2CCO_2Me)$
eco	*trans*-cyclooctene
EI	electron impact
eq	equatorial
Eq.	Equation

esd	estimated standard deviation
FT	Fourier Transform
GWV	Glasswerk Wertheim Filter
HFB	hexafluorobut-2-yne
hν	radiation
HMBC	heteronuclear multiple bond correlation
HMQC	heteronuclear multiple quantum correlation
hr.	hour(s)
Hz	hertz (s^{-1})
I	nuclear spin quantum number
^{i}Pr	isopropyl $(CH_3)_2HC$—
IR	infrared
$^{x}J_{AB}$	X bond coupling constant between nuclei A and B
K	Kelvin
λ	wave length
m	multiplet (NMR spectra)
m	medium intensity (IR spectra)
M^+	molecular ion (mass spectra)
mg	milligrams
MHz	megahertz
min.	minutes
mL	milliliter(s)
mmol	millimoles
MO	molecular orbital(s)

m.p.	melting point
MS	mass spectroscopy
μL	microliter(s)
nm	nanometer
NMR	nuclear magnetic resonance
ν	frequency
Ph	phenyl, C_6H_5—
π*	antibonding pi orbital
ppm	parts per million
psi	pounds per square inch
pz	pyrazolyl-1-yl
q	quartet (NMR spectrum)
s	singlet (NMR spectra)
s	strong intensity (IR spectra)
sept	septet (NMR spectra)
sh	shoulder (IR and NMR spectra)
σ*	antibonding sigma orbital
t	triplet (NMR spectra)
TMEDA	N,N,N′,N′-tetramethylethylenediamine
UV	ultra-violet
v	very
vs.	versus
w	weak (IR spectra)

List of Important Structural Types and Numbering Scheme

Chapter 2 (n = a, $PR_2R' = P^tBu_2Me$; n = b, $PR_2R' = P^iPr_3$; n = c, $PR_2R' = PCy_3$;
n = d, $PR_2R' = P^tBu_3$)

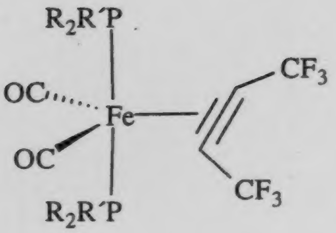
R₂R′P
OC
Fe
OC
R₂R′P
CF₃
CF₃

1n

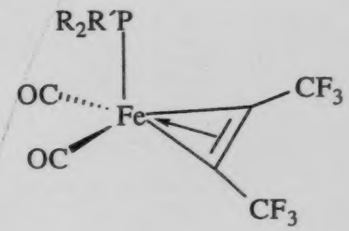
R₂R′P
OC
Fe
OC
CF₃
CF₃

2n

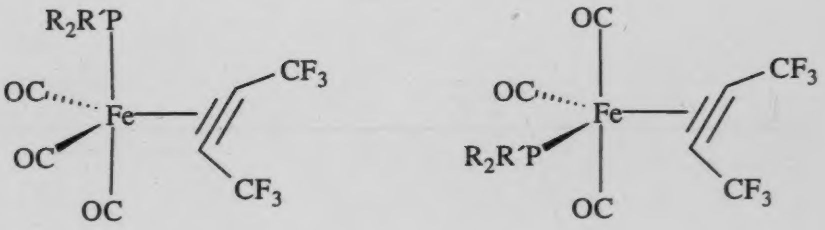
R₂R′P
OC
Fe
OC
OC
CF₃
CF₃
OC
OC
Fe
R₂R′P
OC
CF₃
CF₃

3n

Chapter 3 (n = a, $PR_2R' = P^tBu_2Me$; n = b, $PR_2R' = P^iPr_3$; n = c, $PR_2R' = PCy_3$;

n = d, $PR_2R' = P^tBu_3$)

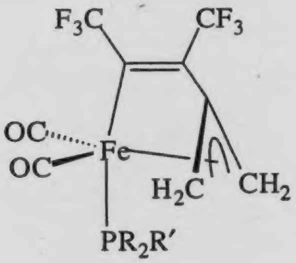

4nI

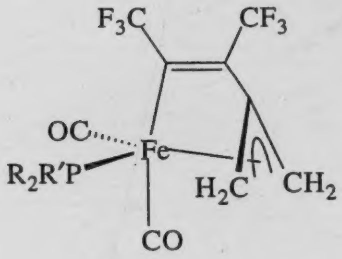

4nII

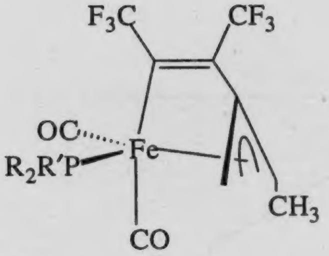

5nI

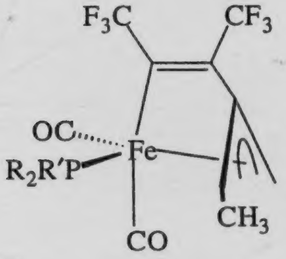

5nII

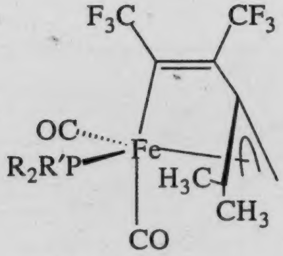

6nI

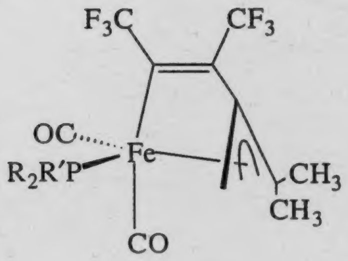

6nII

Chapter 4

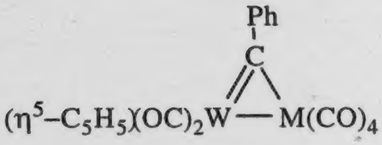

M = Fe, **7**; Os, **8**

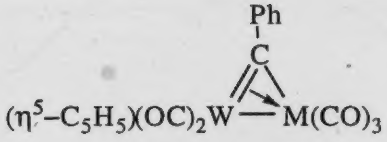

M = Fe, **9**; Os, **10**

Chapter 5

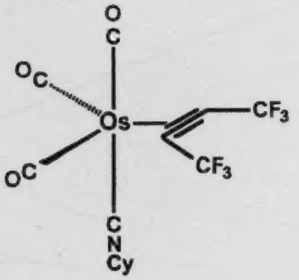

11

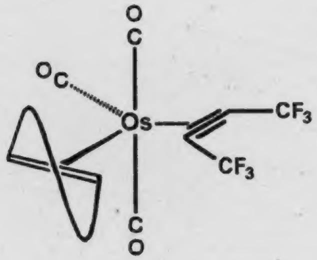

12

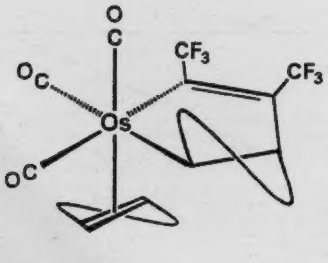

13

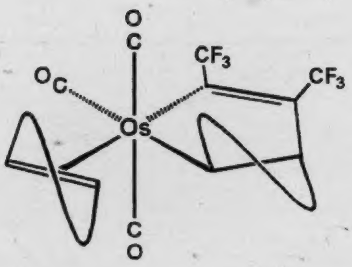

14

Chapter 1

Introduction

1.1 A Brief Introduction to Transition Metal Carbonyl Chemistry

Metal carbonyl compounds are the most common type of molecules found in transition metal organometallic chemistry. Almost all transition metals form compounds with carbon monoxide [1]. It is this breadth of occurrence which allows the metal carbonyls to form much of the foundation of the d-block organometallic chemistry and provide keen insight into those aspects of organometallic chemistry that make this such a fascinating area of science. It is the continued discovery of unusual bonding schemes, the seemingly endless supply of diverse structures, and the unpredictable reactivity patterns of new molecules that distinguishes organometallic chemistry from “classical” inorganic or organic chemistry and creates a domain within which anything can occur and occasionally does. The carbonyls, only one class of many, contribute significantly to the valuable understanding of the formation and reactivity of organometallic molecules.

Carbon monoxide can bind to metal atoms to form homoleptic carbonyls, or more commonly in combination with other ligands to form mixed ligand compounds. Most homoleptic carbonyls are readily available either commercially or by simple preparation. For example, $Ni(CO)_4$ the first homoleptic metal carbonyl complex discovered by Ludwig Mond, Carl Langer and Friedrich Quinke in 1890 forms at a reasonable rate from the direct reaction of nickel metal and carbon monoxide gas at atmospheric pressure and ambient temperature [2]. However, direct synthesis is impracticable for most homoleptic metal carbonyls and other methods must be employed. One such common method, reductive carbonylation, involves the reduction of a transition metal salt or complex, by an appropriate reducing agent, in the presence of carbon monoxide (Eq. 1-1, 1-2). A common method to prepare mixed ligand carbonyl complexes is *via* substitution of carbon monoxide. However, since the vast majority of homoleptic carbonyls are 18-valence electron compounds, they are substitutionally inert. Thus, carbonyl substitution must be initiated in some way, most commonly by thermal, photochemical or chemical activation [3].

$$2CoCO_3 + 2H_2 + 8CO \rightarrow Co_2(CO)_8 + 2CO_2 + 2H_2O \qquad (1\text{-}1)$$

$$Re_2O_7 + 17CO \rightarrow Re_2(CO)_{10} + 7CO_2 \qquad (1\text{-}2)$$

The bonding between metals and π-acceptor ligands in organometallic chemistry is illustrated by the interaction between the carbonyl ligand and the metal. The notion of a CO ligand acting as a simple electron pair donor and the M←CO bond as a simple σ dative bond is a gross oversimplification for this important class of compounds and, by extension, many other types of organometallic compounds. The M←CO σ dative bond is reinforced by a donation from a filled metal π-type *d* orbital into the vacant π* orbital of the CO ligand (back donation). Thus, there exists some multiple bonding character in the M–CO bond. This can be represented in terms of resonance structures and Valence Bond Theory as shown in Scheme 1-1. These two bonding components are mutually reinforcing and they are said to have a synergistic relationship. The σ donation produces a CO ligand with overall electron deficiency, which increases its π acceptor ability. The π back donation causes the CO ligand to be overall electron rich, thus increasing its basicity. Typically the CO ligand is found in one of two bonding modes; terminal or bridging. Each mode can be distinguished by their characteristic IR CO stretching frequency. Terminal carbonyls M–CO and bridging carbonyls M–C(O)–M are found in the 2130–1850 cm^{-1} and 1850–1700 cm^{-1} range, respectively. In addition, the position of the ν_{CO} bands is often useful as a diagnostic to indirectly monitor the charge dynamics occurring at the metal center.

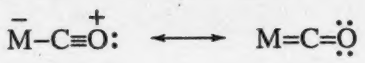

$$\overset{-}{M}-C\equiv\overset{+}{O}: \longleftrightarrow M=C=\ddot{\underset{..}{O}}$$

Scheme 1-1 Valence Bond Representation of Metal-Carbonyl Bonding.

In transition metal organometallic chemistry, as in main group chemistry, the concept of closed shell electronic configuration greatly assists in rationalizing stability, stoichiometry and reactivity patterns of molecules. The concept of the octet rule in main group chemistry is extended to organometallic chemistry in the form of the 18-electron rule [4]. A detailed discussion of this formalism is commonplace in any introductory organometallic text and an explanation here would be redundant. It is, however, important to note that despite some exceptions, the vast majority of carbonyl complexes obey the 18-electron rule.

Metal carbonyl complexes display a variety of structural types, some unexceptional, others new and unusual. Many of these structures are used as a paradigm for other classes of organometallic compounds. Simple mononuclear metal carbonyl molecules often adopt molecular structures that are simple, symmetrical and well defined. For example, the 4-, 5-, and 6-coordinate complexes have tetrahedral, trigonal bipyramidal and octahedral structures, respectively (Figure 1-1) [5].

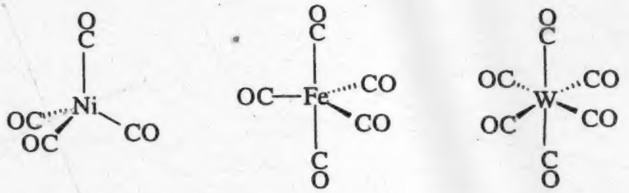

Figure 1-1 Tetrahedral, Trigonal Bipyramidal and Octahedral Geometries of Simple Homoleptic Carbonyls.

Carbonyl complexes exhibit a special capacity to form covalent bonds with other metal atoms to produce cluster compounds. These compounds may be composed of two, three or more metal centers in addition to a number of ancillary ligands. Carbonyl cluster compounds not only enrich organometallic chemistry through their interesting structures but also through unusual bonding modes. Consider, for example, the unusual position of the carbon atom in [$Ru_6C(CO)_{17}$] [6] (Figure 1-2). The carbon atom is completely encapsulated by an octahedral arrangement of six ruthenium atoms, which in turn are surrounded by a shell of carbonyl ligands. The carbon atom in this complex exhibits a coordination number and structure not normally found in classical organic chemistry. Other elements, notably hydrogen [7] and nitrogen [8], have also been encapsulated in a transition metal carbonyl cluster.

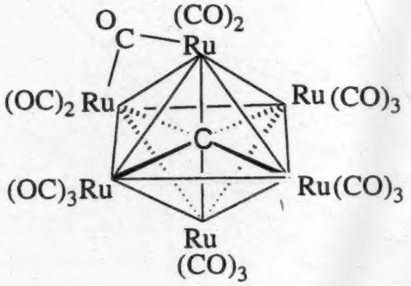

Figure 1-2 An Example of a Cluster Carbide Compound, [$Ru_6C(CO)_{17}$] [6].

Moreover, consider the diverse reactive patterns and structures observed when $Ru_3(CO)_{12}$ and alkynes are combined (Scheme 1-2) [9]. Some products show a variety of bridging coordination modes, while others show alkyne-alkyne and alkyne-CO coupling.

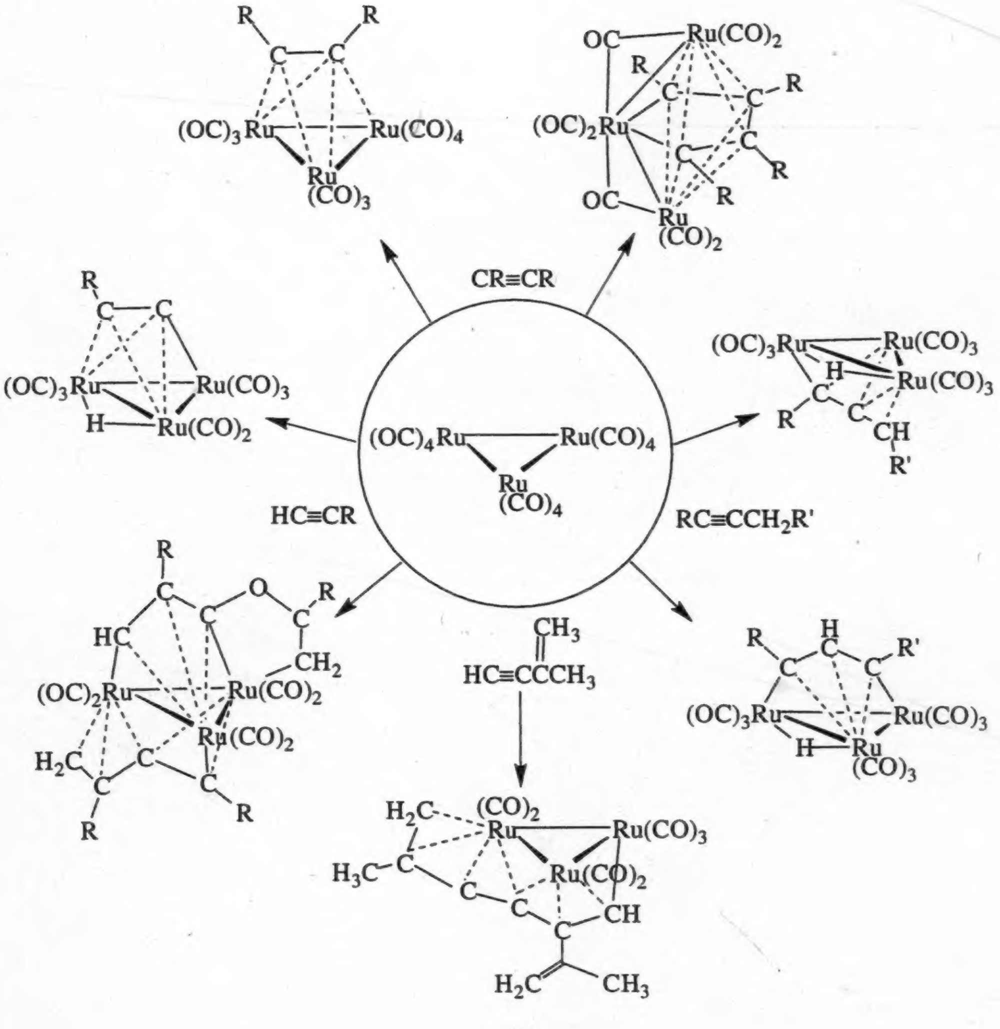
CR≡CR
HC≡CR
RC≡CCH₂R'
HC≡CCCH₃ with =CH₂... CH₃
(OC)₄Ru Ru(CO)₄ Ru (CO)₄
(OC)₃Ru Ru(CO)₄ Ru (CO)₃
OC Ru(CO)₂ (OC)₂Ru OC Ru (CO)₂
(OC)₃Ru Ru(CO)₃ H Ru(CO)₂
(OC)₃Ru Ru(CO)₃ H Ru(CO)₃ CH R'
(OC)₂Ru Ru(CO)₂ Ru(CO)₂ HC H₂C CH₂ O
(OC)₃Ru Ru(CO)₃ H Ru (CO)₃ R R'
H₂C (CO)₂ Ru Ru(CO)₃ Ru(CO)₂ H₃C CH H₂C CH₃
R

Scheme 1-2 Reaction of $Ru_3(CO)_{12}$ with Alkynes [9].

The diverse reactivity patterns of transition metal carbonyls, and organometallic complexes in general, raises the question how best to utilize these important classes of compounds. Much interest is centered on the practical aspects of organometallic compounds. Two areas stand out in this regard; the use of organometallic compounds in organic synthesis and in homogenous catalysis. It is well known that transition metal organometallic compounds assist in the synthesis of both simple and complex organic molecules [10]. Organometallic compounds can act as activating, protecting and stabilizing agents. Binding an organic molecule to a metal may activate the organic functional groups toward reactivity patterns that would otherwise be unavailable or difficult to achieve for the free organic molecule [11(a)]. As a protecting agent the metal complex can deactivate or protect organic functionalities from unwanted involvement in a reaction [11(b)]. Moreover, organometallic compounds are used to stabilize very reactive organic molecules, so they may be used in synthesis [11(c)]. The advantage associated with the use of organometallic complexes for organic synthesis stems from their ability to direct or maintain a preferred chemoselectivity, regioselectivity and stereochemistry. Metal carbonyl complexes make good reagents in organic synthesis as they are relatively stable, inexpensive and display a wide range of reactions [12]. Aside from the protecting and activating abilities of metal carbonyls, they can also act as a source of CO. Through carbonyl insertion (alkyl migration) and olefin insertion the introduction of a CO group into an organic moiety can be achieved.

The ability of organometallic complexes to activate organic functionalities is the basis of homogenous catalysis. Interest in this area is driven, to a large extent, by the need for chemical applications [13]. For some time, the development of existing organometallic catalysts for industrial applications has slowed, largely because the processes and catalysis that were developed in the 1970s and 1980s are economically efficient [14,15]. However, research continues in a number of areas: further development of existing industrial processes with the aim of improving activities and selectivities, development of processes for new materials and the conversion of stoichiometric processes to catalytic processes [14,15]. One such area that has received notable attention, and is associated with a major obstacle in many homogeneous catalytic processes, is the separation of a non- or low-volatile product from the thermally unstable catalyst [16]. In addition to their wide usage in industry to produce synthetic chemicals and petroleum products, organometallic catalysis is intrinsically interesting because the subtle mechanisms by which they operate are often not known. Thus, fundamental mechanistic research continues to be an active area [17].

Catalysis by transition metal carbonyls has played a pivotal role in this area with the development of the hydroformylation of olefins (oxo process), discovered by Otto Roelen in 1938, and the carbonylation of alkynes, alkenes and alcohols (Reppe reactions), discovered by Walter Reppe in the early 1940's [18]. Both processes use transition metal carbonyl complexes as catalysts and both have contributed greatly to the chemical industry [18,19]. The former, in particular, continues to be an important industrial process using cobalt or rhodium carbonyl catalysts [20]. Moreover, research activity into refinement of existing processes and development of new catalysis, based on a carbonyl platform, continues [13a,20,21].

The future bodes well for organometallic chemistry as a number of new areas of interest emerge. It appears that the transition metal carbonyls may play a significant role in two such "cutting edge" areas; bioorganometallic chemistry and surface science. Within the bioorganometallic realm, scientists are attempting to use metal carbonyl fragments as biochemical tracers in the hope of developing a carbonylmetalloimmunoassay (CMIA) procedure [22]. With the metal carbonyl fragment bound to a biological molecule, scientists may be able to follow the molecule through various metabolic pathways. The detection and monitoring of these molecules is based on the ν_{CO} of metal bound carbonyl by FT-IR. This technique has advantages over traditional radioisotope methods in that the exposure to hazardous material and the need for complex detection and disposal facilities are eliminated [22a,c], as well, by labeling different biological molecules with different metal carbonyl groups one can monitor mixtures at the same time, which is not possible with traditional radiolabels [23]. Within surface science, heterogeneous catalysis and, to some extent, organometallic chemistry, organometallic complexes are used as models for reaction sites at metal surfaces in order to elucidate the nature of catalytic process at these surfaces [24]. Scientists seek parallels between transition metal clusters and metal surfaces as they assert that the interaction between ligands and metal clusters models the interaction between small molecules and metal surfaces (cluster-surface analogy) [25]. Carbonyl complexes are very useful in this respect because they have a tendency to form cluster compounds [26] and therefore are potential models for multiple atom surface sites.

From a more fundamental view point, there has been an emergence of a new class of nontraditional or non-classical carbonyl compounds [1d, 27]. It appears that the classical description of M–CO bonding does not accurately portray the bonding for a growing number of metal carbonyl compounds as the average ν_{CO} of these compounds are significantly greater than the 2143 cm^{-1} observed for free CO. These non-classical carbonyl complexes are best described as featuring primarily $M \leftarrow CO$ σ donor interaction, with little or no $M \rightarrow CO$ back donation. This situation is very different from the traditional bonding description in which back donation is considered essential for the formation of stable metal carbonyls [1c,28].

Since the time of Ludwig Mond and the discovery of $Ni(CO)_4$, the transition metal carbonyls have played a significant role in the development of organometallic chemistry, both in terms of practical application and fundamental concepts. It is expected that the carbonyls will continue to contribute to the advancement of organometallic chemistry as new areas unfold.

1.2 The Group 8 Metal Carbonyls

1.2.1 Synthesis and Characterization of Group 8 Metal Carbonyls

The group 8 homoleptic metal carbonyls are either commercially available or can be prepared from commercially available precursors. Physical and spectroscopic properties of the group 8 carbonyls are listed in Table 1-1 [29].

The most common form of the homoleptic iron carbonyl is iron pentacarbonyl. It can be made from the reaction of finely divided iron metal [30] or Fe_2O_3 [31] with CO at elevated temperatures and pressures. $Fe(CO)_5$ is a volatile, toxic yellow liquid that is moderately stable, but will decompose at ambient temperature with time to give the trinuclear compound, $Fe_3(CO)_{12}$, and iron powder which tends to be pyrophoric in air. Upon exposure to ambient light $Fe(CO)_5$ slowly decomposes to give $Fe_2(CO)_9$. Long term storage is possible at low temperatures with protection from ambient light sources. A low temperature solid state crystal structure has been reported [32] and shows a slightly distorted trigonal bipyramidal geometry. However, the solution ^{13}C NMR spectrum indicates the molecule to be fluxional in the temperature range 25 to −170 °C as only one signal for all carbonyls is observed [33].

Table 1-1 Physical and Spectroscopic Properties of the Group 8 Carbonyls.

Compound	$M(CO)_5$ [a]			$M_2(CO)_9$			$M_3(CO)_{12}$ [b]		
M	Fe†	Ru	Os	Fe†	Ru	Os	Fe†	Ru†	Os†
appearance	yellow liquid	colorless liquid	yellow liquid	orange crystals	—	orange-yellow crystals	dark green crystals	orange crystals	yellow crystals
m.p. (°C)	−20.5	−17 to −16	2–2.5	80	—	64–67 (dec.)	—	154–155 (dec.)	—
ν_{CO} (cm^{-1})	2022.5 2000.5 (hexane)	2036.5 2001.5 (hexane)	2035.0 1993.0 (hexane)	2075 2020 1821 (mull)	2077 2018 1814 (heptane)	2080 2038 2024 2013 2000 1778 (heptane)	2045 2015 1850 (THF)	2061 2031 2021 (heptane)	2070 2036 2015 2003 (hexane)
^{13}C NMR (ppm)	210.6 ($CDCl_3$)	200.4 ($CDCl_3$)	182.6 ($CDCl_3$)	—	—	—	210.1 (CD_2Cl_2)	198.0 ($CDCl_3$)	183.9 172.3 (C_6D_6)

† commercially available

[a] Ref. 35a.

[b] ^{13}C NMR data from Ref. 50e.

The Berry pseudorotation is the generally accepted mechanism for this carbonyl scrambling process [34]. The exchange between the nonequivalent axial and equatorial sites occurs as the geometry rapidly converts from a trigonal bipyramid to a square pyramid then back to a trigonal bipyramid (Scheme 1-3)

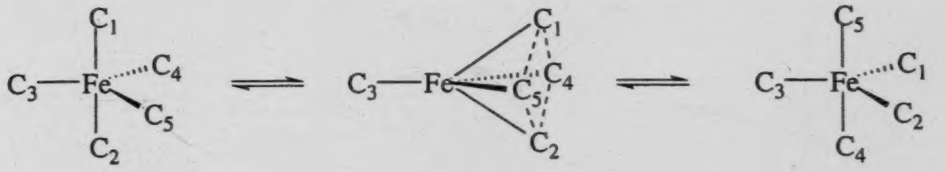

Scheme 1-3 The Berry Pseudorotation Mechanism for $Fe(CO)_5$.

The ruthenium analogue is a volatile colorless liquid and is much more light and temperature sensitive than $Fe(CO)_5$; it readily decomposes at room temperature. It can be formed by carbonylation of $Ru_3(CO)_{12}$ at elevated pressures and temperatures [35], from low temperature photolysis of $Ru_3(CO)_{12}$ in the presence of excess CO [36], or reductive carbonylation of $[Ru(acac)_3]$ with CO/H_2 in heptane (180 °C/200 atm) [37]. $Os(CO)_5$ is best synthesized from reaction of $Os_3(CO)_{12}$ and CO at high temperatures and pressures [35a]. It is a volatile yellow liquid and is comparable in stability to $Fe(CO)_5$. The IR spectrum of $Ru(CO)_5$ or $Os(CO)_5$ show two strong ν_{CO} bands indicating a trigonal bipyramidal structure with D_{3h} symmetry [35a, 37]. As with the iron pentacarbonyl, the ^{13}C NMR spectra of the ruthenium and osmium pentacarbonyls indicate a rapid scrambling of the carbonyl ligands [35a]. A gas phase electron diffraction study of $Os(CO)_5$ supports the trigonal bipyramidal structural assignment [38]; however, an unpublished crystal structure report indicates that $Os(CO)_5$ adopts a distorted trigonal-bipyramidal geometry with only C_{2v} symmetry [39].

Diiron nonacarbonyl was the first binuclear carbonyl complex to be isolated and the first carbonyl complex to be structurally analyzed by X-ray crystallography [40]. It can be synthesized by photolysis of $Fe(CO)_5$ [41] and is a useful source of $Fe(CO)_3$ and $Fe(CO)_4$ fragments in organometallic and organic synthesis [42]. The orange crystals of this compound are air stable; however, it has low solubility in most organic solvents and low volatility for a metal carbonyl of its molecular weight. The solid state structure of the molecule has approximate D_{3h} symmetry, actual symmetry is C_{3h}, with the carbonyl ligands located about the iron centers in a distorted octahedron [40b]. The molecule contains an Fe-Fe bond and three bridging carbonyls along with the six terminal carbonyl ligands (Figure 1-3). Both $Ru_2(CO)_9$ and $Os_2(CO)_9$ can be prepared by low temperature photolysis [43]. The ruthenium dimer has not been isolated in pure form and is much too unstable for structural characterization, it readily decomposes at room temperature, but its formulation has been corroborated by mass spectrometry [43]. The IR spectrum of a mixture of $Ru_2(CO)_9$ and $Ru_3(CO)_{12}$ has been obtained and tentative assignments of the bands of the binuclear complex have been proposed (Table 1-1) [43, 44]. The more robust $Os_2(CO)_9$, orange-yellow crystals, allowed mass and IR spectroscopic analysis [43]. The proposed structure has one bridging carbonyl and eight terminal carbonyls as well as a metal-metal bond (Figure 1-3). Both the ruthenium and osmium compounds decompose to give the trinuclear dodecacarbonyls [43]. Structural analysis by diffraction methods have not been successful for either of the former species thus far.

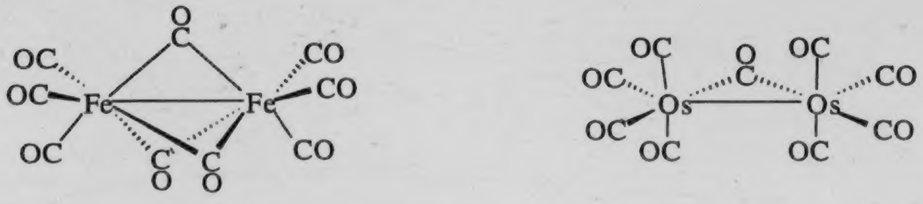

Figure 1-3 Structures of $M_2(CO)_9$ (M = Fe, Os).

The deep green "black" crystals of moderately stable $Fe_3(CO)_{12}$ can be obtained from the thermal decomposition of $Fe_2(CO)_9$ [45] or from the pentacarbonyl complex by reaction with aqueous strongly basic organic amines and subsequent acidification [46]. Alternatively, oxidation of $HFe(CO)_4^-$ by MnO_2 [47] will give the dodecacarbonyl. The generally accepted structure consists of a three iron atom triangle core with three Fe-Fe bonds. Two asymmetric bridging carbonyl ligands span one metal-metal bond while the remaining carbonyls are terminal (Figure 1-4). The crystallographic disorder associated with the X-ray crystal structure casts some doubt on the proposed structure [40c, 48]. However, solid state magic angle spinning ^{13}C NMR spectrum at –93 °C supports the assignment [49]. The structure of $Fe_3(CO)_{12}$ in solution, based on ^{13}C NMR and IR spectroscopy, remains a mystery as the issue is complicated by carbonyl scrambling and a mixture of structures [50]. The ^{13}C NMR spectrum shows a single resonance down to a temperature of –100 °C indicating a rapid equilibration of all carbonyls [50e]. The trimetallic dodecacarbonyls of ruthenium and osmium are the most stable and common forms of the homoleptic carbonyls of these metals. Orange crystals of $Ru_3(CO)_{12}$ are best prepared by direct carbonylation (125 °C/65 atm) of $RuCl_3{\bullet}XH_2O$ in methanol [51]. In the absence of an autoclave, the compound can be synthesized by ambient pressure carbonylation [52]. The osmium analogue is prepared by reaction of OsO_4 and CO in ethanol (175 °C/80 atm) and gives large hexagonal yellow crystals of $Os_3(CO)_{12}$ [53]. Both the ruthenium [54] and osmium [55] dodecacarbonyls crystallize without disorder and the crystal structures show a triangular core of metal atoms with each metal at the center of an approximate octahedron with each metal atom bonded to four terminal carbonyl ligands (Figure 1-4). The ^{13}C NMR spectrum of $Ru_3(CO)_{12}$ [50e,f] is similar to that of the iron analogue, *i.e.* it indicates fluxionality and exchange between axial and equatorial carbonyls, but the ^{13}C NMR spectrum of $Os_3(CO)_{12}$ [50e,f, 56] shows two resonances at room temperature indicating the structure is stereochemically rigid at this temperature.

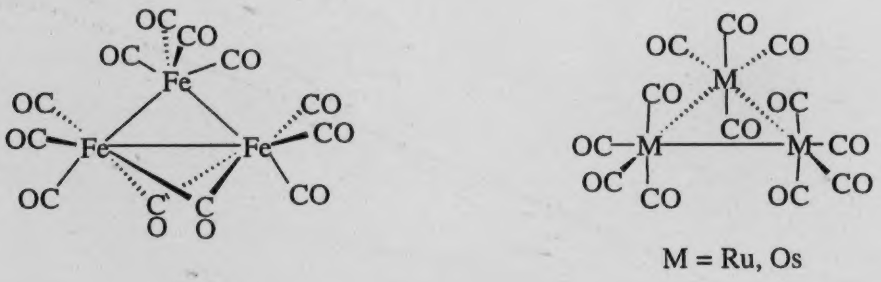

Figure 1-4 Structures of $M_3(CO)_{12}$ (M = Fe, Ru, Os).

1.2.2 Substitution Reactions of $M(CO)_5$ (M = Fe, Ru, Os) Complexes

One of the most common type of reactions displayed by the group 8 pentacarbonyls is carbonyl substitution. The generally accepted mechanism for carbonyl substitution in these systems is CO dissociation, the rate determining step, followed by ligation of the incoming ligand [57]. In general, the $M(CO)_5$ (M = Fe, Ru, Os) complexes are substitutionally inert; carbonyl substitution reactions occur at a slow rate. The reaction must therefore be initiated in some manner. Several methods are described in the literature with the most popular being thermal activation, photolysis [58], and the use of chemical initiators, such as Me_3NO [59].

A variety of simple two-electron donor ligands may substitute for a carbonyl ligand in the group 8 metal carbonyl complexes. Probably the most widely studied substitution reactions are the substitution of a carbonyl by a phosphine or phosphite in iron carbonyl complexes [60], but those of ruthenium [61] and osmium [62] are also well studied. Products of these reactions usually take the form $M(CO)_{5-n}L_n$ (n = 1 - 4) with the mono- and dicarbonyl complexes being relatively rare while products with n = 1 or 2 being most common. Again, these reactions proceed very slowly without activation. Generally, the geometry of the products is found to be trigonal bipyramidal with some distortion toward square pyramidal in the case of the more sterically demanding ligands [60]. In most cases the phosphine ligand occupies the axial position, as expected from site preference arguments of Rossi and Hoffmann [63], but it can be found in the equatorial position. Moreover spectroscopic evidence indicates that axial-equatorial isomerization can occur in these systems [64].

A number of different organic functionalities can also act as incoming ligands in carbonyl substitution reactions and bind to group 8 metals. One area that has shown activity for many years is the use of unsaturated organic molecules as ligands. By far, the most popular class of ligands used are the alkenes. In particular η^2-alkene complexes of iron carbonyl complexes have attracted a great deal of interest [65]. These complexes tend to be thermally sensitive and therefore are synthesized at or below room temperature. Since $Fe_2(CO)_9$ is a good source of $Fe(CO)_4$ and $Fe(CO)_3$ moieties, a good method of preparation is the reaction of alkene with $Fe_2(CO)_9$ [66]. Otherwise, low temperature photosubstitution of $Fe(CO)_5$ in the presence of olefins has proven to be a reliable method for the synthesis of $Fe(CO)_4(\eta^2$-alkene) complexes [67]. Multiple carbonyl substitution is possible as evidenced by the production of $Fe(CO)_3(\eta^2\text{-Z-cyclooctene})_2$ [67b], $Ru(CO)_3(\eta2\text{-}C_2H_4)_2$ [68] and $Os(CO)_3(\eta^2\text{-}C_2H_4)_2$ [69]. These molecules retain the trigonal bipyramidal geometry of the parent homoleptic carbonyls with the olefin in the equatorial plane and adopting an in-plane orientation. Figure 1-5 shows an archetypical structure of $M(CO)_4(\eta^2\text{-alkene})$ (M = Fe, Ru, Os) complexes as determined by gas phase electron diffraction and X-ray diffraction analysis [70]. Like the phosphine containing complexes, spectroscopic evidence suggest stereochemical nonrigidity involving carbonyl scrambling [71, 66a]. Alkynes can also serve as ligands in group 8 carbonyl complexes, but they are not nearly as common as the alkene ligands. Under similar reaction conditions that produced simple alkene complexes, it was found that reactions with alkynes tend to give alkyne coupled products rather than η^2-alkyne derivatives [72].

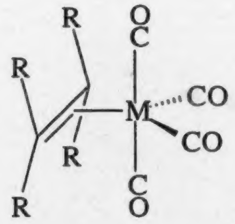

Figure 1-5 Archetypical Structure of $M(CO)_4(\eta^2\text{-alkene})$ (M = Fe, Ru, Os).

1.3 $M(CO)_4(\eta^2\text{-alkyne})$ (M = Fe, Ru, Os) Complexes

1.3.1 Synthesis of $M(CO)_4(\eta^2\text{-alkyne})$ (M = Fe, Ru, Os) Complexes

Prior to the Takats group involvement in the synthesis of simple η^2-alkyne tetracarbonyl complexes of the group 8 transition metals, few examples were reported in the literature. In 1964 Hübel reported the preparation of $Fe(CO)_4(\eta^2\text{–}C_2RR')$ (R, R′

= CMe_3; R, R′ = $SiMe_3$; R = Ph, R′ = $SiMe_3$) [73]. These complexes were prepared by UV irradiation of a mixture of $Fe(CO)_5$ and the free alkyne in petroleum ether at 20 °C. Hübel proposed a trigonal bipyramidal geometry for the complexes in which the alkyne is η^2 bound to the iron center and occupies an equatorial position. However these initial reports were poorly documented and included few details of product characterization. Some years later a publication by Pannell and Crawford detailed the synthesis and characterization of $Fe(CO)_4(\eta^2\text{-}C_2(SiMe_3)_2)$ [74]. The preparation was conducted in a similar manner to that described by Hübel, with the exception that $Fe_3(CO)_{12}$ was used as the source of the metal carbonyl. The yellow crystalline product was recovered in 50-80% yields but was found to be thermally sensitive and decomposed at room temperature, even while being under an inert atmosphere. Despite analytical and spectroscopic characterization (IR), structural details were lacking. Finally, in 1978 Carty *et al.* reported the synthesis and characterization, including a solid state molecular structure, of $Fe_2(CO)_8(Ph_2PC{\equiv}C^tBu)$ which contains the $Fe(CO)_4(\eta^2\text{-alkyne})$ moiety in addition to the $Fe(CO)_4$(phosphine) fragment [75]. The complex forms from a room temperature reaction of $Fe_2(CO)_9$ and $Ph_2PC{\equiv}C^tBu$ in benzene under a carbon monoxide atmosphere. After purification by chromatography and recrystallization, pale yellow crystals were obtained. Carty's report provides the first conclusive structural geometry of a $Fe(CO)_4(\eta^2\text{-alkyne})$ complex (Figure 1-6). The crystal structure concurs with Hübel's earlier purposed structure: a trigonal bipyramidal stereochemistry about the iron center (Fe1 in Figure 1-6) with an η^2-alkyne occupying an equatorial position. In addition, Carty's structure shows the ligating carbon atoms of the alkyne (C9 and C10) lie in the equatorial plane (Fe1, C1, C3) as opposed to an alignment with the axial axis (C2–Fe1–C4).

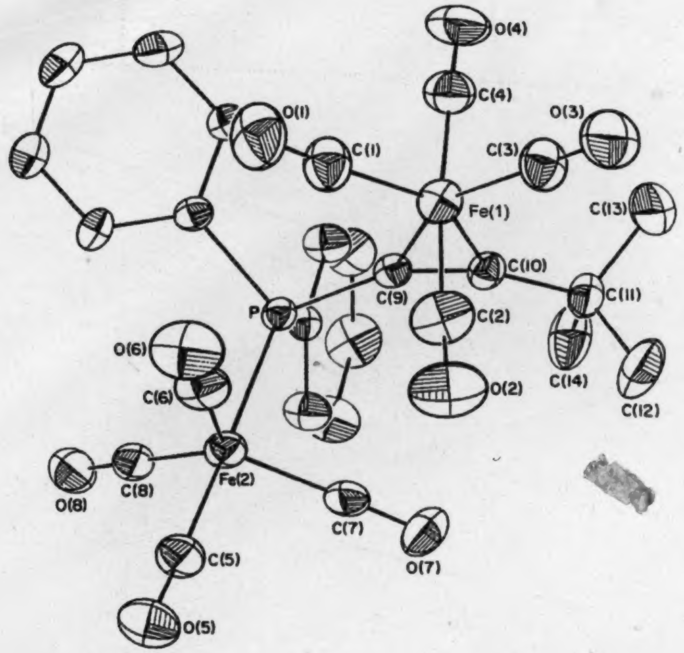

Figure 1-6 Solid State Molecular Structure of $Fe_2(CO)_8(\eta^2\text{-}Ph_2C{\equiv}C^tBu)$ [75].

Takats *et al.* contributed to this area of chemistry in 1987 with a publication detailing the synthesis and characterization of the first simple mononuclear $M(CO)_4(\eta^2\text{-}C_2(SiMe_3)_2)$ (M = Ru, Os) complexes [76]. In addition, the iron analogue was prepared, as described previously by Pannell and Crawford, and a triad comparison was conducted. The preparation of the osmium and ruthenium complexes required some modification to the procedure used to produce $Fe(CO)_4(\eta^2\text{-}C_2(SiMe_3)_2$, as filtered radiation ($\lambda \geq 370$ nm; GWV Glasswerk Wertheim filter) gave the best results. In addition, to obtain the ruthenium product the photolysis had to be performed at low temperature (– 40 °C) and with *in situ* prepared $Ru(CO)_5$ as substrate. Also in this report an X-ray crystal structure of $Os(CO)_4(\eta^2\text{-}C_2(SiMe_3)_2)$ (Figure 1-7) was presented and was shown to closely resemble the $Fe(CO)4(\eta^2$-alkyne) fragment described in Carty's crystal structure of $Fe_2(CO)_8(Ph_2PC{\equiv}C^tBu)$ [75].

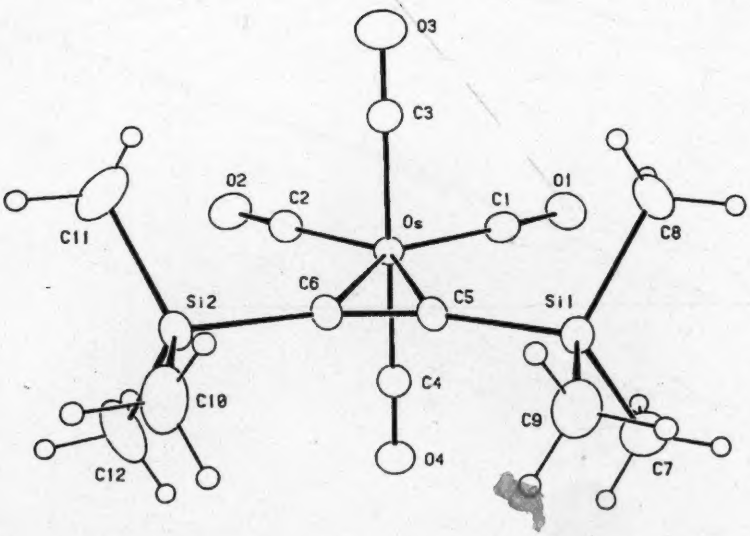

Figure 1-7 Molecular Structure of $Os(CO)_4(\eta^2\text{-}C_2(SiMe_3)_2)$ [76].

Over the years, continuing work in the Takats laboratories with the low temperature photolysis technique has allowed the incorporation of a modest variety of alkyne ligands in the osmium and ruthenium tetracarbonyl complexes [77]. However, until recently, attempts to produce the related iron derivatives, beside the bis(trimethylsilyl)acetylene and minor amounts of the hexafluorobut-2-yne compounds have failed. Finally, in 1997 Cooke and Takats reported the preparation of a series of $Fe(CO)_4(\eta^2\text{-alkyne})$ complexes with the same alkyne ligands that were used in the previous osmium and ruthenium compounds [78]. It was found that the use of an uranium glass filter ($\lambda \geq 330$) and temperatures below −50 °C were needed to achieve reasonable success with the iron compounds. Presently, in our laboratories, the preparation of the simple η^2-alkyne tetracarbonyl complexes of the group 8 transition metals, on a 100-200 mg scale and with a moderate variety of alkyne ligands, is routinely accomplished.

1.3.2 Bonding Between an Alkyne Ligand and a Transition Metal

The modern view of the bonding between an alkyne ligand and a metal center is commonly considered analogous to the Dewar-Chatt-Duncanson model for metal-olefin bonding [79]. Like the metal-olefin bonding, the metal-alkyne interaction is based on a synergistic relationship between ligand to metal donation and metal to ligand back donation. A simple orbital illustration of metal-alkyne bonding is shown in Scheme 1-4. Donation of electron density from the alkyne to the metal occurs through a σ type interaction by overlap of the filled $\pi_{||}$ (π-parallel) orbital of the alkyne with an appropriate vacant σ metal orbital. Back donation occurs through a π interaction from the metal to the alkyne by overlap of a filled metal $d\pi$ orbital (d_{xz} in Scheme 1-4) with the empty $\pi_{||}$* orbital of the alkyne. All metal-alkyne bonding in this case is coplanar and thus referred to as in-plane or parallel bonding. At this point, in terms of the 18-electron rule formalism, the alkyne is considered a two electron donor ligand.

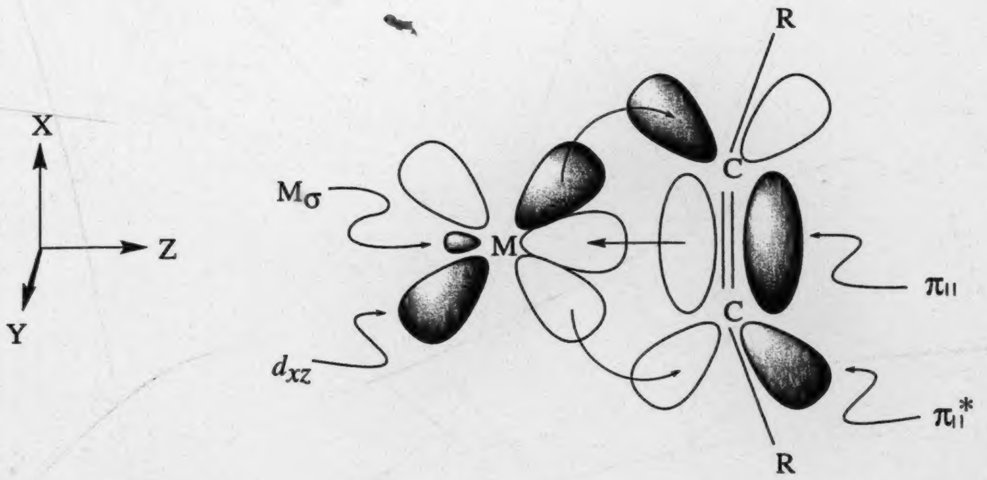

Scheme 1-4 Metal-Alkyne In-Plane Bonding.

Since the $\pi_{||}$* orbital is antibonding with respect to the alkyne triple bond, strong back donation causes a decrease in the triple bond character. As a consequence, a rehybridization of the alkyne carbons from *sp* to increasing sp^2 character occurs. In terms of geometry, the substituents bound to the alkyne carbons bend back away from the metal, analogous to the bending back of hydrogens in a transition metal complexed olefins [80]. Furthermore, the bend back angle is a measure in the deviation of the C≡C–R angle from linearity and of the strength of the metal-alkyne interaction.

Within the valence bond framework, two limiting representations can be constructed to describe two extreme cases of metal-alkyne bonding (Scheme 1-5). Representation **A** shows the extreme of good σ donation from the alkyne to the metal and poor back donation from the metal to the alkyne. Structurally speaking only small changes in both the alkyne carbon-carbon distance and the bending back of the alkyne substituents would be expected. Representation **B** shows the other extreme of weak to moderate donation from the alkyne but with strong back donation from the metal to the alkyne; the metallacyclopropene extreme. In this case one would expect to observe a significant expansion of the alkyne carbon-carbon distance as the triple bond becomes a double bond. Moreover, a significant bending back of the alkyne substituents would be seen as the metal bound alkyne carbons change from *sp* to sp^2 hybridization. Typically metal-alkyne bonding is best represented by **A** when the alkyne has electron donating substituents and **B** when electron withdrawing substituents are present.

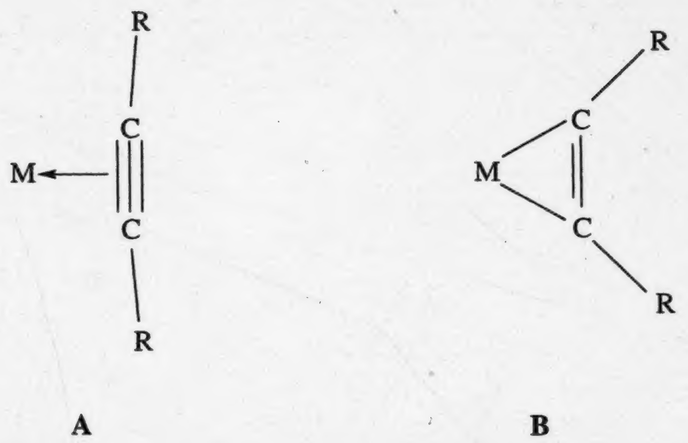

Scheme 1-5 Valence Bond Representations of Metal-Alkyne Bonding; Two Electron Donor Alkyne

In addition to the in-plane σ and π interaction the alkyne ligand may engage in a perpendicular interaction with the metal by utilizing its second set of π and π* orbitals. In a similar manner to the in-plane bonding, the perpendicular bonding is composed of alkyne to metal donation and metal to alkyne back donation. Scheme 1–6 shows the two components of the perpendicular metal-alkyne bonding interaction. Donation of electron density from the alkyne to the metal occurs through a π interaction by overlap of the filled $\pi_\perp$ (π perpendicular) orbital of the alkyne and a vacant metal *d* orbital (d_{yz} in Scheme 1-6(a)) of appropriate symmetry. Back donation from the metal to the alkyne occurs through a δ interaction by overlap of an appropriate metal *d* orbital (d_{xy} in Scheme 1-6(b)) and the vacant $\pi_\perp$* of the alkyne. This back donation from the metal to the alkyne in the δ fashion is found to be weak and can be ignored in most cases [81]. In terms of the 18-electron formalism, the alkyne is considered a four electron donor ligand. However, if the metal d_π orbital is also filled, perpendicular interaction between the alkyne and the metal may have a destabilizing effect on the metal-alkyne bond. This effect is referred to as four electron destabilization and arises from a repulsive interaction between the filled $\pi_\perp$ orbital of the alkyne and a filled metal *d* orbital of the same symmetry (d_{yz} orbital in Scheme 1–6(a)) [81c, 82]. This repulsion results in a decrease in the total bonding of the alkyne to the metal and may cause labilization of the alkyne ligand in cases where the metal has electron density in these *d* orbitals.

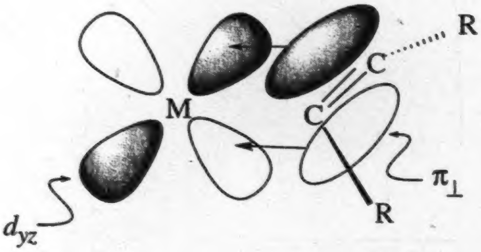

(a) Alkyne $\pi_\perp \rightarrow$ Metal d_{yz} Donation

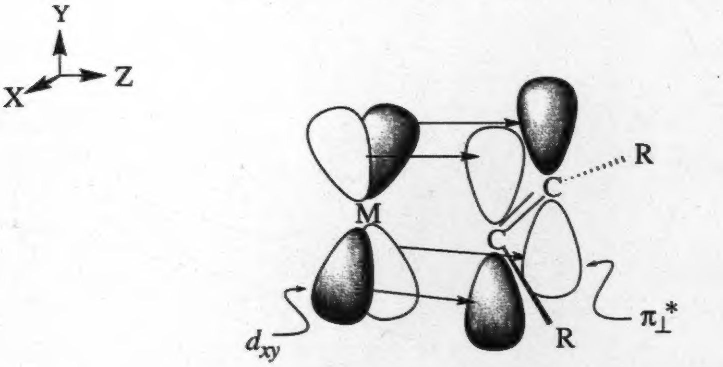

(b) Metal $d_{xy} \rightarrow$ Alkyne $\pi_\perp^*$ Back Donation

Scheme 1-6 Metal-Alkyne Perpendicular Bonding.

The valence bond representations of metal-alkyne bonding in the four electron donor alkyne case are shown in Scheme 1-7. In representation **C** the in-plane two electron bonding is supplemented with marginal perpendicular involvement in the metal-alkyne bonding. On the other hand representation **D** illustrates the case where strong perpendicular involvement occurs and adds considerably to the total metal-alkyne bonding. Structurally, no change in the bond angles about the alkyne carbons may occur but one would expect to see significant contraction of the metal-alkyne carbon distances and an expansion of the carbon-carbon distance of the alkyne carbons as a result of the transition from representation **C** to **D**.

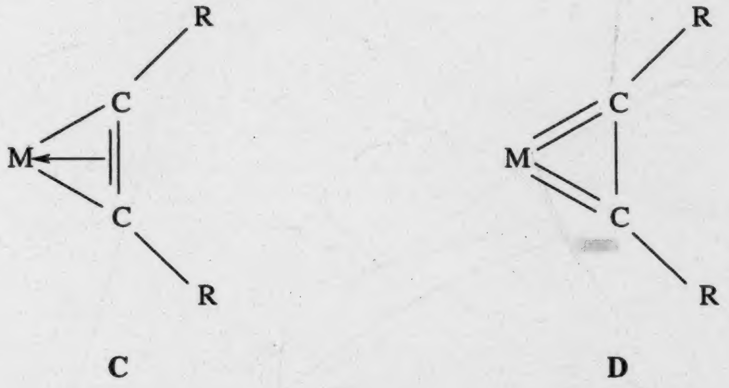

Scheme 1-7 Valence Bond Representation of Metal-Alkyne Bonding: Four Electron Donor Alkyne.

The importance of the perpendicular involvement has been acknowledged by Templeton in a review of molybdenum(II) and tungsten(II) complexes containing four electron donor alkyne ligands [83]. Templeton developed a criterion, based on empirical correlation, for the identification of four electron alkyne donor ligands. The ^{13}C NMR chemical shift of the metal bound alkyne carbons was found to be diagnostic in revealing the electron donating nature of the alkyne ligand. The chemical shift of the alkyne carbons of the two electron donor alkynes were found to be in the

δ 95–130 ppm range, while the alkyne carbons of the four electron donor alkyne were found to resonate at a much lower field, in the δ 170-230 ppm range. Moreover four electron donor alkynes can be identified based on structural parameters. In particular, the metal-alkyne carbon distances in four electron donor alkyne complexes were found to be substantially shorter than the corresponding distances in the two electron donor complexes when the alkyne is bound to the same type of metal atom. In addition, a good deal of consistency in M-C(alkyne) distances of four electron donor alkyne complexes was established even with a diversity in the types of alkynes and auxiliary ligands [83].

A more detailed discussion of bonding in $M(CO)_4(\eta^2\text{-alkyne})$ compounds can shed some light on some of the structural issues involving these compounds. All available structural data indicate that these complexes adopt a trigonal bipyramidal geometry with the η^2-alkyne occupying an in-plane equatorial coordination site in preference to an axial site [75, 76, 81c, 84]. The question of the equatorial preference and the in-plane orientation are at issue. This same question arose in the analogous ethylene complexes and has been addressed by Hoffmann [85]. The approach used by Hoffmann was to compare the interactions between the frontier orbitals of the ML_4 fragment and the ethylene ligand for the complex with the ethylene in the axial position (C_{3v} ML_4) with the corresponding interactions in the complex with the equatorially bound ethylene (C_{2v} ML_4). However, complexes containing the alkyne ligand have an added complexity, that being the presence of the $\pi_{\perp}$ and $\pi_{\perp}^*$ orbitals. Although Hoffmann's approach does not take this added factor into account, it does accurately describe the $\pi_{\parallel}$ and $\pi_{\parallel}^*$ interactions between the alkyne and the metal. Since the molecular orbital descriptions for both of the ML_4 fragments [85, 86] and the alkyne ligand [81a,c] are available and qualitative interaction diagrams have been constructed, a comparison of their orbital interactions, in the Hoffmann tradition, can be conducted to rationalize the preference of in-plane equatorial coordination over axial coordination for the alkyne ligand in trigonal bipyramidal geometry.

Scheme 1-8 shows the orbital interaction diagram for the $M(CO)_4$ fragment with C_{3v} symmetry and an alkyne ligand. Strong bonding interaction occurs between the filled $\pi_{||}$ orbital of the alkyne and the hybridized empty a_1 σ orbital of the $M(CO)_4$ fragment. This was described previously (Scheme 1-4) in terms of parallel σ donation from the alkyne to the metal. The corresponding parallel metal-alkyne back donation is seen in this diagram as interaction between $\pi_{||}^*$ and an element of the lower e set of the $M(CO)_4$ fragment which is mainly metal d_{xz} orbital in character. This interaction, however, is weak as a result of poor energy match between the orbitals. Hoffmann has indicated that the lower e set orbitals experience significant stabilization as a result of good backbonding to the auxiliary ligands, *i.e.* carbonyl ligands [85, 86]. This stabilization opens a significant energy gap between the lower e set and the $\pi_{||}^*$ orbital thus reducing the bonding interaction. A destabilizing interaction occurs between the filled $\pi_{\perp}$ of the alkyne and a filled element of the lower e set (d_{yz}). This interaction was previously described as four electron destabilization. The δ interaction between the vacant $\pi_{\perp}^*$ and a filled element of appropriate symmetry of the upper e set, which is primarily d_{xy} in character, is negligible and thus this upper e set orbital remains a nonbonding orbital. Likewise the remaining element of the upper e set ($d_{x^2-y^2}$) is nonbonding and thus neither adds to or subtracts from the total bonding. In summary the total metal-alkyne bonding between the C_{3v} $M(CO)_4$ fragment and an alkyne is dependent mainly upon the parallel σ donation with only minimal reinforcement from the weak parallel back donation. Moreover, the total bonding is destabilized by the presence of the additional filled $\pi_{\perp}$ orbital through the four electron destabilization effect.

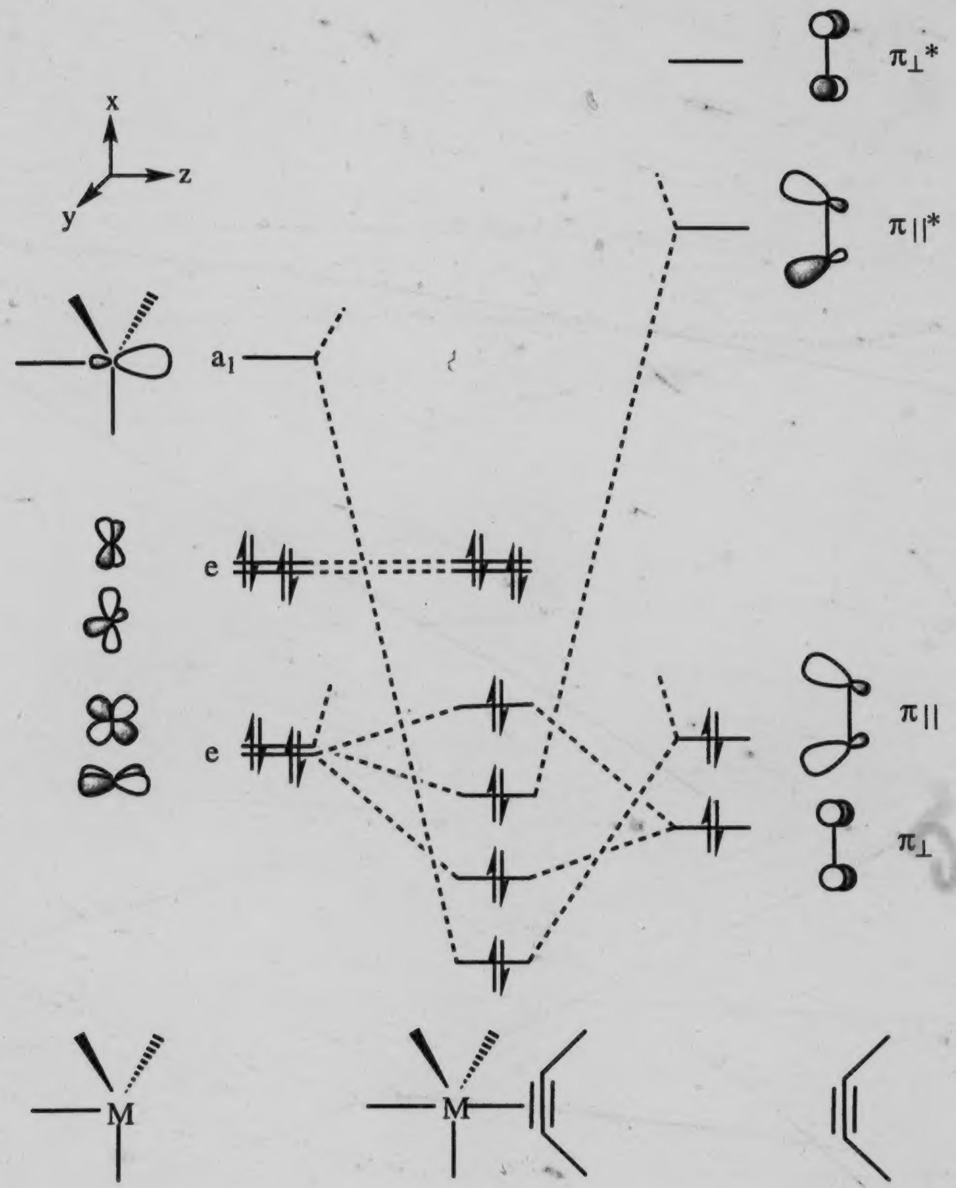
x
z
y
a$_1$
e
e
$\pi_\perp$*
$\pi_{||}$*
$\pi_{||}$
$\pi_\perp$
M
M

Scheme 1-8 Interaction Diagram for a C_{3v} M(CO)$_4$ Fragment (*left*) with a Perturbed Alkyne Ligand (*right*).

The orbital interaction diagram for the C_{2v} $M(CO)_4$ fragment and an in–equatorial plane alkyne is given in Scheme 1-9. The bonding here can be described in much the same manner as in the C_{3v} $M(CO)_4$ case but with some notable differences. As in the above case, a strong bonding interaction occurs for the parallel alkyne σ donation; good interaction between $\pi_{\|}$ and the hybridized $2a_1$ orbital. In contrast to the C_{3v} case, the parallel metal-alkyne back donation, seen here as the interaction between $\pi_{\|}^*$ and b_2, is relatively strong; *i.e.* stronger than the corresponding interaction in the C_{3v} case [85]. One reason for this is that the hybridization advantage in the b_2 orbital was absent in either member of the lower e set in the C_{3v} case. In alkene complexes, Hoffmann indicates that it is precisely this strong metal-alkene back donation that is the deciding factor in the equatorial site preference of the alkene ligand [85]. This argument is also valid for the alkyne case. At this point we are in a position to discuss an alternative orientation of the alkyne ligand, which is a rotation of the alkyne by 90 degrees so it is in parallel alignment with the axial ligands. In this orientation the $\pi_{\|}^*$ now interacts with the b_1 (d_{xz}) orbital. The b_1 metal orbital, however, is already in a strong bonding interaction with the axial carbonyl ligands [85], and this competition for bonding interaction would seriously compromise the metal-alkyne back donation. Thus, it is more energetically favorable for the alkyne to adopt an in-equatorial plane orientation. Returning to the in-equatorial plane orientation of the alkyne, the interaction of the filled $\pi_{\perp}$ and the filled b_1 induces four electron destabilization but this negative bonding effect is more than compensated for by the good parallel bonding. Again the δ interaction can be ignored due to poor overlap, which leaves the a_2 (d_{xy}) as a nonbonding orbital along with the $1a_1$ (d_{z^2}). Thus the total in-equatorial plane bonding is determined by the two mutually reinforcing components of parallel interaction and both components are found to have superior bonding interaction with the metal fragment. The bonding is clearly stronger compared to the case in which the alkyne occupies the axial position.

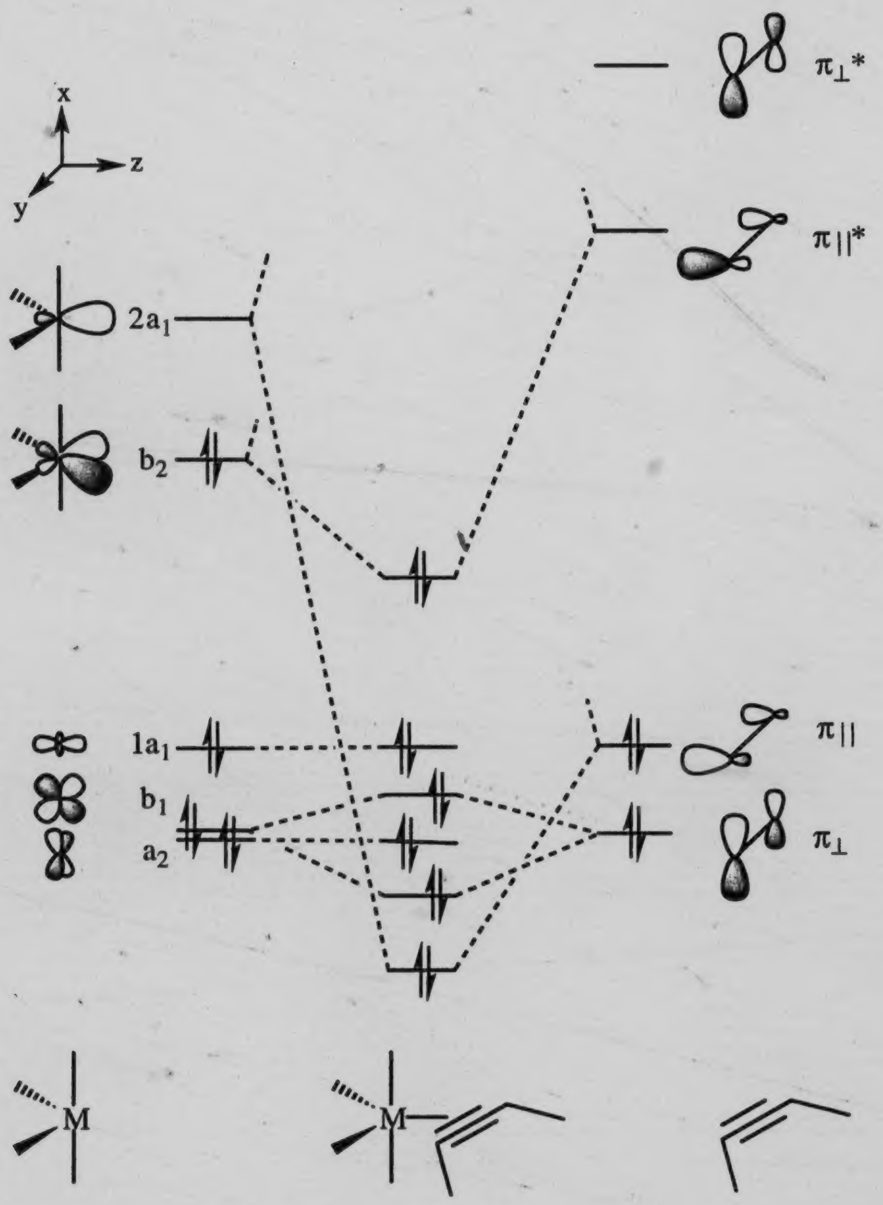
x
z
y
2a$_1$
b$_2$
1a$_1$
b$_1$
a$_2$
π$_\perp$*
π$_{||}$*
π$_{||}$
π$_\perp$
M
M

Scheme 1-9 Interaction Diagram for a C_{2v} M(CO)$_4$ Fragment (*left*) with an In-Plane Orientated Perturbed Alkyne Ligand (*right*).

1.3.3 Substitution Reactions of $M(CO)_4(\eta^2\text{-alkyne})$ (M = Fe, Ru, Os) Complexes

Continuing research in the Takats laboratories with $M(CO)_4(\eta^2\text{-alkyne})$ (M= Fe, Ru, Os) complexes have shown that, despite being 18-electron coordinately saturated species and therefore expected to be kinetically inert, these complexes are remarkably labile toward CO substitution reactions. It has been shown that these complexes undergo facile $^{13}CO/^{12}CO$ exchange and substitution of CO by phosphine ligands [57d, 77b, 87, 88]. Recent kinetic studies show replacement of CO by phosphine ligands (Scheme 1-10) occurs at a much faster rate than that observed with the parent $M(CO)_5$ complexes [57d, 88]. Clearly this facile reactivity is a consequence of some property of the coordinated alkyne ligand. It was concluded that the reaction proceeds by a rate determining CO dissociation step (from **A** to **B** in Scheme 1-10) and that this CO lability is a result of a stabilization of the transition state [57d, 88]. It was proposed that the alkyne stabilizes the 16-electron CO-dissociated intermediate $[M(CO)_3(\eta^2\text{-alkyne})]$ (**B** in Scheme 1-10) by additional π-donation to the vacant coordination site through its filled $\pi_\perp$ orbitals, and in this role the alkyne is effectively acting as a four electron donor ligand [57d, 88]. Reaction with one equivalent of phosphine gives the monosubstituted axial phosphine derivative (**C**) while further reaction with a second equivalent, initiated by a second CO dissociation and through a second intermediate (**D**), gives the disubstituted, diaxial derivative (**E**). Further corroboration of the existence of the four electron donor alkyne ligand was provided when $Fe(CO)_2(PCy_3)(\eta^2\text{-}C_2(CF_3)_2)$ was isolated and its solid state molecular structure determined [89]. This complex shows the archetypical intermediate with four electron donation from the alkyne. Furthermore, a recent theoretical study lends additional support by showing that coordinated acetylene acts a four electron donor (both $\pi_\perp$ and $\pi_{||}$ donate to the metal) in order to stabilize the 16-electron CO dissociation product, $M(CO)_3(\eta^2\text{-}C_2H_2)$ (M = Fe, Ru Os) [90].

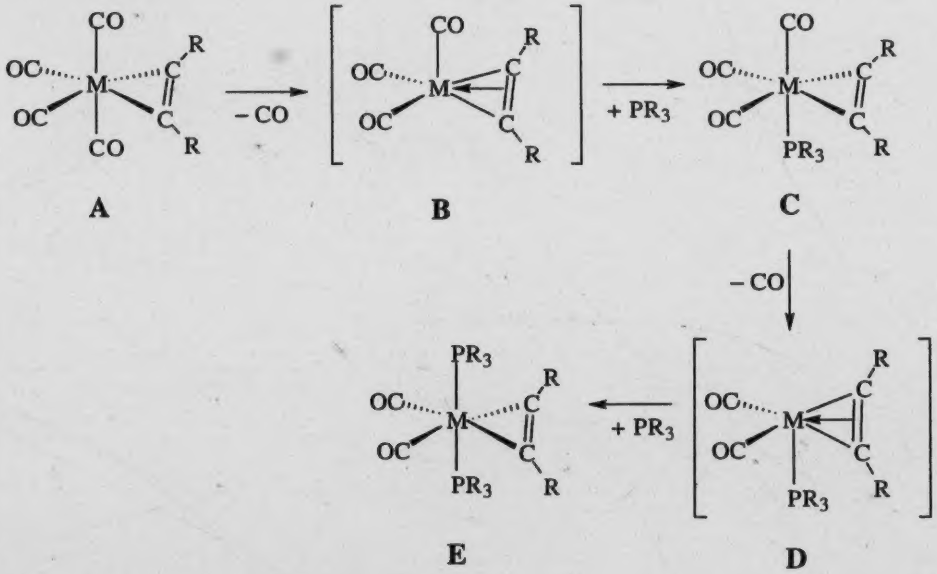

Scheme 1-10 Replacement of Axial Carbonyls with Phosphine Ligands.

1.4 Carbon to Carbon Bond Formation Promoted by Group 8 Carbonyls

It is well known that transition metal complexes promote the formation of carbon to carbon bonds between unsaturated organic molecules, and the group 8 metal carbonyls are no exception [91]. Carbonyl complexes are particularly adept at introducing CO into or removing CO from organic molecules, largely because they act as a readily available source or acceptor of carbon monoxide [92]. Transition metal carbonyls are also known to mediate the coupling of other organic functionalities, most notably olefins and alkynes, and often with inclusion of CO in the product. For example, iron pentacarbonyl can couple two alkyne molecules to produce a cyclobutadiene or a cyclopentadienone ligand from two alkynes and a CO (Eq. 1-3) [93].

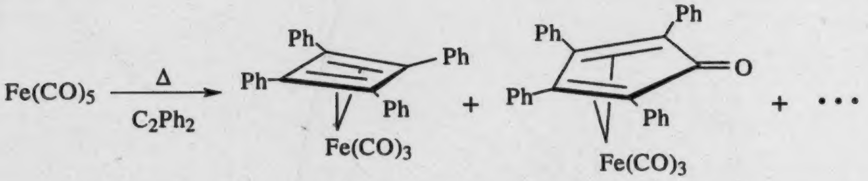

(1-3)

Similarly, the reaction of iron pentacarbonyl with norbornadiene gives cyclobutane and cyclopentanone based derivatives [94]. In addition, coupling of different organic functionalities is also possible. Consider the three component reaction that produces β-methylenecyclopentenones from the iron carbonyl mediated [2+2+1] cycloaddition of alkyne-allene-carbon monoxide (Eq. 1-4) [95]. The reaction may be facilitated by either a $Fe(CO)_5$ or $Fe_2(CO)_9$ metal carbonyl platform.

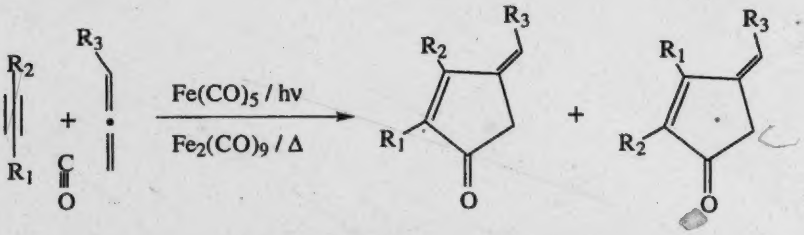

(1-4)

It can be shown that the coupling of organic groups can be easily extended to involve the $M(CO)_4(\eta^2\text{-alkyne})$ (M = Fe, Ru, Os) complexes. In addition to work in the Takats' laboratories with carbonyl substitution chemistry of these complexes, it has been successfully demonstrated that these complexes display a remarkable reactivity toward organic molecules. In particular they are receptive to further alkyne involvement. Washington has shown that $Os(CO)_4(\eta^2\text{-}C_2Me_2)$ mediates a facile three component alkyne-alkyne-CO coupling to produce asymmetrical η^4-cyclopentadienone ligands (Eq. 1-5) [77c]. More recently, Cooke has demonstrated similar reactivity patterns with the iron analogues and, in addition to a cyclopentadienone complex, has observed formation of tropone, and p-quinone iron carbonyl complexes (Eq. 1-6) [78].

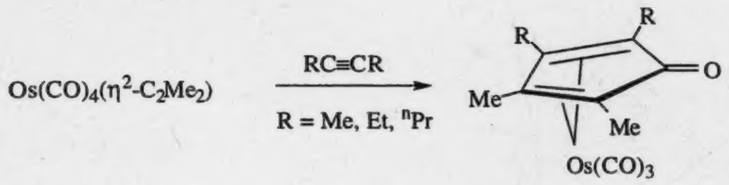
Os(CO)4(η2-C2Me2)
RC≡CR
R = Me, Et, nPr
R
R
O
Me
Me
Os(CO)3

(1-5)

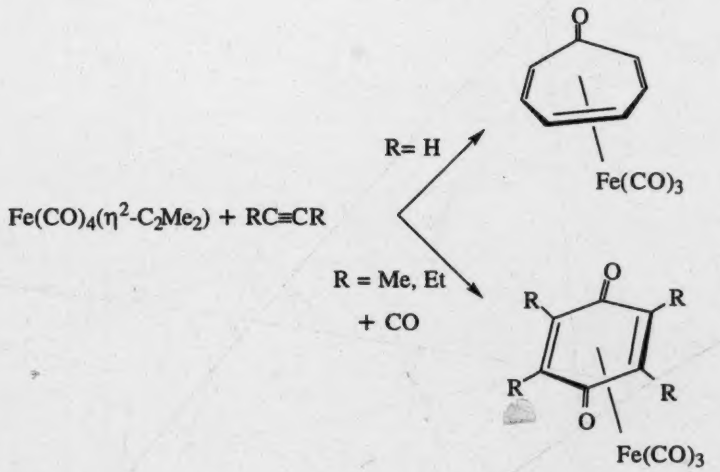
Fe(CO)4(η2-C2Me2) + RC≡CR
R= H
R = Me, Et
+ CO
O
Fe(CO)3
O
R
R
R
R
O
Fe(CO)3

(1-6)

1.5 Scope of the Thesis

From both a fundamental and application perspective the transition metal carbonyls have formed, and, in all probability, will continue to form, much of the backbone of transition metal organometallic chemistry. The bonding model of the M–C≡O linkage provides a paradigm for other types of ligands, while diverse and unpredictable reactivity patterns continue to extend the boundaries of known reactivity. Transition metal carbonyls have proven valuable in the areas of organic synthesis and homogeneous catalysis. All indications are that transition metal carbonyls will continue to aid in the future with continuing research in the areas of homogeneous catalysis, organic synthesis and research in nontraditional areas such as bioorganometallic chemistry and heterogeneous catalysis. As well, the study of non-classical carbonyl complexes looks promising to extend some of the fundamental bonding regimes of the metal carbonyl envelope.

Research in transition metal alkyne carbonyl chemistry is generally thought to have progressed to a mature state as reactions of alkynes with iron carbonyls have been widely studied. However, relatively few studies of simple $M(CO)_4(\eta^2\text{-alkyne})$ (M = Fe, Ru, Os) complexes are known. Their high reactivity towards alkyne-alkyne coupling and CO insertion reactions make these species interesting but difficult to isolate. The development of a convenient and reliable synthesis of the ruthenium and osmium complexes was a breakthrough in this area and allowed the reactivity of these complexes to be explored. The ability of the alkyne to act as a four electron donor to a 16-electron intermediate in these complexes promotes facile CO dissociation and allows fast CO substitution with simple two electron donor ligands, such as phosphines. Studies also examined alkyne-alkyne coupling and CO migration reactions of these complexes. Fortunately, continued efforts finally uncovered a reliable synthetic method for the synthesis of the iron analogues. Subsequently, the reactivity of these species was explored and found to parallel that of the ruthenium and osmium complexes in most respects.

The objective of the present work was to investigate the chemistry of the group 8 metal carbonyl alkyne complexes. More specifically, Chapter 2 is concerned with revisiting and further exploring the reaction of $Fe(CO)_4(\eta^2\text{-HFB})$ with bulky phosphine ligands. We intend to synthesize and characterize a series of $Fe(CO)_2(PR_3)_n(\eta^2\text{-HFB})$ (n = 1, 2) complexes with the purpose of broadening the knowledge base of the two and four electron donating ability of the alkyne ligand within the context of the group 8 carbonyls. In this spirit, it is also desirable to investigate the reactivity of these complexes toward small unsaturated organic molecules; thus, Chapter 3 describes the results of the reactions of $Fe(CO)_2(PR_3)(\eta^2$-HFB) complexes with allenes. Chapter 4 revisits the reactivity of $M(CO)_4(\eta^2$-alkyne) compounds with the reaction of $Fe(CO)_4(\eta^2-C_2H_2)$ with the pseudoalkyne complex $W(\equiv CC_6H_5)(CO)_2(\eta^5-C_5H_5)$. Admittedly, the chemistry of the ruthenium carbonyl alkyne analogues have been ignored in this thesis. However, time has allowed some studies with $Os(CO)_4(\eta^2$-HFB) to be carried out. In keeping with the theme of exploring the facile reactions of the tetracarbonyl alkyne complexes of the group 8 transition metals with simple two electron donor ligands, the osmium analogue has been reacted with cyclohexylisocyanide and *trans*-cyclooctene. Chapter 5 presents the results and discussion of these reactions.

1.6 References

1. (a) Collman, J. P.; Hegedus, L. S.; Norton, J. R.; Finke, R. G. *Principles and Applications of Organotransition Metal Chemistry;* University Science Books: Mill Valley, CA, 1987, pp 110-117. (b) Huheey, J. E.; Keiter, E. A.; Keiter, R. L. *Inorganic Chemistry: Principles of Structure and Reactivity*; 4th ed.; HarperCollins: New York, 1993; pp 630-647. (c) Mingos, D. M. P. In *Comprehensive Organometallic Chemistry*; Wilkinson, G.; Stone, F. G. A.; Abel, E. W., Eds.; Pergamon: New York, 1982; Vol. 3; pp 2-26. (d) Ellis, J. E.; Beck, W. *Angew. Chem. Int. Ed. Engl.* **1995**, *34*, 2489 and references therein.
2. Mond, L.; Langer, C.; Quincke, F. *J. Chem. Soc. (London)* **1890**, *57*, 749.
3. Shriver, D.F.; Whitmire, K.H. In *Comprehensive Organometallic Chemistry*; Wilkinson, G; Stone, F. G. A.; Abel, E. W., Eds.; Pergamon: New York, 1982; Vol. 4; p 249.
4. (a) Mitchell, P. R.; Parish, R. V. *J. Chem. Educ.* **1969**, *46*, 811. (b) Ellis, J. E. *J. Chem. Educ.* **1976**, *53*, 2. (c) Tolman, C. A. *Chem. Soc. Rev.* **1972**, *1*, 337.
5. Huheey, J. E.; Keiter, E. A.; Keiter, R. L. *Inorganic Chemistry: Principles of Structure and Reactivity*; 4th ed.; Harper Collins College: New York, 1993, pp 632-634.
6. Sirigu, A; Bianchi, M.; Benedetti, E. *J. Chem. Soc., Chem. Comm.* **1969**, 596.
7. (a) Eady, C. R.; Johnson, B. F. G.; Lewis, J.; Malatesta, M. C.; Machin, P.; McPartlin, M. *J. Chem. Soc., Chem. Comm.* **1976**, 945. (b) Jackson, P. F.; Johnson, B. F. G.; Lewis, J.; Raithby, P. R.; McPartlin, M.; Nelson, W. J. H.; Rouse, K. D.; Allibon, J.; Mason, S. A. *J. Chem. Soc., Chem. Comm.* **1980**, 295. (c) Eady, C. R.; Jackson, P. F.; Johnson, B. F. G.; Lewis, J.; Malatesta, M. C.; McPartlin, M.; Nelson, W. J. H. *J. Chem. Soc., Dalton. Trans.* **1980**, 383.

8. Tachikawa, M.; Stein, J.; Muetterties, E. L.; Teller, R. G.; Beno, M. A.; Gebert, E.; Williams, J. M. *J. Am. Chem. Soc.* **1980**, *102*, 6648.
9. Gambino, O.; Sappa, E.; Lanfredi, A. M. M.; Tiripicchio, A. *Inorg. Chim. Acta.* **1979**, *36*, 189 and references therein.
10. A number of thematic issues have appeared in the literature in recent years: *Chem. Rev.* **2000**, *100*(8); *Tetrahedron* **2000**, *56*(15), *Polyhedron* **2000**, *19*(5). In addition a recent series of articles on selected topics within this area have appeared: (a) Comely, A. C.; Gibson, S. E.; Sur, S. *J. Chem. Soc., Perkins Trans. 1.* **2000**, 109. (b) Haughton, L.; Willams, J. M. J. *J. Chem. Soc., Perkins Trans. 1.* **1999**, 2645. (c) Comely, A. C.; Gibson, S. E. *J. Chem. Soc., Perkins Trans. 1.* **1999**, 223. (d) Danahoe, T. J.; Harji, R. R.; Moore, P. R.; Waring, M. J. *J. Chem. Soc., Perkins Trans. 1.* **1998**, 819.
11. (a) Davies, S. G. *Organotransition Metal Chemistry: Applications to Organic Synthesis;* Pergamon: Oxford, 1982; pp 1-2. (b) *ibid.* pp 83-93. (c) *ibid.* pp 99-112.
12. Whole books or parts of books have been dedicated to the use of transition metal carbonyls in organic synthesis. A selected list follows: (a) *Organic Synthesis via Metal Carbonyls*; Wender, I.; Pino, P., Eds.; Wiley-Interscience: New York, 1968; Vol. 1 and Vol. 2 (1977). (b) Pearson, A. J. *Iron Compounds in Organic Synthesis*; Academic: San Diego, 1994; Chapter 1. (c) Hegedus, L. S. *Transition Metals in the Synthesis of Complex Organic Molecules*; University Science Books: Mill Valley, CA, 1994; Chapter 5. (d) Collman, J. P.; Hegedus, L. S.; Norton, J. R.; Finke, R. G. *Principles and Applications of Organotransition Metal Chemistry;* University Science Books: Mill Valley, CA, 1987, Chapter 15.
13. (a) Parshall, G. W.; Ittel, S. D. *Homogeneous Catalysis: The Applications and Chemistry of Catalysis by Soluble Transition Metal Complexes*; 2nd ed., Wiley-

Interscience: New York, 1992, Chapter 1. (b) Nakamura, A.; Tsutsui, M. *Principles and Applications of Homogeneous Catalysis*; Wiley-Interscience: New York, 1980, Chapter 1 and 7. (c) Blaser, H. -U.; Indolese, A.; Schnyder, A. *Curr. Sci.* **2000**, *78*, 1336. (d) Bhaduri, S.; Mukesh, D. *Homogeneous Catalysis: Mechanism and Industrial Applications*; Wiley-Interscience: New York, 2000; Chapter 1.

14. Parshall, G. W. *Organometallics* **1987**, *6*, 687.
15. (a) Watkins, K. *Chem & Engng News* **2001**, *79*, 40. (b) Yamamoto, A. *J. Organomet. Chem.* **2000**, *600*, 159. (c) Halpern, J. *Pure Appl. Chem.* **2001**, *73*, 209.
16. (a) Baker, R. T.; Tumas, W. *Science* **1999**, *284*, 1477. (b) Sellin, M. F.; Webb, P. B.; Cole-Hamilton, D. J. *Chem. Comm.* **2001**, 781.
17. (a) Ford, P. C.; Massick, S. *Coord. Chem. Rev.* **2002**, *226*, 39. (b) van der Drift, R. C.; Bouwman, E.; Drent, E. *J. Organomet. Chem.* **2002**, *650*, 1. (c) Grimmer, N. E.; Coville, N. J. *S. Afr. J. Chem.* **2001**, *54*, 1. (d) Clarke, M. L. *Polyhedron* **2001**, *20*, 151. (e) Haji, S.; Erkey, C. *Tetrahedron* **2002**, *58*, 3929. (f) Chaudhari, R. V.; Seayad, A.; Jayasree, S. *Catalysis Today* **2001**, *66*, 371.
18. Herrmann, W. A. *J. Organomet. Chem.* **1990**, *383*, 21.
19. (a) Parshall, G. W.; Ittel, S. D. *Homogeneous Catalysis: The Applications and Chemistry of Catalysis by Soluble Transition Metal Complexes*; 2nd ed., Wiley-Interscience: New York, 1992, pp 106-111. (b) Masters, C. *Homogeneous Transition-Metal Catalysis*; Chapman and Hall: New York, 1981, pp 89-135. (c) Kiss, G. *Chem. Rev.* **2001**, *101*, 3435. (d) Grotjahn, D. B. In *Comprehensive Organometallic Chemistry II*; Hegedus, L. S.; Abel, E. W.; Stone, F. G. A.;

Wilkinson, G.; Eds.; Pergamon: Oxford, 1995; Vol. 12, pp 741-770. (e) Saito, S.; Yamamoto, Y. *Chem. Rev.* **2000**, *100*, 2901.

20. Protzmann, G.; Wiese, K.-D. *Erdoel Kohle Erdgas Petrochemie* **2001**, *117*, 235.

21. (a) Rathke, J. W.; Klinger, R. J. Krause, T. R. *Organometallics* **1991**, *10*, 1350. (b) Knifton, J. F.; Lin, J. J. *J. Mol. Catal.* **1993**, *81*, 27. (c) Sunley, G. J.; Watson, D. J. *Catal. Today* **2000**, *58*, 293. (d) Das, P.; Boruah, M.; Kumari, N.; Sharma, M.; Konwar, D.; Dutta, D. K. *J. Mol. Catal. A Chem.* **2002**, *178*, 283.

22. (a) Vessières, A.; Jaouen, G.; Butler, I. S. *Acc. Chem. Res.* **1993**, *26*, 361. (b) van Staveren, D. R.; Weyhermüller,; Metzler-Nolte, N. *Organometallics* **2000**, *19*, 3730. (c) Metzler-nolte, N. *Angew. Chem. Int. Ed. Engl.* **2001**, *40*, 1040. (d) Salmain, M.; Fischer-Durand, N.; Cavalier, L.; Rudolf, B.; Zakrzewski, J.; Jaouen, G. *Bioconjugate Chem.* **2002**, *13*, 693.

23. (a) Varenne, A. Vessières, A.; Salmain, M.; Durand, S.; Brossier, P.; Jaouen, G. *Anal. Biochem.* **1996**, *242*, 172. (b) Salmain, M.; Vessières, A.; Varenne, A. Brossier, P.; Jaouen, G. *J. Organomet. Chem.* **1999**, *589*, 92.

24. (a) Brown, D. B.; Johnson, B.F.G.; Martin, C. M.; Wheatly, A. E. H. *J. Chem. Soc., Dalton Trans.* **2000**, 2055. (b) Evans, J. *Chem, Soc. Rev.* **1981**, *10*, 159. (c) Brait, S.; Deabate, S.; Knox, S. A. R.; Sappa, E. *J. Cluster Sci.* **2001**, *12*, 139.

25. (a) Muetterties, E. L. *Bull. Soc. Chim. Belg.* **1975**, *84*, 959. (b) *ibid.* **1976**, *85*, 451. (c) Muetteries, E. L.; Rhodin, T. N.; Band, E.; Brucker, C. F.; Pretzer, W. R. *Chem. Rev.* **1979**, *79*, 91. (d) Schaefer, H. F. *Acc. Chem. Res.* **1977**, *10*, 287. (e) Canning, N. D. S.; Madix, R. J. *J. Phys Chem.* **1984**, *88*, 2437. (f) Somorjai, G. A. *Introduction to Surface Chemistry and Catalysis*; Wiley-Interscience: New York, 1994, pp 402-409.

26. (a) Lauher, J. W. *J. Am. Chem. Soc.* **1978**, *100*, 5305. (b) Adams, R. D. In *The Chemistry of Metal Cluster Complexes*; Shriver, D. F., Kaesz, H. D., Adams, R. D., Eds.; VCH, New York, 1990, Chapter 3. (c) Mingos, D. M. P.; May, A. S. In *The Chemistry of Metal Cluster Complexes*; VCH: New York, 1990, pp 21-22.

27. (a) Strauss, S. H. *J. Chem. Soc., Dalton Trans.* **2000**, 1. (b) Willner, H.; Aubke, F. *Angew. Chem. Int. Ed. Engl.* **1997**, *36*, 2403.

28. (a) Pauling, L. *The Nature of the Chemical Bond*; Cornell: Ithaca, 3rd ed., 1960, pp 331-339. (b) Huheey, J. E.; Keiter, E. A.; Keiter, R. L. *Inorganic Chemistry: Princples of Structure and Reactivity*; HarperCollins: New York, 4th ed., 1993, pp 393-394. (c) Elschenbroich, C; Salzer, A. *Organometallics*; VCH: New York, 1989, pp 226-230.

29. Knox, G. R. In *Dictionary of Organometallic Compounds*; Macintyre; J. E.; Hodgson, A. J., Eds.; Chapman and Hall: London, 1995; 2nd ed.; Vol. 2 [Fe] and 3 [Ru, Os].

30. (a) Shriver, D.F.; Whitmire, K.H. In *Comprehensive Organometallic Chemistry*; Wilkinson, G.; Stone, F. G. A.; Abel, E. W., Eds.; Pergamon: New York, 1982; Vol. 4; p 245. (b) Ebenhöch, E. L. In *Ullmann's Encyclopedia of Industrial Chemistry*; Elvers, B.; Kawkins, S.; Ravenscroft, M.; Schulz, G., Eds.; VCH: New York, 5th ed., 1989; Vol. A14, pp 595-597.

31. Hagen, A. P.; Miller, T. S.; Terrell, D. L.; Hutchinson, B.; Hance, R. L. *Inorg. Chem.* **1978**, *17*, 1369.

32. Braga, D.; Grepioni, F.; Orpen, A. G. *Organometallics* **1993**, *12*, 1481.

33. (a) Jesson, J. P.; Meakin, P. *J. Am. Chem. Soc.* **1973**, *95*, 1344. (b) Adams, R. D.; Cotton, F. A. In *Dynamic Nuclear Magnetic Resonance Spectroscopy;* Jackman,

L. M.; Cotton, F. A., Eds.; Academic: New York, 1975; p 491-492. (c) Gansow, O. A.; Burke, A. R.; La Mar, G. N. *J. Chem. Soc., Chem. Comm.* **1972**, 456.

34. (a) Berry, R. S. *J. Chem. Phys.* **1960**, *32*, 933. (b) Muetterties, E. L. *Acc. Chem. Res.* **1970**, *3*, 266. (c) Cotton, F. A.; Wilkinson, G.; Murillo, C. A.; Bochmann, M. *Advanced Inorganic Chemistry*; Wiley-Interscience: New York, 6th ed., 1999; pp 14-16.
35. (a) Rushman, P.; van Buuren, G. N.; Shiralian, M. Pomeroy, R. K. *Organometallics* **1983**, *2*, 693. (b) Piacenti, F.; Bianchi, M.; Frediani, P.; Benedetti, E. *Inorg. Chem.* **1971**, *10*, 2759. (c) Whyman, R. *J. Organomet. Chem.* **1973**, *56*, 339.
36. Johnson, B. F. G.; Lewis, J.; Twigg, M. V. *J. Chem. Soc., Dalton Trans.* **1975**, 1876.
37. Calderazzo, F.; L' Eplattenier, F. *Inorg. Chem.* **1967**, *6*, 1220.
38. Huang, J.; Hedberg, K.; Pomeroy, R. K. *Organometallics* **1988**, *7*, 2049.
39. Grevels, F. -W. (Max-Planck-Institut für Strahlenchemie) and R. Goddard (Max-Planck-Institut für Kohlenforschung, Mülheim an der Ruhr, Germany), unpublished results.
40. (a) Powell, H. M.; Ewens, R. V. G. *J. Chem. Soc.* **1939**, 286. (b) Cotton, F. A.; Troup, J. M. *J. Chem. Soc., Dalton Trans.* **1974**, 800. (c) Cotton, F. A. *Prog. Inorg. Chem.* **1976**, *21*, 1.
41. Braye, E. H.; Hübel, W. *Inorg. Synth.* **1966**, *8*, 178.
42. Pearson, A. J. *Iron Compounds in Organic Synthesis*; Academic: New York, 1994; Chapter 4.
43. Moss, J. R.; Graham, W. A. G. *J. Chem. Soc., Dalton Trans.* **1977**, 95.
44. Bogdan, P.L.; Weitz, E. *J. Am. Chem. Soc.* **1989**, *111*, 3163.

45. Cutforth, H. G.; Selwood, P. W. *J. Am. Chem. Soc.* **1943**, *65*, 2414.

46. McFarlane, W.; Wilkinson, G. *Inorg. Synth.* **1966**, *8*, 181.

47. King, R. B.; Stone, F. G. A *Inorg. Synth.* **1963**, *7*, 193.

48. (a) Wei, C. H.; Dahl, L. F. *J. Am. Chem. Soc.* **1969**, *91*, 1351. (b) Cotton, F. A; Troup, J. M. *J. Am. Chem. Soc.* **1974**, *96*, 4155. (c) Churchill, M. R.; Fettinger, J. C. *Organometallics* **1990**, *9*, 446. (d) Anson, C. E.; Benfield, R. E.; Bott, A. W.; Johnson, B. F. G.; Braga, D. Marseglia, E. A. *J. Chem. Soc., Chem. Comm.* **1988**, 889. (e) Johnson, B. F. G.; Bott, A. *J. Chem. Soc., Dalton Trans.* **1990**, 2437. (f) Braga, D.; Anson, C. E.; Bott, A. Johnson, B. F. G.; Marseglia, E. *J. Chem. Soc., Dalton Trans.* **1990**, 3517. (g) Johnson, B. F. G.; Roberts, Y. V.; Parisini, E. *J. Chem. Soc., Dalton Trans.* **1992**, 2573.

49. Hanson, B. E.; Lisic, E. C.; Petty, J. T.; Iannaconne, G. A. *Inorg. Chem.* **1986**, *25*, 4062.

50. (a) Knight, J.; Mays, M. J. *Chem. Comm.* **1970**, 1006. (b) Gansow, O. A.; Burke, A. R.; Vernon, W. D. *J. Am. Chem. Soc.* **1972**, *94*, 2550. (c) Forster, A.; Johnson, B. F. G.; Lewis, J.; Matheson, T. W.; Robinson, B. H.; Jackson, W. G. *J. Chem. Soc., Chem. Comm.* **1974**, 1042. (d) Cotton, F. A.; Hunter, D. L. *Inorg. Chim. Acta* **1974**, *11*, L9. (e) Aime, S.; Gambino, O.; Milone, L.; Sappa, E.; Rosenberg, E. *Inorg. Chim. Acta* **1975**, *15*, 53. (f) Johnson, B. F. G. *J. Chem. Soc., Chem Comm.* **1976**, 703.

51. Bruce, M. I.; Jensen, C. M.; Jones, N. L. *Inorg. Synth.* **1990**, *28*, 216.

52. Mantovani, A; Cenini, S. *Inorg. Synth.* **1975**, *16*, 47.

53. Drake, S. R.; Loveday, P. A. *Inorg. Synth.* **1990**, *28*, 230.

54. (a) Mason, R.; Rae, A. I. M. *J. Chem. Soc. (A)* **1968**, 778. (b) Churchill, M. R.; Hollander, F. J.; Hutchinson, J. P. *Inorg. Chem.* **1977**, *16*, 2655.

55. Churchill, M. R.; DeBoer, B. G. *Inorg Chem.* **1977**, *16*, 878.

56. Koridze, A. A.; Kizas, O. A.; Astakhova, N. M.; Petrovskii, P.V.; Grishin, Y. K . *J. Chem. Soc., Chem. Comm.* **1981**, 853.

57. (a) Basolo, F. *J. Organomet. Chem.* **1990**, *383*, 579. (b) Huq, R.; Poë, A. J.; Chawla, S. *Inorg. Chim. Acta* **1980**, *38*, 121. (c) Shen, J. -K.; Gao, Y. -C.; Shi, Q. –Z.; Basolo, F. *Inorg. Chem.* **1989**, *28*, 4304. (d) Pearson, J.; Cooke, J.; Takats, J. Jordan, R. B. *J. Am. Chem. Soc.* **1998**, *120*, 1434.

58. (a) Leadbeater, N. *Coord. Chem. Rev.* **1999**, *188*, 35. (b) Ferraud, G. J. *Elements of Inorganic Photochemistry*; Wiley-Interscience: New York, 1988; pp 174-177. (c) Roundhill, D. M. *Photochemistry and Photophysics of Metal Complexes*; Plenum: New York, 1994; Chapter 6. (d) Alway, D. G.; Barnett, K. W. In *Inorganic and Organometallic Photochemistry*; Wrighton, M. S., Ed.; American Chemical Society: Washington, DC, 1978, Chapter 7.

59. (a) Shvo, Y; Hazum, E. *J. Chem. Soc., Chem. Comm.* **1975**, 829. (b) Albers, M. O.; Coville, N. J. *Coord. Chem. Rev.* **1984**, *53*, 2270.

60. Whitmire, K.H. In *Comprehensive Organometallic Chemistry II*; Wilkinson, G.; Stone, F. G. A; Abel, E. W., Eds.; Pergamon: New York, 1995; Vol. 7; pp 35-38.

61. Bruce, M. I. In *Comprehensive Organometallic Chemistry II*; Wilkinson, G.; Stone, F. G. A.; Abel, E. W., Eds.; Pergamon: New York, 1995; Vol. 7; p 294.

62. Adams, R. D.; Selegue, J. P. In *Comprehensive Organometallic Chemistry*; Wilkinson, G.; Stone, F. G. A.; Abel, E. W., Eds.; Pergamon: New York, 1982; Vol. 4, pp 977-978.

63. Rossi, A. R.; Hoffmann, R. *Inorg. Chem.* **1975**, *14*, 365.

64. (a) Martin, L. R.; Einstein, F. W. B.; Pomeroy, R. K. *Inorg. Chem.* **1985**, *24*, 2777. (b) Howell, J. A. S.; Palin, M. G.; McArdle, P.; Cunningham, D.; Goldschmidt, Z.; Gottlieb, H. E.; Hezroni-Langerman, D. *Inorg. Chem.* **1993**, *32*, 3493.

65. (a) Deeming, A. J. In *Comprehensive Organometallic Chemistry*; Wilkinson, G.; Stone, F. G. A.; Abel, E. W., Eds.; Pergamon: New York, 1982; Vol. 4; pp 378-398. (b) Kerber, R. C. In *Comprehensive Organometallic Chemistry II*; Wilkinson, G.; Stone, F. G. A.; Abel, E. W., Eds.; Pergamon: Oxford, 1995; Vol. 7; pp 120-123. (c) Pearson, A. J. *Iron Compounds in Organic Synthesis*; Academic: New York, 1994; Chapter 2.

66. (a) Cosandey, M.; von Büren, M.; Hansen, H. J. *Helv. Chim. Acta* **1983**, *66*, 1. (b) Lei, P.; Vogel, P. *Organometallics* **1986**, *5*, 2500. (c) Schmid, G.; Alraum, F.; Boese, R. *Chem. Ber.* **1991**, *124*, 2255. (d) Thomas, S. E.; Tustin, G. J.; Ibbotson, A. *Tetrahedron* **1992**, *48*, 7629.

67. (a) Fleckner, H.; Grevels, F. -W.; Hess, D. *J. Am. Chem. Soc.* **1984**, *106*. 2027. (b) Angermund, H.; Grevels, F. -W.; Moser, R.; Benn, R.; Krüger, C.; Romano, M. J. *Organometallics* **1988**, *7*, 1994.

68. Wuu, Y. -M.; Bentsen, J. G.; Brinkley, C. G.; Wrighton, M. S. *Inorg. Chem.* **1987**, *26*, 530.

69. Kiel, G. -Y.; Takats, J.; Grevels, F. -W. *J. Am. Chem. Soc.* **1987**, *109*, 2227.

70. (a) Davis, M. I.; Speed, C. S. *J. Organomet. Chem.* **1970**, *21*, 401. (b) Beagley, B.; Schmidling, D. G.; Cruickshank, D. W. J.; *Acta Crystallogr.* **1973**, *B29*, 1499. (c) Enders, D. Schmitz, T; Raabe, G.; Krüger, C. *Acta Cryst. Sect. C* **1991**, *47*, 37. (d) Stainer, M. V.; Takats, J. *Inorg. Chem.* **1982**, *21*, 4044.

71. (a) Kruczynski, L.; LiShingMan, L. K. K.; Takats, J. *J. Am. Chem. Soc.* **1974**, *96*, 4006. (b) Wilson, S. T.; Coville, N. J.; Shapely, J. R.; Osborn, J. A. *J. Am. Chem. Soc.* **1974**, *96*, 4038.

72. Hübel, W, *In Organic Syntheses via Metal Carbonyls*; Wender, I.; Pino, P., Eds.; Interscience: New York, 1968; Vol. 1; pp 273-338.

73. Hoogzand, C.; Hübel, W. *Proc. Intern. Conf. Coordination Chem.* 8th , Vienna, Sept. 1964, p. 258.

74. Pannell, K. H.; Crawford, G. M. *J. Coord. Chem.* **1973**, 2, 251.

75. Carty, A. J.; Smith, W. F.; Taylor, N. J. *J. Organomet. Chem.* **1978**, *146*, C1.

76. Ball, R. G.; Burke, M. R.; Takats, J. *Organometallics* **1987**, *6*, 1918.

77. (a) Gagné, M. R.; Takats, J. *Organometallics* **1988**, *7*, 561. (b) Burn, M. J. Kiel, G -Y. Seils, F.; Takats, J.; Washington, J. *J. Am. Chem. Soc.* **1989**, *111*, 6850. (c) Washington, J.; McDonald, R.; Takats, J.; Menashe, N.; Reshef, D. Shvo, Y. *Organometallics* **1995**, *14*, 3996.

78. Cooke, J.; Takats, J. *J. Am. Chem. Soc.* **1997**, *119*, 11088.

79. (a) Dewar, M. J. S. *Bull. Chem. Soc. Fr.* **1951**, *18*, C79. (b) Chatt, J.; Duncanson, L. A. *J. Chem. Soc.* **1953**, 2939. (c) Dewar, M. J. S.; Ford, G. P. *J. Am. Chem. Soc.* **1979**, *101*, 783.

80. (a) Bombieri. G.; Forsellini, E.; Panattoni, C.; Graziani, R.; Bandoli, G. *J. Chem. Soc A* **1970**, 1313. (b) McGinnety, J. A.; Ibers, J. A.; *Chem. Comm.* **1968**, 235. (c) Love, R. A.; Koetzle, T. F.; Williams, G. J. B.; Andrews, L. C.; Bau, R. *Inorg. Chem.* **1975**, *14*, 2653. (d) Francis, J. N.; McAdam, A; Ibers, J. A. *J. Organomet. Chem.* **1971**, *29*, 131. (e) McAdam, A.; Francis, J. N.; Ibers, J. A. *J. Organomet. Chem.* **1971**, *29*, 149. (f) Ricci, J. S.; Ibers, J. A. *J. Am. Chem. Soc.* **1971**, 2391. (g) Stalick, J. K.; Ibers, J. A. *J. Am. Chem. Soc.* **1970**, 5333. (h) Guggenberger,

L. J.; Cramer, R. *J. Am. Chem. Soc.* **1972**, 3779. (i) Nunzi, F.; Sgamellott; A.; Re, N.; Floriani, C. *J. Chem. Soc., Dalton Trans.* **1999**, 3487. (j) Cedeño, D. L.; Weitz, E.; Bérces, A. *J. Phys. Chem. A* **2001**, *105*, 8077.

81. (a) Tatsumi, K.; Hoffmann, R.; Templeton, J. L. *Inorg. Chem.* **1982**, *21*, 466. (b) Templeton, J. L.; Winston, P. B.; Ward, B. C. *J. Am. Chem. Soc.* **1981**, *103*, 7713. (c) Marinelli, G.; Streib, W. E.; Huffman, J. C.; Caulton, K. G.; Gagné, M. R.; Takats, J.; Dartiguenave, M.; Chardon, C.; Jackson, S. A.; Eisenstein, O. *Polyhedron* **1990**, *9*, 1867. (d) Pidun, U.; Frenking, G. *J. Organomet. Chem.* **1996**, *525*, 269.
82. (a) Birdwhistell, K. R.; Tonker, T. L.; Templeton, J. L. *J. Am. Chem. Soc.* **1987**, *109*, 1401. (b) Caulton, K. G. *New. J. Chem.* **1994**, *18*, 25.
83. Templeton, J. L. *Adv. Organomet. Chem.* **1989**, *29*, 1.
84. (a) Davies, B. D.; Puddephatt, R. J.; Payne, N. C. *Can. J. Chem.* **1972**, *50*, 2276. (b) Kirchner, R. M.; Ibers, J. A. *J. Am. Chem. Soc.* **1973**, *95*, 1095. (c) Davies, B. W.; Payne, N. C. *Inorg. Chem.* **1974**, *13*, 1843.
85. Albright, T. A.; Hoffmann, R.; Thibeault, J. C.; Thorn, D. Z. *J. Am. Chem. Soc.* **1979**, *101*, 3801.
86. Elian, M.; Hoffmann, R. *Inorg. Chem.* **1975**, *14*, 1058.
87. Takats, J. *J. Cluster Sci.* **1992**, *3*, 479.
88. Mao, T.-F.; Zhang, Z.; Washington, J.; Takats, J.; Jordan, R. B. *Organometallics* **1999**, *18*, 2331.
89. Cooke, J. Ph.D. Thesis, University of Alberta. 1998, pp 122-128.
90. Decker, S. A.; Klobukowski, M. *J. Am. Chem. Soc.* **1998**, *120*, 9342.
91. (a) Hegedus, L. S. *Transition Metals in the Synthesis of Complex Organic Molecules*; University Science Books: Mill Valley, CA, 1994, pp 131-135.

(b) Collman, J. P.; Hegedus, L. S.; Norton, J. R.; Finke, R. G. *Principles and Applications of Organotransition Metal Chemistry;* University Science Books: Mill Valley, CA, 1987, pp 739-748. (c) Alper, H. In *New Applications of Organometallic Reagents in Organic Synthesis*; D. Seyferth, Ed.; Elservier Scientific: New York, 1976; pp 305-312.

92. (a) Bates, R. W. In *Comprehensive Organometallic Chemistry II*; G.Wilkinson, F. G. A. Stone, E. W. Abel, Eds.; Pergamon Press: Oxford, 1995; Vol. 12; Chapter 4. (b) Hegedus, L. S. *Transition Metals in the Synthesis of Complex Organic Molecules*; University Science Books: Mill Valley, California, 1994, pp 135-145.
93. Hübel, W. In *Organic Synthesis via Metal Carbonyl;* I. Wender, P. Pino, Eds.; Interscience: New York, 1968; Vol. 1; pp 292-294.
94. (a) Jolly, P. W.; Stone, F. G. A.; Mackenzie, K. *J. Chem. Soc.* **1965**, 6416 and references therein. (b)Weissberger, E.; Laszlo, P. *Acc. Chem. Res.* **1976**, *9*, 209.
95. Aumann, R.; Weidenhaupt, H.-J. *Chem. Ber.* **1987**, *120*, 23.

Chapter 2

Reactions of $Fe(CO)_4(\eta^2\text{-HFB})$ with Bulky Phosphines: Synthesis and Structures of $Fe(CO)_2(PR_2R')_n(\eta^2\text{-HFB})$ (n = 1, 2) Complexes

2.1 Introduction

Studies in the Takats laboratories have shown that $M(CO)_4(\eta^2\text{-alkyne})$ (M = Fe, Ru, Os) undergo facile CO substitution reactions with phosphine ligands [1]. Detailed kinetic studies on $M(CO)_4(\eta^2\text{-HFB})$ (M = Fe, Ru, Os) have established that PR_3 substitution proceeds by a dissociative mechanism [2]. The enhanced CO lability can be attributed to a combination of ground state four electron destabilization (Scheme 2-1), due to filled-filled interaction between metal *d* (d_{xz} in Scheme 2-1) and alkyne $\pi_\perp$ (π donor) orbitals [3], and stabilization of the CO dissociated $[M(CO)_3(\eta^2\text{-alkyne})]$ intermediate by electron donation from the alkyne $\pi_\perp$ orbital, *i.e.* the alkyne acting as a four electron donor (Scheme 2-1). It was argued [2] that the latter effect is dominant for the present complexes and this was confirmed by computational analysis [4]. The rate acceleration for CO substitution compared to the parent $M(CO)_5$ compounds was found to be Ru < Os < Fe, with $Fe(CO)_4(\eta^2\text{-HFB})$ exhibiting a spectacular 1×10^{13} rate increase [2].

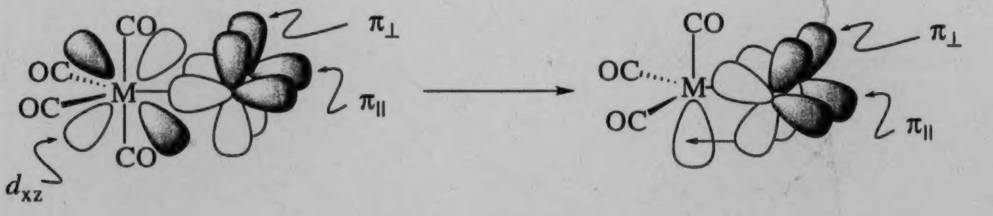

Ground State $M(CO)_4(\eta^2\text{-alkyne})$ $[M(CO)_3(\eta^2\text{-alkyne})]$ Intermediate

Scheme 2-1 η^2-Alkyne as a Two Electron Donor (*left*) or a Four Electron Donor (*right*).

The phosphine substitution reactions proceed in a stepwise fashion but, commonly, the second PR_3 substitution is faster than the first and, although the mono-PR_3 compounds could be detected by NMR spectroscopy, the reactions mostly gave the bis-PR_3 products [1c]. This is illustrated in Eq. 2-1 for the reaction of $Fe(CO)_4(\eta^2$-HFB) with PMe_3 and PPh_3. The reaction with one equivalent of PR_3 gave a mixture of unreacted starting material, small amounts of mono- and large quantities of bis-PR_3 products (PMe_3, bright yellow; PPh_3, bright orange). As shown in the equation the PR_3 ligand occupies the axial position, as expected from the electronic site-preference arguments for σ-donor ligands in five coordinate trigonal bipyramidal molecules [5]. This has been confirmed by X-ray structural work on related $Fe(CO)_2(PR_3)_2(\eta^2$-alkyne) compounds [6].

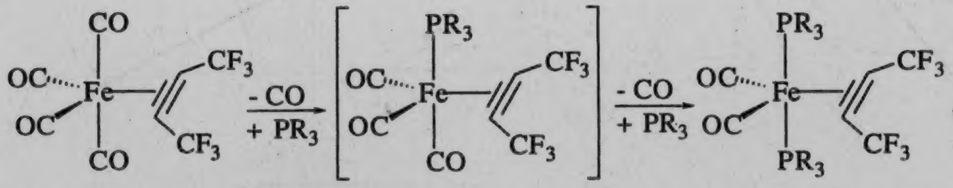

(2-1)

R = Me, Ph

Interestingly, $Fe(CO)_2(PPh_3)_2(\eta^2$-HFB), with the larger PPh_3 ligand (cone angle PPh_3 = 145°, PMe_3 = 118° [7]), underwent reversible PPh_3 dissociation (Eq. 2-2), identified by both IR and $^{31}P\{^1H\}$ NMR spectroscopy [1c]. Similar observations were made by Caulton *et al.* with $Ru(CO)_2(P^tBu_2Me)_2(\eta^2\text{-}C_2Ph_2)$ [8]. Although the phosphine dissociated compound, in this case, could not be detected by IR or ^{31}P NMR spectroscopy, phosphine dissociation could be inferred from line broadening of the ^{31}P NMR signal. Support for the steric origin of PR_3 dissociation comes from the observations that both $Fe(CO)_2(PMe_3)_2(\eta^2$-HFB) [1c] and $Ru(CO)_2(PEt_3)_2(\eta^2\text{-}C_2Ph_2)$ [9], containing smaller PR_3 ligands, are stable toward phosphine dissociation.

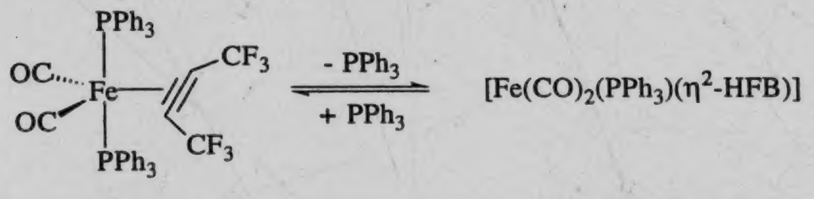

(2-2)

Reaction of $Fe(CO)_4(\eta^2\text{-HFB})$ with the very bulky PCy_3 (cone angle 170° [7]) also produced interesting, indeed surprising and unique, results. Consumption of the starting material still required two equivalents of PCy_3, and led to the isolation of the red-orange, diaxial, bis-PCy_3 substituted derivative, when the reaction solution was kept at low temperatures, Eq. 2-3 [1c]. The structure was corroborated by single crystal X-ray crystallography [1c]. Dissolution of the red-orange material in CH_2Cl_2 at ambient temperature gave an intensely colored purple solution, which reverted to red-orange upon lowering the temperature, clearly indicating reversible PCy_3 dissociation with the equilibrium favoring the dissociated product at the higher temperature, in accord with the larger size of the PCy_3, Eq. 2-4. Unfortunately, attempts to isolate the phosphine dissociated product, presumably with a four electron donor alkyne ligand and a model of the putative intermediate in the CO substitution reactions, proved unsuccessful.

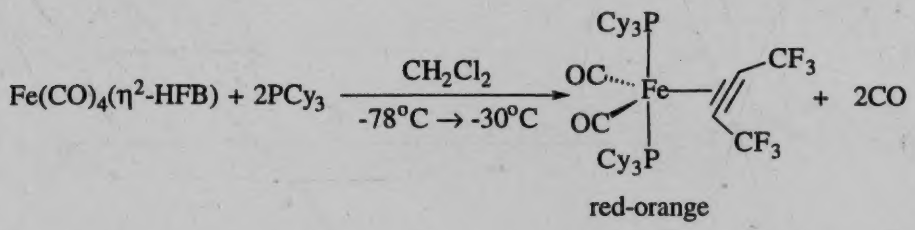

(2-3)

$$\underset{\text{red-orange}}{Fe(CO)_2(PCy_3)_2(\eta^2\text{-HFB})} \rightleftharpoons \underset{\text{purple}}{[Fe(CO)_2(PCy_3)(\eta^2\text{-HFB})]} + PCy_3 \qquad (2\text{-}4)$$

Successful isolation of a compound containing the four electron HFB ligand was finally achieved when it was discovered that reaction of one equivalent of PCy_3, under a

CO atmosphere at low temperature, allowed the conversion of $Fe(CO)_4(\eta^2\text{-HFB})$ to, and isolation of, the thermally sensitive mono-substituted derivative, Eq. 2-5 [1c].

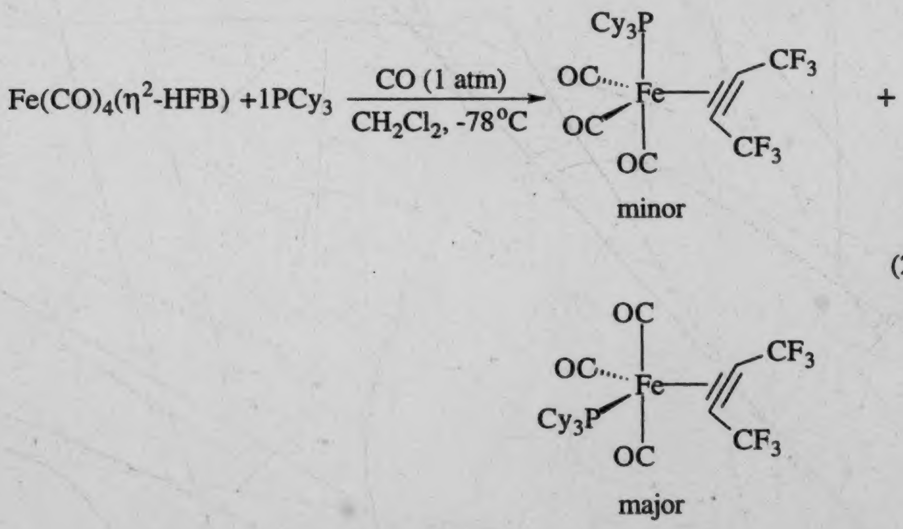

(2-5)

As shown in the equation, the reaction produced an isomeric mixture of two products. The major isomer contains the phosphine ligand in the electronically less but sterically more favored equatorial position, while the minor isomer contains the phosphine ligand in the electronically more but sterically less favored axial position. The fact that the steric size of ligands can also strongly influence the energetics of the five coordinate transition metal complexes is well documented in the chemical literature. An early example is the structures of $Fe(CO)_3(PPh_3)(\eta^2\text{-}CHR{=}CHR)$ ($R = CO_2Et$) complexes [10]. As shown in Figure 2-1, diethyl maleate gives the electronically preferred axial-PPh_3 isomer (olefinic substituents away from PPh_3), but with diethyl fumarate (with olefinic substituents in *trans*-disposition and pointing along the axial sites) the phosphine is forced to occupy the more voluminous equatorial position. Competition between electronic and steric effects was also noted in determining the structure of $Ru(CO)_2(PR_3)_2(PR'_3)$ complexes [9] and the solution behavior of $Fe(CO)_4(PR_3)$ [11] and $M(CO)_4(ER_3)$ (M = Fe, Ru, Os; E = P, As, Sb) [12].

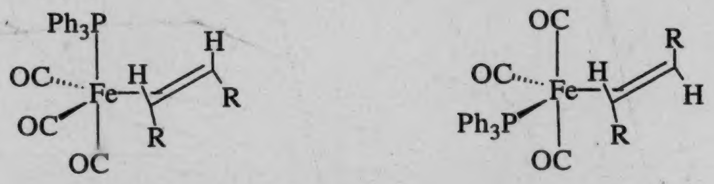

Figure 2-1 Structure of $Fe(CO)_3(PPh_3)(\eta^2$-*cis*-RCH=CHR) (*left*) and $Fe(CO)_3(PPh_3)(\eta^2$-*trans*-RCH=CHR) (*right*) (R = CO_2Et) [10].

Returning to $Fe(CO)_3(PCy_3)(\eta^2$-HFB), warming the cold yellow pentane solution to ambient temperature again resulted in a rapid color change to purple, but in this case, removal of the solvent gave the purple $Fe(CO)_2(PCy_3)(\eta^2$-HFB), Eq. 2-6. The complex was structurally characterized and it was revealed that the alkyne was indeed acting as a four electron donor ligand [1c]. Thus the molecule represents a realistic structural model for the CO dissociated intermediate $[Fe(CO)_3(\eta^2$-HFB)] and corroborates the previous conclusion that the facile CO dissociation is a result of supplemental donation from the $\pi_\perp$ orbital of the alkyne.

$$\underset{\text{yellow}}{Fe(CO)_3(PCy_3)(\eta^2\text{-HFB})} \underset{+\ CO}{\overset{-\ CO}{\rightleftharpoons}} \underset{\text{purple}}{Fe(CO)_2(PCy_3)(\eta^2\text{-HFB})} + CO \qquad (2\text{-}6)$$

In view of these promising early results, it was of interest to revisit the reaction of $Fe(CO)_4(\eta^2$-HFB) with other bulky phosphines in order to determine the range of bulky phosphines capable of forming the bis-ligand complexes, $Fe(CO)_2(PR_3)_2(\eta^2$-HFB), and to expand the series of $Fe(CO)_2(PR_3)(\eta^2$-HFB) compounds, featuring four electron donor alkyne ligands. The results of these studies are described in this chapter.

During the preparation of this thesis a report appeared in the literature which documents the isolation and full characterization, including a solid state molecular structure, of the elusive iron tricarbonyl alkyne complex. The compound in question,

$Fe(CO)_3\{\eta^2\text{-}C_2(NMe_2)_2\}$, is stabilized by the electron rich diaminoalkyne ligand acting as a four electron donor [13]. It appears that the electron poor HFB needs the electron donor PCy_3 ligand to supply the electron density to stabilize $Fe(CO)_2(PCy_3)(\eta^2\text{-}HFB)$.

2.2 Synthetic Aspects and Characterization of $Fe(CO)_2(PR_2R')_n(\eta^2\text{-}HFB)$ (n = 1, 2) Complexes

2.2.1 $Fe(CO)_2(PR_2R')_2(\eta^2\text{-}HFB)$ Complexes (1a-c)

Since previous reactions of $Fe(CO)_4(\eta^2\text{-}HFB)$ with one equivalent of bulky phosphine initially led to a mixture of products, the reaction with two equivalents of phosphine was attempted first.

The reaction of $Fe(CO)_4(\eta^2\text{-}HFB)$, at low temperature, with two equivalents of bulky phosphine resulted in the isolation of red-orange products of the formula $Fe(CO)_2(PR_2R')_2(\eta^2\text{-}HFB)$ (R = ^{t}Bu, R′ = Me, **1a**; R, R′ = ^{i}Pr, **1b**; R, R′ = Cy, **1c**) (Eq. 2-7).

$$Fe(CO)_4(\eta^2\text{-}HFB) + 2PR_2R' \longrightarrow Fe(CO)_2(PR_2R')_2(\eta^2\text{-}HFB) + 2CO \qquad (2\text{-}7)$$

R = ^{t}Bu, R′ = Me; **1a**
R, R′ = ^{i}Pr; **1b**
R, R′ = Cy; **1c**

The progress of the reaction was monitored by IR spectroscopy in the transition metal ν_{CO} region (2200-1600 cm^{-1}). Treatment of a nearly colorless pentane solution of $Fe(CO)_4(\eta^2\text{-}HFB)$ with two equivalents of phosphine at −20 °C resulted in an immediate color change to yellow, which quickly gave way to a dark green solution. Previously, in our laboratories, yellow $Fe(CO)_3(PR_3)(\eta^2\text{-}HFB)$ (R = Me, Ph, Cy) were identified by IR spectroscopy and low temperature NMR spectroscopy [1c]. IR spectroscopy indicated that the yellow solutions contained $Fe(CO)_3(PR_2R')(\eta^2\text{-}HFB)$

complexes as well as unreacted $Fe(CO)_4(\eta^2$-HFB). The IR spectrum of the green solution indicated the presence of these compounds as well as additional strong bands which were consistent with $Fe(CO)_2(PR_2R')(\eta^2$-HFB), as judged by comparison to previous IR spectroscopic characterization of $Fe(CO)_2(PCy_3)(\eta^2$-HFB) [1c]. After 30 minutes at −20 °C the IR spectrum indicated that the reaction had stopped. The green solution was cooled to −50 °C and removal of the solvent, *in vacuo,* resulted in the isolation of an orange solid, very much like the previously obtained $Fe(CO)_2(PR_3)_2(\eta^2$-HFB) (R = PPh_3, PCy_3) complexes [1c]. Upon warming, the orange color of **1a** and **1b** changed to a dark purple, whereas that of **1c** took on a deeper red coloration. Redissolution of the red-orange solids at low temperature produced an orange solution which changed to deep purple in the syringe while a sample was withdrawn for IR analysis. The IR spectrum indicated the presence of only $Fe(CO)_2(PR_2R')(\eta^2$-HFB) compounds, consistent with previous observations [1c]. Crystalline form of the orange solids could be obtained by concentrating a pentane solution of **1a-c** at −20 °C and crystallizing at −80 °C. The crystalline form can be maintained if the material is kept at or below −30 °C.

From the above observations it can be concluded that **1a-c** and $Fe(CO)_2(PR_2R')(\eta^2$-HFB) exist in equilibrium. Low temperatures, −50 °C (PCy_3), and below, −70 °C (P^iPr_3 and P^tBu_2Me), favor the orange bis-phosphine compounds while at higher temperatures, 0 °C to ambient, the solutions contain predominately the purple monophosphine complexes and one equivalent of free phosphine. Within this context the colors of the solutions that were observed during the course of the reaction can be rationalized. As mentioned earlier, the initial yellow color is due to the monophosphine $[Fe(CO)_3(PR_2R')(\eta^2$-HFB)] complexes, as $Fe(CO)_4(\eta^2$-HFB) loses one CO and picks-up a phosphine ligand. The development of the green color is the result of an intermediate mixture of the former complexes and the deep purple $Fe(CO)_2(PR_2R')(\eta^2$-HFB) compounds, these latter compounds being the source of the additional strong bands in the IR spectrum. Removal of the solvent from this green solution at low temperature is accompanied by the removal of liberated CO, while maintaining the second equivalent of phosphine in solution. Removal of CO forces the equilibrium between $Fe(CO)_3(PR_2R')(\eta^2$-HFB) and **1a-c** to favor the latter compounds and restricting the solution to a low temperature forces the equilibrium between **1a-c** and $Fe(CO)_2(PR_2R')(\eta^2$-HFB) to favor the former. It is under these carefully controlled conditions that the best yields of the desired products **1a-c** can be obtained.

Although a previous reaction of $Fe(CO)_4(\eta^2$-HFB) with the very bulky P^tBu_3 reportedly yielded only decomposition products [1c], reinvestigation was deemed necessary. In my hands, reaction with two equivalents of P^tBu_3, after workup, yielded a purple residue and free phosphine. After crystallization, a purple crystalline solid was obtained and was subsequently identified, *vide infra*, as $Fe(CO)_2(P^tBu_3)(\eta^2$-HFB). Since, as judged by Tolman's electronic parameter [7], P^tBu_3 is a better σ donor than P^tBu_2Me or P^iPr_3 but comparable to PCy_3, it is evident that the larger steric bulk of P^tBu_3 relative to P^tBu_2Me, P^iPr_3 and PCy_3 (cone angles 182°, 161° [8a], 160° and 170°, respectively [7]) prevented the coordination of a second equivalent of P^tBu_3 and thus the formation of the bis-substituted complex.

Although **1a-c** can be isolated and are stable enough to be stored for long periods of time at low temperature, the thermally sensitive nature of **1a-c** prevented the use of elemental microanalysis or mass spectrometry for the determination of molecular composition.

As indicated previously, **1a-c** tend to favor the monophosphine derivatives and free phosphine in solution at ambient temperature, thus collection of the room temperature IR solution spectra of the orange-red compounds was not possible. Likewise, in the solid state **1a** and **1b** decompose to give the monophosphine complex and free phosphine ligand. However, a solid state (KBr disc) IR spectrum of **1c** has been obtained and it shows two terminal bands (1973 and 1899 cm^{-1}) in the ν_{CO} region [14]. Furthermore, it was discovered that low temperature solution IR spectra of reasonable quality, given the circumstances, of **1a-c** could be obtained through the use of an improvised low temperature IR cell. A solution IR cell (CaF_2) and a 1 mL glass syringe were cooled by placing them in an ultra low temperature freezer (–80 °C) for two hours. Meanwhile a solution of **1a-b** (pentane) or **1c** (CH_2Cl_2) was prepared and taken to low temperature (–78 °C). The cold solution was quickly transferred to the precooled IR cell and a series of IR spectra were collected as the cell warms. This allowed the recording of a series of low temperature spectra. Unfortunately, frost build-up caused progressive baseline distortion and, of course, the temperature of the IR cell could not be measured with this system, but for the first few minutes, with this crude system, reasonable quality spectra were obtained.

Figure 2-2 displays a stacked representation of four low temperature solution IR spectrum (ν_{CO} region, pentane) of **1a**. The T = 0 (time zero) spectrum was recorded as quickly as possible after loading the IR cell and corresponds to lowest temperature. This spectrum shows four terminal ν_{CO} bands. The remaining three spectra were recorded at consecutive 1.5 minute time intervals and consequently at higher temperatures. As the solution warms, two of the bands, labeled with an asterisk (*), decrease in intensity while the other two bands, labeled with a single dagger (†), increase in intensity. Two bands (2012 and 1951 cm^{-1}), indicated by a single dagger (†) in Figure 2-2, can be identified as belonging to $Fe(CO)_2(P^tBu_2Me)(\eta^2\text{-HFB})$ since they occur at the characteristic frequency of this compound. The remaining two bands at lower frequencies (1978, 1906 cm^{-1}), as expected from the presence of two electron donor phosphine ligands, correspond to **1a**, indicated by an asterisk (*) in Figure 2-2. These observations are consistent with conversion of **1a** to Fe(CO)$_2$(P^{t}Bu$_2$Me)(η^2-HFB) as the solution warms and the equilibrium shifts in favor of the phosphine dissociated product. Eventually, after 10-15 minutes, the bands of **1a** are no longer detected and only the bands of Fe(CO)$_2$(P^{t}Bu$_2$Me)(η^2-HFB) are observed. These data nicely compliment the observation of a yellow solution of **1a-c** at low temperature changing to deep purple color upon warming. Unfortunately, the band associated with the ν_{CC} of the alkyne could not be detected. This is not surprising as the band is typically weak in intensity and **1a-c** have a relatively low solubility in solution at the low temperatures needed to record the IR spectrum. The low temperature FT-IR data for **1a-c** are listed in Table 2-1.

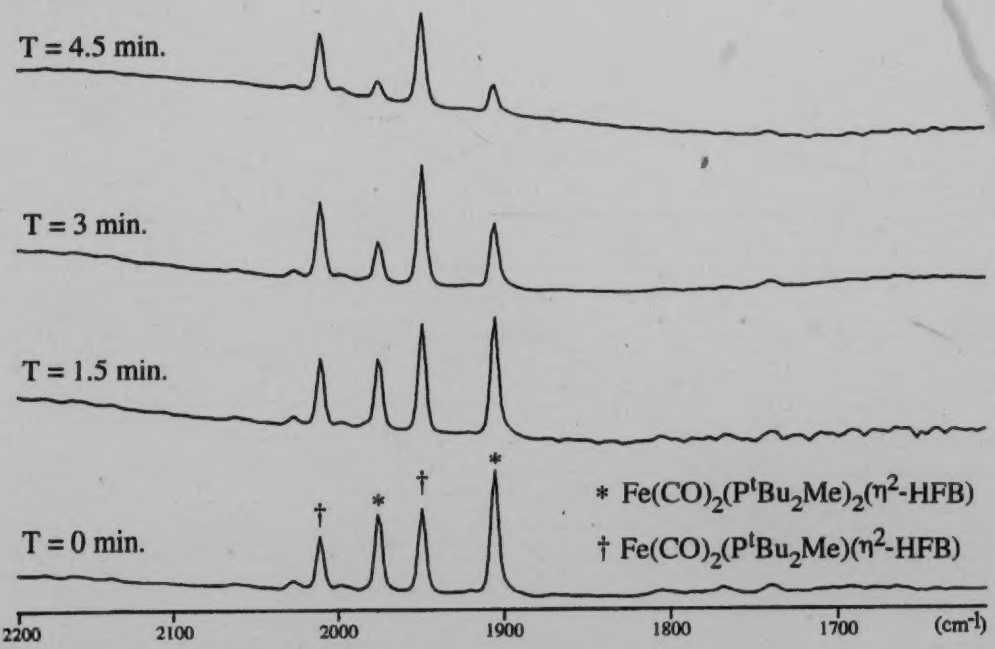

Figure 2-2 Low Temperature FT-IR Spectra (pentane) of Compound **1a.**

Table 2-1 Low Temperature FT-IR Data in the Carbonyl Region, $^{31}P\{^1H\}$, ^{19}F and $^{13}C\{^1H\}$ NMR Data of Compounds **1a-c**.

Compound	$\nu_{CO}{}^{a}$	Average ν_{CO}	$^{31}P\{^1H\}^{b}$	$^{19}F^{b}$	$^{13}C\{^1H\}^{b}$/*$^{13}C\{^{19}F\}^{b}$
1a	1978 (m) 1906 (s)	1942	74.8	–50.2	221.8 s *CO* 124.8 q $^1J_{CF}$ = 269 Hz C*C*F$_3$ 116.8* br s *C*CF$_3$
1b	1978 (m) 1910 (s)	1944	58.9	–47.7	221.2 t $^2J_{CP}$ = 29 Hz, *CO* 125.5 q $^1J_{CF}$ = 271 Hz C*C*F$_3$ 115.4 br s (t* $^2J_{CP}$ = 14 Hz) *C*CF$_3$
1c	1974 (m) 1903 (s)	1939	56.2	–47.8	220.9 t $^2J_{CP}$ = 29 Hz, *CO* 125.4 q $^1J_{CF}$ = 271 Hz C*C*F$_3$ 115.3 br s *C*CF$_3$
P^{t}Bu$_2$Me^{c}	–	–	11.7	–	–
P^{i}Pr$_3{}^{c}$	–	–	21.3	–	–
PCy$_3{}^{c}$	–	–	11.6	–	–
P^{t}Bu$_3{}^{c}$	–	–	62.6	–	–
HFB^{d}	–	–	–	–54.3	112.5 q $^2J_{CF}$ = 261 Hz CF$_3$ 71.4 q $^2J_{CF}$ = 50.3 Hz C$_{alkyne}$

[a] cm^{-1}, **1a**,**b**, pentane; **1c**, CH$_2$Cl$_2$

[b] ppm, CD$_2$Cl$_2$, –90 °C

[c] ^{31}P NMR, CD$_2$Cl$_2$, 27 °C

[d] ^{19}F NMR at 27 °C, ^{13}C NMR at –50 °C, CD$_2$Cl$_2$

Based on previous reports, it is reasonable to assume that compounds **1a-c** have a trigonal bipyramidal geometry and that the η^2-alkyne assumes an equatorial coordination site with an in-plane orientation [1]. The two IR bands of **1a-c** are consistent with a mutually *trans*-diaxial phosphine and *cis*-dicarbonyl arrangement (structure **A** in Figure 2-3). Although the alternative structure (structure **B** in Figure 2–3), with an axial CO and an equatorial phosphine, is also possible, it is not consistent with previous results [1] and has been excluded by NMR spectroscopic considerations, *vide infra*.

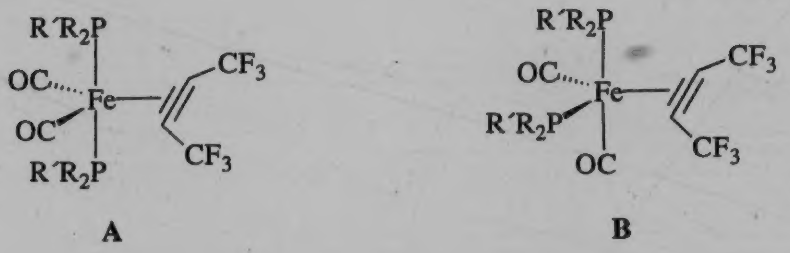

Figure 2-3 Two Possible Structures of $Fe(CO)_2(PR_2R')_2(\eta^2\text{-HFB})$.

There exist a number of NMR active nuclei in **1a-c** and they provide much structural information (Table 2-1). NMR spectra were recorded at low temperature (– 90 °C) in order to force the equilibrium to favor the bis-phosphine complexes. For instance, above these temperatures the ^{31}P signal shows significant broadening as the process of phosphine dissociation and recoordination occurs on a time scale comparable to the NMR experiment. For each **1a-c** the ^1H NMR spectrum showed proton resonances that were consistent with the presence of the respective phosphine ligands. In the spectrum of **1a**, a virtual triplet at δ 0.78 ppm (N = 6 Hz), corresponding to the protons of the PCH_3 group were observed. The triplet is attributed to the virtual coupling phenomenon and is a strong indication of *trans* arrangement of the two phosphine ligands [15]; virtual coupling has been observed in related *trans*–Fe(CO)$_2${PR$_3$/P(OR)$_3$}$_2$(η^2-alkyne) complexes [6b,c, 16]. The ^{31}P{^{1}H} NMR spectrum of each compound showed one resonance that was significantly shifted downfield from the position of the free phosphine ligands. With two phosphine ligands coordinated to the metal, this single signal indicates chemical equivalence and on this basis, and assuming a rigid structure, arrangement **B** in Figure 2-3 can be excluded. The ^{19}F NMR spectrum indicates a structure with additional symmetry as only one resonance is observed for the two CF$_3$ groups of the η^2-HFB ligand. Clearly the spectroscopic data strongly support structure **A** in Figure 2-3.

For each compound, ^{13}C NMR spectra were obtained. One spectrum was recorded with proton decoupled (^{13}C{^{1}H}) and a second spectrum was obtained with flourine-19 decoupling (^{13}C{^{19}F}). Signals in the upfield region could easily be assigned to the alkyl substituents of phosphine ligands. An example of the downfield region of the ^{13}C{^{1}H} NMR spectrum is presented in Figure 2-4. The ^{13}C{^{1}H} NMR spectrum further corroborates the choice of structure **A** with C_{2v} symmetry as it shows chemical equivalence of the two CO groups and the two CCF$_3$ groups, the former is a triplet due to coupling to the chemically equivalent *trans*-phosphine ligands. Assignment of the carbonyl signal is based on the characteristic downfield chemical shift (δ ~220 ppm) [17]. The observed $^2J_{CP}$ in **1b** (29 Hz) and **1c** (29 Hz) lie in the range (27 - 40 Hz) found for the corresponding coupling in similar complexes [6b,c, 16]. The spectrum also shows a binomial quartet at δ 124.8 – 125.5 ppm with typically large $^1J_{CF}$ (269 - 271 Hz), due to *C*F$_3$ carbons. The ^{13}C NMR (CD$_2$Cl$_2$) spectrum of the free HFB shows the *C*F$_3$ carbon resonance as a binomial quartet at δ 112.5 ppm with a $^1J_{CF}$ of 261 Hz. The remaining resonance at δ 115 - 117 ppm is then assigned to the ligating carbons of the alkyne (C$_{alkyne}$). For comparison the *C*CF$_3$ carbons of the free alkyne are observed at δ 71.4 ppm ($^2J_{CF}$ = 50 Hz). The broadness of this signal in **1a-c** can be explained on the basis of comparable coupling to three equivalent fluorine and two equivalent phosphorus nuclei creating a multiplet which is not resolved. Due to poor signal to noise, this signal was not observed in the $^{13}C\{^1H\}$ NMR spectrum of **1a**. Upon conducting $^{13}C\{^{19}F\}$ experiments the broad CCF_3 signal sharpens somewhat to give a slightly broad singlet in **1a** and **1c**, however, for **1b** the expected binomial triplet ($^2J_{CP}$ = 14 Hz) can be clearly observed.

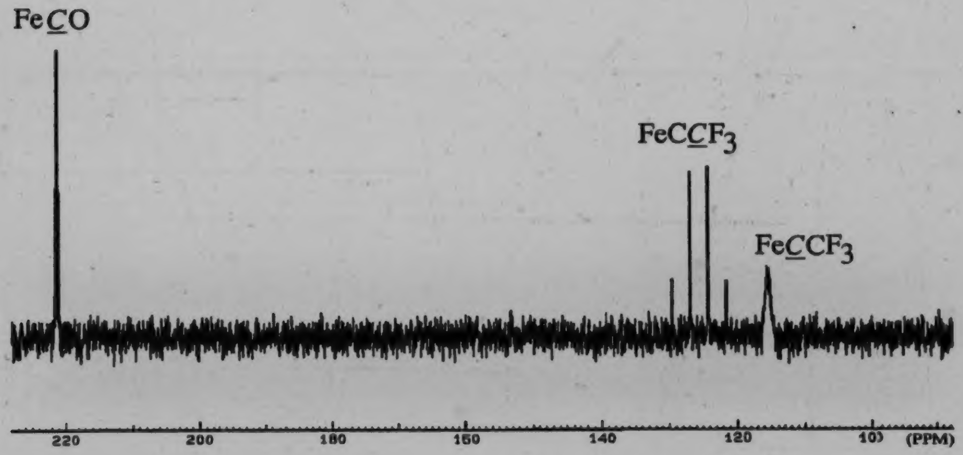

Figure 2-4 The $^{13}C\{^1H\}$ NMR Spectrum (CD_2Cl_2, –70 °C) of **1b**; 100-225 ppm Region.

The ^{13}C NMR chemical shift of the ligating carbons of the alkyne (C_{alkyne}) in **1a-c** are within the range observed for the corresponding parameter in $Fe(CO)_4(\eta^2$-alkyne) [1c] and *trans*-$Fe(CO)_2\{PR_3/P(OR)_3\}_2(\eta^2$-alkyne) [1, 6a,b, 16a] complexes in which the alkyne acts as a two electron donor ligand. The range is broad (C_{alkyne} δ = 48.9 - 117.2 ppm), with the $Fe(CO)_2\{PR_3/P(OR)_3\}_2(\eta^2$-alkyne) compounds at the upper end of this range at δ 77.6 - 117.2 ppm. Coordination of an alkyne to a metal results in a rehybridization of the C_{alkyne} toward sp^2 and, with the more olefinic character of the C_{alkyne}, a shift to higher frequency is expected [18, 19]. This is typically observed with electron withdrawing alkynes, like HFB, although electron rich alkynes often display an upfield coordination shift [1c]. The latter is the reason for some of the unusually high field C_{alkyne} chemical shifts in some of the $Fe(CO)_4(\eta^2$-alkyne) compounds [1c]. The C_{alkyne} chemical shifts in **1a-c** are best compared to the parent $Fe(CO)_4(\eta^2$-HFB) molecule. The progression, free HFB (δ C_{alkyne} = 71.4 ppm), $Fe(CO)_4(\eta^2$-HFB) (δ C_{alkyne} = 88.5 ppm) and **1a-c** (average δ C_{alkyne} = 115.8 ppm) follows the expected trend. The δ 27.3 ppm downfield shift in **1a-c** compared to $Fe(CO)_4(\eta^2$-HFB) provides good empirical evidence of the increased electron richness of iron and hence greatly enhances the $d \rightarrow \pi^*$ back-donation in the former compounds.

2.2.2 $Fe(CO)_2(PR_2R')(\eta^2$-HFB) Complexes (2a-d)

In view of the observations of Cooke [1c] and Washington [1a] with **1c** and the facile phosphine dissociation equilibrium observed with **1a/1b**, the isolation of the coordinatively unsaturated derivatives looked promising. The original procedure called for treating $Fe(CO)_4(\eta^2$-HFB) with one equivalent of PCy_3 under a CO atmosphere followed by solvent removal at room temperature, but this procedure proved to be somewhat unreliable. We discovered that the CO atmosphere was not necessary and that conducting the reaction and workup at low temperature gave the desired compounds in good yield. Thus, the reaction of $Fe(CO)_4(\eta^2$-HFB) with one equivalent of bulky phosphine yields deep purple-blue products of the formula $Fe(CO)_2(PR_2R')(\eta^2$-HFB) (R = ^{t}Bu, R′ = Me, **2a**; R, R′ = ^{i}Pr, **2b**; R, R′ = Cy, **2c**; R, R′ = ^{t}Bu, **2d**) Eq. 2-8.

$$\mathrm{Fe(CO)_4(\eta^2\text{-HFB}) + PR_2R'} \xrightarrow[\text{2) workup at } 0\ ^{\circ}\text{C}]{\text{1) pentane, } -20\ ^{\circ}\text{C to } 0\ ^{\circ}\text{C}} \mathrm{Fe(CO)_2(PR_2R')(\eta^2\text{-HFB}) + 2CO}$$

R = ^{t}Bu, R′ = Me; **2a**
R, R′ = ^{i}Pr; **2b**
R, R′ = Cy; **2c** (2-8)
R, R′ = ^{t}Bu; **2d**

Treatment of a near colorless pentane solution of $Fe(CO)_4(\eta^2$-HFB) with one equivalent of P^tBu_2Me, P^iPr_3, or PCy_3, at −20 °C resulted in an immediate color change to yellow, due to formation of $Fe(CO)_3(PR_2R')(\eta^2$-HFB), which quickly gave way to dark green, as a result of the presence of a mixture of $Fe(CO)_3(PR_2R')(\eta^2$-HFB) and **2a-c** as determined by IR spectroscopy. After 30 minutes at −20 °C the IR spectrum indicated that the reaction had stopped but had not yet reached completion. Upon warming to 0 °C, the solution color quickly changed to deep purple. The solvent and volatiles were removed, *in vacuo,* at 0 °C to produce a deep purple residue. Redissolution of the purple residue in pentane and subsequent removal of solvent, *in vacuo,* at 0 °C, and repeating the procedure, ensured complete conversion of $Fe(CO)_3(PR_2R')(\eta^2$-HFB) to **2a-c**. This low temperature synthetic procedure minimizes the production of, at least, three decomposition products, one of which was unambiguously identified by single crystal structure analysis as $[Fe(PCy_3)(CO)_2\{\mu$-$\eta^1,\eta^1:\eta^4$-$C_4(CF_3)_4\}Fe(CO)_3]$. The final purple residue was then dissolved in a minimum amount of pentane at 0 °C and crystallized at −78 °C to give deep purple crystals. However, upon warming **2b** melted between −10 °C and 0 °C to give a deep purple viscous liquid.

Contrary to previous observations [1c], the reaction with P^tBu_3 did not result in complete decomposition of the $Fe(CO)_4(\eta^2$-HFB) but rather upon addition of one equivalent of P^tBu_3 to a pentane solution of $Fe(CO)_4(\eta^2$-HFB) at −20 °C there was an immediate color change from colorless to deep blue with, notably, no indication of the intermediate yellow or green coloration. Subsequent workup produced deep blue crystalline **2d**.

All compounds are moderately air and temperature stable as they can be handled under ambient conditions for short periods of time. In the solid state, **2c** and **2d** are stable for days under inert atmosphere at ambient temperature, while **2a** and, especially liquid **2b**, are somewhat less robust and begin to show decomposition after 12 hours.

The elemental microanalysis (%C, %H) results are consistent with the proposed formulation of **2a,c,d**. However, several attempts to obtain the elemental analysis of **2b** failed to produce consistent results. Nevertheless, a high resolution mass spectrum of **2b** was obtained. The results show a weak but distinct molecular ion signal (*m/z* = 434) that is consistent with the proposed formulation. In addition to the molecular ion peak, two fragment ions corresponding to M^{+}–nCO (n = 1, 2) were observed, each showing excellent agreement with the calculated isotope pattern for **2b**.

The FT-IR spectra of **2a-d** each showed two strong terminal ν_{CO} stretching bands in the range 1943-2012 cm^{-1} (Table 2-2). In terms of structure this pattern is indicative of a *cis*-dicarbonyl arrangement. A comparison of the average frequencies of **2a-c** with that of **1a-c** shows a 37 - 39 cm^{-1} shift to higher frequency and implies that the relative amount of electron density at the metal center in **2a-c** has decreased. This is consistent with the loss of a good donor phosphine ligand.

In addition to the ν_{CO} bands, a weak band in the range 1730-1740 cm^{-1}, assigned to ν_{CC} of the alkyne, was observed. In the IR spectra of the $Fe(CO)_4(\eta^2$-alkyne) complexes Cooke has also observed bands in the range 1700-1890 cm^{-1} and has shown, through ^{13}CO labeling studies, that indeed these signals belong to the ν_{CC} stretching vibration of the alkyne ligand [1c]. Typically, coordinated alkynes show a ν_{CC} band in the range 1700-2000 cm^{-1} [20]. This shift to lower frequencies from around 2200 cm^{-1} (IR or Raman) for the free alkyne is indicative of a decrease in the C≡C bond order. The ν_{CC} of the free HFB is found at 2300 cm^{-1} [21]. The decrease in the ν_{CC} frequency is consistent with a considerable weakening of the C≡C bond strength in **2a-d**. It would be interesting to compare the ν_{CC} frequencies of **2a-c** with the corresponding frequencies given by **1a-c** in which the alkyne acts as a two electron donor.

Table 2-2 FT-IR Data in the Carbonyl Region, $^{31}P\{^1H\}$, ^{19}F, ^1H and $^{13}C\{^1H\}$ NMR Data of Compounds **2a**-**d**.

Compound	$\nu_{CO}{}^a$ (average)	$\nu_{CC}{}^a$	$\Delta(\nu_{CC})^b$	$^{31}P\{^1H\}^c$	$^{19}F^c$	$^{13}C\{^1H\}^c$
2a	2012 (s)	1740	560	115.4	–56.7	217.1 s *C*O
	1951 (s)					170.9 q $^2J_{CF}$ = 48 Hz, *C*CF$_3$
	(1981)					124.3 q $^1J_{CF}$ = 270 Hz, C*C*F$_3$
2b	2011 (s)	1735	565	127.2	–56.3	216.9 d $^2J_{CP}$ = 29 Hz, *C*O
	1951 (s)					172.2 q $^2J_{CF}$ = 46 Hz, *C*CF$_3$
	(1981)					124.3 q $^1J_{CF}$ = 270 Hz, C*C*F$_3$
2c	2009 (s)	1734	566	116.9	–56.4	216.7 d $^2J_{CP}$ = 28 Hz, *C*O
	1947 (s)					171.1 q $^2J_{CF}$ = 43 Hz, *C*CF$_3$
	(1978)					123.8 q $^1J_{CF}$ = 270 Hz, C*C*F$_3$
2d	2005 (s)	1730	570	148.2	–56.2	218.5 d $^2J_{CP}$ = 26 Hz, *C*O
	1943 (s)					170.4 q $^2J_{CF}$ = 42 Hz, *C*CF$_3$
	(1974)					124.7 q $^1J_{CF}$ = 271 Hz, C*C*F$_3$

[a] cm^{-1}, pentane

[b] cm^{-1}, $\Delta(\nu_{CC}) = \nu_{CC}(\text{free HFB}) - \nu_{CC}(\text{complexed HFB})$, $\nu_{CC}(\text{free HFB}) = 2300\ cm^{-1}$ [20]

[c] ppm, CD_2Cl_2, 25 °C

Unfortunately, the ν_{CC} signals in **1a-c** were too weak to be observed. However, by placing hydrocarbon solutions of **2a-c** under a CO atmosphere (~1 atm) at low temperature (–78 °C) and quickly measuring the IR spectrum, it was possible to obtain the frequencies of both the ν_{CO} and ν_{CC} stretches of the corresponding tricarbonyl species $Fe(CO)_3(PR_2R')(\eta^2\text{-HFB})$ (R = ^{t}Bu, R′ = Me, **3a**; R, R′ = ^{i}Pr, **3b**; R, R′ = Cy, **3c**). (Table 2-3). Interestingly, the P^tBu_3 analogue, $Fe(CO)_3(P^tBu_3)(\eta^2\text{-HFB})$, did not form. Apparently, the large bulk of the phosphine ligand prevents the formation of the tricarbonyl species, much the same as the bis-phosphine complex $Fe(CO)_2(P^tBu_3)_2(\eta^2\text{-HFB})$. Comparing the ν_{CC} frequencies of **3a-c**, in which the alkyne acts as a two electron donor, with those of **2a-c**, it is seen that the band has shifted some 100 cm^{-1} to lower frequency. This frequency shift indicates a lower bond order in **2a-c** than in **3a-c** and is consistent with stronger metal-alkyne interaction. However what is not so clear is the form of this interaction. There may exist increased alkyne to metal donation or metal to alkyne back-donation, or a combination thereof.

Templeton has noted an empirical correlation between the IR frequencies of ν_{CC} stretches and their formal electron donation to the metal in two electron and four electron donor alkyne Mo(II) and W(II) complexes [19]. Of course, inconsistencies exist in the correlation when complexes contain different alkynes or ancillary ligands. However, for closely related complexes the data correlates reasonably well with the formal electron donation from the alkyne. For example, the frequency of the ν_{CC} stretch of the coordinated DMAD ($MeO_2CC{\equiv}CCO_2Me$) ligand is observed as a function of the formal electron donation from the $\pi_\perp$ orbital. A two electron donor DMAD shows a ν_{CC} band in the IR spectrum at 1895 cm^{-1}, while a four electron donor DMAD absorbs at a much lower frequency, 1730 cm^{-1}.

Table 2-3 FT-IR Data in the Carbonyl Region of Compounds **3a-c**.

Compound[a]	ν_{CO}[b]	ν_{CC}[b]	$\Delta(\nu_{CC})$[c]
3a	2064 (m) 2000 (s) 1987 (m) 1974 (m)	1841 (w)	459
3b	2068 (m) 2004 (s) 1987 (m) 1976 (m)	1840 (w)	460
3c	2063 (m) 1995 (s) 1987 (m) 1973 (m)	1840 (w)	460

[a] Solution contains two isomers of **3a-c**; PR_3 (axial) and PR_3 (equatorial), see Eq.2-5.
[b] cm^{-1}, pentane
[c] cm^{-1}, $\Delta(\nu_{CC}) = \nu_{CC}(\text{free}) - \nu_{CC}(\text{complex})$, $\nu_{CC}(\text{free HFB}) = 2300\ cm^{-1}$ [20]

It has been suggested that for a proper comparison of IR or NMR parameters between compounds the coordination shift (Δ) is the parameter of choice [22]. Comparison of $\Delta(\nu_{CC})$ of **2a-c** and **3a-c** shows a ~100 cm^{-1} smaller value associated with **2a-c**, a result which parallels the direct comparison above, and thus the conclusion is the same; the bond order of the C≡C in **2a-c** is substantially reduced relative to that observed in **3a-c**. Having established this, one cannot definitively conclude from the IR data that the alkyne in **2a-c** is acting as a four electron donor ligand but these observations are consistent with additional, *i.e.* beyond $\pi_{||}$ donation, metal-alkyne interaction.

Several NMR active nuclei are present in **2a-d** and can provide information germane to both the structure and nature of the metal-alkyne interaction. Each ^1H NMR spectra showed signals in the aliphatic region that are consistent with the presence of a phosphine ligand. Table 2-2 shows selected NMR data of **2a-d**. The $^{31}P\{^1H\}$ NMR spectrum of each spectrum showed a single resonance with a chemical shift that is considerably downfield of the free phosphine ligand and shifted somewhat downfield of the ^{31}P resonances observed in **1a-c**. Both the ^{19}F and ^{13}C NMR spectra indicated a structure with chemically equivalent CCF_3 and carbonyl groups as only one resonance was observed for each group. Variable temperature ^{19}F NMR studies, in the temperature range +27 °C to −90 °C, did not detect stereochemical nonrigidity. The assignment of the ligating carbon atoms of the alkyne, *C*CF$_3$, to the δ 170-172 ppm resonance is based on the smaller $^2J_{CF}$ coupling relative to the large $^1J_{CF}$ observed of the signals located at δ 124-125 ppm. The carbon-fluorine coupling was confirmed by $^{13}C\{^{19}F\}$ experiments. Interestingly, coupling of the alkyne carbons to the phosphorus nuclei was not observed. The resonance associated with the ligating carbons of the alkyne in **2a-d** show a striking downfield shift when compared to the corresponding signals in **1a-c**, in which the alkyne acts as a two electron donor. A good illustration of this downfield shift is shown in Figure 2-5 in which the low field region of the $^{13}C\{^1H\}$ NMR spectra (CD_2Cl_2, −70 °C) of **1b** and **2b** are shown. Templeton has noticed a dramatic downfield chemical shift of the ligating carbons of η^2-alkyne ligands in Mo(II) and W(II) complexes when the alkyne was acting as a four electron donor (δ 170 - 230 ppm) compared to being a two electron donor alkyne (δ 95 - 130 ppm) [19]. Clearly the characteristic chemical shift in **2a-d** strongly suggests a four electron donor bonding mode for the alkynes in these complexes if this empirical correlation established with the Mo(II) and W(II) compounds can be extended to the iron compounds.

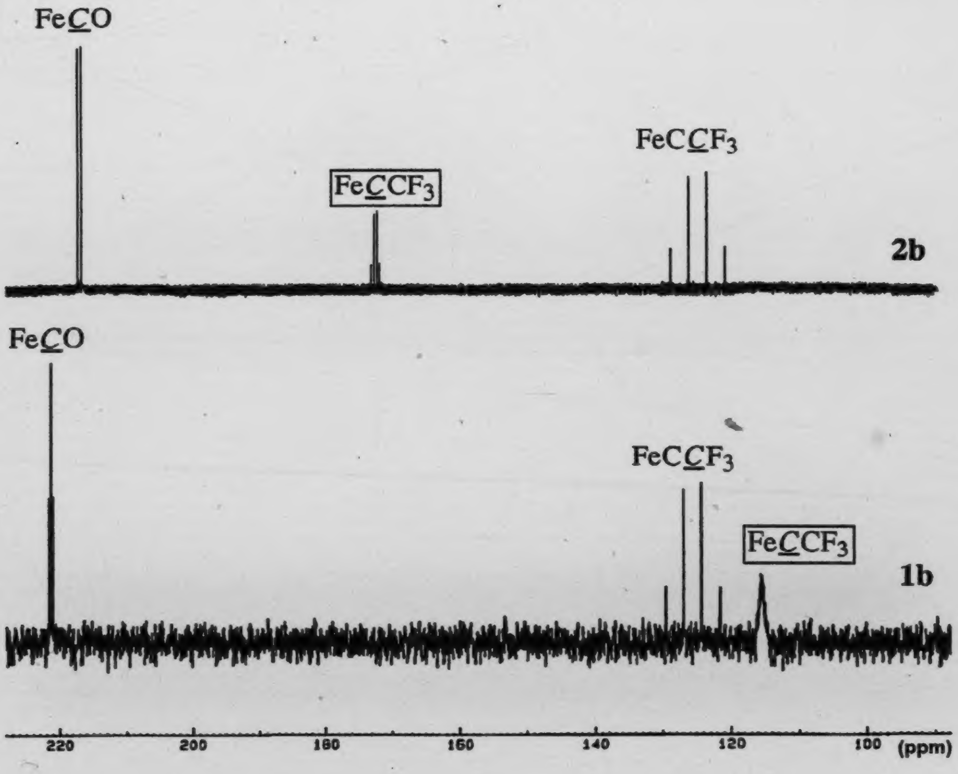

Figure 2-5 The $^{13}C\{^1H\}$ NMR Spectra (CD_2Cl_2, – 70 °C) of **1b** and **2b**; 100-225 ppm Region.

Surprisingly, there are only two reports of a four electron donor alkyne complexes of iron in which the report quotes ^{13}C NMR data, $Fe\{(PMe_2CH_2)_3SiMe\}(C_2RR')$ (R, R′ = Ph; R = Me, R′ = Et; R, R′ = Et; R, R′ = $SiMe_3$) [23] and the very recently reported $Fe(CO)_3\{\eta^2\text{-}C_2(NMe_2)_2\}$ [13]. The ^{13}C NMR chemical shift of the ligating carbons of the alkynes in these compounds are observed in the range δ 181 - 204 ppm. Unfortunately, no comparison to analogous two electron donor alkyne complexes of this type can be made since none are reported. However a comparison of the ^{13}C NMR chemical shift of the Fe-C_{alkyne} carbons in the above complexes and **2a-d** to the range of δ 85-117 ppm, indicated for the related parameter in two electron donor alkyne iron complexes **1a-c** and the related *trans*–$Fe(CO)_2\{PR_3/(OR)_3\}_2(\eta^2\text{-alkyne})$ [6a,b, 16a] mentioned earlier, clearly shows that there is a considerable chemical shift difference. The compounds with, presumably, a four electron donor alkyne show a chemical shift of 50-60 ppm downfield of that in the two electron donor complexes. It appears that indeed the chemical shift of the ligating carbons of an alkyne ligand in iron complexes can be an indicator of four electron donation in much the same manner as that shown in Mo(II) and W (II) complexes [19].

While the evidence for four electron donation from the alkyne in **2a-d** appears convincing, based on the ν_{CC} and ^{13}C NMR data, additional information from solid state analysis is desirable since comparison to precedent making examples from the chemical literature are severely limited; very few four electron donor alkyne group 8 complexes are reported in the chemical literature. Furthermore, given the formulation of **2a-d** the question of coordination saturation arises. Are these compounds coordinatively saturated or stable 16-electron species? If they obey the 18-electron rule, how then is electronic saturation achieved? Determination of the structure of **2a-d** is key to answering these questions.

2.3 Molecular Structures of $Fe(CO)_2(PR_2R')_n(\eta^2\text{-HFB})$ (n = 1, 2) Complexes

2.3.1 $Fe(CO)_2(PR_2R')_2(\eta^2\text{-HFB})$ Complexes (1a-c)

Single crystal X-ray structure analyses were conducted on **1a,b** and the X-ray structure analysis of **1c** [14] has been previously completed in our laboratories. The structures are, in general, similar but some differences are notable, in particular between **1a** and **1b** or **1c**. For comparison purposes the molecular structures of **1a** and **1b** are shown in Figure 2-6. As we will shortly see, the structures of **1b** and **1c** are much more similar and **1b** serves well as a representative of this subgroup. Selected interatomic distances and angles for **1a-c** are presented in Table 2-4.

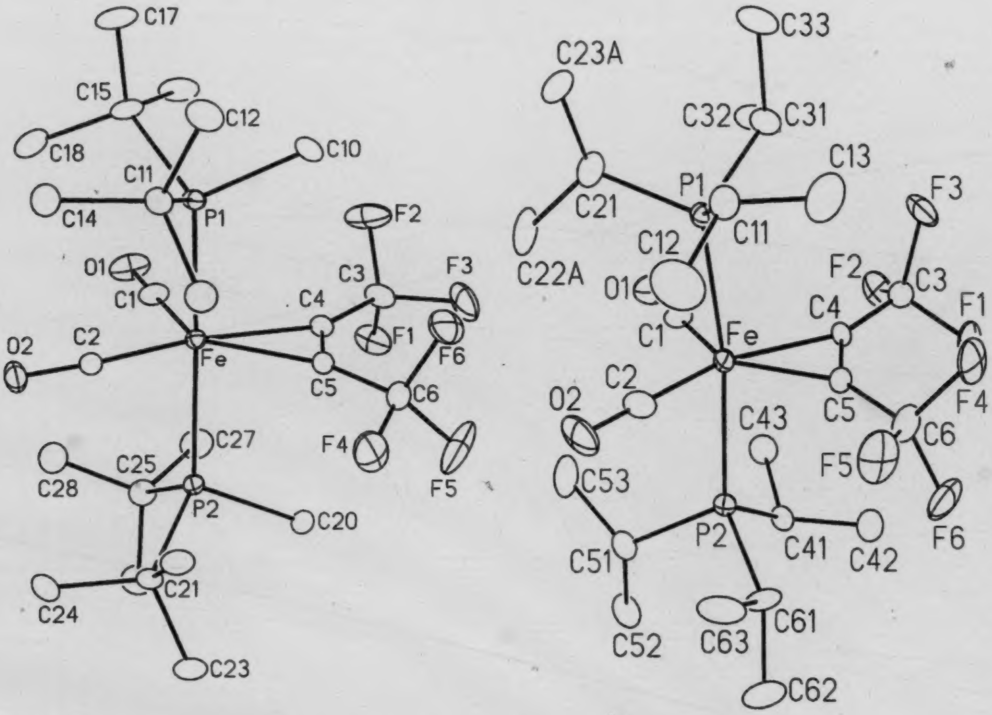
C17
C15
C12
C18
C10
C11
C14
P1
F2
O1
C3
F3
C1
C4
F1
O2
C2
Fe
F6
C5
C6
C27
F4
C25
C28
P2
F5
C20
C21
C24
C23
C33
C23A
C32
C31
C13
P1
C21
F3
C12
C11
C22A
O1
F2
C3
F1
C4
C1
Fe
C2
F4
O2
C5
C6
C43
F5
C53
P2
C41
C42
F6
C51
C61
C52
C63
C62

Figure 2-6 Solid State Molecular Structure of **1a** (*left*) and **1b** (*right*).

The geometry about the iron center is best described as approximating a trigonal bipyramid with the phosphines occupying axial positions while two carbonyls and the η^2-HFB ligand take up positions in the equatorial plane. As expected, the alkyne assumes an in-equatorial plane orientation. The iron and equatorial atoms, C1, C2, C4, and C5 form a good plane as none of the atoms deviated from a calculated least squares plane by more than 0.056(3)Å in **1a**, 0.039(3)Å in **1b** and 0.038(12)Å in **1c**.

Table 2-4 Selected Interatomic Distances (Å) and Angles (deg.) in **1a-c**.

Parameter	**1a**	**1b**	**1c**
Fe–P1	2.3811(5)	2.339(1)	2.363(1)
Fe–P2	2.3905(5)	2.339(1)	2.350(1)
Fe–C1	1.776(2)	1.752(5)	1.764(4)
Fe–C2	1.759(2)	1.746(6)	1.761(4)
Fe–C4	1.980(2)	1.998(4)	1.991(4)
Fe–C5	2.045(2)	2.020(4)	2.030(4)
O1–C1	1.142(3)	1.150(5)	1.161(5)
O2–C2	1.157(2)	1.154(5)	1.156(4)
C4–C5	1.278(3)	1.252(5)	1.267(5)
P1–Fe–P2	169.89(2)	170.92(6)	168.20(4)
P1–Fe–C1	94.38(6)	89.9(2)	90.9(1)
P1–Fe–C2	86.61(6)	86.5(2)	83.7(1)
P1–Fe–C4	91.74(5)	92.9(1)	94.7(1)
P1–Fe–C5	88.63(5)	94.5(1)	96.0(1)
P2–Fe–C1	94.52(7)	89.9(2)	89.1(1)
P2–Fe–C2	87.43(6)	84.8(2)	84.9(1)
P2–Fe–C4	91.80(5)	96.0(1)	96.9(1)
P2–Fe–C5	88.50(5)	91.6(1)	92.0(1)
C1–Fe–C2	97.88(9)	103.8(2)	105.5(2)
C1–Fe–C4	97.76(9)	103.0(2)	100.4(2)
C2–Fe–C5	127.38(8)	117.1(2)	117.45(2)
C4–Fe–C5	36.99(8)	36.3(2)	36.7(2)
C4–C5–C6	133.9(2)	135.5(5)	133.7(4)
C5–C4–C3	140.4(2)	137.1(5)	137.8(4)
Fe–C1–O1	179.0(2)	177.3(5)	177.1(4)
Fe–C2–O2	174.6(2)	177.8(5)	176.4(4)

Two distortions from ideal trigonal bipyramidal geometry do, however, occur. First, the P1–Fe–P2 angle deviates from 180° by about 10° (P1–Fe–P2 = 169.89(2)° **1a**; 170.92(6)° **1b**; 168.20(4)° **1c**). The phosphines are bent in the direction of the space between C2 and C5 in **1a**, and more towards C2 in **1b** and **1c**. Secondly, the bond angles in the equatorial plane show some curiosities. The C2–Fe–C5 angle in **1a** is 127.38(8)° while the adjacent angle C1–Fe–C4 angle is 97.76(9)°, this represents a difference of 30°. This pattern is also reflected, albeit to a lesser extent, in **1b** (14° difference) and **1c** (17° difference). Thus, compounds **1a-c** are asymmetric, while, in contrast, analogous iron compounds from the chemical literature, with an analogous labeling scheme, show much more symmetric structures; a twofold axis contains the iron atom and bisects the alkyne triple bond in *trans*-$Fe(CO)_2(PR_3)_2(\eta^2\text{-}C_2R'R'')$ (R = OPh, R′, R″ = Ph; R = OMe, R′, R″ = Ph; R = Et, R′, R″ = SiMe3), and in $Fe(CO)_2(PEt_3)_2(\eta^2\text{-}HC_2Ph)$ a plane of symmetry relates the two axial phosphine ligands (Table 2-5) [6].

Close examination of the space filling models of **1a-c** reveals that the large steric bulk of the phosphines causes the distortion in these structures. Consider, for example, the space filling model of the molecular structure of **1a** in Figure 2-7, which exhibits the greatest distortion. Component **A** shows a view in the equatorial plane and along a vector that roughly bisects the C2–Fe–C5 angle, while component **B** shows a view that is in the equatorial plane along a vector that roughly bisects the C1–Fe–C4 angle. It can be seen (Figure 2-7 **A**) that the ^{t}Bu substituents of the phosphines "wedge" into the equatorial plane forcing the carbonyl (C2O2) and the alkyne carbon (C5) away from each other and causing the C2–Fe–C5 angle to open up, while in the adjacent angle (Figure 2-7 **B**) the phosphine substituents are much farther removed from the equatorial plane and thus have much less of an influence, if any, on the C1–Fe–C4 angle. The implication here is that the large steric profile of the phosphine ligands in **1a-c** causes this distortion.

Table 2-5 Interatomic Distances (Å) and Angles (deg.) in $Fe(CO)_2(PR_3)_2(\eta^2\text{-}C_2R'R'')$[a]

Parameter	R = OPh	R = OMe	R = Et	R = Et
	R′ = Ph	R′ = Ph	R′ = $SiMe_3$	R′ = H
	R″ = Ph	R″ = Ph	R″ = $SiMe_3$	R″ = Ph
Fe–P1/P2	2.1702(5)	2.177(2)	2.243(2)	2.221(2)
Fe–C1	1.769(2)	1.758(4)	1.72(1)	1.752(8)
Fe–C2	1.769(2)	1.758(4)	1.72(1)	1.753(8)
Fe–C4	2.057(2)	2.048(2)	2.123(9)	2.046(8)
Fe–C5	2.057(2)	2.048(2)	2.123(9)	2.014(8)
C4–C5	1.274(4)	1.263(6)	1.29(5)	1.24(1)
P1–Fe–P2	177.04(2)	1.77.4(1)	1.75.0(1)	1.771(1)
C1–Fe–C2	111.1(1)	109.7(2)	112.2(7)	105.7(4)
C1–Fe–C4	106.53(8)	107.2(2)	–	112.1(3)
C2–Fe–C5	106.53(8)	107.2(2)	–	147.7(3)
C4–Fe–C5	36.1(1)	35.9(2)	–	35.6(3)
C4–C5–C6[b]	148.42(9)	148.9(2)	141.9(5)	147(5)
C5–C4–C3[c]	148.42(9)	148.9(2)	141.9(5)	147.3(8)

[a] Refs. [6]

[b] C≡C–H in $Fe(CO)_2(PEt_3)_2(\eta^2\text{-}HC{\equiv}CPh)$

[c] C≡C–Ph in $Fe(CO)_2(PEt_3)_2(\eta^2\text{-}HC{\equiv}CPh)$

Furthermore, it can be seen from Figure 2-6 or Figure 2-7 that in **1a** the phosphine adopts a conformation in which the smallest substituent, the Me group, is adjacent to the alkyne. Understandably this is a preferred arrangement since the alkyne is much more sterically demanding than a carbonyl. The structures from the literature, *trans*-$Fe(CO)_2(PR_3)_2(\eta^2\text{-}C_2R'R'')$ [6], have phosphine ligands that are not nearly as bulky as the phosphines in **1a-c** and so these structures do not show this distortion in the equatorial plane. In the case of $Fe(CO)_2(PEt_3)_2(\eta^2\text{-}HC_2Ph)$ [6d], the equatorial distortion, which is much less than that seen in **1a-c**, originates from the different substituents on the alkyne.

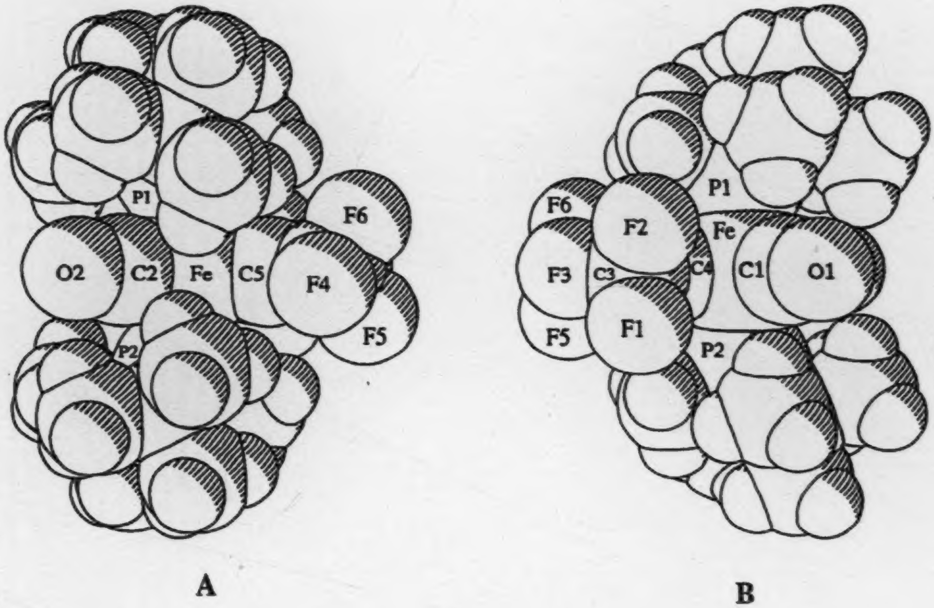

Figure 2-7 Space Filling Model of the Molecular Structure of **1a**.

The geometric features of the alkyne ligand also show signs of steric strain. Most telling are the distinct differences between the two $Fe\text{–}C_{alkyne}$ separations. For example the Fe–C5 separation in **1a** is larger by 0.065 Å (32 esd's) than the Fe–C4 separation. This trend is also reflected in **1b** and **1c** but to a lesser extent: **1c** shows a difference of 0.039 Å (10 esd's) while **1b** shows a 0.022 Å (5 esd's) difference. Moreover, there are differences between alkyne $C{\equiv}C\text{–}CF_3$ angles within each structure.

The C4–C5–C6 angle (133.9(2)°, **1a**; 135.5(5)°, **1b**; 133.7(4)°, **1c**) is slightly smaller (*i.e.* more bent away from linearity) than the C5–C4–C3 angle (140.4(2)°, **1a**; 137.1(5)°, **1b**; 137.8(4)°, **1c**). Again these effects are more pronounced in **1a**, 6.5° (32 esd's) while the differences in **1b** and **1c** are less at 1.6° (3 esd's) and 4.1° (8 esd's). In the more symmetric structures of $M(CO)_4(\eta^2\text{-HFB})$ (M = Ru, Os) [24], there is virtually no difference between the $C{\equiv}C{-}CF_3$ angles within each structure. Clearly, the difference in **1b** is negligible and within a range typically observed, however the difference in **1a** and arguably **1c** seem to be beyond this range. Thus, the ranking of steric profile of the phosphine ligands in the current systems appears to be P^tBu_2Me > PCy_3 > P^iPr_3. The cone angles, quoted from the chemical literature [7, 8a], for these three phosphines suggests a somewhat different order; PCy_3 (cone angle 170°) > P^tBu_2Me (average cone angle 161°) ≅ P^iPr_3 (cone angle 160°). This dichotomy arises from the inability of the cone angle model to accurately describe the steric profile of the P^tBu_2Me ligand and points to the danger in using the average cone angle value for a ligand such as P^tBu_2Me. This phosphine, unlike P^iPr_3 or PCy_3, has two different substituents; two very sterically demanding ^{t}Bu groups and one small Me group. The average cone angle model does not take into account the preferred rotational orientation of the ligand which in turn can cause specific but significant distortions.

The amount of metal-alkyne interaction might be measured in terms of the $Fe{-}C_{alkyne}$ distance, the C≡C separation and the C≡C–R angles. Between the group members **1a-c** there is no meaningful difference between the average values of the $Fe{-}C_{alkyne}$ separations. When compared to the average value associated with the known structures, *trans*-$Fe(CO)_2(PR_3)_2(\eta^2\text{-}C_2R'R'')$ (2.06(1) Å) [6], the average value of **1a-c** as a group (2.01(1) Å) is slightly smaller by 0.05 Å (5 esd's). This is consistent with expectation since the superior π-acidity of the HFB, relative to that of electron rich alkynes like C_2Ph_2, $C_2(SiMe_3)_2$ and HC_2Ph, allows the HFB ligand to accept more back-donation from the metal and thus strengthen the Fe-alkyne interaction. The average C≡C separation for the group **1a-c** (1.266(8) Å) is not significantly different from the average C≡C distance observed in the *trans*-$Fe(CO)_2(PR_3)_2(\eta^2\text{-}C_2R'R'')$ compounds [6] as a group (1.27(1) Å) or those found in $M(CO)_4(\eta^2\text{-HFB})$ (M = Ru, 1.276(6)Å; Os, 1.276(9)Å) [24]. One might expect a lengthening of the C≡C bond in **1a-c** since back-donation involves the π^* orbitals of the alkyne but it appears that the C≡C distances are somewhat insensitive to changes in the metal-alkyne bonding. The C≡C–R angles of coordinated alkynes indicate a rehybridization at the C_{alkyne} centers; the smaller this angle, the more deviation from linearity and the more rehybridization. Within the **1a-c** group, the C≡C–R bond angles are similar and indicate similar rehybridization. The average for the group is 136 (1)°, a deviation of 44° from 180°, indicating significant M→alkyne back donation and rehybridization at the C_{alkyne} centers. In comparison with the known *trans*-$Fe(CO)_2(PR_3)_2(\eta^2\text{-}C_2R'R'')$ structures [6], the bending back of the alkyne substituents is more pronounced by about 10° and this suggests more back bonding from the metal to the HFB ligand in **1a-c**. Furthermore, when compared to the C≡C–R angles in $M(CO)_4(\eta^2\text{-HFB})$ (M = Ru, Os) [24], it is found that the average of the C≡C–R angles in **1a-c** are 6° (6 esd's) and 5° (5 esd's) smaller, respectively. Again an indication of more back donation in **1a-c** which is consistent with replacement of two good π acid carbonyl ligands with two good σ donor phosphines. However, it was concluded previously that the equatorial distortions in **1a-c**, due to the steric bulk of the phosphine ligand, had some effect on the bending back of the alkyne substituents and the Fe–C_{alkyne} distances, *vide supra*. In light of this, it is not possible to conclude that the bending back of the HFB substituents is solely a result of metal-alkyne back donation. The distortions observed in **1a-c** clearly complicate the comparison of the metal-alkyne structural parameters with those of similar but less distorted structures; nevertheless, there is a suggestion, through the comparison of the Fe–C_{alkyne} separations, that metal-alkyne interaction in **1a-c** are stronger than that in the analogous $Fe(CO)_2(PR_3)_2(\eta^2\text{-}C_2R'R'')$ compounds.

2.3.2 $Fe(CO)_2(PR_2R')(\eta^2\text{-HFB})$ Complexes (2a,c,d)

The X-ray crystal structure of **2c** has previously been determined [1c] and it was of interest to obtain the X-ray crystal structures of **2a**, **2b** and **2d** for comparison purposes. The single crystal structure analyses of **2a** and **2d** were successful. In general, the structures are similar, and as such **2a** and **2d** serve well as a representative examples (Figure 2-8). Table 2-6 presents selected interatomic distances and angles for **2a,c,d**.

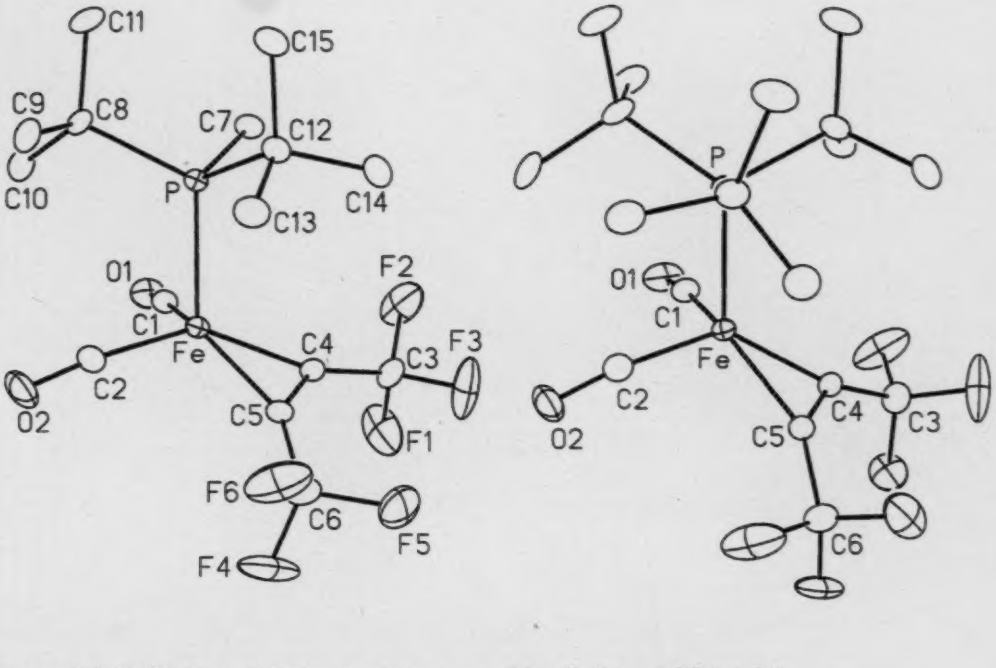

Figure 2-8 Solid State Molecular Structure of **2a** (*left*) and **2d** (*right*).

Table 2-6 Selected Interatomic Distances (Å) and Angles (deg.) in **2a-c**.

Parameter	**2a**	**2c**	**2d**
Fe–P	2.224(1)	2.210(1)	2.2609(8)
Fe–C1	1.752(5)	1.778(4)	1.764(3)
Fe–C2	1.788(5)	1.759(4)	1.771(3)
Fe–C4	1.854(4)	1.871(4)	1.868(3)
Fe–C5	1.876(4)	1.864(4)	1.871(3)
O1–C1	1.149(5)	1.144(5)	1.147(3)
O2–C2	1.147(5)	1.154(5)	1.152(4)
C4–C5	1.290(5)	1.294(5)	1.296(4)
P–Fe–C1	88.1(1)	91.6(1)	93.4(1)
P–Fe–C2	98.4(1)	90.2(1)	95.3(1)
P–Fe–C4	112.6(1)	120.5(1)	122.2(1)
P–Fe–C5	124.8(1)	116.6(1)	126.0(1)
C1–Fe–C2	104.4(2)	103.3(2)	103.1(1)
C1–Fe–C4	102.6(2)	101.3(2)	99.1(1)
C2–Fe–C5	99.9(2)	104.5(2)	98.4(1)
C4–Fe–C5	40.5(2)	40.5(2)	40.6(1)
C5–C4–C3	138.2(4)	138.0(4)	137.0(3)
C4–C5–C6	140.2(4)	136.2(4)	138.4(3)
Fe–C1–O1	173.4(4)	176.8(3)	171.0(3)
Fe–C2–O2	173.2(4)	175.9(3)	171.3(3)

Results of the crystal structure analyses show that the structures consist of well separated monomeric units with no unusual intermolecular contacts. The geometry about the iron can be described in terms of either a square pyramid or tetrahedron but in either case the structure must be considered highly distorted. In terms of a tetrahedral geometry, C1, C2 and the midpoint of the C4–C5 vector form the trigonal base while P occupies the apex position. The metal lies slightly above the plane of the atoms that define the trigonal base. If a least squares plane is constructed using C1, C2, C4 and C5 then the distance from the Fe atom to this plane is 0.414(2) Å in **2a**, 0.371(2) Å in **2c** and 0.500(2) Å in **2d**.

The most notable distortion is the large difference between the P–Fe–C_{alkyne} and P–Fe–CO angles. In all structures the P–Fe–Cn (n = 4, 5) angles are considerably larger than the P–Fe–Cm (m = 1, 2) angles; the latter being close to 90°. In other words the alkyne bends down away from the phosphine and toward the vacant axial site of a trigonal bipyramidal structure formally occupied by a phosphine in **1a-c** or a carbonyl in $Fe(CO)_3(PR_3)(\eta^2$-HFB). Intuitively, this distortion seems to be a result of steric repulsion between the bulky phosphine and the alkyne ligand. However there is evidence that this phenomenon is the result of mainly electronic factors. Klobukowski and Decker have calculated (DFT) the optimized geometry for $M(CO)_3(\eta^2\text{-}C_2H_2)$ (M = Fe, Ru, Os) under C_s symmetry constraints [4]. The results show that the structures obtained are similar to **2a,c,d**. In the case of M = Fe (Figure 2-9) the C3–Fe–Cn (n = 4, 5) angles are 117.6° [4], a value close to the corresponding angles in **2c** (120.5(1)° and 116.6(1)°). If steric effects alone were the dominate factor in these complexes one would expect a considerably larger P–Fe–Cn (n = 4, 5) angle in **2c** than in $Fe(CO)_3(\eta^2\text{-}C_2H_2)$ since both PCy_3 is larger than CO and HFB is larger than C_2H_2. Moreover, Klobukowski and Decker have found that upon changing the metal from Fe to Ru and Os , *i.e.* increasing the size of the metal in the order Fe < Ru ≅ Os, this same angle slightly increases (117.6°, Fe; 121.4° Ru; 122.8° Os), which is counter intuitive and further discredits the steric argument [4]. Having said this, steric factors still play a role in these structures, when bulky phosphine ligands are involved, because the average of the P–Fe–Cn (n = 4, 5) angles in **2d** (124.1(2)°) is larger than the corresponding value in **2c** (118.6(2)°). It is apparent, since P^tBu_3 and PCy_3 have similar donor properties (Section 2.2.1), that the larger P^tBu_3 experiences more steric interaction with the alkyne than the smaller PCy_3. Moreover, in **2a,c,d** an asymmetry in both the P–Fe–Cn (n = 1, 2) and P–Fe–Cn (n = 4, 5) angles is observed. That is, the phosphine ligand tilts toward the space between one carbonyl and one terminus of the alkyne. The asymmetry in these angles is most prominent in **2a**, evidently a result of the unusual steric profile of a PR_2R' type phosphine versus a PR_3 type ligand. In **2a** the phosphine tilts in the direction of the space above and between C1 and C4 as the P–Fe–C1 angle is 88.1(1)° while the P–Fe–C2 is 98.4(1)° and the P–Fe–C4 angle is 112.6(1)° while the P–Fe–C5 angle is 124.8(1)°. Not surprisingly it is the least spatially demanding substituent, Me (C7), of the P^tBu_2Me ligand which occupies this space.

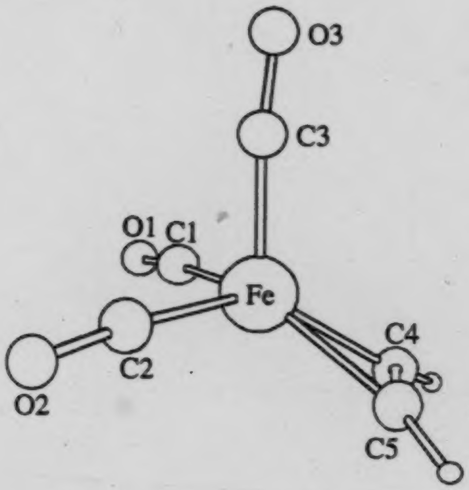

Figure 2-9 Structure of $Fe(CO)_3(\eta^2\text{-}C_2H_2)$ [4].

The geometric features of the Fe–alkyne linkage (M–C_{alkyne} separations, C≡C separations, and C≡C–R deviation from linearity) are of particular interest in **2a,c,d** since one would expect that it is these parameters that will be the most revealing concerning the issue of the bonding role played by the alkyne. In his analysis of monomeric Mo(II) and W(II) complexes with four electron donor alkynes, Templeton indicates that the M–C_{alkyne} separations are particularly useful in determining the level of involvement of the alkyne $\pi_{\perp}$ orbital with the metal [19]. He has found that the M–C_{alkyne} distances in four electron donor alkyne complexes are some 0.10 Å shorter than the corresponding distances in two electron donor complexes. He further cites the case of $[Co(PMe_3)_3(\eta^2\text{-}C_2Ph_2)]^+$ and $[Co(PMe_3)_3(CH_3CN)(\eta^2\text{-}C_2Ph_2)]^+$ in which a 0.13Å contraction of the M–C_{alkyne} distances occurs in the four electron donor alkyne, the former complex, relative to the corresponding distance in the two electron donor complex [19]. In addition, Klobukowski and Decker have calculated a 0.236 Å contraction of the Fe–C_{alkyne} distance in $Fe(CO)_3(\eta^2\text{-}C_2H_2)$ relative to the corresponding distances in $Fe(CO)_4(\eta^2\text{-}C_2H_2)$ [4]. The results here show that in comparison to **1a** and **1c** the average Fe–C_{alkyne} separation in **2a** and **2c** are approximately 0.14 Å shorter. Furthermore, the average of the Fe–C_{alkyne} distances in **2a,c,d** are 0.14 - 0.25 Å shorter than the corresponding distances in the previously mentioned two electron donor alkyne $Fe(CO)_2(PR_3)_2(\eta^2\text{-}C_2R'R'')$ complexes (Table 2-5 Section 2.3.1). Templeton has shown that, despite a variety of alkynes and spectator ligands, in four electron donor alkyne complexes the M–C_{alkyne} distances show a high degree of consistency [19]. In **2a,c,d** the average Fe–C_{alkyne} separation is 1.867(3)Å. This separation is short and consistent with an alkyne-metal interaction that can be characterized as being greater than that usually observed in similar iron complexes in which the alkyne acts as a two electron donor.

As additional π bonding resources are donated from the alkyne to the metal and additional metal-alkyne back bonding into π* C≡C orbitals occurs, one would expect a weakening of the C≡C bond and consequently a greater C≡C separation in making the transition from a two electron donor to a four electron donor alkyne ligand. This argument seems to be supported by the recent DFT calculations that predict an elongation of 0.051Å of the C≡C bond in $Fe(CO)_3(\eta^2-C_2H_2)$ relative to $Fe(CO)_4(\eta^2-C_2H_2)$ [4]. Moreover, the C≡C stretches in the IR spectra of closely related Mo(II) and W(II) complexes show a considerable shift, of the order of 100 cm^{-1} or more, to lower frequencies in four electron donor alkynes relative to their two electron donor counterparts [19], and this was also seen in the present compounds. It is therefore curious that the C≡C distance in **2a** is not significantly different (Δ = 0.012 Å, 2 esd's) from that found in **1a**, while the C≡C separation in **2c** is only slightly longer (0.027Å, 5 esd's) than that in **1c**. Furthermore, in comparison to the C≡C separations found in the $Fe(CO)_2(PR_3)_2(\eta^2-C_2R'R'')$ complexes (Table 2-5 Section 2.3.1) and $M(CO)_4(\eta^2$-HFB) (M = Ru, Os) [24], **2a,c,d** no consistent correlation is observed. Templeton [19] and others [25] have indicated that the C≡C structural parameter is a poor indicator of metal-alkyne bonding but have not addressed the dichotomy in the use of ν_{CC} stretches from IR spectra as a fair indicator of metal-alkyne interaction while the C≡C distances from solid state structures are considered inadequate for this purpose. The results here provide no avenue for a definitive conclusion on this issue and the C≡C parameters from X-ray structures indeed appear to be an inadequate indicator of metal-alkyne interaction beyond the two electron donor type.

Another indicator of metal to alkyne interaction is the deviation of the C≡C–C angles from linearity. In Mo(II) and W(II) alkyne complexes the typical deviation from linearity is 40° for both two electron and four electron donor alkyne ligands [19].

Comparing the C≡C–C angles of **2a,c,d** to **1a-c** it is clear that there exists no significant difference between the two groups as there is less than a 2° difference between their average values. For the two groups as a whole the deviation from linearity is 42-43°. Although C≡C–C angles from solid state structures are a good indicators of alkyne coordination it is apparent that they are not relevant in the detection of the involvement of the $\pi_\perp$ orbital in the metal-alkyne bonding.

Only four crystal structures of four electron donor alkyne complexes containing group 8 metals appear in the literature. A preliminary structure of $Fe\{P(OMe)_3\}_3(\eta^2\text{-}C_2Ph_2)$ has been reported but the only data offered is that it is monomeric, its geometry can be described as either pseudotetrahedral or square pyramidal and the C≡C distance is 1.332(10) Å [26]. Recently, crystal structures of a pair of closely related Os(II) compounds containing two and four electron alkyne ligands have been reported [27]. The most meaningful comparison that can be made between the iron and the osmium compounds is the contraction of the $M\text{–}C_{alkyne}$ separation upon going from a two electron to a four electron donor alkyne complex. The $M\text{–}C_{alkyne}$ distances in the four electron donor alkyne complex $[Os(\eta^5\text{-}C_5H_5)(P^iPr_3)(\eta^2\text{-}HC{\equiv}CC(OH)Ph_2)]^+$ are 0.15 and 0.18 Å shorter than the related parameters in the two electron donor alkyne complex $Os(\eta^5\text{-}C_5H_5)Cl(P^iPr_3)(\eta^2\text{-}HC{\equiv}CC(OH)Ph_2)$, which is very close to the contraction (0.14 Å) observed from **1a,c** to **2a,c**. These osmium complexes also show the expected shift of the C_{alkyne} in the ^{13}C NMR spectra to lower field in the four electron donor alkyne complex relative to the two electron donor complex [27]. Also, the crystal structure of the four electron donor alkyne complex $Os(CO)(P^iPr_3)_2(\eta^2\text{-}C_2Ph_2)$ has been reported [28] and the average of the $Os\text{–}C_{alkyne}$ separations is not significantly different (within 3 esd's) from the corresponding parameter in $[Os(\eta^5\text{-}C_5H_5)(P^iPr_3)(\eta^2\text{-}HC{\equiv}CC(OH)Ph_2)]^+$, but they are 0.12 Å (6 esd's) shorter than the corresponding parameter in $Os(\eta^5\text{-}C_5H_5)Cl(P^iPr_3)(\eta^2\text{-}HC{\equiv}CC(OH)Ph_2)$. Therefore, it appears that in group 8 metal complexes the M–C_{alkyne} separations in four electron donor alkynes are about 0.1 Å shorter than those found in their two electron counterparts and the correlation that Templeton noted for Mo(II) and W(II) complexes [19] holds for the group 8 metals as well.

Most recently, Filippou and Rosenauer have published the solid state molecular structure of $Fe(CO)_3\{\eta^2\text{-}C_2(NMe_2)_2\}$ [13]. Figure 2-10 shows the structure, which is similar to those of **2a,c,d**, while Table 2-7 gives selected interatomic distances and angles. The structure, as in **2a,c,d**, can be described as a distorted square pyramid with the basal plane consisting of the alkyne (C1, C2) and the two carbonyls C3O1 and C4O2, while the third carbonyl C5O3 occupies the apical position. As in **2a,c,d** there is a tilting of the apical ligand away from the alkyne (113°), however not nearly to the extent as that observed in **2a,c,d** (121°). Unlike in **2,a,c,d**, the apical ligand is symmetrically positioned over the basal plane, *i.e.* C5–Fe–C1 = C5–Fe–C2 and C5–Fe–C3 = C5–Fe–C4. Clearly the apical carbonyl, as expected, does not cause the structural distortions that are observed in **2a,c,d** with the bulky phosphines. As discussed previously, a comparison of the C≡C distances is a moot point since this structural parameter was found to be a poor indicator of $\pi_\perp$ orbital involvement in the M-alkyne bonding. Moreover, Templeton has found that the C≡C distances in Mo(II) complexes with diaminoalkyne ligands are unusually long and suggests that the reason for this phenomenon stems from a π delocalization in the $R_2N\text{-}C{\equiv}C\text{-}NR_2$ system [19]. Indeed Filippou *et al.* have indicated that there is considerable π-electron delocalization along the alkyne moiety involving the NMe_2 groups [13]. Templeton further discovered that comparison of the C≡C–R angles with these complexes is problematic since it seems that the diaminoalkyne ligands are unique in this respect; the C≡C–N angle is typically 128-130° compared to the more common 140° for other alkyne ligands [19]. Interestingly in $Fe(CO)_3\{\eta^2\text{-}C_2(NMe_2)_2\}$ the C≡C–N angles are 143°; a value more consistent with typical alkyne ligands and close to the C≡C–R angles in **2a,c,d**.

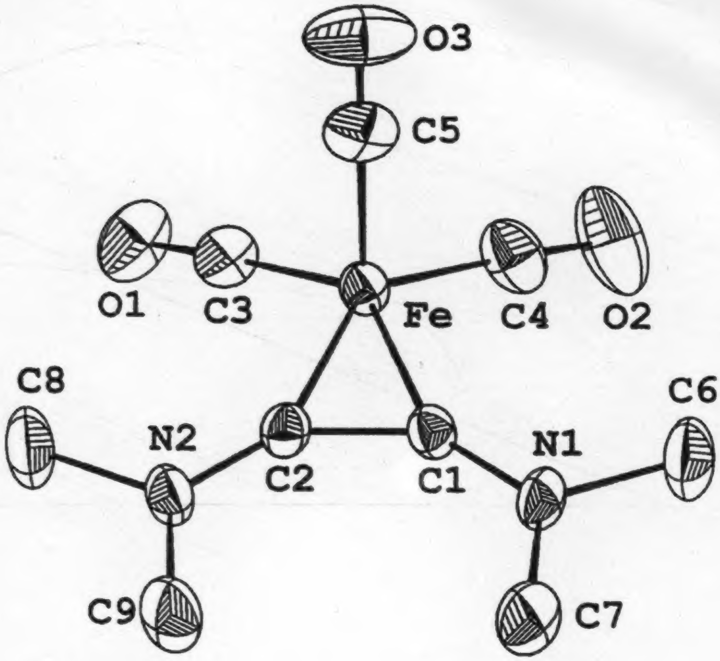

Figure 2-10 Solid State Molecular Structure of $Fe(CO)_3\{\eta^2\text{-}C_2(NMe_2)_2\}$ [13].

Table 2-7 Selected Interatomic Distances (Å) and Angles (deg.) in $Fe(CO)_3\{\eta^2\text{-}C_2(NMe_2)_2\}$.

Fe–C1	1.845(3)	C1–Fe–C5	113.1(2)
Fe–C2	1.844(3)	C2–Fe–C3	100.1(2)
Fe–C3	1.773(4)	C2–Fe–C5	112.9(2)
Fe–C4	1.785(4)	C3–Fe–C4	99.0(2)
Fe–C5	1.787(4)	C3–Fe–C5	99.7(2)
O1–C3	1.168(4)	C4–Fe–C5	99.0(2)
O2–C4	1.145(5)	C1–C2–N2	143.2(3)
O3–C5	1.146(5)	C2–C1–N1	143.1(3)
C1–C2	1.375(4)	Fe–C3–O1	177.3(3)
C1–Fe–C2	43.8(1)	Fe–C4–O2	177.4(4)
C1–Fe–C4	101.1(2)	Fe–C5–O3	176.6(3)

The most meaningful comparison that can be made between $Fe(CO)_3\{\eta^2\text{-}C_2(NMe_2)_2\}$ and **2a,c,d** are the Fe–C_{alkyne} separations. The average Fe–C_{alkyne} separation of 1.867(8) Å in **2a,c,d** is within 3 esd's of the corresponding parameter in $Fe(CO)_3\{\eta^2\text{-}C_2(NMe_2)_2\}$ (1.845(1) Å). This would lead one to believe that the strength of the metal-alkyne interaction is similar between these two types of compounds. Indeed, Filippou *et al.* have concluded that there is strong evidence, both structural and spectroscopic, that the diaminoalkyne ligand is acting as a four electron donor. Despite the very different alkyne ligands, the striking similarities between **2a,c,d** and $Fe(CO)_3(\eta^2\text{-}C_2(NMe_2)_2)$ led us to conclude that these compounds belong to the same class of four electron donor alkyne complexes of iron.

2.4 Conclusions

It has been demonstrated that $Fe(CO)_2(PR_2R')_2(\eta^2\text{-HFB})$ and $Fe(CO)_2(PR_2R')(\eta^2\text{-HFB})$ complexes can be synthesized from $Fe(CO)_4(\eta^2\text{-HFB})$ and bulky phosphines. The $Fe(CO)_2(PR_2R')_2(\eta^2\text{-HFB})$ complexes have been structurally characterized. In solution the spectroscopic data indicates a geometry with C_{2v} symmetry with mutually *trans*-phosphines and *cis*-carbonyls. In the solid state the compounds adopt a distorted trigonal bipyramidal geometry that closely approximates C_s symmetry. The phosphines take up the axial positions while the carbonyls and alkyne ligand claim equatorial sites. The alkyne assumes an η^2 in-plane orientation as expected. Distortion from ideal geometry is the result of the presence of bulky phosphine ligands. Solution spectroscopy of the $Fe(CO)_2(PR_2R')(\eta^2\text{-HFB})$ complexes indicate a structure with C_s symmetry while the solid state structure reveals a distorted tetrahedral or, alternatively, a distorted square pyramidal geometry approaching a C_s symmetry. The alkyne is η^2 bound and spectroscopic and structural evidence supports its four electron donor role. The significance of this result is realized in that these structures, along with $Fe(CO)_3(\eta^2\text{-}C_2(NMe_2)_2\}$, represent a prototypical model for the $[M(CO)_3(\eta^2\text{-alkyne})]$ intermediate in the carbonyl substitution reactions of $M(CO)_4(\eta^2\text{-alkyne})$ with phosphine ligands. Upon loss of an axial CO the alkyne bends toward the vacant axial site and away from the equatorial plane. In this manner maximum overlap of the $\pi_\perp$ orbital and the vacant *d* orbital occurs (Figure 2-11). Moreover, in light of the extremely limited number of reports of group 8 four electron alkyne complexes in the annals of chemical literature, the spectroscopic and structural data establish a standard for the detection and identification of such species.

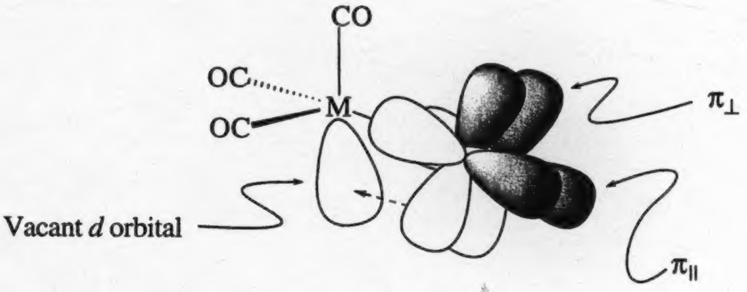

Figure 2-11 Intermediate $[Fe(CO)_3(\eta^2\text{-alkyne})]$.

2.5 Experimental

2.5.1 Solvents, Techniques and Physical Measurements

Solvents were dried from appropriate drying agents [29] and distilled under a nitrogen atmosphere. CD_2Cl_2 (99.9 %) was purchased from Cambridge Isotope Laboratories and was dried over CaH_2, then bulb to bulb vacuum distilled and stored over 4 Å molecular sieves. Glassware was cleaned by submersion in alcoholic KOH bath and subsequently soaked in a dilute HCl bath then rinsed with distilled water. Glassware was then dried at 250 °C for a 12 hour period. All reactions were performed under nitrogen atmosphere using Schlenk techniques. Prepurified nitrogen was passed through a deoxygenating column (BASF Cu catalyst R3-11, 125 °C) and a P_2O_5 drying column (Mallinkrodt Aquasorb) before use.

Elemental analyses were performed by the Microanalytical Laboratory Department of Chemistry, University of Alberta. Mass spectrometry analyses were performed by the Mass Spectrometry Laboratory, Department of Chemistry, University of Alberta. Infrared spectroscopy was performed on a Fourier Transformer Bomem MB-100 spectrometer. Solution cells (KBr/CaF_2) of path length of approximately 0.1 mm were used to contain solution samples. Nuclear magnetic resonance spectra were obtained on a Bruker AM-400 or Varian INOVA-400 spectrometers. ^1H and ^{13}C NMR chemical shifts (δ) were referenced to solvent signals and are reported in ppm units relative to tetramethylsilane (TMS). ^{31}P NMR chemical shift were referenced externally to 85% H_3PO_4 while ^{19}F NMR chemical shifts were referenced externally to $CFCl_3$. NMR samples were prepared under nitrogen atmosphere using standard Schlenk methods and tubes were sealed with rubber septa.

2.5.2 Reagents

Hexafluoro-2-butyne (99%) was purchased from Sigma-Aldrich Canada and used without further purification. The phosphines, P^iPr_3 (98%), PCy_3 (97%) and P^tBu_3 (98%) were purchased from Strem Chemicals and stored under nitrogen atmosphere. P^tBu_2Me was either purchased from Strem Chemicals (98%) or prepared according to the procedure described below [30] and stored under nitrogen. When deemed necessary (^{31}P and ^1H NMR essays) the phosphines were purified by either vacuum distillation (P^tBu_2Me, P^iPr_3, P^tBu_3) or crystallization (PCy_3 from EtOH). $Fe(CO)_5$ was purchased from Johnson-Matthey and used without further purification. $Fe(CO)_4(\eta^2\text{-HFB})$ was prepared as described in literature with one exception; 2-3 mL of HFB was condensed at −78 °C then transferred into the photochemical reaction chamber instead of being "bubbled through the solution for five minutes" [31].

2.5.3 Synthetic Procedures

Synthesis of P^tBu_2Me [30]. A three neck 500 mL round bottom flask with reflux condenser was dried and degassed. Diethyl ether, 210 mL, was distilled, degassed and added to the flask. P^tBu_2Cl (6.75 g, 37 mmol) was added to the Et_2O *via* cannula transfer. MeLi (27 mL of 1.4 M in Et_2O, 38 mmol), was added to the colorless solution *via* cannula in approximately 5 mL portions to minimize the heat generated by the exothermic reaction. A colorless precipitate formed immediately. The reaction mixture was then heated to reflux for approximately 18 hours. The reflux was stopped and the mixture allowed to cool. A degassed NH_4Cl solution (17.5 g in 70 mL H_2O) was added *via* cannula in approximately 5 mL portions in order to minimize heat generated by the exothermic quenching. The Et_2O layer was decanted and the aqueous layer washed with 2×20 mL degassed Et_2O. The original Et_2O layer and washes were combined. The solution was concentrated to approximately 50 mL, *in vacuo*, (0.25 mmHg) at –30 °C. The solution was then dried over Na_2SO_4 with stirring for several hours. The solution was filtered and the Na_2SO_4 washed with 2×20 mL degassed Et_2O. The washings and Et_2O solution were combined. The Et_2O was removed by vacuum (0.25 mmHg) at –30 °C, leaving colorless crude P^tBu_2Me (2.84 g, 17.7 mmol, 48% yield) . The phosphine was vacuum distilled (0 °C, 0.25 mmHg). Purity was determined by ^1H and ^{31}P NMR spectroscopy. Purification by vacuum distillation was repeated on occasion.

P^tBu_2Me is an air sensitive colorless liquid (d = 0.89 g/mL) that can be vacuum distilled at 25 °C at 5 mm Hg.

F.W. 160.23

^1H NMR (CD_2Cl_2, 400.1 MHz, 27 °C) δ 0.93 (d, $^2J_{HP}$ = 4 Hz, PCH_3), 1.08 (d, $^3J_{HP}$ = 11 Hz, $PC(CH_3)_3$).

$^{31}P\{^1H\}$ NMR (CD_2Cl_2, 161.9 MHz) δ 11.7 (s).

Synthesis of $Fe(CO)_2(PR_2R')_2(\eta^2$-HFB) (1a-c). Two equivalents of phosphine were added to a 50 ml pentane solution of $Fe(CO)_4(\eta^2$-HFB) (90 – 120 mg, 0.27-0.36 mmol) at –20 °C. The solution was stirred for 30 minutes at this temperature. The solvent was then removed, *in vacuo*, at –50 °C, leaving an orange-red solid. The solid was dissolved in a minimum amount of pentane at –20 °C and crystallized at –80 °C. The reaction with PCy_3 was performed in CH_2Cl_2. Due to the temperature sensitive nature of the compounds, with the exception of **1c** (84% yield), yields could not be determined.

$Fe(CO)_2(P^tBu_2Me)_2(\eta^2$-HFB) (1a)

F.W. 594.4

IR (pentane, cm^{-1}) ν_{CO} 1978 (m), 1906 (s)

^{1}H NMR (CD_2Cl_2, 400.1 MHz, – 90 °C) δ 0.78 (virtural triplet, N = 6 Hz, $\mathrm{PC}H_3$), 1.20 (br s, $\mathrm{PC(C}H_3)_3$)

^{19}F NMR (CD_2Cl_2, 376.4 MHz, – 90 °C) δ – 50.2 (s, $\mathrm{CC}F_3$)

^{31}P{^{1}H} NMR (CD_2Cl_2, 161.9 MHz, – 90 °C) δ 74.8 (s)

^{13}C{^{1}H} NMR (CD_2Cl_2, 100.6 MHz, – 90 °C) δ 221.8 (s, *C*O), 124.8 (q, $^1J_{CF}$ = 269 Hz, $\mathrm{C}C\mathrm{F}_3$), 33.8 (s, $\mathrm{P}C\mathrm{(CH_3)_3}$), 22.4 (s, $\mathrm{PC(}C\mathrm{H_3)_3}$), 13.8 (s, $\mathrm{P}C\mathrm{H_3}$)

^{13}C{^{19}F} NMR (CD_2Cl_2, 100.6 MHz, – 90 °C) δ 221.8 (br s, *C*O), 124.8 (br s, $\mathrm{C}C\mathrm{F}_3$), 116.8 (br s, $C\mathrm{CF}_3$) 33.8 (br, $\mathrm{P}C\mathrm{(CH_3)_3}$), 22.4 (t, $^1J_{CH}$ = 119 Hz $\mathrm{PC(}C\mathrm{H_3)_3}$), 13.8 (q, $^1J_{CH}$ = 125 Hz $\mathrm{P}C\mathrm{H_3}$)

Fe(CO)$_2$(P^{i}Pr$_3$)$_2$(η^2-HFB) (1b)

F.W. 594.4

IR (pentane, cm^{-1}) ν_{CO} 1978 (m), 1910 (s)

^{1}H NMR (CD_2Cl_2, 400.1 MHz, – 90 °C) δ 1.12 (br, $\mathrm{PCC}H_3$), 1.77 (m, $\mathrm{PC}H$)

^{19}F NMR (CD_2Cl_2, 376.4 MHz, – 90 °C) δ – 47.7 (s, $\mathrm{CC}F_3$)

^{31}P{^{1}H} NMR (CD_2Cl_2, 161.9 MHz, – 90 °C) δ 58.9 (s)

^{13}C{^{1}H} NMR (CD_2Cl_2, 100.6 MHz, – 90 °C) δ 221.2 (t, $^2J_{CP}$ = 29 Hz, *C*O), 125.5 (q, $^1J_{CF}$ = 271 Hz, $\mathrm{C}C\mathrm{F}_3$), 115.3 (br, $C\mathrm{CF}_3$), 23.9 (s, $\mathrm{P}C\mathrm{H}$), 20.2 (s, $\mathrm{PC}C\mathrm{H_3}$)

^{13}C{^{19}F} NMR (CD_2Cl_2, 100.6 MHz, – 90 °C) δ 221.2 (t, $^2J_{CP}$ = 29 Hz, *C*O), 125.5 (s, $\mathrm{C}C\mathrm{F}_3$), 115.4 (t, $^2J_{CP}$ = 14 Hz, $C\mathrm{CF}_3$), 23.9 (d, $^1J_{CH}$ = 132 Hz $\mathrm{P}C\mathrm{H}$), 20.2 (q, $^1J_{CH}$ = 129 Hz $\mathrm{PC}C\mathrm{H_3}$)

Fe(CO)$_2$(PCy$_3$)$_2$(η^2-HFB) (1c)

F.W. 834.8

IR (pentane, cm^{-1}) ν_{CO} 1974 (m), 1903 (s)

^1H NMR (CD_2Cl_2, 400.1 MHz, – 90 °C) δ 1.0-2.1 (br) PC_6H_{11}

^{19}F NMR (CD_2Cl_2, 376.4 MHz, – 90 °C) δ – 47.8 (s, CCF_3)

$^{31}P\{^1H\}$ NMR (CD_2Cl_2, 161.9 MHz, – 90 °C) δ 56.2 (s)

$^{13}C\{^1H\}$ NMR (CD_2Cl_2, 100.6 MHz, – 90 °C) δ 220.9 (t, $^2J_{CP}$ = 29 Hz, *C*O), 125.4 (q, $^1J_{CF}$ = 271 Hz, $C\mathit{C}F_3$), 115.3 (br s, $\mathit{C}CF_3$), 34.8-25.6 (br, $P\mathit{C}_6H_{11}$)

$^{13}C\{^{19}F\}$ NMR (CD_2Cl_2, 100.6 MHz, – 90 °C) δ 220.9 (t, $^2J_{CP}$ = 29 Hz, *C*O), 125.4 (s, $C\mathit{C}F_3$), 115.3 (br s, $\mathit{C}CF_3$), 34.8-25.6 (br, $P\mathit{C}_6H_{11}$)

Synthesis of $Fe(CO)_2(PR_2R')(\eta^2$-HFB) (2a-d). One equivalent of phosphine was added to a 50 ml pentane solution of $Fe(CO)_4(\eta^2$-HFB) (90 - 120 mg, 0.27-0.364 mmol) at –20 °C. The solution was stirred for 30 minutes at this temperature and then brought to 0 °C over several minutes. The solvent was removed, *in vacuo*, at 0 °C leaving a deep purple residue (deep blue in the case of **2d**). The residue was redissolved in pentane and the solvent removed and this procedure repeated. The residue was dissolved in a minimum amount of pentane at 0 °C and crystallized at –80 °C, producing deep purple (blue in the case of **2d**) crystalline material with yields of 79%, **2a**; 68%, **2b**; 76%, **2c**; 74%, **2d**. The reaction with PCy_3 was performed in CH_2Cl_2 but the crystallization was done in pentane. The compound **2b** melts to a purple liquid at room temperature.

$Fe(CO)_2(P^tBu_2Me)(\eta^2$-HFB) (2a)

F.W. 434.1

Elemental Analysis $C_{15}H_{21}F_6FeO_2P$; Calculated: C, 41.50%; H, 4.88%,

Observed: C, 41.35%; H, 4.89%.

IR (pentane, cm^{-1}) ν_{CO} 2012 (s), 1951(s); ν_{CC} 1740

^1H NMR (CD_2Cl_2, 400.1 MHz, 27 °C) δ 1.18 (d, $^3J_{HP}$ = 14 Hz, $PC(CH_3)_3$), 1.50 (d, $^2J_{HP}$ = 10 Hz, PCH_3)

^{19}F NMR ($\mathrm{CD_2Cl_2}$, 376.4 MHz, 27 °C) δ – 56.7 (s, $\mathrm{C}C\mathit{F}_3$)

^{31}P{^{1}H} NMR ($\mathrm{CD_2Cl_2}$, 161.9 MHz, 27 °C) δ 115.4 (s)

^{13}C{^{1}H} NMR ($\mathrm{CD_2Cl_2}$, 100.6 MHz, 27 °C) δ 217.1 (s, *C*O), 170.9 (q, $^2J_{CF} = 48$ Hz, *C*CF$_3$), 124.3 (q, $^1J_{CF} = 270$ Hz, C*C*F$_3$), 35.8 (d, $^1J_{CP} = 18$ Hz, P*C*(CH$_3$)$_3$), 28.3 (s, PC(*C*H$_3$)$_3$), 13.2 (d, $^1J_{CP} = 25$ Hz, P*C*H$_3$)

^{13}C{^{19}F} NMR ($\mathrm{CD_2Cl_2}$, 100.6 MHz, 27 °C) δ 217.1 (s, *C*O), 170.9 (s, *C*CF$_3$), 124.3 (s, C*C*F$_3$), 35.8 (br s, P*C*(CH$_3$)$_3$), 28.3 (q, $^1J_{CH} = 128$ Hz, PC(*C*H$_3$)$_3$), P*C*H$_3$ not observed.

Fe(CO)$_2$(P^{i}Pr$_3$)(η^2-HFB) (2b)

F.W. 434.053

EI-MS (*m/z*): 434.052 [M$^+$], 406.058 [M$^+$–CO], 387.059 [M$^+$–2CO].

IR (pentane, cm^{-1}) ν_{CO} 2011 (s), 1951(s) ν_{CC} 1735

^{1}H NMR ($\mathrm{CD_2Cl_2}$, 400.1 MHz, 27 °C) δ 1.15 (dd, $^3J_{HH} = 16$ Hz, $^3J_{HP} = 7$ Hz, PCC*H*$_3$), 1.93 (br m, PC*H*)

^{19}F NMR ($\mathrm{CD_2Cl_2}$, 376.4 MHz, 27 °C) δ – 56.3 (s, $\mathrm{C}C\mathit{F}_3$)

^{31}P{^{1}H} NMR ($\mathrm{CD_2Cl_2}$, 161.9 MHz, 27 °C) δ 127.2 (s)

^{13}C{^{1}H} NMR ($\mathrm{CD_2Cl_2}$, 100.6 MHz, 27 °C) δ 216.9 (d, $^2J_{CP} = 29$ Hz, *C*O), 172.2 (q, $^2J_{CF} = 46$ Hz *C*CF$_3$), 124.3 (q, $^1J_{CF} = 270$ Hz, C*C*F$_3$), 26.5 (d, $^1J_{CP} = 23$ Hz, P*C*H), 18.4 (s, PC*C*H$_3$).

Fe(CO)$_2$(PCy$_3$)(η^2-HFB) (2c)

F.W. 554.3

Elemental Analysis $\mathrm{C_{24}H_{33}F_6FeO_2P}$; Calculated: C, 52.00%; H, 6.00%, Observed: C, 52.18%; H, 6.11%.

IR (pentane, cm^{-1}) ν_{CO} 2009 (s), 1947(s) ν_{CC} 1734

^{1}H NMR ($\mathrm{CD_2Cl_2}$, 400.1 MHz, 27 °C) δ 0.90-1.85 (br, PC$_6$*H*$_{11}$)

^{19}F NMR (CD_2Cl_2, 376.4 MHz, 27 °C) $\delta - 56.4$ (s, CCF_3)

$^{31}P\{^1H\}$ NMR (CD_2Cl_2, 161.9 MHz, 27 °C) δ 116.9 (s)

$^{13}C\{^1H\}$ NMR (CD_2Cl_2, 100.6 MHz, 27 °C) δ 216.7 (d, $^2J_{CP} = 28$ Hz, *C*O),
171.1 (q, $^2J_{CF} = 43$ Hz CCF_3), 123.8 (q, $^1J_{CF} = 270$ Hz, CCF_3),
38.0 (d, $^1J_{CP} = 21$ Hz, PC_6H_{11}), 29.9 (d, $^3J_{CP} = 2$ Hz, PC_6H_{11}),
27.8 (d, $^2J_{CP} = 11$ Hz, PC_6H_{11}), 26.5 (s, PC_6H_{11})

$Fe(CO)_2(P^tBu_3)(\eta^2$-HFB) (2d)

F.W. 476.22

Elemental Analysis $C_{18}H_{27}F_6FeO_2P$; Calculated: C, 45.40%; H, 5.71%,

Observed: C, 45.15%; H, 5.78%.

IR (pentane, cm^{-1}) ν_{CO} 2005 (s), 1943(s) ν_{CC} 1730

^{1}H NMR (CD_2Cl_2, 400.1 MHz, 27 °C) δ 1.45 (d, $^3J_{HP} = 13$ Hz, $PC(CH_3)_3$)

^{19}F NMR (CD_2Cl_2, 376.4 MHz, 27 °C) $\delta - 56.2$ (s, CCF_3)

$^{31}P\{^1H\}$ NMR (CD_2Cl_2, 161.9 MHz, 27 °C) δ 148.2 (s)

$^{13}C\{^1H\}$ NMR (CD_2Cl_2, 100.6 MHz, 27 °C) δ 218.5 (d, $^2J_{CP} = 26$ Hz, *C*O),
170.4 (q, $^2J_{CF} = 42$ Hz CCF_3), 124.7 (q, $^1J_{CF} = 271$ Hz, CCF_3),
41.0 (d, $^1J_{CP} = 9$ Hz, $PC(CH_3)_3$), 31.8 (br s, $PC(CH_3)_3$).

2.5.4 X-ray Crystal Structure Determination of $Fe(CO)_2(PR_2R')_2(\eta^2$-HFB) (1a,b)

The crystal structure of **1c** has been previously determined [14].

Orange crystals of suitable quality of **1a,b** were eventually obtained by repeated cooling a concentrated pentane solution from –20 °C to –80 °C. Data collection and structure refinement were performed by Dr. M. J. Ferguson (**1a**) or Dr. R. McDonald (**1b**) of the X-ray Crystallography Laboratory, Department of Chemistry, University of Alberta. Crystals were mounted on a glass fiber and transferred to a goniometer. Data collection was carried out on a Bruker PLATFORM/SMART 1000 CCD (**1a**) or a Bruker P4/R4/SMART 1000 CCD (**1b**) diffractometer. Programs for diffractometer operation, data collection, data reduction and absorption correction were those supplied by Bruker. Unit cell parameters were obtained from least-squares refinement of 6052 (**1a**) or 3353 (**1b**) centered reflections. The structure was solved using a Patterson search/structure expansion (DIRDIF-96) [32] (**1a**) or direct methods/fragment search (DIRDIF-96) [32] (**1b**) method. Structure refinement was performed using a full-matrix least-squares on F^2 (SHELXL-93) [33] method for both structures. All non-hydrogen atoms were located. Hydrogen atoms were place in calculated positions and geometrically constrained during final refinement. Summaries of data collection parameters are presented in Tables 2-8, **1a**; Table 2-9, **1b**. Final atomic coordinates and displacement parameters may be obtained from X-ray Crystallography Laboratory, Department of Chemistry, University of Alberta with the file codes TAK 0106, **1a**; TAK 0004, **1b**; TAK 9603, **1c**.

Table 2-8 Crystallographic Experimental Details for Compound **1a**

formula	$C_{24}H_{42}F_6FeO_2P_2$
formula weight	594.37
crystal dimensions (mm)	0.54 × 0.38 × 0.36
crystal system	monoclinic
space group	$P2_1/c$ (No.14)
unit cell parameters	
a (Å)	10.5815 (6)
b (Å)	25.9255 (15)
c (Å)	10.9539 (6)
β (deg)	105.0159 (11)
V (Å^3)	2902.4 (3)
Z	4
ρ_{calcd} (g cm^{-3})	1.360
μ (mm^{-1})	0.687
radiation (λ [Å])	graphite-monochromated Mo Kα (0.71073)
temperature (°C)	- 80
scan type	ω scans (0.2°) (25 s exposures)
data collection 2θ limit (deg)	52.80
total data collected	15923 ($-13 \leq h \leq 9$, $-32 \leq k \leq 32$, $-12 \leq l \leq 13$)
independent reflections	5922 (R_{int} = 0.0200)
number of observed reflections (*NO*)	5254 [$F_o^2 \geq 2\sigma(F_o^2)$]
absorption correction method	empirical (*SADABS*)
range of transmission factors	0.7900-0.7079
data/restraints/parameters	5922 [$F_o^2 \geq -3\sigma(F_o^2)$] / 0 / 317
goodness of fit (S)[a]	1.022 [$F_o^2 \geq -3\sigma(F_o^2)$]
final R indices[b]	
R_1 [$F_o^2 \geq 2\sigma(F_o^2)$]	0.0349
wR_2 [$F_o^2 \geq -3\sigma(F_o^2)$]	0.0996
largest difference peak and hole	0.633 and -0.370 e Å^{-3}

[a] $S = [\Sigma w(F_o^2 - F_c^2)^2/(n - p)]^{1/2}$ (n = number of data; p = number of parameters varied; $w = [\sigma^2(F_o^2)+(0.0545P)^2 + 1.7681P]^{-1}$ where $P = ([\mathrm{Max}(F_o^2, 0) + 2F_c^2]/3)$.

[b] $R_1 = \Sigma||F_o| - |F_c||/\Sigma|F_o|$; $wR_2 = [\Sigma w(F_o^2 - F_c^2)^2/\Sigma w(F_o^4)]^{1/2}$

Table 2-9 Crystallographic Experimental Details for Compound **1b**

formula	$C_{24}H_{42}F_6FeO_2P_2$
formula weight	594.37
crystal dimensions (mm)	0.23 × 0.09 × 0.08
crystal system	monoclinic
space group	$P2_1/c$ (No.14)
unit cell parameters	
a (Å)	16.2498 (15)
b (Å)	11.6610 (11)
c (Å)	16.2866 (15)
β(deg)	110.542 (2)
V (Å^3)	2889.9 (5)
Z	4
ρ_{calcd} (g cm^{-3})	1.366
μ (mm^{-1})	0.690
radiation (λ([Å])	graphite-monochromated Mo Kα (0.71073)
temperature (°C)	- 80
scan type	ϕ rotations (0.3°)/ω scans (0.3°)(30 s exposures)
data collection 2θ limit (deg)	52.82
total data collected	14161 ($-20 \le h \le 15$, $-10 \le k \le 14$, $-15 \le l \le 20$)
independent reflections	5939
number of observed reflections (*NO*)	2478 [$F_o^2 \ge 2\sigma(F_o^2)$]
absorption correction method	*SADABS*
range of transmission factors	0.9486-0.6979
data/restraints/parameters	5939 [$F_o^2 \ge -3\sigma(F_o^2)$] / 0 / 324
goodness of fit (S)[a]	0.804 [$F_o^2 \ge -3\sigma(F_o^2)$]
final R indices[b]	
R_1 [$F_o^2 \ge 2\sigma(F_o^2)$]	0.0565
wR_2 [$F_o^2 \ge -3\sigma(F_o^2)$]	0.0996
largest difference peak and hole	0.337 and -0.328 e Å^{-3}

[a] $S = [\Sigma w(F_o^2 - F_c^2)^2/(n - p)]^{1/2}$ (n = number of data; p = number of parameters varied; $w = [\sigma^2(F_o^2)+(0.0189P)^2]^{-1}$ where $P = ([\mathrm{Max}(F_o^2, 0) + 2F_c^2]/3)$.

[b] $R_1 = \Sigma||F_o| - |F_c||/\Sigma|F_o|$; $wR_2 = [\Sigma w(F_o^2 - F_c^2)^2/\Sigma w(F_o^4)]^{1/2}$

2.5.5 X-ray Crystal Structure Determination of $Fe(CO)_2(PR_2R')(\eta^2\text{-HFB})$ (2a,d)

The crystal structure of **2c** has been previously completed in our laboratories[1c].

Deep purple crystals of **2a** or deep blue crystals of **2d** of suitable quality were obtained by repeated ~~cooling~~ a concentrated pentane solution from 0 °C to –30 °C or –80 °C. Data collection and structure refinement were performed by Dr. M. J. Ferguson (**2a**) or Dr. R. McDonald (**2d**) of the X-ray Crystallography Laboratory, Department of Chemistry, University of Alberta. Crystals were mounted on a glass fiber and transferred to a goniometer. Data collection was carried out on a Bruker P4/R4/SMART 1000 CCD diffractometer. Programs for diffractometer operation, data collection, data reduction and absorption correction were those supplied by Bruker. Unit cell parameters were obtained from least-squares refinement of 3714 (**2a**) or 3256 (**2d**) centered reflections. The structure was solved using a Patterson interpretation (SHELXS-86) [34] (**2a**) or direct methods/fragment search (DIRDIF-96) [32] (**2d**) method. Structure refinement was performed using a full-matrix least-squares on F^2 (SHELXL-93) [33] method for both structures. All non-hydrogen atoms were located. Hydrogen atoms were place in calculated positions and geometrically constrained during final refinement.

Summaries of data collection parameters are presented in Tables 2-10, **2a**; Table 2-11, **2d**. Final atomic coordinated and displacement parameters may be obtained from the X-ray Crystallography Laboratory, Department of Chemistry, University of Alberta with the file codes TAK 9907, **2a**; TAK 9811, **2c**; TAK 9912, **2d**.

Table 2-10 Crystallographic Experimental Details for Compound **2a**

formula	$C_{15}H_{21}F_6FeO_2P$
formula weight	434.14
crystal dimensions (mm)	0.26 × 0.06 × 0.05
crystal system	monoclinic
space group	$P2_1/c$ (No.14)
unit cell parameters	
a (Å)	8.8406 (6)
b (Å)	16.0620 (11)
c (Å)	13.8812 (9)
β (deg)	104.7950 (10)
V (Å^3)	1905.7 (2)
Z	4
ρ_{calcd} (g cm^{-3})	1.513
μ (mm^{-1})	0.936
radiation (λ [Å])	graphite-monochromated Mo Kα (0.71073)
temperature (°C)	- 80
scan type	ϕ rotations(0.3)/ω scans (0.3°) (30 s exposures)
data collection 2θ limit (deg)	51.40
total data collected	10156 ($-10 \le h \le 10$, $-18 \le k \le 19$, $-16 \le l \le 16$)
independent reflections	3623
number of observed reflections (*NO*)	2119 $[F_o^2 \ge 2\sigma(F_o^2)]$
absorption correction method	*SADABS*
range of transmission factors	0.9547-0.7895
data/restraints/parameters	3623 $[F_o^2 \ge -3\sigma(F_o^2)]$ / 0 / 226
goodness of fit (S)[a]	0.895 $[F_o^2 \ge -3\sigma(F_o^2)]$
final R indices[b]	
R_1 $[F_o^2 \ge 2\sigma(F_o^2)]$	0.0490
wR_2 $[F_o^2 \ge -3\sigma(F_o^2)]$	0.1153
largest difference peak and hole	0.515 and -0.410 e Å^{-3}

[a] $S = [\Sigma w(F_o^2 - F_c^2)^2/(n - p)]^{1/2}$ (n = number of data; p = number of parameters varied; $w = [\sigma^2(F_o^2)+(0.0506P)^2]^{-1}$ where $P = ([\mathrm{Max}(F_o^2, 0) + 2F_c^2]/3)$.

[b] $R_1 = \Sigma||F_o| - |F_c||/\Sigma|F_o|$; $wR_2 = [\Sigma w(F_o^2 - F_c^2)^2/\Sigma w(F_o^4)]^{1/2}$

Table 2-11 Crystallographic Experimental Details for Compound **2d**

formula	$C_{18}H_{27}F_6FeO_2P$
formula weight	476.22
crystal dimensions (mm)	0.30 × 0.14 × 0.09
crystal system	monoclinic
space group	$P2_1$/n (a nonstandard setting of $P2_1$/c [No. 14])
unit cell parameters	
a (Å)	8.4644 (7)
b (Å)	17.3678 (16)
c (Å)	14.8479 (14)
β (deg)	98.571 (2)
V (Å3)	1000.0 (10)
Z	4
ρ_{calcd} (g cm^{-3})	1.465
μ (mm^{-1})	0.834
radiation (λ [Å])	graphite-monochromated Mo Kα (0.71073)
temperature (°C)	- 80
scan type	ϕ rotations(0.3)/ω scans (0.3°) (30 s exposures)
data collection 2θ limit (deg)	51.40
total data collected	11443 ($-10 \le h \le 10$, $-19 \le k \le 21$, $-16 \le l \le 18$)
independent reflections	4108
number of observed reflections (NO)	2815 [$F_o^2 \ge 2\sigma(F_o^2)$]
absorption correction method	*SADABS*
range of transmission factors	0.9144-0.6315
data/restraints/parameters	4108 [$F_o^2 \ge -3\sigma(F_o^2)$] / 0 / 307
goodness of fit (S)[a]	0.921 [$F_o^2 \ge -3\sigma(F_o^2)$]
final R indices[b]	
R_1 [$F_o^2 \ge 2\sigma(F_o^2)$]	0.0397
wR_2 [$F_o^2 \ge -3\sigma(F_o^2)$]	0.0898
largest difference peak and hole	0.286 and -0.424 e Å^{-3}

[a] $S = [\Sigma w(F_o^2 - F_c^2)^2/(n - p)]^{1/2}$ (n = number of data; p = number of parameters varied; $w = [\sigma^2(F_o^2)+(0.0391P)^2]^{-1}$ where P = ([Max(F_o^2, 0) + $2F_c^2$]/3).

[b] $R_1 = \Sigma||F_o| - |F_c||/\Sigma|F_o|$; $wR_2 = [\Sigma w(F_o^2 - F_c^2)^2/\Sigma w(F_o^4)]^{1/2}$

2.6 References

1. (a) Mao, T. -F.; Zhang, Z.; Washington, J.; Takats, J.; Jordan, R. B. *Organometallics* **1999**, *18*, 2331. (b) Mao, T. -F. Ph. D. Thesis, University of Alberta, 1996, Chapters 2 and 3. (c) Cooke, J. Ph. D. Thesis, University of Alberta, 1998, Chapter 4.
2. Pearson, J.; Cooke, J.; Takats, J.; Jordan, R. B. *J. Am. Chem. Soc.* **1998**, *120*, 1434.
3. Caulton, K. G. *New J. Chem.* **1994**, *18*, 25.
4. Decker, S. A.; Klobukowski, M. *J. Am. Chem. Soc.* **1998**, *120*, 9342.
5. Rossi, A. R.; Hoffmann, R. *Inorg. Chem.* **1975**, *14*, 365.
6. (a) Barrow, M.; Cromhout, N. L.; Cunningham, D.; Manning, A. R.; McArdle, P. *J. Organomet. Chem.* **2000**, *612*, 61, (b) Gauss, C.; Veghini, D.; Berke, H. *Chem. Ber.* **1997**, *130*, 183. (c) Meier-Brocks, F.; Albrecht, R.; Weiss, E. *J. Organomet. Chem.* **1992**, *439*, 65. (d) Birk, R,; Berke, H.; Huttner, G.; Zsolnai, L. *Chem. Ber.* **1988**, *121*, 471.
7. Tolman, C. A. *Chem. Rev.* **1977**, *77*, 313.
8. (a) Li, C.; Ogasawara, M.; Nolan, S. P.; Caulton, K. G. *Organometallics* **1996**, *15*, 4900. (b) Ogasawara, M.; Macgregor, S. A.; Streib, W. E.; Folting, K.; Eisenstein, O.; Caulton, K. G. *J. Am. Chem. Soc.* **1996**, *118*, 10199.
9. Ogasawara, M.; Maseras, F.; Galleo-Planas, N.; Kawamura, K.; Ito, K.; Toyota, K.; Streib, W. E.; Komiya, S.; Eisenstein, O.; Caulton, K. G. *Organometallics* **1997**, *16*, 1979.
10. Stainer, M. V. R.; Takats, J. *Inorg. Chem.* **1982**, *21*, 4044.
11. Barnard, T. S.; Mason, M. R. *Inorg. Chem.* **2001**, *40*, 5001.

12. (a) Martin, L. R.; Einstein, F. W. B.; Pomeroy, R. K. *Inorg. Chem.* **1983**, *22*, 1959. (b) Martin, L. R.; Einstein, F. W. B.; Pomeroy, R. K. *Inorg. Chem.* **1985**, *24*, 2777.

13. Filippou, A. C.; Rosenauer, T. *Angew. Chem. Int. Ed. Engl.* **2002**, *41*, 2393.

14. Washington, J. unpublished results.

15. (a) Harris, R. K. *Can. J. Chem.* **1964**, *42*, 2275. (b) Verkade, J. G.; McMarley, R. E.; Hendricker. D. G.; King, R. W. *Inorg. Chem.* **1965**, *4*, 228.

16. (a) Barrow, M.; Cromhout, N. L.; Manning, A. R.; Gallagher, J. F. *J. Chem. Soc., Dalton Trans.* **2001**, 1352. (b) Birk, R.; Grössmann, U.; Hund, H. –U.; Berke, H. *J. Organomet. Chem.* **1988**, *345*, 321.

17. (a) Mann, B. E.; Taylor, B. F. *^{13}C NMR Data for Organometallic Compounds*; Academic: New York, 1981; pp 151-182. (b) Crabtree, R. H. *The Organometallic Chemistry of the Transition Metals*; Wiley-interscience: New york, 2001; Chapter 10. (c) Chisholm, M. H.; Godleski, S *Prog. Inorg. Chem.* **1976**, *20*, 299. (d) Gansow, O. A.; Vernon, W. D. In *Topics in Carbon-13 NMR Spectroscopy*; Levy, G. C., Ed.; Wiley-Interscience: New York, 1976; Chapter 5.

18. Chisholm, M. H.; Clark, H. C.; Manzer, L. E.; Stothers, J. B. *J. Am. Chem. Soc.* **1972**, *94*, 5087.

19. Templeton, J. L. *Adv. Organomet. Chem.* **1989**, *29*, 1.

20. Lukehart, C. M. *Fundamental Transition Metal Organometallic Chemistry*; Brooks/Cole: Monterey, CA, 1985; pp 160-162.

21. Berney, C. V.; Cousins, L. R.; Miller, F. A. *Spectrochim. Acta* **1963**, *19*, 2019.

22. Ball, R. G.; Burke, M. R.; Takats, J. *Organometallics* **1987**, *6*, 1918.

23. Boncella, J. M.; Green, M. L. H. *J. Organomet. Chem.* **1987**, *325*, 217.

24. Marinelli, G.; Streib, W. E.; Huffman, J. C.; Caulton, K. G.; Gagné, M. R.; Takats, J.; Dartiguenave, M.; Chardon, C.; Jackson, S. A.; Eisenstein, O. *Polyhedron* **1990**, *9*, 1867.

25. Ricard, L.; Weiss, R.; Newton, W. E.; Chen, G. J.-J.; McDonald, J. W. *J. Am. Chem. Soc.* **1978**, *100*, 1318.

26. Harris, T. V.; Rathke, J. W.; Muetterties, E. L. *J. Am. Chem. Soc.* **1978**, *100*, 6966.

27. (a) Carbó, J. J.; Crochet, P.; Esteruelas, M. A.; Jean, Y.; Lledós, A.; López, A. M.; Oñate, E. *Organometallic* **2002**, *21*, 305. (b) Crochet, P.; Esteruelas, M. A.; López, A. M.; Ruiz, N.; Tolosa, J. I. *Organometallics* **1998**, *17*, 3479. (c) Esteruelas, M. A.; López, A. M.; Ruiz, N.; Tolosa, J. *Organometallics* **1997**, *16*, 4657.

28. Espuelas, J.; Esteruelas, M. A.; Lahoz, F. J.; López, A. M.; Oro, L. A.; Valero, C. *J. Organomet. Chem.* **1994**, *468*, 223.

29. (a) Perrin, D. D.; Armarego, W. L. F.; Perrin, D. R. *Purification of Laboratory Chemicals*; Pergamon: New York, 1980. (b) Harwood, L. M.; Moody, C. J. *Experimental Organic Chemistry: Principles and Practice*; Blackwell: Oxford, 1992.

30. The procedure for the preparation of P^tBu_2Me was kindly provided by A. Cooper (Ph. D. Thesis, Indiana University, 1997) and K. G. Caulton (Department of Chemistry, Indiana University, Bloomington, Indiana). Caulton has indicated that the procedure was adapted from the preparation of PEt_2Ph described in Adams, D. M.; Raynor, J. B. *Advanced Practical Inorganic Chemistry*; John Wiley and Sons: London, 1965; p. 116.

31. Cooke, J. Ph. D. Thesis, University of Alberta, 1996, Chapter 2

32. Beurskens, P. T.; Beurskens, G; Bosman, W. P.; de Gelder, R.; Garcia Granda, S.; Gould, R. O.; Israel, R; Smits, J.M. (1996). The DIRDIF-96 program system. Crystallography Laboratory, University of Nijmegen, The Netherlands.

33. Sheldrick, G. M. SHELXL-93. Program for crystal structure determination. University of Göttingen, Germany, 1993.

34. Sheldrick, G. M. *Acta Crystallogr.* **1990**, **A46**, 467.

Chapter 3

Reactions of Four Electron Donor Alkyne $Fe(CO)_2(PR_2R')(\eta^2\text{-HFB})$ Complexes with Allenes: The Serendipitous Discovery of Metal Mediated Alkyne-Allene Coupling

3.1 Introduction

Continuing studies in the Takats laboratories with $M(CO)_4(\eta^2\text{-alkyne})$ (M = Fe, Os) complexes have shown that these compounds react with alkynes to form alkyne-alkyne and alkyne-carbonyl coupled products [1]. In particular, Cooke has shown that $Fe(CO)_4(\eta^2\text{-HFB})$ slowly reacts at ambient temperature with additional HFB to give a cyclopentadienone complex (Eq. 3-1) [2].

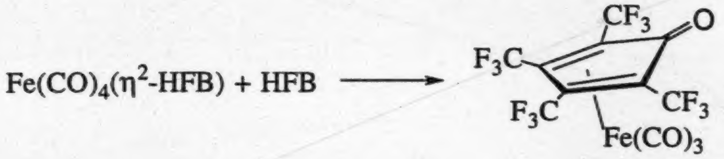

(3-1)

In 1962, Wilkinson *et al.* showed that the yellow-orange crystals of this product could be isolated from reaction of $Fe(CO)_5$ and excess HFB at high temperatures and high pressures [3]. In 1970 Green *et al.* produced the parallel products $Fe(CO)_2(PR_2R')\{\eta^4\text{-}C_4(CF_3)_4(CO)\}$ (R = Me, R′ = Ph; R, R′ = OEt) by photolysis of $Fe(CO)_3(PR_2R')_2$ in the presence of excess HFB [4]. Thus it appears that the presence of a coordinated phosphine or phosphite ligand does not hinder the coupling ability of these complexes. In light of these results it was of interest to explore the alkyne-alkyne coupling capabilities of the four electron donor compounds **2a-d**. It was felt that the kinetic barrier to a second alkyne coordination, presumably the first step in alkyne-alkyne coupling [5], would be small since coordination of two-electron donors, *i.e.* CO and PR_3, has already been demonstrated to be facile, even at low temperatures (Chapter 2). Furthermore it was anticipated that the formation of the C–C bonds in the product would provide the thermodynamic force that would drive the reaction to completion.

3.2 Experimental Aspects

3.2.1 Initial Attempts

Reactions were carried out between **2a-d** with a variety of alkynes and olefins (terminal, internal and diynes/dienes) in a manner that is similar to that described for the reaction with phosphines (Chapter 2). A pentane solution of **2a-d** was allowed to warm slowly from –78 °C to room temperature in the presence of an excess of alkyne. The reaction was monitored by FT-IR spectroscopy. Throughout the warming no color change occurred and no reaction was indicated by IR spectroscopy. Once the solution reached ambient temperature the reaction mixture was allowed to stir for several days. After a few days the solution began to show the familiar signs of decomposition; deposition of a precipitate and darkening of the solution. Results were not promising as the IR spectrum of the solution was very similar to that obtained for the near complete decomposition of isolated **2a-d**. Solvent extraction and NMR spectroscopic characterization of the resulting residue indicated a number of compounds and from the reaction of **2c** with 2-butyne a few crystals of $Fe(PCy_3)(CO)_2\{\mu\text{-}\eta^1,\eta^1\text{:}\eta^4\text{-}CF_3CC(CF_3)C(CF_3)CCF_3\}Fe(CO_3)$ were isolated. Clearly **2a-d** did not react with alkynes but instead slowly decomposed to give a number of products that were identical to the decomposition products in the absence of a second alkyne.

Just when it appeared that many months of work would end with no results, again, reaction of a pentane solution of **2a** with excess propyne at –78 °C resulted in a rapid color change from deep purple to bright yellow. The IR spectrum showed two strong terminal ν_{CO} IR bands in the same region as the starting material but at distinctly different frequencies. Reaction of **2b-c** with propyne gave very similar results while no reaction with **2d** was indicated. The latter result was not altogether unexpected because, as discussed in Chapter 2, **2d** failed to react with CO or a second equivalent of phosphine. Nevertheless, it appeared that a reaction of **2a-c** with propyne had occurred. Strangely though, a mixture of **2a** and perfluoropropyne under identical conditions did not give any indication of reaction. Even more puzzling, a repeat of reaction of **2a** with one, two or three equivalents of propyne did not exhibit any indication of reaction. It seemed that the reaction with propyne would only occur when a very large excess of the alkyne was present. After work-up of the crude reaction product, yellow crystals were isolated and structural elucidation, including X–ray crystal structure analysis, was carried out. The results showed that the product did not contain propyne ($HC{\equiv}C{-}CH_3$) but rather the isomeric allene ($H_2C{=}C{=}CH_2$) moiety. A quick analysis of the propyne source revealed that it contained small amounts of allene, suggesting that it was allene and not propyne that reacted with **2a–c**. Indeed reaction of **2a–c** with one equivalent of high purity allene gave the yellow compounds in high yield. To examine the effect of substituents the reaction of **2a–c** with methylallene and 1,1-dimethylallene were also carried out and the results are described in this chapter.

3.2.2 Reaction of $Fe(CO)_2(PR_2R')(\eta^2$-HFB) with Allenes; Experimental Observations

In a typical synthesis, **2a-c** were treated with excess allene or methylallene (~1:50) or one equivalent of liquid 1,1-dimethylallene. With gaseous allenes, a 50 mL Schlenk flask was evacuated and back filled with allene (~ 1 atm). The flask was then sealed and taken to –78 °C. At this temperature the allenes condensed to a colorless liquid. The flask was backfilled with a nitrogen atmosphere and a 30 mL pentane solution of **2a-c** was cannula transferred into the flask. The deep purple solution of **2a-c** turned to a bright yellow color almost immediately. The reaction with methylallene or 1,1-dimethylallene took slightly longer and turned to a bright orange color. The solution was slowly brought to room temperature over a period of 15 minutes at which time the IR spectrum indicated that all the starting material had been consumed. The solution was taken to 0 °C and the solvent was removed, *in vacuo*, leaving a yellow solid-residue which was dissolved in a minimum amount of pentane at 0 °C and crystallized at –30 to –80 °C. In most cases, and with some experience, large, crystallographer friendly, crystals in good yield (75 – 95 %) were obtained. The reaction with 1,1-dimethylallene was performed in a similar manner except that its liquid form allowed the delivery of one equivalent *via* a syringe into a pentane solution of **2a–c**.

As will be shown, the reaction proceeded by C–C bond formation between HFB and the central carbon of the allene moiety and the products contain the η^1,η^3-2-vinylallyl ligand (Eq. 3-2). Thus, the formulation of the compounds is $Fe(CO)_2(PR_2R')(\eta^1,\eta^3\text{-}\{F_3CC{=}C(CF_3)C(CH_2)CR^1R^2\})$ with labels shown in Table 3-1, for ease and convenience in future discussion.

$$\mathbf{2a\text{-}c} + H_2C{=}C{=}R^1R^2 \longrightarrow Fe(CO)_2(PR_2R')(\eta^1,\eta^3\text{-}\{F_3CC{=}C(CF_3)C(CH_2)CR^1R^2\})$$

$R^1, R^2 = H$; **4a-c** (3-2)
$R^1 = H, R^2 = Me$; **5a-c**
$R^1, R^2 = Me$; **6a-c**

Table 3-1 $Fe(CO)_2(PR_2R')(\eta^1,\eta^3\text{-}\{F_3CC{=}C(CF_3)C(CH_2)CR^1R^2\})$ Compounds

	R = ^{t}Bu R′ = Me	R, R′ = ^{i}Pr	R, R′ = Cy
$R^1, R^2 = H$	**4a**	**4b**	**4c**
$R^1 = H, R^2 = Me$	**5a**	**5b**	**5c**
$R^1, R^2 = Me$	**6a**	**6b**	**6c**

The compounds **4a-c** and **5a-c** are thermally sensitive in solution and begin to show decomposition after a few hours at ambient temperature, while **6a-c** are more stable and only begin to show decomposition after 24 hours. The complexes that contain the PCy_3 ligand tend to be more stable than the complexes that contain P^iPr_3 or P^tBu_2Me. In the solid state, the compounds are much more robust and can be easily handled in air at ambient temperature for several hours.

3.3 Characterization of $Fe(CO)_2(PR_2R')(\eta^1,\eta^3\text{-}\{F_3CC{=}C(CF_3)C(CH_2)_2\})$ (4a-c)

The molecular formulation of **4a-c** was based on elemental microanalysis.

The IR spectrum of **4a-c** showed two terminal carbonyl stretches with an intensity pattern indicative of a *cis*-carbonyl arrangement [6] (Table 3-2). The IR spectrum of **4a** initially showed two bands (2014, 1963 cm^{-1}) but after 30 minutes two additional bands (2018, 1968 cm^{-1}) were observed at a frequency that was very close to the initial bands (Figure 3-1). This phenomenon was not observed in the IR spectrum of **4b** or **4c** and was the first indication of isomerism in **4a-c**, *vide infra*.

Table 3-2 FT-IR Data (cm^{-1}, pentane) in the Carbonyl Region of **4a-c**

Compound	ν_{CO}
4a	2014 (s), 1963 (s)
	2018 (s), 1968 (s)
4b	2015 (s), 1964 (s)
4c	2011 (s), 1960 (s)

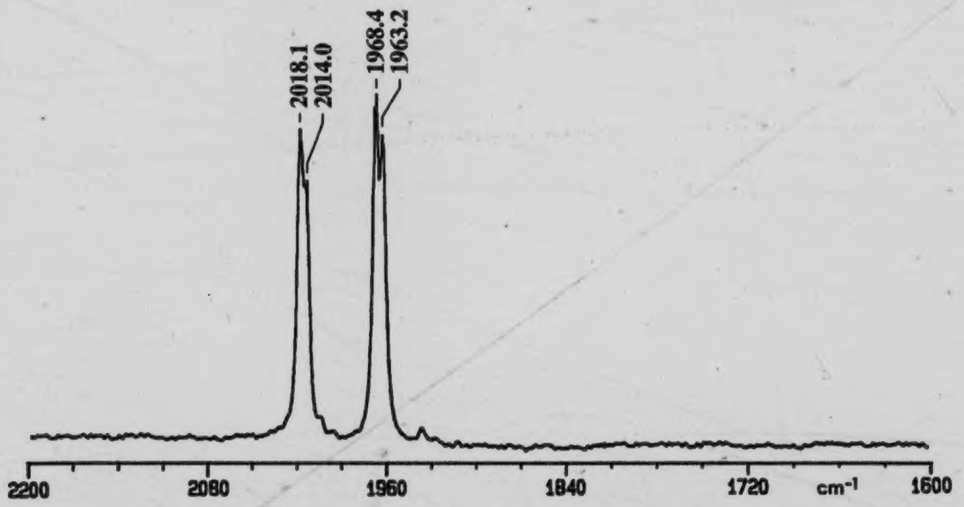

Figure 3-1 FT-IR Solution Spectrum of **4a** (cm^{-1}, pentane).

The NMR data revealed some intriguing and complex behavior. The spectra were too complicated for the presence of only one compound and were more indicative of the existence of two isomeric species in solution. Before the collection of additional NMR data or analysis of the initial NMR data could be completed, successful X-ray crystal structure analyses, which were invaluable in the elucidation of the solution chemistry, were obtained. In order to facilitate discussion of the complex behavior of **4a-c** in solution the crystal structure results will be discussed first.

3.3.1 X-ray Crystal Structure Analysis of $Fe(CO)_2(PR_2R')(\eta^1,\eta^3\text{-}\{F_3CC{=}C(CF_3)C(CH_2)_2\})$ (4a-c)

Figure 3-2 displays the solid state molecular structure of **4a** with atom labeling scheme, while Table 3-3 lists selected interatomic distances and angles. The positions of the hydrogen atoms of the phosphine ligand have been omitted for clarity. There is some minor disorder in the positions of the three fluorine atoms attached to C6. Two positions were calculated for each fluorine and designations of "A" and "B" were assigned; *e.g.* F4A, F4B, etc. Each position was allotted an occupancy of 50%. The figure shows the positions of the "A" designation only.

The crystal structure results of **4a** showed some surprising features. Four ligands are coordinated to the iron center; two carbonyls, the P^tBu_2Me ligand, and, most interestingly, a chelating η^1,η^3-2-vinylallyl ligand. Thus, the reaction between **2a** and allene proceeded by coupling between HFB and allene and the formation of a C–C bond between one of the acetylenic carbons of the HFB and the central allene carbon. The geometry about the iron center is best described as a distorted octahedron. The tridentate vinylallyl ligand perforce occupies one face of the octahedron, such that the P^tBu_2Me ligand is *trans* to the Fe–C4 vector. The C4–Fe–P vector is roughly orthogonal to the equatorial plane defined by Fe, C1, C2, C7 and C9.

Formally, the metal is Fe(II), and contributes six to the electron count, while the vinylallyl and each of the carbonyls and P^tBu_2Me contributes six and two, respectively, to the electron count. Thus, the iron atom achieves a saturated 18 electron configuration.

The geometry about the iron center in **4a** can be described as octahedral. The Fe–C4 and Fe–P vectors are largely perpendicular with respect to the equatorial plane.

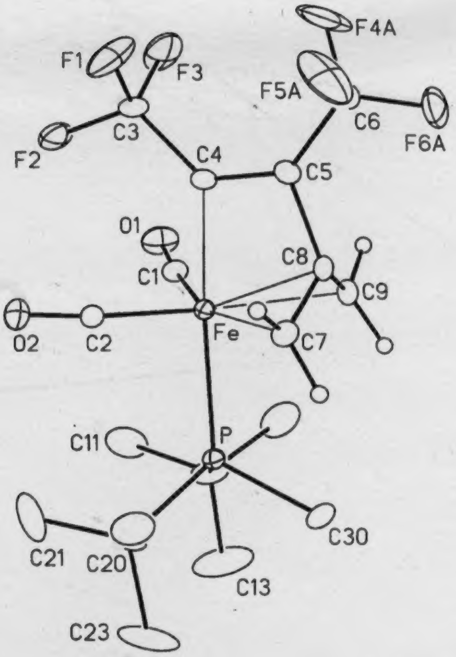
F4A
F1
F3
F5A
C6
F6A
F2
C3
C4
C5
O1
C8
C1
C9
O2
C2
Fe
C7
C11
P
C30
C21
C20
C13
C23

Figure 3-2 Solid State Molecular Structure of **4a.**

Table 3-3 Selected Interatomic Distances (Å) and Angles (deg.) in **4a**.

Fe–P	2.3844(7)	P–Fe–C2	95.6(1)
Fe–C1	1.778(2)	P–Fe–C4	176.1(1)
Fe–C2	1.765(2)	P–Fe–C7	91.2(1)
Fe–C4	2.019(2)	P–Fe–C9	91.6(1)
Fe–C7	2.168(2)	C1–Fe–C2	99.9(1)
Fe–C8	2.051(2)	C1–Fe–C4	85.4(1)
Fe–C9	2.156(2)	C1–Fe–C9	93.9(1)
C4–C5	1.321(4)	C2–Fe–C4	86.6(1)
C5–C8	1.498(3)	C2–Fe–C7	96.1(1)
C7–C8	1.400(3)	C4–Fe–C7	85.4(1)
C8–C9	1.408(3)	C4–Fe–C9	85.5(1)
O1–C1	1.142(3)	C7–Fe–C9	68.8(1)
O2–C2	1.150(3)	Fe–C1–O1	173.2(2)
P–Fe–C1	97.4(1)	Fe–C2–O2	174.7(2)

However, the carbonyls bend upwards slightly, toward the vinyl moiety and away from the phosphine ligand. The C4–Fe–Cn (n = 1, 2) angles are 85-86° while the P–Fe–Cn (n = 1, 2) angles are about 96°. Moreover, the carbonyls show a noticeable deviation from linearity with the Fe–Cn–On (n = 1, 2) angles being about 174°. The P–Fe–Cn (n = 7, 9) angles are essentially ideal, but the C4–Fe–Cn (n = 7, 9) angles are about 5° less than 90°. The cause of these latter distortions are not clear. While we have seen how the P^tBu_2Me bulky phosphine can be quite sterically demanding (Chapter 2), the steric and geometric requirements of the chelating 2–vinylallyl ligand are unknown since no structures with this ligand bound to a mononuclear center are reported in the literature. It may very well be that the C4–Fe–Cn (n = 7, 9) angles are slightly smaller than ideal because of geometric constraints of the vinylallyl ligand. A larger distortion occurs in the equatorial plane. While the C1–Fe–C9 angle and the opposite C2–Fe–C7 angle of 93.9(1)° and 96.1(1)°, respectively, and are nearly equal, the C1–Fe–C2 angle of 99.9(1)° is considerable larger than the 68.8(1)° of the opposite C7–Fe–C9 angle. This is clearly due to the geometric constraints of the η^3-allyl fragment of the vinylallyl ligand as demonstrated by a number of known solid stated molecular structures with simple terminal η^3-allyl ligands. In these known structures the H_2C–Fe–CH_2 angles are invariably in the narrow 61–75° range [7].

Although the overall geometry of the molecular structures of **4b** and **4c** were similar to that of **4a**, the distribution of the ligands show are some interesting differences. The structures **4b** and **4c** are similar and as such **4b** will serve as a representative example. Figure 3-3 displays the molecular structure of **4b** with atom labeling scheme (omitting the hydrogen atoms of the phosphine ligand) and Table 3-4 lists selected interatomic distances and angles.

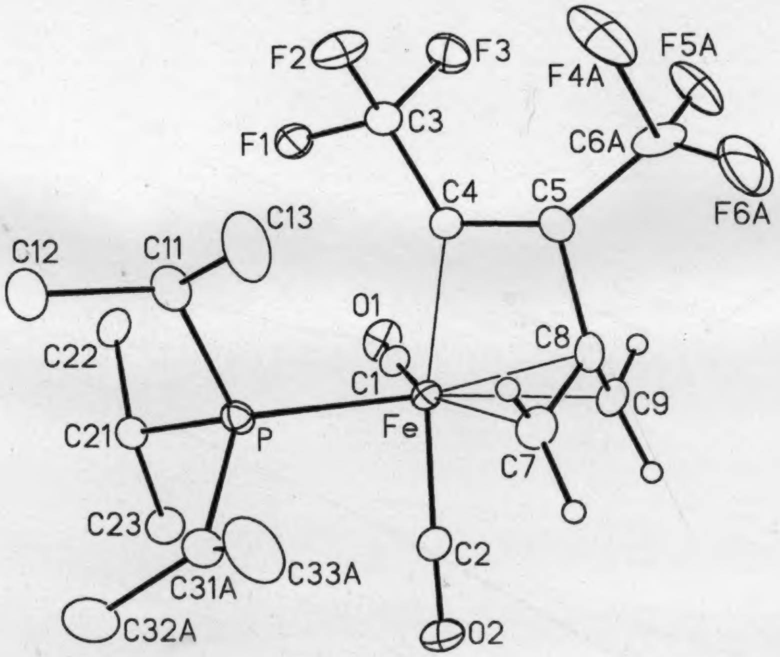
F2
F3
F4A
F5A
F1
C3
C6A
C4
C5
F6A
C13
C12
C11
O1
C8
C22
C1
C9
C21
P
Fe
C7
C23
C2
C31A
C33A
C32A
O2

Figure 3-3 Solid State Molecular Structure of **4b.**

Table 3-4 Selected Interatomic Distances (Å) and Angles (deg.) in **4b**.

Fe–P	2.3032(8)	P–Fe–C2	90.5(1)
Fe–C1	1.763(3)	P–Fe–C4	98.0(1)
Fe–C2	1.782(3)	P–Fe–C7	98.3(1)
Fe–C4	2.039(3)	C1–Fe–C2	94.0(1)
Fe–C7	2.180(3)	C1–Fe–C4	88.0(1)
Fe–C8	2.056(3)	C1–Fe–C9	93.1(1)
Fe–C9	2.170(3)	C2–Fe–C4	170.7(1)
C4–C5	1.320(4)	C2–Fe–C7	88.5(1)
C5–C8	1.496(4)	C2–Fe–C9	85.0(1)
C7–C8	1.401(4)	C4–Fe–C7	86.6(1)
C8–C9	1.398(4)	C4–Fe–C9	85.8(1)
O1–C1	1.147(3)	C7–Fe–C9	67.4(1)
O2–C2	1.142(3)	Fe–C1–O1	175.8(3)
P–Fe–C1	101.4(1)	Fe–C2–O2	176.4(3)

As with **4a**, the structure of **4b** also exhibits some disorder of the CF_3 group attached to the β-carbon of the vinyl group and, in addition, some disorder of the positions of one of the ^{i}Pr groups of the phosphine ligand. For each atom involved two positions were calculated and designated A or B, and each position was given an occupancy of 50%. Only the A-positions are shown in the figure.

The structure shows the presence of the same number and type of ligands as seen in **4a**; two carbonyls, a phosphine ligand and a 2-vinylallyl ligand, but in the structures of **4b**, and **4c**, one of the carbonyls is now *trans* to the α-carbon (C4) of the vinyl moiety, while the phosphine ligand is in an equatorial position and roughly *trans* to one terminus of the allyl moiety (C9). The reason for this may be a function of the phosphine ligand. In **4a** (Figure 3-2) the $P^{t}Bu_2Me$ phosphine ligand is able to occupy coordination site *trans* to C4 by minimizing the steric interaction between the phosphine ligand and the allyl moiety. It does this by positioning the relatively small Me substituent (C30) adjacent to, and between, the two terminus (C7 and C9) of the allyl moiety (torsional angles; C30–Fe–P–Cn = –36.1(1)° and 32.8(1)° for n = 7 and 9, respectively), while in **4b** the $P^{i}Pr_3$ ligand with its larger ^{i}Pr substituents, relative to Me, is forced into an equatorial position in which one terminus of the allyl moiety (C7) is positioned adjacent to, and roughly between two ^{i}Pr substituents (C11 and C31A) of the $P^{i}Pr_3$ ligand (torsional angles; C7–Fe–P–Cn = 76.2(1)° and –41.4(4)° for n = C11 and C31A, respectively). In this way **4b** is able to minimize the steric interaction between the allyl moiety and the phosphine ligand.

The geometry in **4b** is best described as a distorted octahedral. Positioning the bulky phosphine ligand in the equatorial plane causes the P–Fe–C4 angle (98.0(8)°) to be greater than ideal by 8° while the P–Fe–C2 angle (90.5(1)°) remains virtually ideal. Presumably, this is a result of steric interaction between the phosphine ligand and the vinyl moiety. The effect on the equatorial carbonyl is small as the C1–Fe–Cn (n = 2, 4) angles are within 4° of ideal. In regards to the vinylallyl ligand, the C4–Fe–Cn (n = 7, 9) angles show conformity to the related angles in **4a** as they are about 86°. Considering the position of the phosphine ligand in **4b** the angles within the equatorial plane show a similar pattern to that observed in **4a**. The difference between the C1–Fe–C9 and P–Fe–C7 angles is small at 5°. As expected the P–Fe–C7 angle is the larger of the two, while the difference between the C1–Fe–P and C7–Fe–C9 angles is 33.96(15)°. Here again the allyl C7–Fe–C9 angle is within the range indicated by the previously mentioned known complexes with simple η^3-allyl ligands [7].

The most interesting ligand in **4a-c** is the rarely observed chelating 2-vinylallyl ligand. Chelated allyl compounds are a subclass of simple η^3-allyl compounds. A good range of chelated allyl compounds of iron are known and several crystal structures have been reported [8]. In the case of mononuclear iron compounds the vast majority of structures are based on an octahedral geometry about the iron center with one face occupied by simple two electron donor ligands, usually carbonyls, and the second by the "bidentate" η^1,η^3-allyl ligand. The η^3-allyl group is connected to a 2-4 atom chain, usually carbon, that is η^1 bound to the metal. Figure 3-4 shows two examples of the more commonly encountered structures of this type. Compound **A** [9] exhibits a structure in which the allyl is within a bicyclic framework while, **B** [10] shows a typical structure in the absence of a fused ring system. The 2-vinylallyl ligand observed in **4a-c** is a rare find for three reasons. First, the η^1-chain of the chelating allyl ligand is most often comprised of a 3 atom linkage [8, 11]. A two atom chain is uncommon and usually only observed in systems in which the allyl is part of a fused ring system (**A**). Secondly, relatively few examples are know in which the central atom of the allyl acts as the bridgehead carbon of the η^1-chain [12]. In the vast majority of cases the η^1-chain is bound to a terminus of the allyl and is in an *anti*–orientation with respect to the metal. Lastly, while a vinyl or olefinic functionality along the η^1-chain are not unknown, they are relatively rare [13].

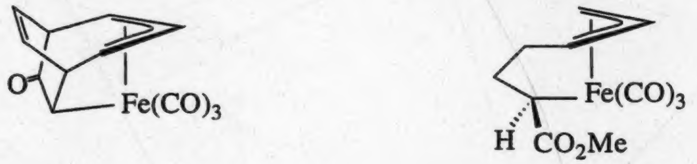

A **B**

Figure 3-4 Iron Carbonyl Compounds with Chelating Allyl Ligands.

The structural features of the vinylallyl ligand in the molecular structures of **4a-c** show a conformity to known molecular structures with simple vinyl or simple ally ligands. Considering the vinyl part first, the average of the Fe–C4 separations in **4a-c** (2.033(7) Å) is within the range (1.995 – 2.030 Å) indicated by several crystal structures of known Fe(II) d^6 complexes that contain a simple vinyl (Fe–CR=CR_2) linkage [14]. In addition, the C4–C5 distances are identical, within the group, and the average value for the group (1.320 (4) Å) is within the range indicated by the known structures (1.30-1.35 Å) and within the 4 esd's of the accepted C_{sp^2}–C_{sp^2} double bond separation of 1.334(3) Å [15]. The Fe–C4–C5 angles are, however, considerably smaller than the related parameter in the above mentioned literature structures [14]. This value in **4a-c** (average value 99.0(5)°) is smaller by about 26-30° and is the result of the geometrical constraints of the chelating vinylallyl ligand. In the literature structures the vinyl is monodentate and is "dangling" free, and the angle is closer to the expected value associated with sp^2 hybridization at the α-carbon, while in **4a-c** the β-carbon of the vinyl is highly constricted to a location near the iron (Fe$\cdots$C5 = 2.586(3) Å) by the ligation of the allyl moiety. The carbon backbone of the vinyl moiety is planar in **4a** and **4c** while near planar in **4b,** as the C3–C4–C5–C6 torsional angles are 0.7 (5), 2.4(6)° and 9.5(10)/14.1(9), respectively. Two values are quoted for **4b** because of the disorder, *vide supra*, associated with the CF_3 group attached to the β-carbon of the vinyl moiety. The allyl part of the vinylallyl ligand is largely unremarkable as there are no significant differences between the structural parameters within the group. As a group they correlate well with the principal structural features found in simple η^3-allyl compounds from the chemical literature [16]; the allylic carbons are typically sp^2 hybridized and the angles about the central carbon are 120° ± 5°, the C–C separations are typically about 1.40 Å, and the $M–C_{terminal}$ distances are greater than the $M–C_{central}$ distance by about 0.1 Å.

The C5–C8 linkage bridges the vinyl and allyl moieties. The average value of the C5–C8 separations in **4a-4c** (1.499 (3) Å) is slightly longer than the 1.44-1.48 Å range of a $C_{sp^2}–C_{sp^2}$ single bond with about 15% double bond character [17]. Moreover, the average value of the C5–C8 distances in **4a-4c** is close to the $C_{sp^2}–C_{sp^2}$ single bond separation between the olefin and cyclohexadienyl in the π–cyclohexadienyl–σ-propenoyl bridging linkage in $Fe(CO)_2\{\eta^5,\eta^1\text{-}C(O)CH{=}CHC_6H_6\}$ (Figure 3-5) [18]. Thus, the π-systems of the vinyl and allyl moieties in **4a-c** do not interact, that is, the π-bonding of the vinyl and of the allyl group do not extend over the C5–C8 linkage.

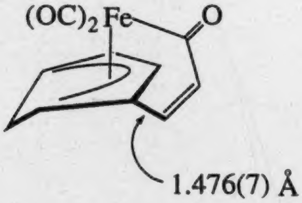

Figure 3-5 Iron Carbonyl Compound with a Cyclohexadienyl Chelating Ligand.

With the solid state molecular structures in-hand we now return to the discussion of the solution behavior of the compounds.

3.3.2 Initial NMR Spectroscopic Analysis of $Fe(CO)_2(P^tBu_2Me)(\eta^1,\eta^3\text{-}\{F_3CC{=}C(CF_3)C(CH_2)_2\})$ (4a)

The NMR data of **4a** are shown in Table 3-5. The $^{31}P\{^1H\}$ and ^{19}F NMR data indicated the presence of two compounds in solution. The $^{31}P\{^1H\}$ NMR spectrum of **4a** showed two singlets δ 68.2 and 71.1 ppm of intensity ratio 3:1, respectively. The ^{19}F NMR spectrum showed four signals; one set of dominant signals and a set of smaller signals, again, the intensity ration between the two sets was 3:1. The larger set of signals consisted of a doublet of quartets at δ –58.0 ppm and a quartet at δ –64.7 ppm, while the smaller set of signals appeared as a quartet at δ –53.5 ppm and a doublet of quartets at δ –65.2 ppm. Each of the doublet of quartets collapse into quartets upon selectively decoupling the ^{31}P resonances. This decoupling indicates that the doublet of quartets at δ –58.0 and –65.2 ppm were part of the same molecule as the ^{31}P signals at δ 68.2 and 71.1 ppm, respectively. The fluorine–fluorine coupling ($^5J_{FF}$) was determined to be 8 Hz for the dominant signals, while a $^5J_{FF} = 9$ Hz was observed for the set of smaller signals. Since the elemental analysis, %C and %H, are consistent with the proposed formulation it is clear that these two compounds are isomers. The major isomer is labeled **4aI** and the minor isomer is labeled **4aII**.

The ^1H NMR spectrum of **4aI** (Figure 3-6) also showed a set of decidedly dominant signals and a set of smaller signals. Considering the resonances of the major isomer, **4aI**, the downfield region showed a singlet at δ 3.34 ppm and a doublet at δ 2.25 ppm. In light of the crystal structure results these signals are consistent with two chemically equivalent *syn*- and *anti*-hydrogens, respectively, of an allyl group.

Table 3-5 The $^{31}P\{^1H\}$, ^{19}F, ^1H and $^{13}C\{^{19}F\}$ NMR Data (ppm, CD_2Cl_2, 27 °C) of **4aI** and **4aII**

Compound	$^{31}P\{^1H\}$	^{19}F	^1H	$^{13}C\{^{19}F\}$/*$^{13}C\{^1H\}$APT
4aI	68.2	− 58.0 dq $^5J_{FF}$ = 8 Hz	3.34 s H_{syn}	217.1 d $^2J_{CP}$ = 16 Hz CO
(major isomer)		J_{FP} = 3 Hz	2.25 d $^3J_{HP}$ = 9 Hz H_{anti}	151.9 d $^2J_{CP}$ = 17 Hz $C_\alpha(CF_3)$
		− 64.7 q $^5J_{FF}$ = 8 Hz	1.35 d $^3J_{HP}$ = 12 Hz $PC(\mathit{CH}_3)_3$	135.5 s $C_\beta(CF_3)$
			0.90 d $^2J_{HP}$ = 6 Hz $P\mathit{CH}_3$	125.4 s CF_3
				117.0 s CF_3
				86.6* br s $C_{central}$
				70.9* s CH_2
				36.3* d $^1J_{CP}$ = 14 Hz $P\mathit{C}(CH_3)_3$
				29.9* (–) d $^2J_{CP}$ = 3 Hz $PC(\mathit{CH}_3)_3$
				6.5* (–) d $^1J_{CP}$ = 16 Hz $P\mathit{CH}_3$
4aII	71.1	− 53.5 q $^5J_{FF}$ = 9 Hz	3.57 dd $^4J_{HH}$ = 3 Hz	217.4 d $^2J_{CP}$ = 7 Hz CO
(minor isomer)		− 65.2 dq $^5J_{FF}$ = 9 Hz	$^3J_{HP}$ = 3 Hz H_{syn}	215.1 d $^2J_{CP}$ = 20 Hz CO
		J_{FP} = 3 Hz	3.05 d $^4J_{HH}$ = 3 Hz H_{syn}	155.8 d $^2J_{CP}$ = 19 Hz $C_\alpha(CF_3)$
			2.37 s H_{anti}	134.3 s $C_\beta(CF_3)$
			2.09 s H_{anti}	126.6 s CF_3
			1.43 d $^2J_{HP}$ = 8 Hz $P\mathit{CH}_3$	117.8 s CF_3
			1.35 d $^3J_{HP}$ = 13 Hz $PC(\mathit{CH}_3)_3$	85.4* br s $C_{central}$
			1.31 d $^3J_{HP}$ = 13 Hz $PC(\mathit{CH}_3)_3$	70.3* s CH_2
				66.3* d $^2J_{CP}$ = 10 Hz CH_2
				30.2* (–) d $^2J_{CP}$ = 4 Hz $PC(\mathit{CH}_3)_3$
				29.7* (–) d $^2J_{CP}$ = 4 Hz $PC(\mathit{CH}_3)_3$
				11.6* (–) d $^1J_{CP}$ = 15 Hz $P\mathit{CH}_3$

Indeed, the typical chemical shifts for *syn*-proton resonances in an η^3-allyl ligand are δ 2-5 ppm while that for *anti*-protons are 1-3 ppm [19]. Substitution at the central carbon does not have a significant influence on these values [12c, 20]. The three bond ^1H-^{31}P coupling of the doublet was confirmed by selectively decoupling the ^{31}P resonance at δ 68.2 ppm. Not surprisingly a two bond H_{syn}–H_{anti} coupling is not observed as these are typically found to be small; $^2J_{H_{syn}H_{anti}} = 0 - 2$ Hz [19b]. Upfield of these signals the spectrum shows two doublets at δ 1.35 and 0.90 ppm. These signals are consistent in intensity and chemical shift with the protons of two chemically equivalent ^{t}Bu groups and a methyl group of the phosphine ligand, respectively. The $^3J_{HP}$ and $^2J_{HP}$ was confirmed by selectively decoupling the ^{31}P resonance at δ 68.2 ppm. The ^1H NMR data of the major isomer are fully consistent with the crystal structure and a C_s symmetry solution structure.

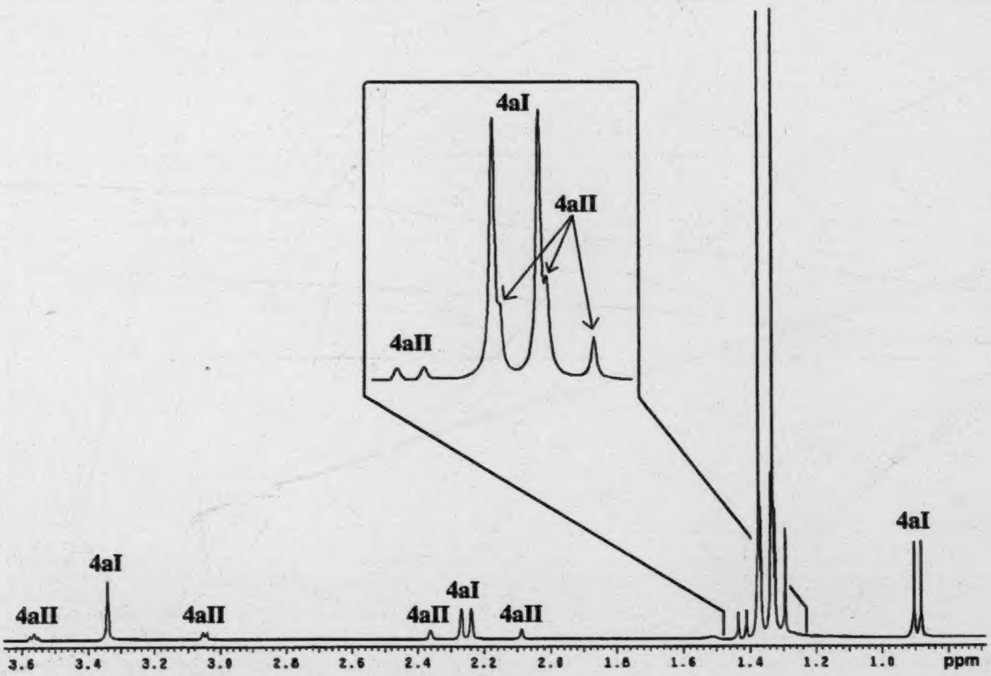

Figure 3-6 ^1H NMR Spectrum (ppm, CD_2Cl_2) of **4a**.

The ^1H NMR spectrum of isomeric **4aII** suggest quite a different structure. The spectrum shows four signals that are consistent in intensity and chemical shift with a set of chemically inequivalent *syn*- and *anti*-protons of an η^3-allyl group. The signals associated with the *syn*-hydrogens are located at δ 3.57 and 3.05 ppm and appear as a triplet and a doublet, respectively. The pseudotriplet at δ 3.57 ppm is in reality a doublet of doublets. The $^1H\{^{31}P$; 71.1 ppm$\}$ spectrum shows this signal as a doublet thus confirming ^1H-^{31}P coupling. In addition, the $^1H\{^1H$; 3.05 ppm$\}$ spectrum shows this signal also to be a doublet thus confirming ^1H-^1H coupling. Furthermore, the doublet at δ 3.05 ppm appears as a singlet when the δ 3.57 ppm signal is selectively decoupled. It is clear that the two *syn*-protons are spin-spin coupled through a four bond linkage. The signals associated with the *anti*-hydrogens are observed as singlets at δ 2.37 and 2.09 ppm. Turning to the resonances of the substituents of the phosphine ligand, the signal for the methyl protons and the signal of one of the ^tBu groups are clearly visible and appear as doublets, due to coupling to phosphorus. However, the resonance of the second ^tBu substituent is nearly coincident with the ^tBu resonance of the major isomer and is masked by this dominant signal. However, upon selectively decoupling the ^{31}P signal at 71.1 ppm the signal for the second ^tBu group of the minor isomer collapses into a singlet and appears within the doublet of the ^tBu groups of the major isomer, at δ 1.35 ppm. One interesting observation is that the resonance of the methyl protons is observed much further downfield (δ 1.43 ppm) than the corresponding signal of the major isomer (δ 0.90 ppm). The ^1H resonances associated with the phosphine substituents show a pattern that is consistent with the phosphine ligand bound to a chiral auxiliary moiety; two chemically inequivalent ^tBu groups (diastereotopic) and a Me group with a 3:3:1 intensity ratio. Clearly the ^1H spectrum of **4aII** suggests an asymmetric structure

(Figure 3-7). By interchanging the positions of one carbonyl and the phosphine ligand of the crystal structure so that the carbonyl is *trans* to the α-carbon of the vinyl group and the phosphine ligand is in an equatorial position one obtains an asymmetric structure that is analogous to the solid state molecular structures of **4b** and **4c**, and is a geometric isomer of **4aI** (Figure 3-7). The ^1H data of the minor isomer is fully consistent with this structure.

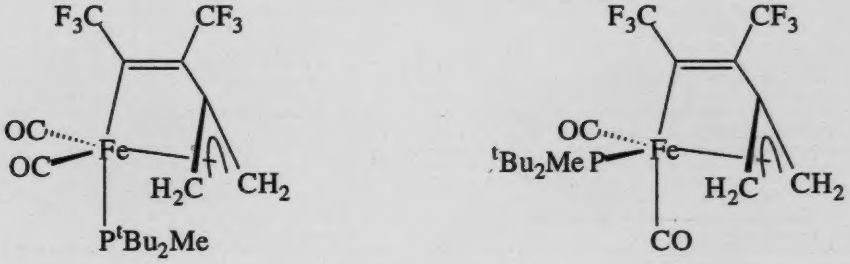

4aI **4aII**

Figure 3-7 Structures of the Major Isomer **4aI** (*left*) and Minor Isomer **4aII** (*right*). (*enantiomers not shown*)

The $^{13}C\{^{19}F\}$ and $^{13}C\{^1H\}$APT (Attached Proton Test) NMR spectra of **4aI** and **4aII** are also in accord with two isomers in solution. It was discovered that the $^{13}C\{^{19}F\}$ spectra gave the best data for the vinyl part of the molecules, while the $^{13}C\{^1H\}$ NMR spectra gave the best data for the allyl part of the molecules (Table 3–5). The $^{13}C\{^{19}F\}$ NMR spectrum from δ 60-220 ppm is displayed in Figure 3-8.

First, considering the resonances of the major isomer **4aI** in the carbonyl region, as expected, for two chemically equivalent carbonyls, there is a single doublet, obviously due to the major isomer, at δ 217.1 ppm.

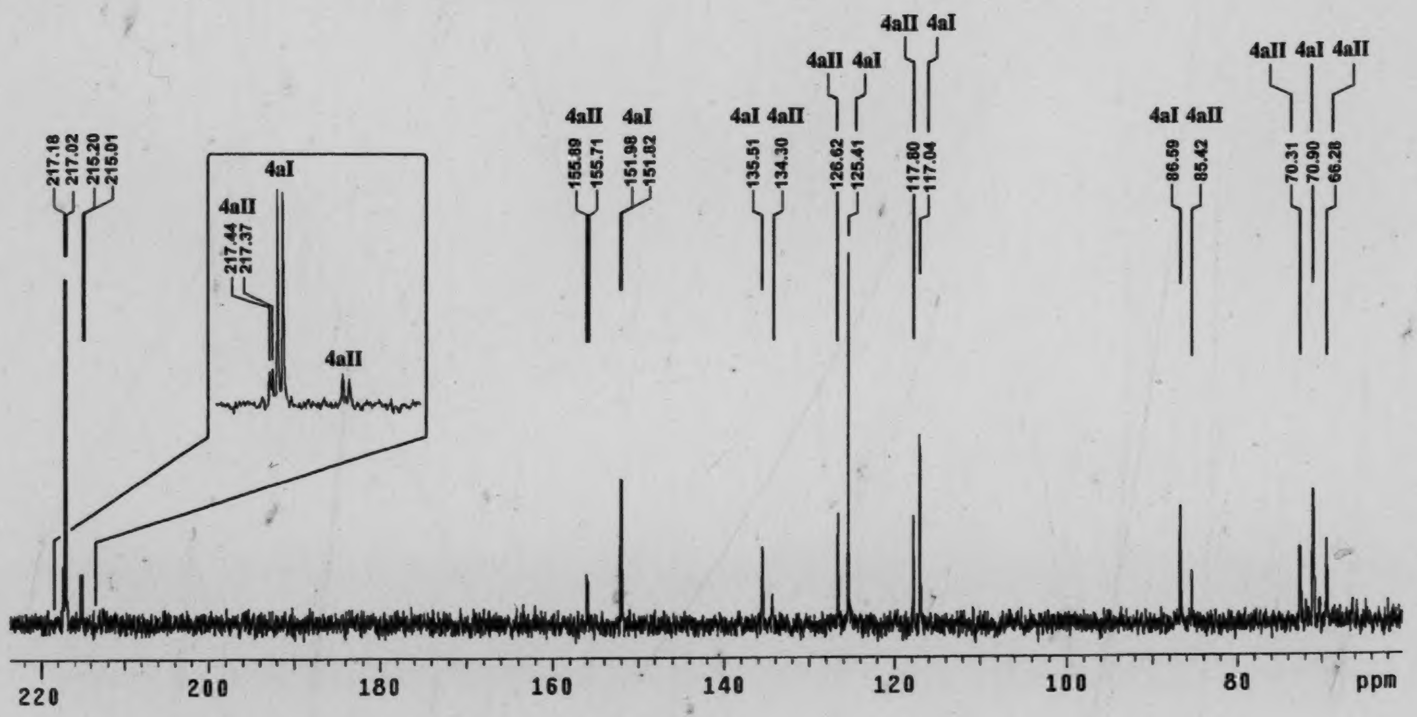

Figure 3-8 The $^{13}C\{^{19}F\}$ NMR Spectrum (60-220 ppm, CD_2Cl_2) of 4a.

The doublet multiplicity is due to two bond coupling to ^{31}P. This was shown by selectively decoupling the ^{31}P nucleus ($^{13}C\{^{31}P\}$). The α- and β-carbons of the vinyl group were not observed in the $^{13}C\{^{1}H\}$APT spectrum but were observed in the $^{13}C\{^{19}F\}$ spectrum. A doublet at δ 151.9 ppm was assigned to the α-carbon (C_α) of the vinyl group while the resonance of the β-carbon appears at δ 135.5 ppm (C_β). Both signals are in the wide range (δ 130–170 ppm) for the chemical shift of the α- and β–carbons in simple Fe(II) vinyl complexes from the chemical literature [14b-d, 21]. However the doublet is obviously due to coupling to the phosphorus nuclei which would support the assignment of the lowfield signal to the α-carbon. Moreover, in the HMBC (Heteronuclear Multiple Bond Correlation) spectrum the *syn*- and *anti*-protons at δ 3.34 and 2.25 ppm correlate with the δ 135.5 ppm resonance and not the δ 151.9 ppm signal. This further corroborates assignment of the highfield resonance to the β–carbon of the vinyl. Two quartets with large one bond carbon-fluorine coupling constants were observed at δ 125.4 ($^{1}J_{CF}$ = 274 Hz) and 117.0 ($^{1}J_{CF}$ = 273 Hz) ppm in the $^{13}C\{^{1}H\}$APT NMR spectrum. These signals are assigned to the carbons of the CF_3 substituents of the vinyl group. Upon ^{19}F decoupling the quartets collapse into singlets. The resonances of the allyl moiety were also identified. Typically, the central carbon of an η^3-bonded allyl appears downfield of the terminal carbons [19a, 22]. This suggest that the signal at δ 86.6 ppm is due to the central carbon of the allyl group ($C_{central}$). This signal showed no correlation to proton signals in the HMQC (Heteronuclear Multiple Quantum Correlation), suggesting no directly bonded hydrogens, but did exhibit a correlation with the *syn*- and *anti*-proton signals at δ 3.34 and 2.25 ppm in the HMBC spectrum. This correlation is consistent with a two bond coupling between the *syn*- and *anti*-protons, and the central carbon of the ally group. The terminal carbons (CH_2) of the allyl group give rise to a single signal at δ 70.9 ppm which was observed to correlate with the *syn*- and *anti*-protons in the HMQC spectrum, suggesting a direct ^{13}C-^{1}H coupling. The single resonance for the two termini of the allyl indicate chemical equivalence and is consistent with C_s symmetry in the molecule. The ^{13}C resonances of the phosphine substituents were identified through a number of experiments: $^{13}C\{^{1}H\}$APT, HMQC, and HMBC. Most notably, the two ^{t}Bu groups were found to be chemically equivalent and gave rise to one resonance for each type of carbon. The ^{13}C NMR data for the major isomer supports the ^{1}H NMR data and is indicative of a structure with C_s symmetry.

The $^{13}C\{^{19}F\}$ and $^{13}C\{^{1}H\}$ NMR spectra (Table 3-5) of the minor isomer, **4aII**, were in accord with an asymmetric structure. Two doublets, at δ 217.4 and 215.1 ppm, signaled the presence of two chemically inequivalent carbonyls. The α- and β-carbons of the vinyl group were located at chemical shifts that are similar to those shown by the major isomer for the related carbons. The β-carbon of the vinyl group (δ 134.3 ppm) was observed to correlate with both of the chemically distinct *anti*-protons of the allyl in the HMBC spectrum. The carbons of the CF_3 groups and the central carbon of the allyl were clearly observed, and at a chemical shift similar to those of the major isomer. Asymmetry of the complex was further corroborated by two signals at δ 70.3 and 66.3 ppm which were assigned to two chemically inequivalent terminal carbons of the allyl group. The assignment of these signals was confirmed as they were observed to correlate with both the *syn*- and *anti*-protons in the HMQC spectrum. The two resonances at δ 30.2 and 29.7 ppm were assigned to the chemically inequivalent primary carbons of the ^{t}Bu groups (diastereotopic). These signals could not be confirmed by HMQC because overlap on the ^{1}H axis with signals of the major isomer occurred. The assignment of these signals is based on the qualitative intensity, relative to each other and to the corresponding carbon resonance of the major isomer ($\delta = 29.9$ ppm), and on the inverted form of these signals in the $^{13}C\{^{1}H\}$APT, indicating one or three hydrogens attached to the carbon. The quaternary carbons of the ^{t}Bu groups ($PC(CH_3)_3$) could not be observed in the ^{13}C NMR spectrum. However, a correlation in the HMBC spectrum indicated that the protons of the methyl substituent are connected through scalar coupling to the δ 37.8 ppm position in the ^{13}C spectrum. In the major isomer, the resonance of the quaternary carbons of the phosphine ligand were observed near this position. The signal of a second quaternary carbon signal could not be located. However, it is possible that it is very near δ 37.8 ppm and not resolved in the HMBC spectrum. The carbon of the methyl substituent of the phosphine ligand was observed at δ 11.6 ppm and was found to correlate with its attached protons in the HMQC spectrum.

The NMR data for **4a** shows that two isomers exist in solution (**4aI** and **4aII**). Clearly, the intensity of one set of signals dominate the spectrum. These dominant signals are fully consistent with the crystal structure obtained for **4a**. Thus **4aI** has the structure shown in Figure 3-7. In regards to the minor signals in the NMR spectra, one might predict, in light of the crystal structures of **4b** and **4c**, that the minor compound is the geometric isomer of **4aI** in which a carbonyl is now trans to the α-carbon of the vinyl moiety and the phosphine ligand is in an equatorial position. Indeed the NMR data supports this conclusion and the structure of **4aII** is given in Figure 3-7.

Surprisingly, by conducting several NMR experiments on solutions of **4aI/4aII** it was discovered that different samples of crystals gave different proportions of the two isomers. Crystals that were crystallized directly from the reaction at very low temperatures (–78 °C) consistently showed **4aII** to be the dominant isomer in solution. Over time, and quickly at room temperature, nearly all **4aII** converts to **4aI**. Complete conversion was never observed and a final ratio of between 5:1 and 10:1 in favor of

4aI was reached. The conversion of **4aII** to **4aI** is complicated by the decomposition of one or both species at room temperature over a few days. The conversion of **4aII** to **4aI** is slow on the NMR time scale as resonances for both isomers are relatively sharp, even at ambient temperature. Material that was obtained from crystallization over long periods of time at −20 °C, or higher temperatures, consistently showed NMR spectra in which **4aI** dominates. Again these mixtures showed a conversion of **4aII** to **4aI** with a product ratio identical to that found above at which time decomposition sets in.

These observations suggest that in the reaction of $Fe(CO)_2(P^tBu_2Me)(\eta^2$-HFB) with allene the kinetic product is **4aII** which then converts to the thermodynamically preferred isomer **4aI**. In an attempt to observe this process from the beginning, an experiment was conducted in which the starting materials were combined in THF-d_8 at −78 °C and the reaction was followed by variable temperature $^{31}P\{^1H\}$, ^{19}F and ^1H NMR spectra from −110 °C to ambient temperature (+27 °C). The NMR spectra obtained revealed some very interesting results.

3.3.3 Low Temperature and Variable Temperature NMR Studies of $Fe(CO)_2(P^tBu_2Me)(\eta^1,\eta^3\text{-}\{F_3CC{=}C(CF_3)C(CH_2)_2\})$ (4a)

The following procedure was performed to follow the reaction of $Fe(CO)_2(P^tBu_2Me)(\eta^2$-HFB), **2a**, and allene by variable temperature NMR spectroscopy. Excess allene was condensed into an NMR tube at −78 °C. A THF-d_8 solution of **2a**, prepared at −78 °C, was cold cannula transferred into the NMR tube. The deep purple solution turned yellow within a few minutes. The NMR tube was then transferred to the NMR probe which was already at a temperature of −110 °C. The ^1H, $^{13}C\{^1H\}$, $^{31}P\{^1H\}$ and ^{19}F NMR spectra were recorded at this temperature. The sample was then taken to progressively warmer temperatures and the ^1H, $^{31}P\{^1H\}$ and

^{19}F were taken at various temperature intervals. At 0 °C and +27 °C the ^{13}C{^{1}H} was again recorded. The ^{31}P{^{1}H}, ^{19}F, ^{1}H and ^{13}C{^{1}H} NMR data at −110 °C, −10 °C and 27 °C are listed in Tables 3.6 and 3.7.

The variable temperature ^{31}P{^{1}H} spectra are shown in Figure 3-9. At −110 °C the spectrum shows two signals at δ 75.5 and 65.9 ppm, labeled **4aII′** and **4aII″**, with an intensity ratio of 0.7:1, respectively. Surprisingly, neither of these signals are at the chemical shift indicative of **4aI** or **4aII** and have not been previously observed. Trace amounts of unidentified compounds were also detected at δ 78.4, 72.8 and 64.4 ppm but will be ignored. Upon progressively warming the sample the dominant resonances showed the characteristic features of stereochemical nonrigidity; broadening of signals, intensity build-up between signals, coalescence, and finally a sharpening of the averaged signal. The coalescence at higher temperatures indicate that the two signals at lower temperatures belong to two species with the same chemical formulation. The initial signals at δ 75.5 and 65.9 ppm (−110 °C) combined to give the averaged resonance at δ 70.6 ppm (−10 °C), which is shifted to δ 71.1 ppm at +27 °C. This resonance was previously assigned to **4aII**. At −10 °C small amounts of **4aI** are detected, and at +27 °C, as previously observed, the near complete conversion of **4aII** to **4aI** occurs. If the warming of the sample is stopped at −10 °C and the temperature lowered, the low temperature spectra are completely reproducible. However, the conversion of **4aII** to **4aI** was not observed to be reversible.

The variable temperature ^{31}P{^{1}H} NMR spectrum has shown that **4aII** forms prior to **4aI** but it has also shown that the spectra of **4aII** at the higher temperatures (≥ −10 °C) is actually an averaged spectra of two compounds (**4aII′** and **4aII″**) and that these compounds are in a fast isomerization process.

Table 3-6 The $^{31}P\{^1H\}$, ^{19}F, ^1H and $^{13}C\{^1H\}$ (carbonyl region) NMR Data (ppm, THF-d_8, −10°C, −110°C) of **4aII**, **4aII′** and **4aII″**

Compound	$^{31}P\{^1H\}$	^{19}F	^1H	$^{13}C\{^1H\}$
		−110 °C		
4aII′	65.9	− 52.9 s	3.79 br s H_{syn}	219.1 br *CO*
(major		− 65.7 s	3.11 br s H_{syn}	215.4 br d $^2J_{CP}$ = 18 Hz *CO*
conformer)			2.49 br s H_{anti}	
			2.31 br s H_{anti}	
4aII″	75.5	− 53.8 s	3.48 br s H_{syn}	219.1 br *CO*
(minor		− 64.1 s	3.20 br s H_{syn}	216.4 br d $^2J_{CP}$ = 19 Hz *CO*
conformer)			2.77 br s H_{anti}	
			2.32 br s H_{anti}	
		−10 °C		
4aII	70.6	− 53.2 s	3.63 dd $^4J_{HH}$ = 3 Hz	218.4 d $^2J_{CP}$ = 7 Hz *CO*
		− 65.1 s	$^3J_{HP}$ = 3 Hz H_{syn}	215.9 br d $^2J_{CP}$ = 20 Hz *CO*
			3.06 d $^4J_{HH}$ = 3 Hz H_{syn}	
			2.47 s H_{anti}	
			2.17 s H_{anti}	
			1.49 d $^2J_{HP}$ = 7 Hz PCH_3	
			1.38 d $^3J_{HP}$ = 13 Hz $PC(CH_3)_3$	
			1.32 d $^3J_{HP}$ = 13 Hz $PC(CH_3)_3$	

Table 3-7 The $^{31}P\{^{1}H\}$, ^{19}F, ^{1}H and $^{13}C\{^{1}H\}$ (carbonyl region) NMR Data (ppm, THF-d_8, 27 °C) of **4aI** and **4aII**

Compound	$^{31}P\{^{1}H\}$	^{19}F	^{1}H	$^{13}C\{^{1}H\}$
4aI	69.8	− 58.4 dq $^{5}J_{FF} = 8$ Hz,	3.35 s H_{syn}	218.0 d $^{2}J_{CP} = 16$ Hz CO
		$J_{FP} = 3$ Hz	2.34 d $^{3}J_{HP} = 9$ Hz H_{anti}	
		− 65.2 q $^{5}J_{FF} = 8$ Hz	1.38 d $^{3}J_{HP} = 12$ Hz $PCCH_3$	
			0.96 d $^{2}J_{HP} = 6$ Hz PCH_3	
4aII	71.1	− 53.8 dq $^{5}J_{FF} = 9$ Hz	3.62 dd $^{4}J_{HH} = 3$ Hz	218.2 d $^{2}J_{CP} = 8$ Hz CO
		$J_{FP} = 1$ Hz	$^{3}J_{HP} = 3$ Hz H_{syn}	215.9 br CO
		− 65.6 dq $^{5}J_{FF} = 9$ Hz	3.04 d $^{4}J_{HH} = 3$ Hz H_{syn}	
		$J_{FP} = 2$ Hz	2.46 s H_{anti}	
			2.14 s H_{anti}	
			1.47 d $^{2}J_{HP} = 8$ Hz PCH_3	
			1.37 d $^{3}J_{HP} = 12$ Hz $PC(CH_3)_3$	
			1.32 d $^{3}J_{HP} = 13$ Hz $PC(CH_3)_3$	

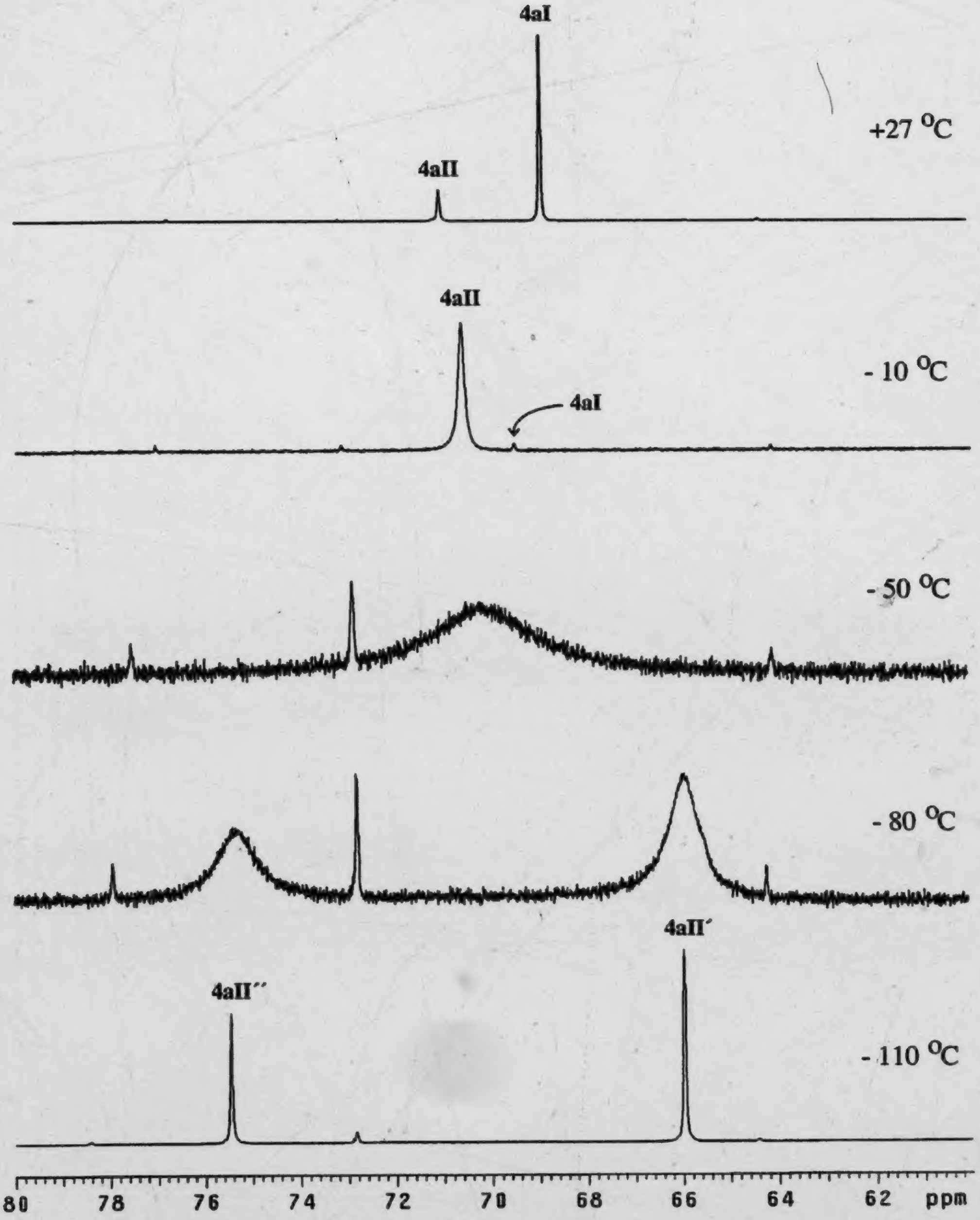

Figure 3-9 The Variable-Temperature $^{31}P\{^{1}H\}$ NMR Spectra (ppm, THF-d_8) of the Reaction of **2a** with Allene.

Furthermore, the low temperature $^{31}P\{^1H\}$ NMR data (–110 °C) shows that **4aII′** and **4aII″** are chemically inequivalent. As will be discussed shortly, the ^{19}F, $^{13}C\{^1H\}$ and ^1H NMR data support these conclusions and further elucidated the behavior of these compounds in solution. In particular it is the ^1H NMR spectra that were instrumental in revealing the true nature of the relationship between **4aII′**, **4aII″** and **4aII**.

It will be shown that **4aII′** and **4aII″** are the result of slowed dynamic process of the P^tBu_2Me ligand, more specifically slowed rotation about one or more bonds involving the phosphine ligand. It is proposed that **4aII′** and **4aII″** are conformers and at –110 °C rotation is slowed to the extent that these two rotomers are effectively "frozen out", on the NMR time scale, and these compounds can be characterized at this temperature. Upon warming the solution, free rotation of the phosphine ligand occurs, rapid interconversion between the two conformers proceeds, and an "averaged" structure, **4aII**, and spectrum is observed. This is followed by the slow, on the NMR time scale, and irreversible conversion of **4aII** to **4aI**.

Slow rotation involving the P^tBu_2Me ligand is known in the chemical literature. Bushweller *et al.* investigated the intramolecular stereodynamics of a number of P^tBu_2R type ligands, including P^tBu_2Me, in four coordinate square planar Pd(II), Pt(II), Rh(I) and Ir(I) complexes using, among other techniques, dynamic ^{31}P and ^{13}C NMR spectroscopy [23]. They have shown that rotation about the M–P and/or P–C bonds in these complexes is fast, on the NMR time scale, at or near room temperature, but at low temperature rotation can be slow. The ^{31}P and ^{13}C NMR spectra were interpreted in terms of slow exchange between different conformers. Caulton *et al.* have detected hindered M–P rotation in P^tBu_2Me in five and six coordinate Ru or Ir complexes using dynamic ^{31}P NMR spectroscopy [24], and observed slow rotation (on the NMR time scale) at room temperature [24c]. Again the results were interpreted in terms of interconversion of conformers.

Returning to **4a**, the ^{19}F NMR variable temperature spectra are consistent with the conclusions derived from the ^{31}P{^{1}H} NMR results with respect to a stereochemically nonrigid process occurring between **4aII′** and **4aII″** and a conversion of these two compounds into **4aI**. At −110 °C four signals are observed. Two signals at δ −52.9 and −65.7 ppm, with an intensity ratio of 1:1, are assigned to **4aII′** and two signals at δ −53.8 and −64.1 ppm with an intensity ratio of 0.7:0.7 are assigned to **4aII″**. Upon warming, the spectra show coalescence of the −52.9 and −53.8 ppm, and of the −65.7 and −64.1 ppm signals. These signals sharpen at room temperature to give the resonances that were previously assigned to **4aII**. In terms of structure it is clear that the two CF_3 groups of each **4aII′** and **4aII″** are chemically inequivalent.

The ^{13}C{^{1}H} spectra were recorded at −110 °C, −10 °C and +27 °C. The most useful region was found to be the carbonyl region (Figure 3-10). At −110 °C three signals were observed and it was concluded, based on intensity measurements, that the broad signal at δ 219.0 ppm is comprised of two carbonyls signals, one from each **4aII′** and **4aII″**. The signal at δ 216.3 ppm, possibly a doublet with an estimated $^{2}J_{CP}$ = ~20 Hz, is due to one carbonyl of **4aII″** while the δ 215.40 ppm resonance is clearly a doublet ($^{2}J_{CP}$ = 18 Hz) and is assigned to a carbonyl of **4aII′**. The resonance at δ 213.2 ppm is due to the central carbon of free allene in solution. Two CO signals for each compound are consistent with a structure that was originally proposed for **4aII**, *i.e.* an asymmetric structure with the α-carbon of a vinyl group *trans* to a carbonyl, while the phosphine ligand and the other carbonyl occupy positions in the equatorial plane (Figure 3-7). The spectrum at −10 °C shows two doublets of equal intensity, consistent with **4aII′** and **4aII″** in fast isomerization, *i.e.* **4aII**. At +27 °C the spectrum shows the dominant signal of **4aI** with a small amount of **4aII′** and **4aII″**, again in fast isomerization.

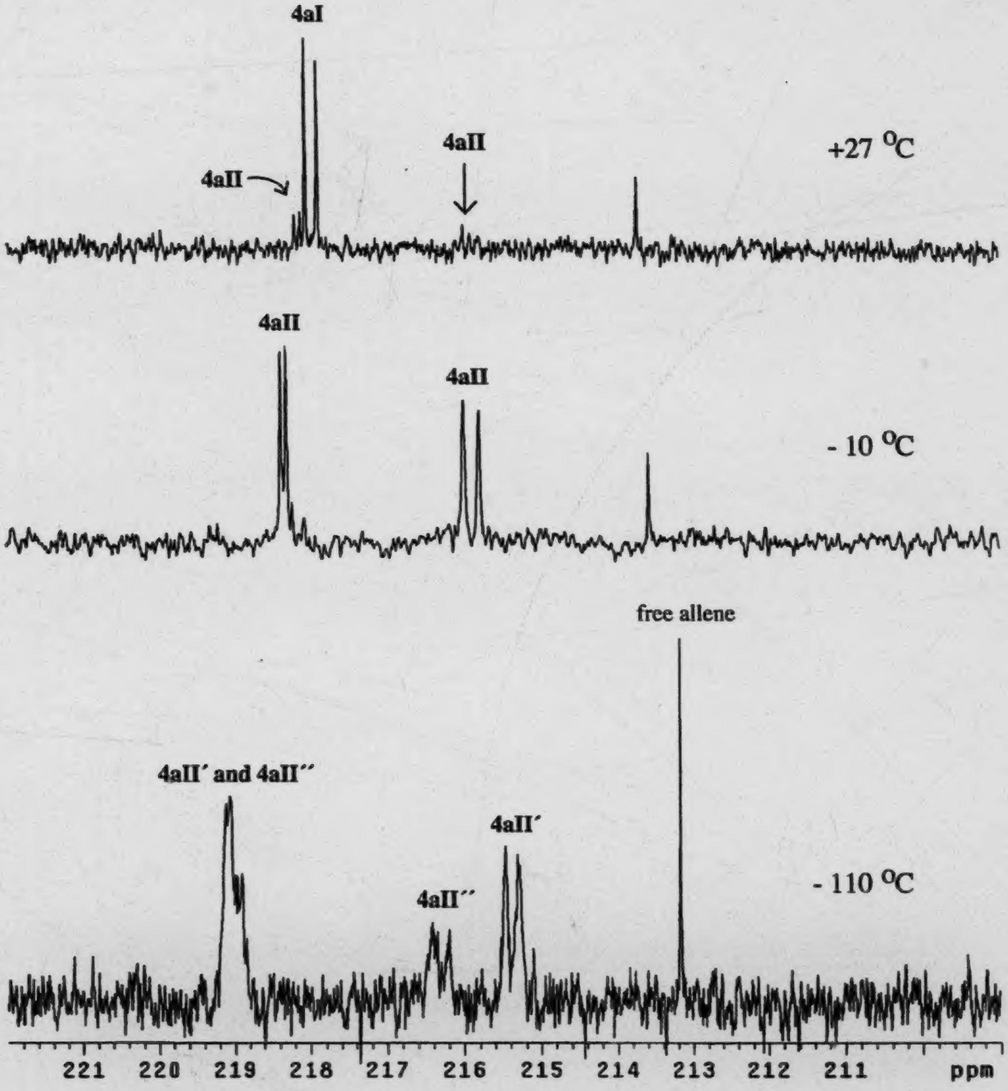

Figure 3-10 The Variable-Temperature $^{13}C\{^1H\}$ NMR Spectra (ppm, THF-d_8) of the Reaction of **2a** with Allene.

The upfield regions of the ^{13}C NMR spectrum at −110 °C indicate the structure of **4aII′** and **4aII″** to be similar to each other and are consistent with an asymmetric structure. Two signals or two sets of signals were located in nearly all of the chemical shift regions associated with a vinylallyl ligand. Two broad signals at δ 157.1 and 156.0 ppm are assigned to the α-carbon of the vinyl moiety. Two signals at δ 136.1 and 132.9 ppm are consistent with the β-carbon of a vinyl ligand. Two sets of two quartets in the CF_3 region were observed to have $^1J_{CF}$ = ~271–275 Hz. A relatively intense signal at δ 85.9 ppm and a smaller signal at δ 86.5 ppm are assigned to the central carbons of the allyl group. Four signals are expected in the region normally associated with the terminal carbons of the allyl group. However, in addition to the terminal carbons of free allene (δ 74.1 ppm), only three signals are observed. Unfortunately, the solvent shows a large signal in this region at δ 67.5 ppm and may conceal the fourth signal. Interpretation of the signals in the region normally associated with the substituents of the phosphine ligand is problematic. It was expected that a total of 10 signals, assuming fast P–C and C–C bond rotation for the two complexes, would be observed. However this was not the case as only six signals are clearly definable. The area also exhibits a large solvent resonance centered at δ 25.4 ppm and a broad signal(s) that covers a ~ 9 ppm range from δ ~ 32.5 – 24.0 ppm. With these two factors complicating matters any definitive interpretation is impossible given the data in its present form.

As expected, the variable temperature ^1H NMR spectra exhibit the characteristic spectral perturbation associated with stereochemical nonrigidity and show the conversion of **4aII′** and **4aII″** into **4aI** (Figure 3-11). At −110 °C the spectrum shows a number of resonances, a result of **4aII′** and **4aII″** in slow isomerization, which broaden, coalesce and sharpen upon warming the sample. Note that the signals are still somewhat broad at −110 °C and thus the dynamic process is not completely arrested at this temperature. At −10 °C **4aII′** and **4aII″** are in fast isomerization and the spectrum shows relatively sharp averaged signals, *i.e.* **4aII**.

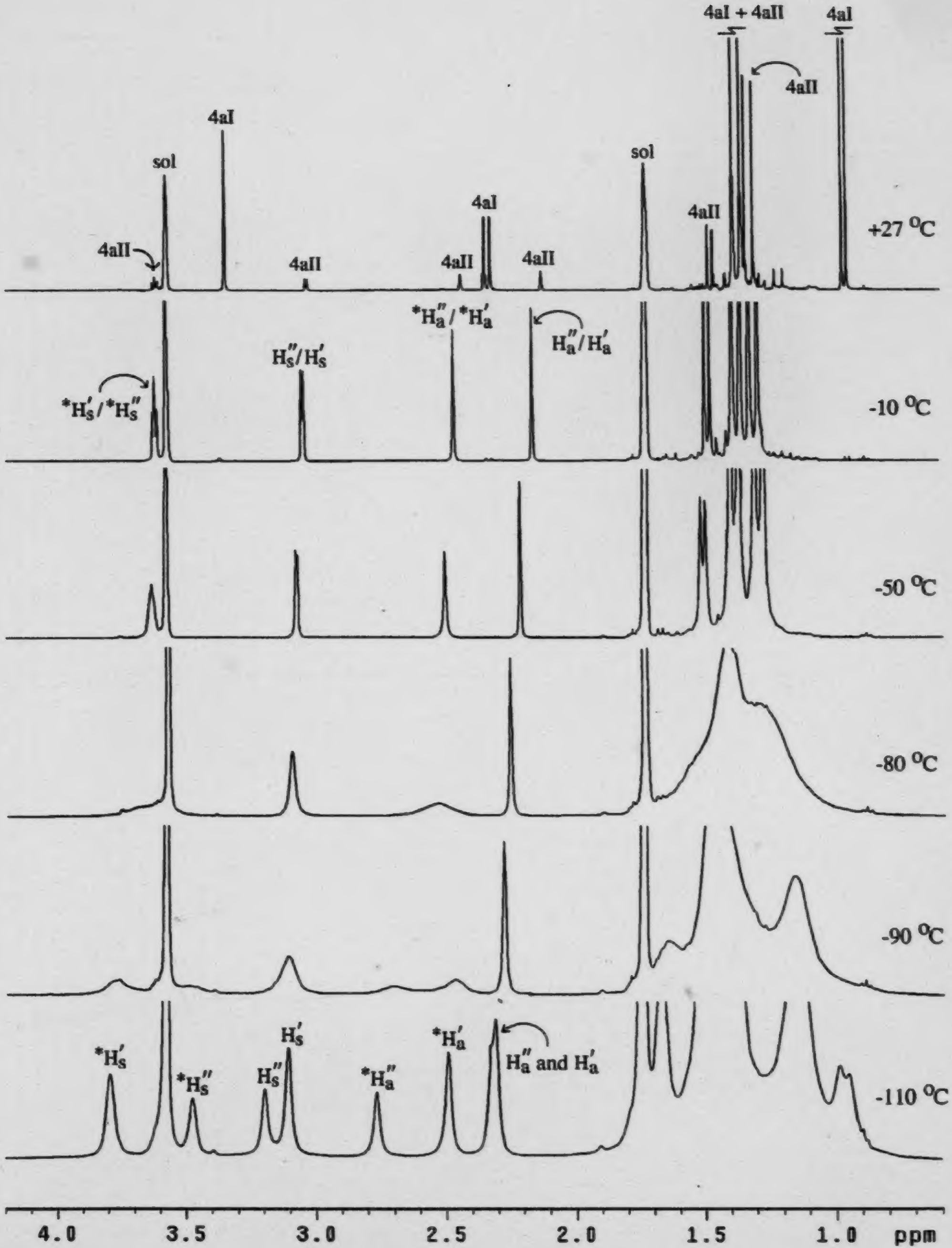

Figure 3-11 The Variable-Temperature ^{1}H NMR Spectra (ppm, THF-d_8) of the Reaction of **2a** with Allene.

At +27 °C **4aII′** and **4aII″** have mostly converted to **4aI**. In terms of the structures of **4aII′** and **4aII″** the −110 °C spectrum is most informative. In the range normally associated with the allyl protons the spectrum shows, in addition to one of the two solvent signals, what appear to be seven proton signals. These signals can be divided into two groups. With the exception of the highfield signal centered at δ 2.28 ppm, the various signals are found to have a relative intensity of either 0.7 or 1.0. These intensities are consistent with previously measured intensities of **4aII″** and **4aII′**, respectively, from the $^{31}P\{^1H\}$ and ^{19}F NMR spectra. The highfield signal centered at δ 2.28 ppm shows a relative intensity of 1.7. This would indicate that this highfield signal is comprised of one signal of each of the two complexes **4aII′** and **4aII″**. Upon closer examination of the line shape of this highfield signal it becomes clear that a shoulder exists and indeed two signals, one at δ 2.32 (weaker intensity) and another at δ 2.31 (stronger intensity) ppm, are nearly superimposed to give the appearance of a single signal. In terms of allyl ligands the four downfield signals can be attributed to *syn*-protons while the four upfield signals can be attributed to *anti*-protons. To clarify the labeling scheme in Figure 3-11 a label of H_s indicates a *syn*-hydrogen while H_a indicates an *anti*-hydrogen. A single prime symbol indicates a hydrogen of **4aII′** while a double prime indicates a hydrogen of **4aII″**. The significance of the asterisks (*) will be explained shortly. The upfield area of the spectrum, the area in which the signals of protons of the phosphine substituents are expected to occur, shows very intense and broad resonances in the range δ 1.65-0.9 ppm. The second solvent signal can be immediately identified at δ 1.73 ppm, otherwise no assignments in this region can be made. Integrations gave rise to a number of possible interpretations. It appears that at this low temperature the rotation about the P–C and/or C–C bond of the phosphine ligand substituents are slowed enough to cause this broadening (*cf.* $^{13}C\{^1H\}$ NMR data). Based on the information provided by the allyl protons it is clear that both **4aII′** and **4aII″** have as asymmetric allyl moiety. This, combined with the other NMR data, indicate that both **4aII′** and **4aII″** have a geometric orientation of ligands similar to that observed in **4aII** (Figure 3-7). Nevertheless, **4aII′** and **4aII″** are distinctly different from each other in some way, evident from the NMR data at –110 °C, and that the two complexes are involved in an isomerization process. The key to solving these mysteries, the differential structures of **4aII′** and **4aII″** and the nature of the isomerization process, lies in the ^{1}H NMR spectrum.

Returning to the ^{1}H NMR spectrum at –110 °C (Figure 3-11), notice that upon raising the temperature $^*H_s'$ and $^*H_s''$ at δ 3.79 and 3.48 ppm, respectively, broaden (–90 °C), coalesce (–80 °C) and sharpen to give the averaged signal $^*H_s'/^*H_s''$ at δ 3.63 ppm (–10 °C) , likewise H_s'' and H_s' combine to give H_s''/H_s' at δ 3.06 ppm, $^*H_a''$ and $^*H_a'$ merge to give the $^*H_a''/^*H_a'$ resonance at δ 2.47 ppm, and H_a'' and H_a' combine to give the H_a''/H_a' signal at δ 2.17 ppm. The asterisk label (*) further differentiates H_s and H_s, and H_a and H_a within each **4aII′** and **4aII″**. All protons of the allyl group in **4aII′** and **4aII″** are involved in the dynamic process. However this process has a dramatic anisotropic effect on the allyl ligand. In the –90 °C spectrum $^*H_s'$, $^*H_s''$, $^*H_a''$ and $^*H_a'$ (asterisk labeled H's) have only begun to broaden while H_s'' and H_s', and, H_a'' and H_a' have already coalesced and begun to sharpen. This inhomogeneous effect on the allyl hydrogens is clearly an indication that the origin of the dynamic behavior is localized within the molecule. Since one CH_2 group of the allyl is more affected than the other and considering the proposed structure of **4aII′** and **4aII″**, the dynamic process must involve the phosphine ligand. Since phosphine dissociation can be excluded, based on the absence of free phosphine in the slow regime exchange, the logical choice for the process is restricted rotational freedom involving the phosphine ligand. This would cause conformational "locking" of the phosphine ligand and could give rise to rotational isomers. In Figure 3-7, the phosphine ligand in **4aII** is *cis* to one terminus of the allyl and *trans* to the other. One would expect that the chemical shift differences between corresponding allyl protons in the two conformers would be larger in the *cis*-CH_2 groups and less in the *trans*-CH_2 groups. This is because the source of the chemical inequivalence in the two rotomers, the two conformations of the phosphine ligand, is physically closer to the *cis*-CH_2 terminus. Assuming **4aII′** and **4aII″** are rotomers, the chemical shift difference between the *syn*-proton closest to the phosphine ligand in **4aII′** and the *syn*-proton closest to the phosphine ligand in **4aII″** would be expected to be larger than the chemical shift difference between the *syn*-proton farthest from the phosphine ligand in **4aII′** and the *syn*-proton farthest from the phosphine ligand in **4aII″**. The same can be said of the *anti*-protons. Indeed, the ^{1}H NMR spectrum at −110 °C exhibits a pattern that is consistent with this expectation. The difference in chemical shift between corresponding nuclei of the two rotomers, as shown by the coalescence behavior of the signals, is particularly evident for the *anti*-protons. The chemical shift difference between $*H'_a$ and $*H''_a$ is large, whereas the chemical shift of Ha′ and Ha″ are nearly coincident. Thus, the asterisk label (*) in Figure 3-11 identifies the *syn*-hydrogens and the *anti*-hydrogens that are closest to the phosphine ligand in each rotomer.

This effect is also observed, albeit in a less dramatic fashion, in the ^{19}F NMR spectra. The two signals at δ −52.9 (**4aII′**) and −53.8 (**4aII″**) ppm (−110 °C) merge upon warming to give the signal at δ −53.2 ppm (−10 °C) likewise the signals at δ −65.7 (**4aII′**) and −64.1 (**4aII″**) ppm merge to give the signal at δ −65.1 ppm (−10 °C). Upon warming the sample the former signals broaden, coalesce and sharpen faster than the latter pair of signals. Furthermore the difference in the chemical shift at

–110 °C of the former pair is smaller (Δ = 0.9 ppm) than that for the latter pair (Δ = 1.6 ppm). Upon this basis it can be surmised that the resonances at δ –52.9 and –53.8 ppm are due to the trifluoromethyl group that is closer to the phosphine ligand, *i.e.* bound to the α-carbon of the vinyl moiety.

Determining the specific orientation of the phosphine substituents in each conformer and the details of the dynamic process is problematic for two reasons. First, the model is relatively complex. The P^tBu_2Me ligand has 10 degrees of rotational freedom; rotation about the Fe–P bond, rotation about the three P–C bonds and rotation about the six C–C bonds. Also it is quite possible and maybe probable that these various degrees of rotational freedom are not independent, and there exists a correlated rotation or a concerted motion which, of course, makes for a much more complex model to study because then one must consider combinations of dependent motions as opposed to only isolated motions of the phosphine substituents. Secondly, there is a severe shortage of data on-hand. The process is not yet completely arrested as evident from the broad signals of the allyl proton signals which makes the ^{13}C and ^1H NMR probes of the phosphine substituents uninformative. Furthermore, successful determination of the steric and electronic intramolecular interaction between the phosphine ligand and the metal fragment are typically dependent upon the use of a combination of powerful and complementary methods; dynamic NMR, computational molecular modeling, NOE experiments and X-ray crystal structure analysis [25]. With the exception of the NMR data, data from these other methods have not been obtained for the present case. These two compounding problems prevent the drawing of any truly insightful and defendable conclusions. However, it can be said that at –110 °C in THF some rotations of the phosphine ligand have been slowed enough to identify the origin of the process. Furthermore, the fast exchange regime is consistent with a model in which all degrees of rotational freedom of the phosphine ligand are unhindered or, alternatively, only the Fe–P bond is arrested while the P–C and the C–C are in fast rotation. With either of these two possibilities one would expect to observe two chemically inequivalent ${}^tBu$ groups, identical to the pattern observed at –10 °C in the ${}^1H$ NMR spectrum. In regards to the slow exchange regime, the broad signals in the δ 1.7-0.9 ppm region of the ${}^1H$ NMR spectrum at –110 °C indicate hindered rotation of the P–C and or C–C linkages. On an intuitive basis, it seems paradoxical to suggest that stoppage of the P–C or C–C rotation of the phosphine substituents could occur without restricted motion about the Fe–P bond. Thus, it is reasonable to conclude that the Fe–P rotation is hindered in the slow exchange regime and that this occurs in combination with the arrest of rotation about some or all P–C or C–C bonds.

The low temperature NMR data and the evidence of rotomers **4aII′** and **4aII″** clearly shows that the P^tBu_2Me phosphine experiences considerable steric congestion when it occupies an equatorial position. In contrast, the low temperature NMR data of **4aI**, shows no evidence of rotational restriction down to –110 °C. Despite **4aII′/4aII″** (or **4aII**) being formed first, the demanding steric envelope of the phosphine ligand populationally disfavors this geometric isomer and the complex quickly converts to the preferred isomer **4aI** in which the phosphine ligand occupies the axial position. Complete conversion to **4aI** is not realized and the persistence of **4aII** in solution at ambient temperature may suggest an equilibrium between the kinetic product and the thermodynamically favored product but, as discussed previously, the processes(s) of decomposition prevent a definitive conclusion on this matter.

3.3.4 NMR Spectroscopic Analysis of $Fe(CO)_2(PR_2R')(\eta^1,\eta^3\text{-}\{F_3CC{=}C(CF_3)C(CH_2)_2\})$ (4b,c)

The solution spectra of **4b** and **4c** are similar. Of course the different phosphine ligands give rise to different NMR resonances but the resonances of the 2–vinylallyl and the carbonyls exhibit good conformity. As with **4a**, the NMR data of **4b,c** (Tables 3-8 and 3-9) indicated two unequally populated isomers in solution. It was found that the major isomer is favored by a ratio of approximately 2:1 in both **4b** and **4c**. Given their similarity, the NMR data of **4b** serves well as a representative example. For reasons which will become obvious later the major and minor isomers were labeled **4nII** and **4nI** (n = b, c), respectively.

The $^{31}P\{^1H\}$ and ^{19}F NMR spectra of **4b** show a strong resemblance to that of **4a**. As with **4a**, the relationships between the phosphorus and fluorine resonances were confirmed by selective $^{19}F\{^{31}P\}$ experiments and the intensity ratios from both the $^{31}P\{^1H\}$ and ^{19}F NMR data were used to calculate the population ratios of **4nI/4nII** (n = b, c).

The ^1H NMR spectrum of **4bI/4bII** is shown in Figure 3-12. Contrary to the situation in **4a**, the resonances in the "allyl region" in **4b** showed comparable intensity ratios. This made assignment of these resonances to **4bI** or **4bII** challenging. This problem was overcome through the use of COSY (Correlation Spectroscopy) experiments in which through-bond connectivity between proton nuclei was established. In this way proton resonances were grouped. The proton resonances associated with the phosphine ligands clearly showed one set of dominant signals and one set of minor signals, and thus could directly be assigned to either **4bI** or **4bII**.

Table 3-8 The $^{31}P\{^1H\}$, ^{19}F, ^1H and $^{13}C\{^{19}F\}$ NMR Data (ppm, CD_2Cl_2, 27 °C) of **4bI** and **4bII**

Compound	$^{31}P\{^1H\}$	^{19}F	^1H	$^{13}C\{^{19}F\}/{*}^{13}C\{^1H\}APT$
4bI (minor isomer)	62.1	– 58.5 dq $^5J_{FF} = 8$ Hz $J_{FP} = 3$ Hz – 64.7 q $^5J_{FF} = 8$ Hz	3.24 s H_{syn} 2.51 d $^3J_{HP} = 8$ Hz H_{anti} 2.21 dsept $^3J_{HH} = 7$ Hz $^2J_{HP} = 8$ Hz PC*H* 1.30 dd $^3J_{HH} = 7$ Hz $^3J_{HP} = 13$ Hz PCCH_3	216.7 d $^2J_{CP} = 18$ Hz *C*O 153.8 d $^2J_{CP} = 16$ Hz $C_\alpha(CF_3)$ 133.9 br $C_\beta(CF_3)$ 125.2 s CF_3 117.0 s CF_3 86.4* br s $C_{central}$ 67.7* dq $^2J_{CP} = 4$ Hz $^4J_{CF} = 1$ Hz CH_2 27.6* (–) d $^1J_{CP} = 17$ Hz s PCH 19.1* (–) br s PCCH_3
4bII (major isomer)	72.0	– 54.5 q $^5J_{FF} = 9$ Hz – 65.3 dq $^5J_{FF} = 9$ Hz $J_{FP} = 2$ Hz	3.74 dd $^4J_{HH} = 3$ Hz $^3J_{HP} = 3$ Hz H_{syn} 3.18 d $^4J_{HH} = 3$ Hz H_{syn} 2.36 dsept $^3J_{HH} = 7$ Hz $^2J_{HP} = 8$ Hz PC*H* 2.28 s H_{anti} 2.26 s H_{anti} 1.29 dd $^3J_{HH} = 7$ Hz $^3J_{HP} = 13$ Hz PCCH_3	217.5 d $^2J_{CP} = 7$ Hz *C*O 214.0 d $^2J_{CP} = 21$ Hz *C*O 155.5 d $^2J_{CP} = 19$ Hz $C_\alpha(CF_3)$ 134.0 br s $C_\beta(CF_3)$ 126.3 s CF_3 117.7 s CF_3 84.8* dq $^2J_{CP} = 3$ Hz $^2J_{CF} = 1$ Hz $C_{central}$ 67.4* dq $^2J_{CP} = 9$ Hz $^4J_{CF} = 1$ Hz CH_2 66.8* dq $^2J_{CP} = 5$ Hz $^4J_{CF} = 1$ Hz CH_2 29.0* (–) d $^1J_{CP} = 19$ Hz PCH 20.4* (–) s PCCH_3 20.0* (–) s PCCH_3

Table 3-9 The $^{31}P\{^{1}H\}$, ^{19}F, ^{1}H and $^{13}C\{^{19}F\}$ NMR Data (ppm, CD_2Cl_2, 27 °C) of **4cI** and **4cII**

Compound	$^{31}P\{^{1}H\}$	^{19}F	^{1}H	$^{13}C\{^{19}F\}$/*$^{13}C\{^{1}H\}$APT
4cI	53.4	− 58.0 dq $^{5}J_{FF}$ = 8 Hz	3.23 s H_{syn}	216.6 d $^{2}J_{CP}$ = 19 Hz CO
(minor isomer)		J_{FP} = 3 Hz	2.51 d $^{3}J_{HP}$ = 8 Hz H_{anti}	154.3 br $C_{\alpha}(CF_3)$
		− 64.1 q $^{5}J_{FF}$ = 8 Hz	2.13-1.20 br PC_6H_{11}	125.7 s CF_3
				117.1 s CF_3
				86.3 br s $C_{central}$
				67.6* br s CH_2
4cII	60.3	− 53.7 q $^{5}J_{FF}$ = 9 Hz	3.73 dd $^{4}J_{HH}$ = 3 Hz Hz	217.9 d $^{2}J_{CP}$ = 6 Hz CO
(major isomer)		− 64.6 dq $^{5}J_{FF}$ = 9 Hz	$^{3}J_{HP}$ = 3 Hz H_{syn}	214.0 d $^{2}J_{CP}$ = 21 Hz CO
		J_{FP} = 2 Hz	3.11 d $^{4}J_{HH}$ = 3 Hz H_{syn}	155.5 d $^{2}J_{CP}$ = 19 Hz $C_{\alpha}(CF_3)$
			2.23 s H_{anti}	133.7 br s $C_{\beta}(CF_3)$
			2.19 s H_{anti}	126.1 s CF_3
			2.13-1.20 br PC_6H_{11}	117.7 s CF_3
				84.4 br s $C_{central}$
				66.3* br s CH_2
				66.6* br s CH_2

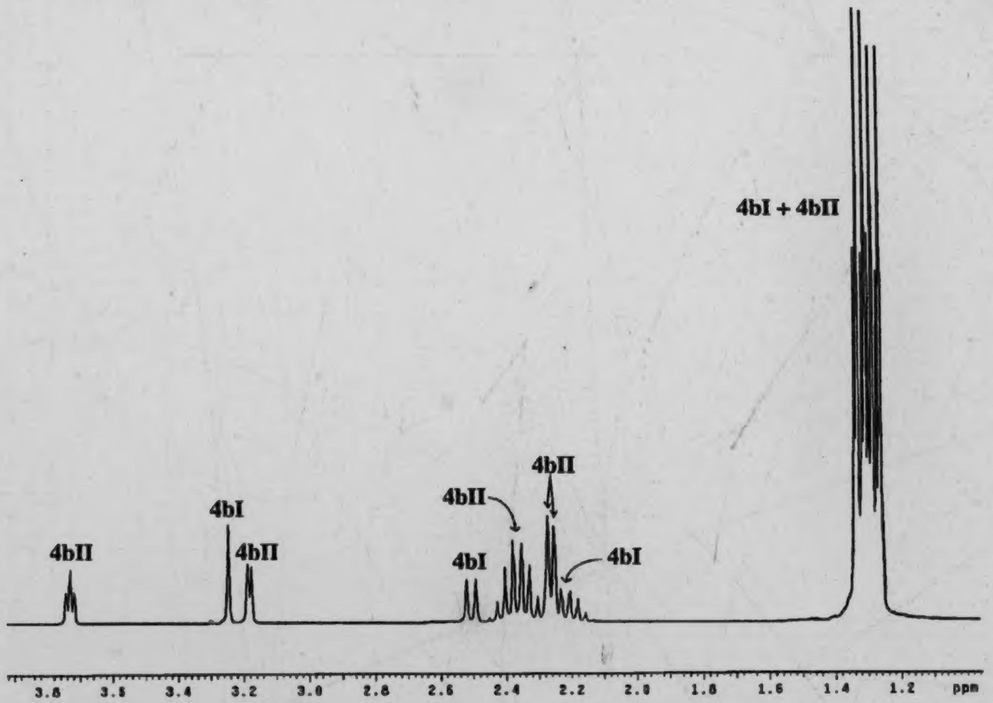

Figure 3-12 The ^1H NMR Spectrum (ppm, CD_2Cl_2) of **4b**.

Four signals of equal intensity are observed in the downfield region associated with allyl protons of **4bII**. A pseudotriplet, assigned to a H_{syn} is observed at δ 3.74 ppm. In reality this signal is a doublet of doublets resulting from $^4J_{HH}$ and $^3J_{HP}$ coupling of equal coupling values (3 Hz). The heteronuclear coupling was confirmed by selectively decoupling the dominant signal in the ^{31}P spectrum at δ 72.0 ppm while the homonuclear coupling was confirmed by selectively decoupling the doublet at δ 3.18 ppm after it was located by a COSY experiment. Selectively decoupling the ^{31}P signal at δ 72.0 ppm showed that this signal is associated with the major isomer. The δ 3.74 and 3.18 ppm signals are in a chemical shift region associated with *syn*-hydrogens of the allyl group. The two signals due to the *anti*-hydrogens of the major isomer were located at δ 2.28 and 2.26 ppm as singlets that, rather unfortuitously, overlap with the pseudooctet resonance of the PCH proton of **4bI**. Their integration, consistent with 1H and 1H in the major isomer, can be calculated by subtraction of the overlapping signals. Moreover, it was observed in the COSY spectrum that a correlation exists between the H_{anti} at δ 2.28 ppm and both the H_{syn} at δ 3.18 ppm and the H_{syn} at δ 3.74 ppm. From the width of the lines the coupling constants can be estimated to be at most 1 Hz. It is not known if the H_{anti}–H_{syn} coupling is a result of allylic $^4J_{HH}$ or geminal $^2J_{HH}$. At this point this question cannot be answered. These results show that these four signals arise from the same allyl group and all protons are chemically inequivalent, suggesting an asymmetric structure similar to the minor isomer in **4a**, *i.e.* **4aII**, and consistent with the solid state molecular structure of **4b**.

The signal of the isopropyl PC*H* protons of **4bII** appear as a pseudooctet at δ 2.36 ppm while, as mentioned above, that of the minor isomer appears at δ 2.21 ppm. The "octet" pattern arises from overlap of a doublet of septets which arises from $^2J_{HP}$ (8 Hz) and $^3J_{HH}$ (7 Hz), this latter coupling occurs as a result of spin-spin interaction with the CH_3 protons of the two methyl groups. It is expected that in the P^iPr_3 ligand, which is bonded to an asymmetric metal moiety, the three ^{i}Pr groups are made equivalent by fast rotation about the Fe–P bond, while within the ^{i}Pr groups the two methyl groups are chemically inequivalent (diastereotopic). This is analogous to the diastereotopic ^{t}Bu groups of the phosphine ligand in **4aII** (Section 3.3.2). Thus, it is expected that one proton resonance will be observed for each of the two chemically distinct methyls of the ^{i}Pr groups. Furthermore, in light of the pattern and $^3J_{HH} = 7$ Hz associated with the signal of the PC*H* protons, the signals will be observed as a doublet. Also two bond coupling to the phosphorus nuclei may also be observed. In the upfield region of the ^{1}H NMR spectrum four peaks of equal intensity are centered at δ 1.29 ppm. These signals are, based on their dominant intensity, associated with the phosphine ligand of the major isomer, **4bII**. Upon selectively decoupling the phosphorus at δ 72.0 ppm the signal pattern collapses into a doublet with $^3J_{HH}$ = 7 Hz. Alternatively, selectively homonuclear decoupling of the isopropyl PC*H* resonance causes the four peak pattern to collapses into a doublet of $^2J_{HP}$ = 13 Hz. Thus, it appears that the proton signals of the two chemically inequivalent $PCCH_3$ groups are coincident in chemical shift and have equal $^3J_{HH}$ and $^3J_{HP}$ constants.

By a process of elimination the signals of **4bI**, the minor isomer, were identified. A singlet and doublet of equal intensity are observed in the allylic region of the spectrum. The singlet occurs within the characteristic region associated with H_{syn} protons of an allyl group (δ 3.24 ppm) while the doublet is located at a chemical shift consistent with allyl H_{anti} protons (δ 2.51 ppm). The doublet collapses into a singlet upon selectively decoupling the ^{31}P signal at δ 62.1 ppm. The COSY spectrum shows that these two proton signals are part of the same molecule. The pattern for the allyl protons suggests a symmetry within the molecule that relates the two terminal groups of the allyl. This of course is not consistent with the crystal structure of **4b** but is consistent with its geometrical isomer in which the phosphine ligand is *trans* to the α–carbon of the vinyl group. This structure is analogous to the crystal structure of **4a** (i.e. **4aI**). In a structure with C_s symmetry all ^iPr units of the phosphine ligand are chemically equivalent, as well the two methyl groups within each ^iPr unit are chemically equivalent. As discussed above, the isopropyl PC*H* resonance is located at δ 2.21 ppm. Further upfield and nearly coincident with the resonances of the $PCCH_3$ signals of **4bII**, a four line signal of equal intensity is centered at δ 1.30 ppm. This signal was confirmed as the $PCCH_3$ proton resonance by first selectively decoupling the ^{31}P singlet at δ 62.1 ppm then homonuclear decoupling of the pseudooctet at δ 2.21 ppm. Each spectrum gave a doublet centered at δ 1.30 ppm.

The ^{13}C NMR data is very informative on the issues of the structure of **4bI** and **4bII**. Figure 3-13 shows the $^{13}C\{^1H\}$APT NMR spectrum of **4b** in CD_2Cl_2. The carbonyl region shows three doublets of equal intensity. The two signals of **4bII** were identified by selectively decoupling the ^{31}P resonance at δ 72.0 ppm. The signal of **4bI** was identified in a likewise manner. A broad resonance at δ 155.5 ppm was assigned to the α-carbon of the vinyl ligand in the major isomer. The corresponding signal for the minor isomer was only observed upon ^{19}F decoupling. Assignment of the δ 155.5 and 153.8 ppm signals to the major or minor isomer is based on selective ^{31}P decoupling experiments. Assignment of these signals as the ligating carbons of the vinyls was based on the coupling to phosphorus nuclei. Another broad resonance was observed at δ 134.0 ppm and assigned to the β-carbon of the vinyl group in the major isomer. The related signal for the minor isomer was not observed in either the $^{13}C\{^{31}P\}$ of ^{13}C $\{^1H\}$ spectra. However a small signal at δ 133.8 ppm, along with the 134.0 ppm resonance, was observed in the $^{13}C\{^{19}F\}$ NMR spectrum. In addition, some of the allylic protons of both the major and minor isomer showed correlation with a broad signal centered at δ 133.9 ppm on the ^{13}C NMR axis in the HMBC spectrum. The broad appearance of this signal suggests that the signals for the β–carbon of the major and minor isomer are very close in chemical shift and not resolved in the HMBC spectrum. The CF_3 carbons of the vinyl are observed in two regions in the $^{13}C\{^{19}F\}$ spectrum; two signals in each of the δ 125-126 and 117-118 ppm regions. Only the signals of the major isomer were observed in the $^{13}C\{^1H\}$APT spectrum. These signals had the characteristic large $^1J_{CF}$ coupling of about 273-276 Hz. The bridgehead carbon of the allyl, *i.e.* the central carbon of the allyl moiety, was shown in **4a** to resonate in the narrow region δ 85-87 ppm.

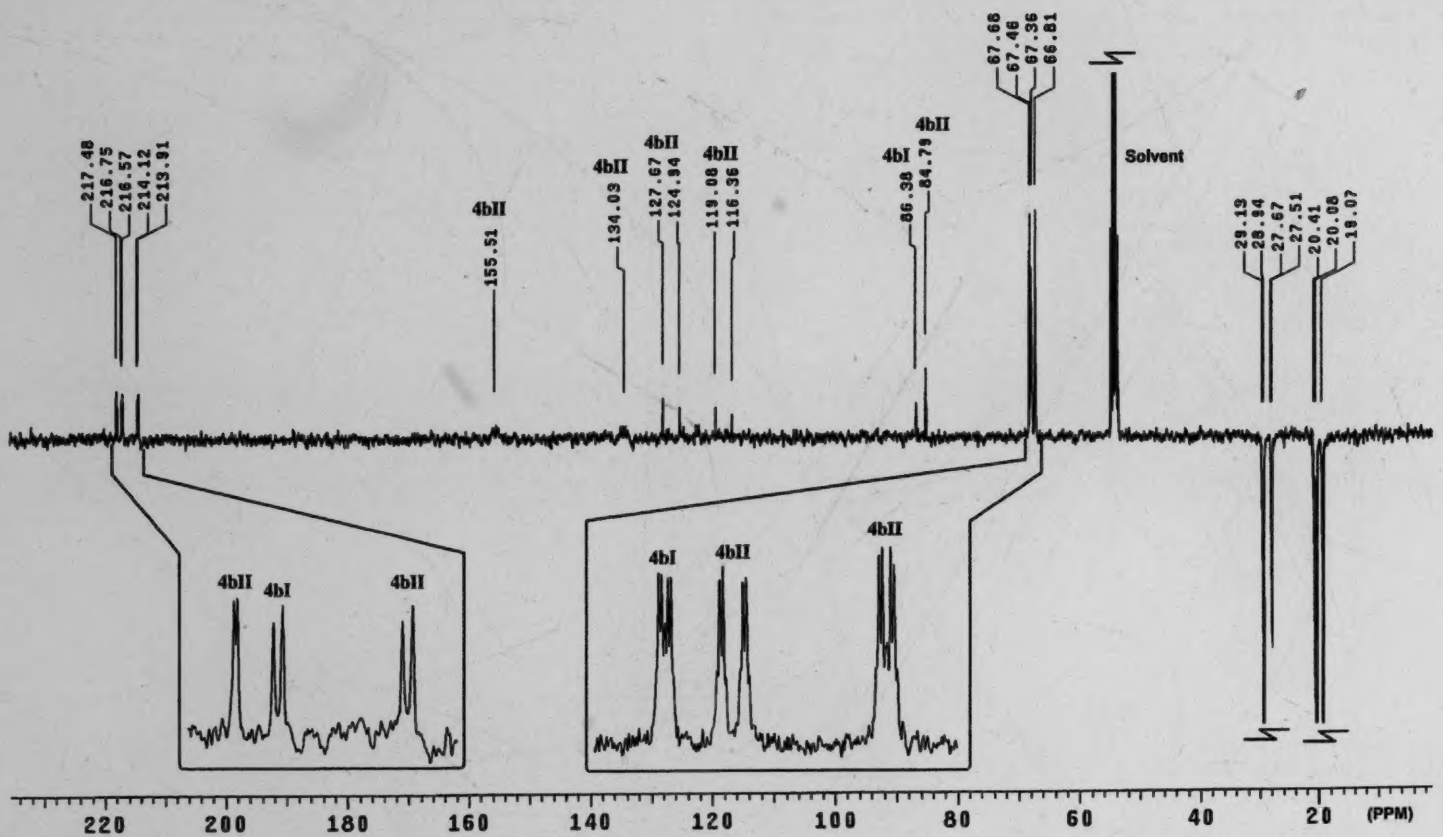

Figure 3-13 The $^{13}C\{^1H\}$ APT NMR Spectrum (ppm, CD_2Cl_2) of **4b**.

Two signals were observed in this region in **4b**. Each signal was clearly detected in the HMBC spectrum and showed a correlation to both H_{syn} and H_{anti}. The terminal carbons of the allyl are observed in the δ 66-68 ppm range (inset in Figure 3-13) and as expected **4bII** shows two signals in this region while **4bI** only shows one signal. These signals show strong correlation in the HMQC spectrum to the H_{syn} and H_{anti} of the allyl moiety indicating direct connections, *i.e.* $^1J_{HC}$. Resonances due to the substituents of the phosphine ligand were found below δ 30 ppm. Two doublets at δ 29.0 and 27.6 ppm were assigned to the tertiary carbon of the ^{i}Pr group in **4bII** and **4bI**, respectively. These assignments were based on the correlation in the HMQC with the attached proton and the inverted form of the signal in the $^{13}C\{^1H\}$APT spectrum. The two singlets at δ 20.4 and 20.0 ppm were assigned to the two chemically inequivalent primary carbons of the ^{i}Pr group in **4bII**. Corroboration was provided by correlation with the proton attached to the tertiary carbon in the HMBC spectrum. The slightly broad singlet at δ 19.1 ppm was assigned to the primary carbon of the ^{i}Pr groups of **4bI**. Again this assignment was supported by HMBC experiments. Coupling to phosphorus was confirmed by selectively decoupling the ^{31}P NMR signals.

As discussed above the NMR data of **4cI** and **4cII** conform closely to **4bI** and **4cII**, respectively. No assignments with respect to the cyclohexyl units of the phosphine ligands could be made as they produced a very broad signals in the 2.1-1.2 ppm region in the ^{1}H NMR spectrum. A number of signals in the ^{13}C NMR spectrum were observed for the Cy groups, but the presence of the two isomers produced overlapping and broadened signals, and no definitive assignments could be made.

The spectroscopic data supports the conclusion that geometric isomers of the title compounds exist in solution. The crystal structures of **4b** and **4c** show an α–carbon of the vinyl, while the phosphine ligand assumes an equatorial position, trans to a CH_2 group of the allyl. The NMR signals of the major isomer in solution are fully consistent with this structure. The NMR data of the minor isomer indicates a structure with C_s symmetry and is consistent with a structure with the phosphine ligand in the axial position and the two carbonyls in the equatorial position. These structures are analogous to **4aI** and **4aII** in Figure 3-7. One significant difference is however observed; the major isomer in **4b** and **4c** is the asymmetric isomer (**4nII**, n = b, c) while in **4a** the major isomer is the symmetric isomer (**4aI**), and the minor isomer in **4b** and **4c** is the symmetric isomer (**4nI**, n = b, c) while in **4a** the minor isomer is the asymmetric isomer (**4aII**).

3.3.5 Low Temperature and Variable Temperature NMR Studies of $Fe(CO)_2(PCy_3)(\eta^1,\eta^3\text{-}\{F_3CC{=}C(CF_3)C(CH_2)_2\})$ (4c)

It was discovered that different samples of **4b** or **4c** gave different proportions of isomers. In one sample **4bI** or **4cI** was the dominant isomer while in another sample **4bII** or **4cII** was the dominant isomer. At room temperature, the population ratio, as measured by NMR integrations, quickly stabilizes in all samples and favors **4bII** or **4cII** over **4bI** or **4cI** at a ratio of 2:1. This ratio persists at room temperature over several hours until degradation of the sample makes reliable integrations impossible to obtain.

In order to monitor the reaction from the beginning, a reaction of $Fe(CO)_2(PCy_3)(\eta^2\text{-HFB})$ and allene was followed by variable temperature NMR. A sample was prepared at –78 °C in CD_2Cl_2 and directly inserted into the NMR probe which was already at –90 °C. The reaction was monitored by obtaining the ^1H, $^{31}P\{^1H\}$ and ^{19}F NMR spectra at temperature intervals. After reaching +27 °C the sample was held at this temperature for several hours, after which the sample began to degrade. The ^1H NMR spectra at –90 °C, 0 °C, and at +27 °C (after 1.5 hours at +27 °C) are presented in stacked form in Figure 3-14. At –90 °C, **4cII**, the asymmetric isomer, is the first isomer to form. This is evident from its characteristic four ally proton pattern; H_{syn} protons at δ 3.63 and 3.12 ppm and H_{anti} protons at δ 2.23 and 2.14 ppm. The broad signal centered at δ 2.37 ppm is part of the PC_6H_{11} signal. The $^{31}P\{^1H\}$ and ^{19}F NMR spectra also show only **4cII** at this temperature. At 0 °C **4cII** begins to convert into **4cI**. The characteristic pattern for **4cI** is just detectable at this temperature; H_{syn} protons at δ 3.22 ppm and H_{anti} protons at δ 2.49 ppm. The +27 °C spectrum shows a 2:1 mixture of **4cII** and **4cI** that has been held at ambient temperature for 1.5 hours. This ratio does not change after several hours at room temperature but by the next day (~16 hours) decomposition becomes significant. A number of signals in the $^{31}P\{^1H\}$ spectrum indicate multiple decomposition products.

As with **4a**, the variable temperature results revealed that the asymmetric isomer is first to form. In addition, the conversion of **4nII** (n = b, c) to **4nI** occurs with warming of the solution and this conversion is slow on the NMR time scale as relatively sharp lines are observed. Contrary to the behavior of **4a** the dominant isomer in **4b,c** is the asymmetric isomer. Moreover, a fast isomerization process like that observed with **4aII** (i.e. **4aII′** and **4aII″**) was not observed with either **4bII** or **4cII**. The differences in the solution behavior between **4a** and **4b,c** again draws attention to the problem of comparing the steric demands of a phosphine of the form PR_2R' to a phosphine of the form PR_3. It seems that the P^tBu_2Me ligand experiences greater steric congestion in **4aII** than do P^iPr_3 or PCy_3 in the analogous structure **4bII** or **4cII**. This may very well be the result of a relatively disadvantageous match between the unique spacial surface of the phosphine ligand and spacial surface of the metal and its ligand environment. Unfortunately, the orientations of the substituents of the phosphine ligand in **4aII** are not known. The structures of **4nII** (n = b, c) are, however, known but it is not clear from a comparison of the three structures, **4a-c**, why **4nII** (n = b, c) are preferred while **4aII** is not. Alternatively, we may consider compounds **4nI** (n = a, b, c).

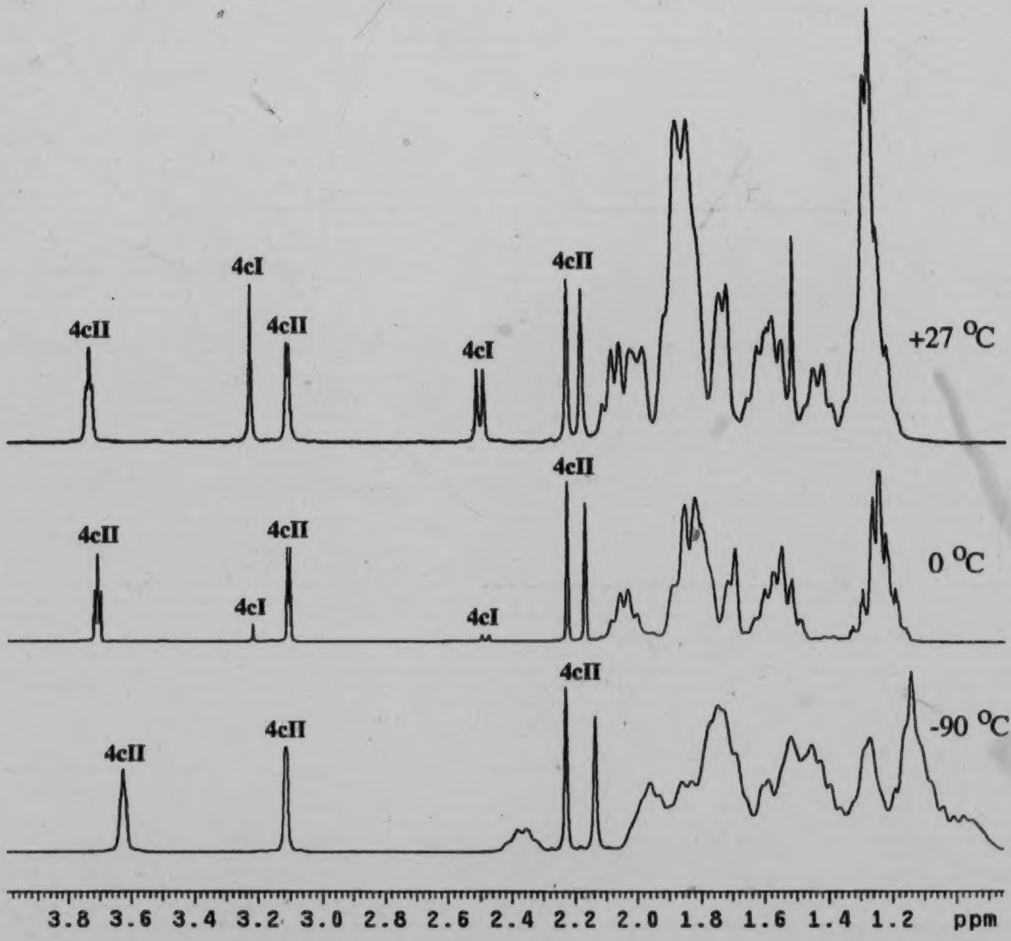

Figure 3-14 The Variable-Temperature ^{1}H NMR Spectra (ppm, CD_2Cl_2) of the Reaction of **2c** with Allene.

The molecular structure of **4aI** (Figure 3-2) shows the P^tBu_2Me ligand in an orientation, in which its small substituent, the Me, is positioned between the terminus of the allyl moiety. In regards to **4nI** (n = b, c) the molecular structures or the preferred orientations of the phosphine substituents are not known but we may hazard a guess that the phosphine ligands cannot minimize steric interaction in the same way because the substituents are relatively large, relative to Me, and all three substituent are identical. In this way we explain the differences in the solution chemistry of these complexes.

3.4 Characterization of $Fe(CO)_2(PR_2R')(\eta^1,\eta^3\text{-}\{F_3CC{=}C(CF_3)C(CH_2)CHMe\})$ (5a-c)

The molecular formulation of **5a-c** was based on the elemental microanalysis.

The IR spectra of **5a-c** showed two terminal carbonyl stretches, the intensity pattern of which are indicative of a *cis* carbonyl arrangement (Table 3-10).

Table 3-10 FT-IR Data (cm^{-1}, pentane) in the Carbonyl Region of **5a-c**

Compound	ν_{CO}
5a	2010 (s), 1958 (s)
5b	2008 (s), 1957 (s)
5c	2006 (s), 1955 (s)

Among the first data obtained for samples of **5a-c** was a successful X-ray crystal structure of **5b**. This structure was the only structure of this group to be successfully determined. It will be discussed first and the discussion of the NMR data will follow.

3.4.1 X-ray Crystal Structure Analysis of $Fe(CO)_2(P^iPr_3)(\eta^1,\eta^3\text{-}\{F_3CC{=}C(CF_3)C(CH_2)CHMe\})$ (5b)

Figure 3-15 shows the solid state molecular structure of **5b**, without phosphine hydrogens, while Table 3-11 lists selected interatomic distances and angles.

As expected, the structure of **5b** is, in general, similar to the previous structures **4a-c**, in particular it is analogous to **4b**. The structure shows two carbonyls, the P^iPr_3 and a 2-vinylmethylallyl ligand coordinated to an iron center. The geometry about the iron center is again best described as a distorted octahedron. The equatorial plane and axial axis as defined in the discussion of **4b** will be extended to this structure. The C2–Fe–C4 axis, which deviates from ideal angle of 180° by about 8°, is very close to the 170.7(1)° in **4b**. The axial–Fe–equatorial angles (Cn–Fe–P/Cm, n = 2, m =1, 7, 9; n = 4, m = 1, 7, 9) in **5b** are within 2° of the corresponding angles in **4b**. Moreover, the intraequatorial plane angles (P/C9–Fe–Cn, n = 1, 7) in **5b** are within 3° of the corresponding angles in **4b**. The two molecules are so similar that even the phosphine substituents have a very similar orientation with respect to the other ligands since the vast majority of the Cn–Fe–P–Cm (n = 1, 2, 4, 7; m = 11, 22, 31) and Fe–P–Cn–Cm (n = 11, m = 12, 13; n = 21, m = 22, 23; n = 31, m = 32, 33) torsional angles are within ± 5° of each other between the two structures. The geometric dimensions of the vinyl fragment show no chemically significant deviations from the corresponding parameters of the vinyl fragment in **4b**; the C4–C5, Fe–C4 distances and the planarity of the carbon backbone, *i.e.* C3–C4–C5–C6 torsional angle, in **5b** are in close agreement with the corresponding dimensions in **4b**.

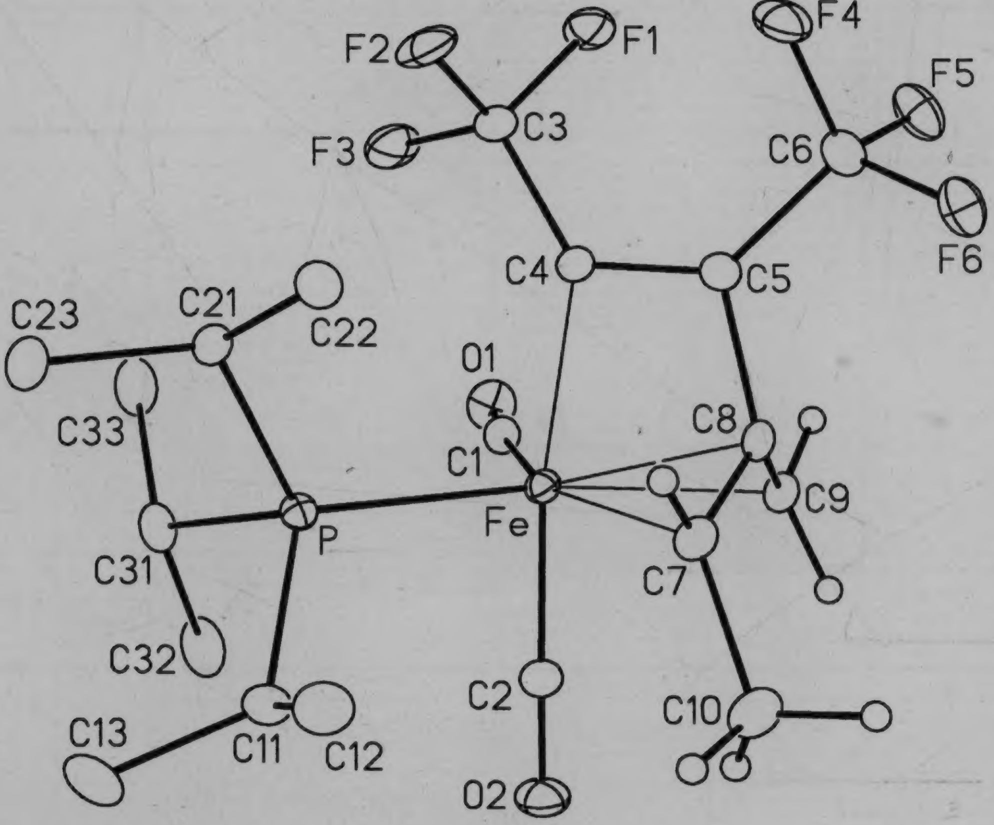
F1
F2
F3
C3
F4
F5
C6
F6
C4
C5
C23
C21
C22
O1
C33
C8
C1
C9
Fe
P
C31
C7
C32
C2
C10
C13
C11
C12
O2

Figure 3-15 Solid State Molecular Structure of **5b**.

Table 3-11 Selected Interatomic Distances (Å) and Angles (deg.) in **5b**.

Fe–P	2.3093(7)	P–Fe–C2	89.27(8)
Fe–C1	1.774(2)	P–Fe–C4	97.86(6)
Fe–C2	1.784(2)	P–Fe–C7	98.44(7)
Fe–C4	2.037(2)	C1–Fe–C2	93.7(1)
Fe–C7	2.236(2)	C1–Fe–C4	87.5(1)
Fe–C8	2.051(2)	C1–Fe–C9	90.7(1)
Fe–C9	2.172(2)	C2–Fe–C4	172.3(1)
C4–C5	1.325(3)	C2–Fe–C7	89.5(1)
C5–C8	1.504(3)	C2–Fe–C9	86.7(1)
C7–C8	1.402(3)	C4–Fe–C7	86.6(1)
C8–C9	1.411(3)	C4–Fe–C9	85.7(1)
O1–C1	1.144(3)	C7–Fe–C9	67.9(1)
O2–C2	1.145(3)	Fe–C1–O1	173.6(2)
P–Fe–C1	103.21(7)	Fe–C2–O2	177.3(2)

In regards to the η^3-1-methylallyl moiety, the methyl substituent (C10) is in an *anti*-position and the CHMe unit is *cis* to the P^iPr_3 ligand. The central carbon (C8) shows strong indications of primarily *sp*^{2} hybridization as the C7–C8–C9 angle is 122.3(2)° and the C8–Cn (n = 7, 9) separations are within 3σ of each other and are not significantly different from those in **4b**. As expected, the Fe–Cn (n = 7, 9) separations are larger that the Fe–C8 (2.051(2) Å) distance, but while the Fe–C9 (2.172(2) Å) distance is 0.121 Å (60 esd's) larger, a value typical of this parameter, the Fe–C7 distance (2.236 (2) Å) is much larger than expected and shows a strong asymmetry in the π-bonding of the allyl moiety. It has long been known that asymmetric metal-allyl bonding of this type can be caused by an asymmetric distribution of auxiliary ligands about the metal center. In the classic examples $[(\eta^3\text{-2-Me-}C_3H_4)(Cl)(PPh_3)Pd]$ [26] and $[(\eta^3\text{-2-Me-}C_3H_4)\{SC(Ph)C(H)C(Ph)O\}Pd]$ [27] the asymmetry in the metal-allyl bonding is explained in terms of the differing *trans* influence of the auxiliary ligands. Initially it might be concluded that the relatively strong *trans* influence of the C1O1 carbonyl, relative to that of the P^iPr_3 ligand, in **5b** is the cause of the unusually large Fe–C7 separation (C1–Fe–C7 = 158.14(10)°), but this is not the case since in **4b** and **4c**, the Fe–Cn (n = 7, 9) distances are within 3 and 4 esd's of each other, respectively. The marginally longer Fe–C7 distances in **4c** might suggest that the asymmetry in the *trans* ligand set plays a small role in the uneven metal-allyl bonding but it seems that this phenomenon is largely the result of some other effect.

Given the similarities between **5b** and **4b**, the root of the asymmetry in the metal-allyl bonding seems to be associated with the methyl substituent of the allyl. One obvious possibility is that this asymmetry is a result of increased intramolecular steric interaction involving the *anti*-methyl and the adjacent ligand environment since in going from **4b** to **5b** a hydrogen atom was replaced with a methyl group. This line of thought is not without precedent as Welch and Murrall have used steric crowding to explain the asymmetric metal-allyl bonding in the structure of [(η^3-1-Ph-C_3H_4)Pd(TMEDA)][BF_4] (TMEDA = N, N, N', N'-tetramethylethylenediamine) [28]. In the cation, the allylic Pd–CHPh separation (2.173(3) Å) is 0.049 Å (10 esd's) larger than the Pd–CH_2 separation (2.124(5) Å). The lack of a *trans* influence phenomenon coupled with the close contacts between the phenyl and one methyl of the TMEDA ligand led the authors to conclude that steric crowding was the primary cause of the asymmetry in the metal-allyl bonding. Returning to the solid state molecular structure of **5b**, a possible steric interaction between the bulky phosphine ligand and the allyl methyl seems the most obvious choice for steric crowding. Indeed, close proximity of the allyl methyl (C10) and one methyl (C12) of one ^{i}Pr group of the phosphine ligand suggests steric interaction between these two groups. The "effective" van der Waals radius of a methyl group has been estimated at 2.0 Å [29]. The C10···C12 separation of 3.65 Å in **5b** is decidedly within twice the sum of the van der Waals radii of two methyl groups, indicating possible steric repulsion.

Having that been said, a second intramolecular ligand-ligand crowding to consider in **5b**, and a less obvious one, is the close contact between C10 and the axial carbonyl (C2O2). The C2···C10 separation of 2.98 Å is clearly within the sum of the van der Waals radii of carbon (1.68 Å) [30] and a methyl group. Steric interaction between a carbonyl ligand and an *anti*-substituent of a π-allyl ligand in a somewhat similar structure has been reported in the literature. Dewan *et al.* have suggested that the bending back of an *anti*-methyl substituent (C1–C2–C3–R torsional angle = 40°, A in Figure 3-16) in the nonchelating η^3-*anti*-1-methylallyl ligand of [NEt_4][$Cr(CO)_3(P(OMe)_3)$(η^3-*anti*-1-methylallyl)] is not simply a result of "pyramidalization" but rather a consequence of intramolecular steric crowding since the *anti*-hydrogen, in the same ligand, showed a torsional angle of only 30° [31]. Furthermore, in the same molecule, they found that after independently refining the *anti*-methyl hydrogens one of them was positioned approximately eclipsed with the adjacent allylic C–C bond. This positioning of the methyl hydrogens maximizes the steric interaction between the allylic C–C bond and the methyl but minimizes the steric interaction between the methyl and a neighboring carbonyl ligand (C4O4 in Figure 3-16). In the same report, a bending back, away from the metal, of an ethenyl substituent (torsional angle = 45°) of an η^3-allyl ligand was observed in $Mn(CO)_3(PMe_3)(\eta^3$-*anti*-1-ethenylallyl) (**B** in Figure 3-16) [31,32]. For comparison purposes the methyl in **5b** is bent out of the allyl plane, away from the metal, by 44.3(3)° (C10–C7–C8–C9). Both the Cr and Mn structures show a noticeable bending of the axial ligands away from the allyl ligand (P–M–C4 = 170.8(1)°, **A**; 170.8(3)°, **B**). Strangely, in **5b** the axial carbonyl (C2O2 in Figure 3-15) is slightly leaning toward the allyl with a symmetric disposition between the two termini and this is also the case in **4b**.

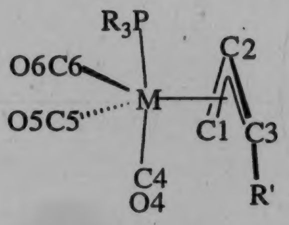

$M = Cr^-$, R = OMe, R' = Me, **A**;
M = Mn, R = Me, R' = $CHCH_2$, **B**

Figure 3-16 Structure of $[NEt_4][Cr(CO)_3(P(OMe)_3)(\eta^3$-*anti*-1-methylallyl)] (**A**) and $Mn(CO)_3(PMe_3)(\eta^3$-*anti*-1-ethenylallyl) (**B**) [31,32].

Table 3-12 Selected Interatomic Distances (Å) and Angles (deg.) in $[NEt_4][Cr(CO)_3(P(OMe)_3)(\eta^3\text{-}anti\text{-}1\text{-methylallyl})]$ (**A**) and $Mn(CO)_3(PMe_3)(\eta^3\text{-}anti\text{-}1\text{-ethenylallyl})$ (**B**) [31,32].

Parameter	A	B
M–C1	2.313(4)	2.199(13)
M–C2	2.164(4)	2.124(10)
M–C3	2.287(4)	2.255(11)
C1–C2	1.371(6)	1.381(19)
C2–C3	1.410(6)	1.440(17)
C3–R	1.499(6)	1.450(18)
P–M–C4	170.8(1)	170.8(3)
C1–C2–C3–R	40	45

It was concluded that in the Cr and Mn complexes the bending back of the *anti*-substituent is a result of steric interaction between the allyl substituent and the neighboring axial carbonyl ligand. Both of these complexes exhibit an asymmetry in the allyl $M–C_{terminal}$ distances. However, in the chromium anion, and in contrast to the related parameter in **5b**, the substituted allyl carbon is closer to the metal while in the manganese complex it is the unsubstituted allyl carbon which is closer to the metal (Table 3-12). The reasons for this inconsistency was not addressed in the report and a number of other structures of middle transition metal complexes with a η^3-*syn*/*anti*-1-methylallyl ligand show no correlation between the longer $M–C_{terminal}$ separation and the position of the allyl methyl [33]. This is troublesome and implies no simple correlation exists, and the issue of asymmetry in the allyl $M–C_{terminal}$ distances is more complex than the simple *trans* influence of auxiliary ligands or steric interaction between adjacent ligands and the allyl substituent.

Turning our attention to the allyl ligand itself, a third factor may affect the bonding of the allyl to the metal, namely the electronic properties of the substituted allyl ligand. It has been suggested that the electronic properties of the allyl termini in the asymmetrically substituted allyl ligand can be considerably different and this can lead to an non-uniform bonding to the metal [34]. Returning to the report by Murrall and Welch, mentioned previously, a second solid state molecular structure of a platinum complex with asymmetric metal-allyl bonding was presented [28]. In $[(\eta^5\text{–}C_5H_5)Pd(\eta^3\text{-1-Ph-}C_3H_4)]$ there are no *trans* influences or inter-/intramolecular steric factors that would explain why the substituted carbon atom of the allyl is further from the metal atom than the unsubstituted allyl carbon atom. The authors suggest that the origin of the metal-allyl distortion is associated with an anisotropy of the electronic properties of the substituted allyl ligand, which in turn is a consequence of the asymmetrical substitution of the allyl ligand. A second report by Welch *et al.* shows that in the molecular structure of $[(\eta^3\text{-1-}CO_2Et\text{-}C_3H_4)PdCl]_2$ and in the $[(\eta^3\text{–1–}CO_2Et\text{-}C_3H_4)Pd(TMEDA)]^+$ cation it is the substituted allylic carbon that is closer to the metal, albeit slightly, than the unsubstituted allylic carbon when the opposite is expected [35]. In these molecules the authors conclude that the counter intuitive asymmetric allylic bonding is a result of differing electronic properties across allyl ligand. In light of these findings Welch *et al.* conducted theoretical studies (Extended Hückel Molecular Orbital) on $[(\eta^3\text{-1-R-}C_3H_4)Pd(TMEDA)][BF_4]$ (R = Ph, CO_2Et) and although a full report of the results has not been published the authors claim that the results show the asymmetry in the metal-allyl bonding is a result of perturbation of the allyl frontier orbitals caused by substitution at one of the allyl terminus [36]. If this is true then this would explain the lack of correlation in regards to the asymmetry in the metal-allyl distances of substituted allyl ligands. This is because the inhomogeneous electronic properties of the asymmetrically substituted allyl ligand must be added to the *trans* influence of auxiliary ligands and the steric interaction between adjacent ligands and the allyl substituent as contributing factors that may influence the metal-allyl distances and presumable metal-allyl bonding in asymmetrically substituted η^3-allyl complexes.

In **5b** no theoretical studies have been conducted. Thus, in the absence of obvious electronic factors we are left with the steric interaction between the *anti*-methyl and both the axial carbonyl and the phosphine ligand accounting for the large Fe–C7 separation relative to the Fe–C9 separation. The large asymmetry in the metal-allyl bonding may be indicative of a move from an η^3-bonding mode to an η^1,η^2-bonding mode. However, there is still a high degree of delocalization among the allylic carbons as the C8–Cn (n = 7, 9) separations are identical, within 3σ of each other, and no indication of an asymmetry in the bond order is observed.

Concerning the other geometric parameters in the CHMe moiety, the C8–C7–C10 angle is 123.0(2)° which is close to ideal for a pure sp^3 hybridized C7. The C7–C10 distance of 1.525(3) Å is between the 1.542 Å of a typical covalent C_{sp^3}–C_{sp^3} separation and the 1.51 Å of a C_{sp^2}–C_{sp^3} separation and is comparable to the related parameter in the above mentioned structures from the chemical literature.

3.4.2 NMR Spectroscopic Analysis of

$Fe(CO)_2(PR_2R')(\eta^1,\eta^3\text{-}\{F_3CC{=}C(CF_3)C(CH_2)CHMe\})$ (5a-c)

With the crystal structure of **5b** in-hand, the best approach to discussing the solution spectroscopy of **5a-c** is by starting with **5b**. The NMR data of **5b** (Table 3–13), **5c** (Table 3-14) and **5a** (Table 3-15) are similar and for purposes of this discussion **5b** will serve as a representative example.

Table 3-13 The $^{31}P\{^1H\}$, ^{19}F, ^1H and $^{13}C\{^1H\}$ NMR Data (ppm, CD_2Cl_2, 27 °C) of **5bI** and **5bII**

Compound	$^{31}P\{^1H\}$	^{19}F	^1H/*COSY	$^{13}C\{^1H\}$/*$^{13}C\{^{19}F\}$
5bI (major isomer)	70.6	− 54.5 q $^5J_{FF}$ = 9 Hz − 65.3 dq $^5J_{FF}$ = 9 Hz, $^4J_{FP}$ = 2 Hz	4.06 dq $^3J_{HH}$ = 7 Hz, $^3J_{HP}$ = 2 Hz $CHCH_3$ 3.85 m H_{syn} 2.60 s H_{anti} 2.36 dsept $^3J_{HH}$ = 7 Hz, $^2J_{HP}$ = 7 Hz PCH 1.34* $CHCH_3$ 1.29 dd $^3J_{HH}$ = 7 Hz, $^3J_{HP}$ = 14 Hz $PCCH_3$ 1.29 dd $^3J_{HH}$ = 7 Hz, $^3J_{HP}$ = 14 Hz $PCCH_3$	217.7 d $^2J_{CP}$ = 4 Hz CO 214.0 d $^2J_{CP}$ = 20 Hz CO 154.7 dqq $^2J_{CP}$ = 19 Hz, $^2J_{CF}$ = 34 Hz, $^3J_{CF}$ = 4 Hz $C_\alpha(CF_3)$ 135.4 br $C_\beta(CF_3)$ 126.2 q $^1J_{CF}$ = 274 Hz CF_3 117.7 q $^1J_{CF}$ = 274 Hz CF_3 85.8 d $^2J_{CP}$ = 10 Hz $CHCH_3$ 84.7 br s $C_{central}$ 64.7 d $^2J_{CP}$ = 5 Hz CH_2 29.1 d $^2J_{CP}$ = 19 Hz PCH 20.4 s $PCCH_3$ 19.1 s $PCCH_3$ 17.5 s $CHCH_3$
5bII (minor isomer)	67.6	− 54.7 q $^5J_{FF}$ = 9 Hz − 65.4 dq $^5J_{FF}$ = 9 Hz, $^4J_{FP}$ = 2 Hz	4.68 m $CHCH_3$ 3.25 br s H_{syn} 2.66 br s H_{anti} 2.36 dsept $^3J_{HH}$ = 7 Hz, $^2J_{HP}$ = 7 Hz PCH 1.27* $CHCH_3$	218.1 d $^2J_{CP}$ = 7 Hz CO 213.7 d $^2J_{CP}$ = 21 Hz CO 156.4* d $^2J_{CP}$ = 20 Hz $C_\alpha(CF_3)$ 134.7* br s $C_\beta(CF_3)$ 117.5* s CF_3 84.0 br s $C_{central}$ 83.9 s $CHCH_3$ 64.8 d $^2J_{CP}$ = ~8 Hz CH_2 29.4 d $^2J_{CP}$ = 19 Hz PCH 20.3 s $PCCH_3$ 18.9 s $PCCH_3$ 16.1 s $CHCH_3$

Table 3-14 The $^{31}P\{^1H\}$, ^{19}F, ^1H and $^{13}C\{^1H\}$ NMR Data (ppm, CD_2Cl_2, 27 °C) of **5cI** and **5cII**

Compound	$^{31}P\{^1H\}$	^{19}F	^1H/*COSY	$^{13}C\{^1H\}$
5cI (major isomer)	61.2	– 54.2 q $^5J_{FF} = 9$ Hz – 65.1 dq $^5J_{FF} = 9$ Hz $^4J_{FP} = 3$ Hz	4.00 dq $^3J_{HH} = 8$ Hz $^3J_{HP} = 2$ Hz $CHCH_3$ 3.87 m H_{syn} 2.55 s H_{anti} 1.30* $CHCH_3$	218.1 d $^2J_{CP} = 5$ Hz CO 214.1 d $^2J_{CP} = 21$ Hz CO 154.9 dqq $^2J_{CF} = 34$ Hz $^2J_{CP} = 19$ Hz $^3J_{CF} = 4$ Hz $C_\alpha(CF_3)$ 135.3 qq $^2J_{CF} = 37$ Hz $^2J_{CF} = 10$ Hz $C_\beta(CF_3)$ 126.2 q $^5J_{FF} = 274$ Hz CF_3 117.7 q $^5J_{FF} = 274$ Hz CF_3 87.0 d br s $C_{central}$ 85.5 d $^2J_{CP} = 10$ Hz $CHCH_3$ 64.4 s CH_2 17.5 s $CHCH_3$
5cII (minor isomer)	56.4	– 54.6 q $^5J_{FF} = 9$ Hz – 65.3 dq $^5J_{FF} = 9$ Hz $^4J_{FP} = 3$ Hz	4.70 m $CHCH_3$ 3.19 s H_{syn} 2.64 s H_{anti} 1.21* $CHCH_3$	218.5 d $^2J_{CP} = 5$ Hz CO 213.8 d $^2J_{CP} = 22$ Hz CO 156.8 dqq $^2J_{CF} = 34$ Hz $^2J_{CP} = 19$ Hz $^3J_{CF} = 4$ Hz $C_\alpha(CF_3)$ 134.8 m $C_\beta(CF_3)$ 126.3 q $^1J_{CF} = 274$ Hz CF_3 117.6 q $^1JC_F = 274$ Hz CF_3 84.6 d br s $C_{central}$ 83.5 s $CHCH_3$ 64.6 d $^2J_{CP} = 9$ Hz CH_2 16.0 s $CHCH_3$

Table 3-15 The ^{31}P{^{1}H}, ^{19}F, ^{1}H and ^{13}C{^{1}H}APT NMR Data (ppm, CD_2Cl_2, 27 °C) of **5aI** and **5aII**

Compound	^{31}P{^{1}H}	^{19}F	^{1}H/*COSY	^{13}C{^{1}H}APT/*^{13}C{^{19}F}
5aI	68.7	– 52.7 q $^{5}J_{FF}$ = 8 Hz	3.87 q $^{3}J_{HH}$ = 7 Hz $C\mathit{H}CH_3$	217.6* br s $\mathit{C}O$
(major isomer)		– 64.5 br q $^{5}J_{FF}$ = 8 Hz	3.66 br m H_{syn}	215.0 d $^{2}J_{CP}$ = 20 Hz $\mathit{C}O$
			2.65 s H_{anti}	155.1 br $C_{\alpha}(CF_3)$
			1.41 d $^{2}J_{HP}$ = 7 Hz $PC\mathit{H}_3$	135.6 br $C_{\beta}(CF_3)$
			1.35 d $^{3}J_{HP}$ = 13 Hz $PC(C\mathit{H}_3)_3$	126.4 q $^{1}J_{CF}$ = 273 Hz $\mathit{C}F_3$
			1.30 d $^{3}J_{HP}$ = 13 Hz $PC(C\mathit{H}_3)_3$	117.7 q $^{1}J_{CF}$ = 275 Hz $\mathit{C}F_3$
			1.25* $CHC\mathit{H}_3$	83.8 (–) d $^{2}J_{CP}$ = 10 Hz $\mathit{C}HCH_3$
				85.3 br s $C_{central}$
				67.8 s $\mathit{C}H_2$
				38.1 m $P\mathit{C}CH_3/P\mathit{C}CH_3$
				30.3 (–) s $PC(\mathit{C}H_3)_3$
				29.8 (–) s $PC(\mathit{C}H_3)_3$
				17.5 (–) s $CH\mathit{C}H_3$
				11.8 (–) d $^{2}J_{CP}$ = 19 Hz $P\mathit{C}H_3$
5aII	64.2	– 52.7 q $^{5}J_{FF}$ = 8 Hz	4.57 br m $C\mathit{H}CH_3$	214.4 d $^{2}J_{CP}$ = 22 Hz $\mathit{C}O$
(minor isomer)		– 64.8 br q $^{5}J_{FF}$ = 8 Hz	3.12 s H_{syn}	157.5 br $C_{\alpha}(CF_3)$
			2.46 s H_{anti}	87.5 (–) s $\mathit{C}HCH_3$
			1.48 d $^{2}J_{HP}$ = 7 Hz $PC\mathit{H}_3$	84.2 br s $C_{central}$
			1.36 d $^{2}J_{CP}$ = 13 Hz $PC(C\mathit{H}_3)_3$	63.3 d $^{2}J_{CP}$ = 9 Hz $\mathit{C}H_2$
			1.31* $CHC\mathit{H}_3$	30.0 (–) s $PC(\mathit{C}H_3)_3$
				29.4 (–) s $PC(\mathit{C}H_3)_3$
				16.4 (–) s $CH\mathit{C}H_3$
				11.6 (–) d $^{2}J_{CP}$ = 20 Hz $P\mathit{C}H_3$

The data showed that two isomers of unequal population exist in solution. The major isomers are labeled **5nI** (n = a, b, c) while the minor isomers are labeled **5nII** (n = a, b, c). The ^{31}P NMR spectrum of **5b** showed two singlets in an intensity ratio of 5:1 (4:1, **5c**; 2:1, **5a**,) while the ^{19}F spectrum showed two sets of two signals each. Each set of ^{19}F signals consisted of a quartet and a quartet of doublets. The intensity ratio is consistent with that measured in the ^{31}P{^{1}H} spectrum. As in **4a-c** it is evident that a mixture of isomers coexist in solution.

The ^{1}H NMR spectrum of **5b** (Figure 3-17) also indicates two isomers in solution. The spectrum shows six signals above δ 2.5 ppm, in the typical allylic region. On the basis of their relative intensity, the six signals can be divided into two groups of three signals each. Considering the major isomer **5bI** first, it is clear from the relative intensities that the allyl methyl is not in this region.

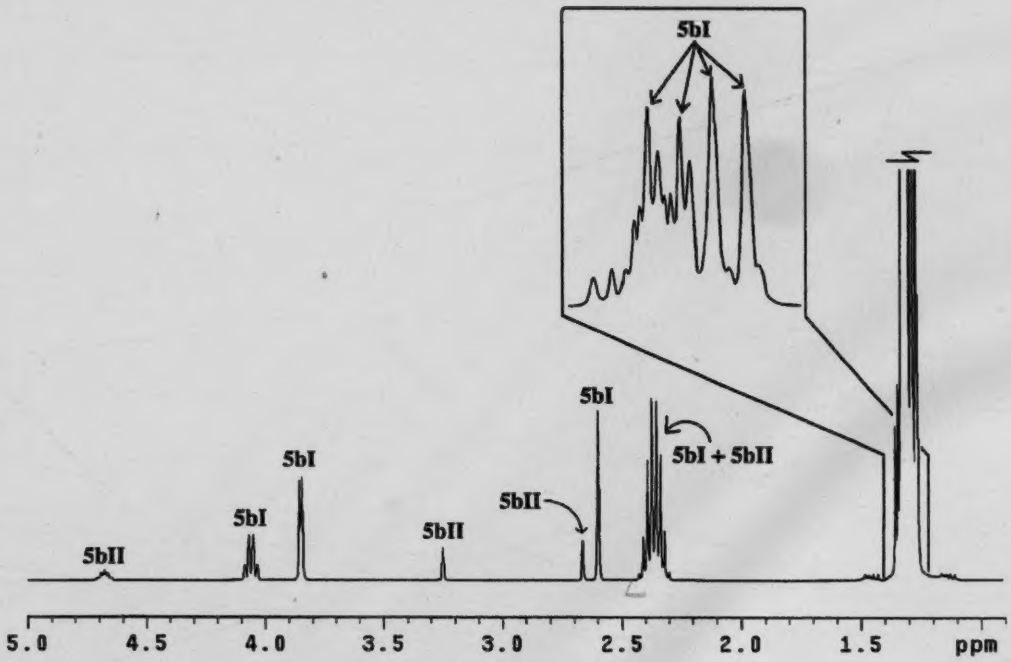

Figure 3-17 The ^{1}H NMR Spectrum (ppm, CD_2Cl_2) of **5b**.

The solid state molecular structure indicates an *anti*-methyl substituent, thus we expect two *syn*-protons and an *anti*-proton signal. The two resonances that appear at δ 4.06 and 3.85 ppm are in a region usually associated with *syn*-hydrogens. Thus, the remaining signal at δ 2.60 ppm is presumably due to the *anti*-hydrogen. The doublet of quartets at δ 4.06 ppm collapses into a quartet upon ^{31}P decoupling, implying that the quartet multiplicity is due to coupling with the methyl protons ($CHCH_3$). Indeed, the COSY spectrum shows a correlation between this signal and a signal at δ 1.34 ppm which cannot be observed in the ^1H NMR spectrum since it is masked by a mass of signals centered at δ 1.3 ppm and thus the intensity cannot be measured. This chemical shift is within the range indicated for the *anti*-methyl protons in known molecules (δ 1.40-1.21 ppm) [12c, 32, 33d]. Thus, the resonances at δ 4.06 and 1.34 (COSY) are assigned to the *syn*-hydrogen, $CHCH_3$, and the *anti*-methyl hydrogens, $CHCH_3$, of the substituted terminus of the allyl, respectively. For all **5a-c** the chemical shift of the $CHCH_3$ protons had to be located in the COSY spectrum (Tables 3-13, 14, 15). The multiplet at δ 3.85 ppm in **5b** collapses into a triplet upon ^{31}P decoupling and the COSY spectrum shows a correlation between this signal and the signals at δ 4.06 and 2.60 ppm. Hence, the "triplet" in the $^1H\{^{31}P\}$ is actually a doublet of doublets of similar coupling constants (~1.5 Hz) and this same signal in the ^1H spectrum is a result of an unresolved doublet ($^3J_{HP}$) of doublets ($^2J_{HH}$) of doublets ($^4J_{HH}$). Upon this basis the δ 3.85 ppm multiplet is assigned to the *syn*-hydrogen of the unsubstituted terminus. By elimination, and based on its chemical shift, the δ 2.60 ppm signal is assigned to the *anti*-hydrogen of the unsubstituted terminus of the allyl.

Upfield of the allylic resonances, we find the familiar pseudooctet of the PC*H* protons (cf. **4b**) located at a chemical shift (δ 2.36 ppm) that is unfortunately nearly coincident with the corresponding signal of **5bII**. These signals are separated by 1Hz and collapse into septets upon ^{31}P decoupling, a $^3J_{HH} = 7$ Hz was measured form each signal. Further upfield, the δ 1.36-1.26 ppm region is highly congested with a number of signals, presumably due to the other resonances of the phosphine ligand, that appear as a broad intense absorption. This is not wholly unexpected since, given the asymmetrically substituted allyl moiety, both isomers must be asymmetric. Thus, as in **4bII,** the phosphine ligand should give rise to one signal, probably a doublet ($^3J_{HH}$ = 7Hz) of doublets ($^3J_{HP}$), for each of the diastereotopic methyl of the ^{i}Pr groups and it is expected that these signals would appear with a similar chemical shift. In addition, we know from the COSY spectrum that the allylic methyls ($CHCH_3$) also appear in this region, probably with a multiple coupling pattern, adding yet more potential for overlap of signals. A detailed analysis of this region revealed that definitive NMR parameters, *i.e.* chemical shifts, integrations, multiplicities and thus coupling constants, for the $PCCH_3$ methyls of **5bII** could not be obtained from the ^1H NMR spectrum. However the resonances due to the methyls of the ^{i}Pr groups of **5bI** were identified. Upon selectively decoupling the ^{31}P resonance at δ 70.6 ppm, the dominant 1:1:1:1 quartet at δ 1.29 ppm (inset Figure 3-17), collapses into two barely resolved doublets ($^3J_{HH}$ = 7Hz), separated by 0.9 Hz. These doublets clearly dominate the $^1H\{^{31}P$; 70.6 ppm$\}$ spectrum. It is evident that this 1:1:1:1 quartet in the ^1H NMR spectrum is a result of two nearly superimposed or unresolved ($\Delta = 0.9$ Hz) doublet of doublets, each due to one diastereotopic methyl of the ^{i}Pr groups of the phosphine ligand in **5bI**. Unfortunately the $^1H\{^{31}P$; 67.6 ppm$\}$ or $^1H\{^{31}P\}$ spectrum failed to provide any additional information on the multiplicity or chemical shift of the methyls of the ^{i}Pr substituents of the minor isomer. Likewise, the multiplicity and chemical shift of the allylic methyls in **5bI** and **5bII** could not be definitively identified.

However the chemical shift was obtained from the COSY spectrum through correlation with the neighboring *syn*-hydrogen (C*H*Me) for both **5bI** and **5bII**.

Assignments in the ^1H NMR spectrum of **5bII** were made using a similar analysis to that used in **5bI**. Most notable is the assignment of the H_{syn} that is two bonds away from the methyl of the allyl group. This resonance appears at δ 4.68 ppm as a poorly resolved multiplet due to multiple coupling. Upon ^{31}P decoupling the signal appears as a broad quartet with $^3J_{HH} = 7$ Hz. The line shape indicates further coupling but the COSY spectrum indicated only coupling to the methyl of the allyl. A *syn*-hydrogen resonance at δ 3.25 ppm appears as a broad singlet but converts into a barely resolved doublets of doublets with $J_{HH} = 1$ and 2 Hz upon ^{31}P decoupling. The H_{anti} at δ 2.66 ppm also appears as a broad singlet. This line shape does not change upon ^{31}P decoupling. As discussed above, the protons of the allylic methyl appear within the mass of signals at δ 1.35-1.26 ppm and could not be unambiguously identified, but this signal was located at δ 1.27 ppm in the COSY spectrum through correlation with the C*H*CH$_3$ resonance.

The $^{13}C\{^1H\}$ NMR spectrum of **5b** is similar to that of **4b**, as such most assignments for the resonances of **5b** were made in a similar manner to that previously discussed. The data shows all resonances of **5bI** and nearly all the resonances of **5bII,** one *C*F$_3$ signal of the minor isomer was not observed. The $^{13}C\{^{19}F\}$ spectrum helped to identify some of the signals of the minor isomer. Obviously, the low concentration of the minor isomer prevents the detection of some of its signals. The carbonyl region clearly shows four doublets. Two signals are obviously more intense and show a 5:1 intensity advantage over the two minor signals. The two chemically inequivalent carbonyl signals for each isomer are consistent with ^1H NMR data and indicates two asymmetric structures. The region associated with the resonances of the vinyl group (δ 156-117 ppm) shows four signals for the major isomer. The CF_3 carbons were observed in their characteristic chemical shift region with their characteristically large one bond ^{13}C-^{19}F coupling. As in **4b**, the signals due to the α- and β-carbons of the vinyl group were initially observed as broad resonances. However additional information on their multiplicity was obtained. Upon closer examination, the resonance at δ 154.7 ppm, presumably due the α-carbon of the major isomer, was observed as a complex multiplet (Figure 3-18; **5bI**, *top and left*). Initially, its multiplicity could not be determined due to poor signal to noise ratio. Later excellent data was collected on a sample of **5c**, a result of an overnight $^{13}C\{^1H\}$ data collection, (Figure 3-18; **5cI**, *bottom and left*) and this led to a reinterpretation of the **5b** signal, based on the corresponding signal in **5c**. The signal of **5cI** (δ 154.9 ppm) appears as eight strong lines of equal intensity with additional smaller lines at the base. The eight lines of equal intensity can only be the result of coupling to the ^{31}P nucleus and the fluorine nuclei of both CF_3 groups, producing a doublet ($^2J_{CP}$) of quartets ($^2J_{CF}$) of quartets ($^3J_{CF}$). Upon decoupling ^{19}F the signal appeared as a doublet, confirming coupling to phosphours-31 with a $^2J_{CP}$ = 19 Hz. With the carbon-phosphorus coupling constant in hand the $^2J_{CF}$ and $^3J_{CF}$ were measured from the spectrum. To illustrate this, and further delineate the observed pattern, a reconstruction of the multiplicity was undertaken. Figure 3-19 shows a step-by-step reconstruction of a quartet of doublets of quartets using the measured coupling constants (*bottom*) and the actual δ 154.9 ppm signal in the $^{13}C\{^1H\}$ NMR spectrum of **5c** (*top*). Frame **A** (*bottom*) in Figure 3-19 shows the ^{13}C signal of the α-carbon in the absence of all coupling. Frame **B** shows this signal split into a binomial quartet due to coupling to the three chemically equivalent fluorines of one CF_3 group ($^2J_{CF}$ = 34 Hz). Frame **C** shows further splitting of the signals into doublets due to coupling to the ^{31}P nucleus ($^2J_{CP}$ = 19 Hz).

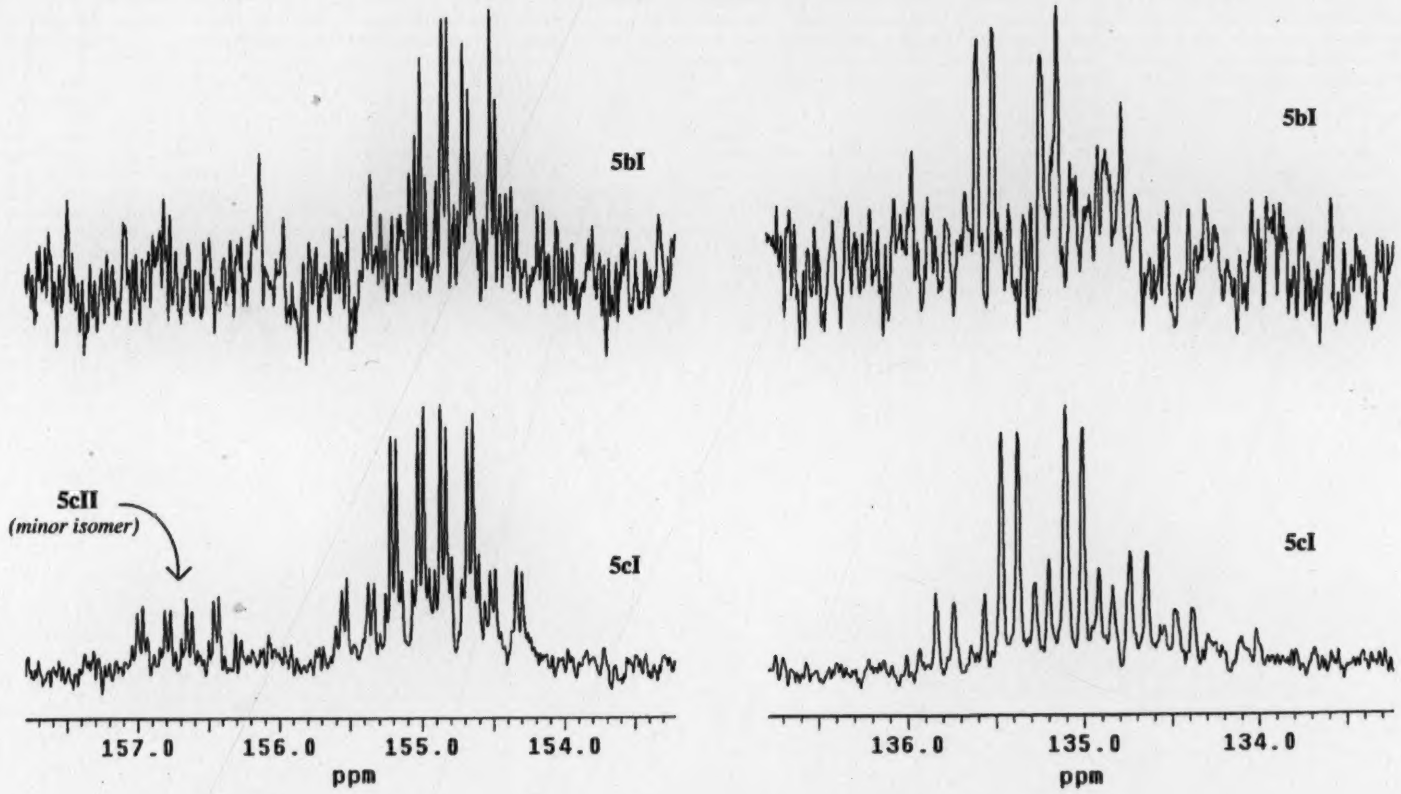

Figure 3-18 The $^{13}C\{^1H\}$ NMR Spectra (ppm, CD_2Cl_2) of α-Carbon (*left*) and β- Carbon (*right*) Region of **5b** (*top*) and **5c** (*bottom*).

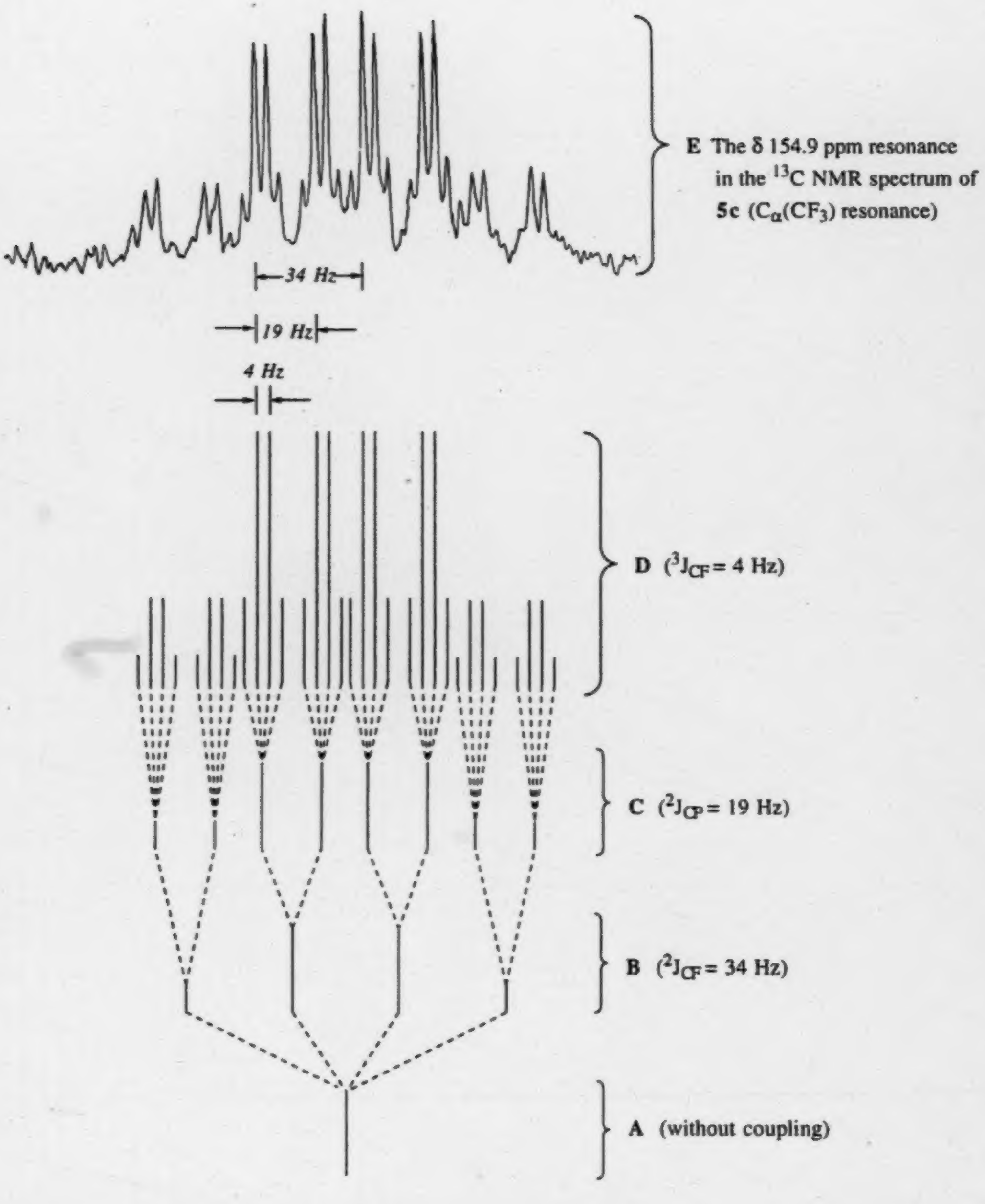
E The δ 154.9 ppm resonance in the ^{13}C NMR spectrum of 5c ($C_\alpha(CF_3)$ resonance)
34 Hz
19 Hz
4 Hz
D ($^3J_{CF}$ = 4 Hz)
C ($^2J_{CP}$ = 19 Hz)
B ($^2J_{CF}$ = 34 Hz)
A (without coupling)

Figure 3-19 Reconstruction of the α-Carbon Signal (δ 154.9 ppm) in the $^{13}C\{1H\}$ NMR Spectra (ppm, CD_2Cl_2) of **5c** .

Frame **D** shows the final multiplicity (q×d×q) upon factoring in the last carbon-fluorine coupling ($^3J_{CF}$ = 4 Hz). Comparison of the final reconstructed pattern to the signal observed at δ 154.9 ppm (frame **E**) shows a high degree of consistency, thus supporting the assignment of multiplicity. The resonance at δ 135.4 ppm in the $^{13}C\{^1H\}$ NMR spectrum of **5b** also appeared as a broad multiplet (Figure 3-18; *top and right*). Again, poor signal to noise prevented the unambiguous identification of the multiplicity. However, in the $^{13}C\{^1H\}$ NMR spectra of **5c**, the multiplicity of the corresponding signal at δ 135.3 ppm was identified as a quartet ($^2J_{CF}$) of quartets ($^3J_{CF}$) that arises from coupling to the two chemically inequivalent fluorine groups (Figure 3-18; *bottom and right*). Presumably, the same multiplicity pattern occurs in **5b** at δ 135.4 ppm. Again a comparison of a reconstruction and the actual signal shows a high degree of consistency (Figure 3-20).

The assignment of the δ 154.7 and 135.4 ppm signals as the α- and β-carbon, respectively, of the vinyl moiety was based on the observed $^2J_{CP}$ associated with the former and the correlation between the δ 2.60 ppm resonance (H_{anti}) and the latter in the HMBC spectrum. Although the signal of the α-carbon of the minor isomer of **5c** was clearly observed in the $^{13}C\{^1H\}$ NMR spectrum (Figure 3-18, **5cII**, *bottom left*), the α- and β-carbon of **5bII**, and the β-carbon of **5cII** could only be observed in the $^{13}C\{^{19}F\}$ NMR spectrum.

The region associated with the resonances of the bridgehead carbon of the allyl group (δ 83 - 88 ppm), surprisingly, shows four signals (Table 3-13). The two resonances at δ 84.7 and 84.0 ppm were assigned to the bridgehead carbons ($C_{central}$) of **5bI** and **5bII**, respectively, since each signal showed a correlation in the HMBC spectrum to the *anti*-hydrogen and the protons of the allylic methyl groups of the respective isomers.

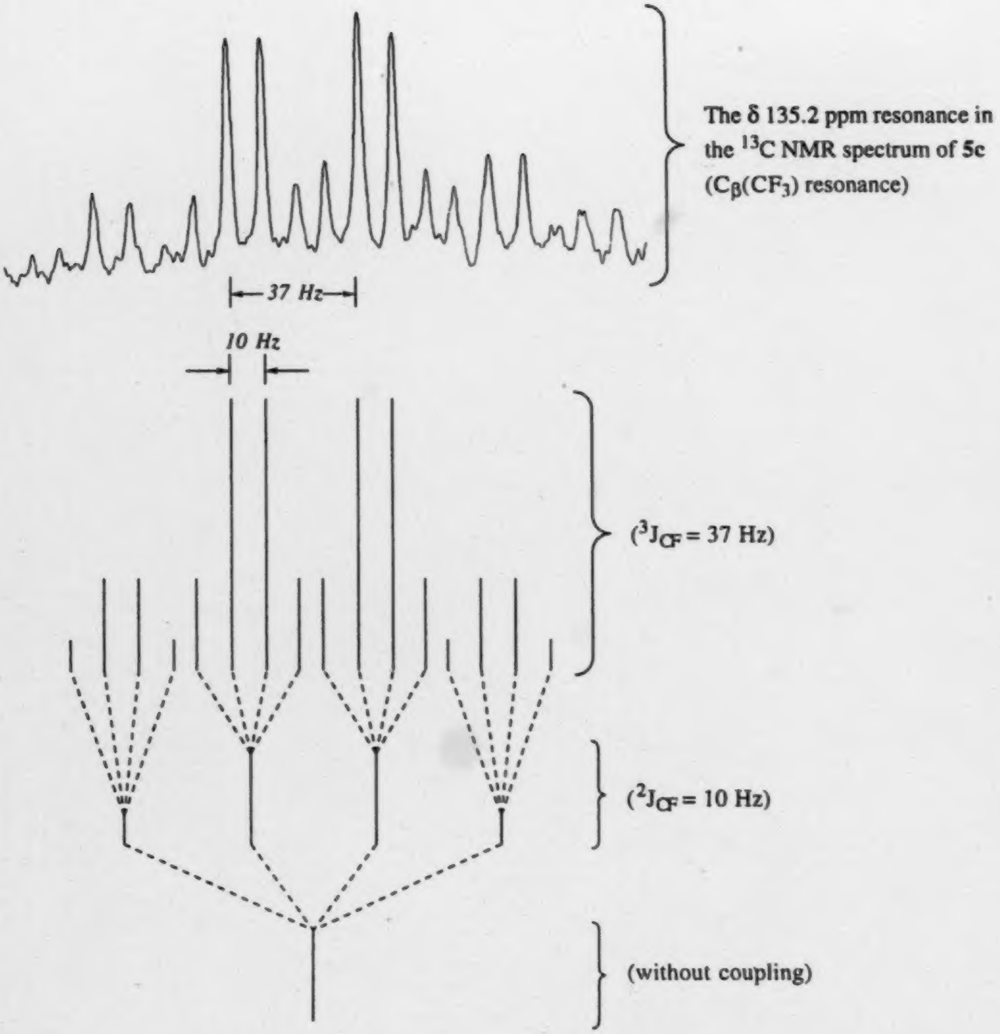

Figure 3-20 Reconstruction of the β-Carbon Signal (δ 135.2 ppm) in the $^{13}C\{1H\}$ NMR Spectra (ppm, CD_2Cl_2) of **5c** .

The two remaining signals, at δ 85.8 (doublet) and 83.9 (singlet) ppm, belong to **5bI** and **5bII**, respectively.The δ 84.0 ppm signal appears as a shoulder on the latter resonance. These signals were observed to correlate with their $C\mathit{H}CH_3$ (HMQC) and $CHC\mathit{H}_3$ (HMBC) protons of the corresponding isomer, and the corresponding signals in **5a** appeared in an inverted form in the $^{13}C\{^1H\}$APT spectrum. Clearly these resonances are due to the substituted carbon of the allyl (*C*HMe). This finding is significant because in **4nI/II** (n = a, b, c) the terminal carbons of the allyl (*C*H_2) were found in the δ 66-64 ppm region. In **5bI/II** this carbon, now with a methyl replacing a hydrogen, is shifted by 19-24 ppm downfield. Several transition metal complexes from the literature show a similar phenomenon [31, 33a, 33c, 33d]. In these compounds the chemical shift of the terminal allylic carbon with either a *syn*- or *anti*-methyl substituent was observed 10-20 ppm downfield relative to the resonance of the unsubstituted terminal carbon in the same allylic ligand. No explanation for the differing chemical shifts is offered in these reports and no correlation between the chemical shift of the terminal allylic carbons and the position of the methyl, either *syn* or *anti*, or the symmetry in the allylic bonding, or lack thereof, can be found, with one exception; the chemical shift of the substituted terminal carbon always appears downfield of the unsubstituted terminal carbon. This effect has also been observed in known allylic complexes with unsubstituted allyl ligands. In these complexes the metal-allyl bonding is either strongly asymmetric or the complex features a η^1-allyl ligand. It was concluded in these cases that the dramatic downfield shift of the allylic resonance is a result of the carbon taking on a more olefinic character [37]. This olefinic character is a result of the change from an η^3 toward an η^1,η^2 or η^1 bonding mode. As discussed previously, the solid state molecular structure of **5b** shows a definite asymmetry in the allylic Fe–$C_{terminal}$ separations (Fe–CH_2 = 2.172(2) Å; Fe–CHMe = 2.236(2) Å). However the allylic C–C separations are within error of the measurements and there is no indication of more olefinic character in one allylic C–C bond than the other. The chemical shift of the substituted allylic carbon in **5bI** (δ = 85.8 ppm) or **5bII** (δ = 83.9 ppm) is not significantly different than that of the corresponding carbon in free methylallene (*C*HMe, δ = 84.4 ppm). Thus, this phenomenon may simply be a result of substitution of a hydrogen by a methyl group in the allene molecule [38].

The chemical shift of the unsubstituted terminal carbons of the allyl (CH_2) in **5bI** and **5bII** were observed very close to the chemical shift of the related parameter in **4n** (n = a, b, c). However their resonances at δ 64.7 and 64.8 ppm, respectively, are partially overlapped; one half of the doublet of the δ 64.8 ppm signal appears as a shoulder on the much stronger signal at δ 64.7 ppm. In the $^{13}C\{^1H\}$ NMR spectrum of **5c** a very similar pattern is observed and although the two CH_2 signals are close together they are clearly separated. In **5b** these two positions are not resolved on the ^{13}C axis in the HMQC spectrum and appear as one, but the *syn*-hydrogen and *anti*-hydrogen of both **5bI** and **5bII** show a clear correlation with this single ^{13}C position. In the HMQC spectrum of **5c**, two distinct positions on the ^{13}C axis were resolved and correlation with the directly bonded *syn*- and *anti*-hydrogens of the corresponding isomer was clearly indicated.

As expected, the carbons of the phosphine ligand appear in the range 30–16 ppm. The two doublets centered at δ 29.1 and 29.4 ppm are assigned to the P*C*H carbon of **5bI** and **5bII**, respectively. These resonances were observed to correlate with the two nearly superimposed PC*H* signals (δ 2.36 ppm) in the HMQC spectrum. Upfield of these signals were observed an additional six signals. Their number and intensity (qualitative) are consistent with each isomer giving rise to two chemically inequivalent methyls of the ^{i}Pr groups (diastereotopic) and one methyl substituent of the allyl group. Specific correlations in the HMQC and HMBC could not be made due to overlap of multiple signals on the ^{1}H axis but these signals show a correlation to the mass of signals at δ 1.2–1.4 ppm.

As discussed above, the NMR data of **5c** (Table 3-14) closely resembled that of **5b**. No assignments with respect to the ^{1}H or ^{13}C NMR data of the cyclohexyl units of the phosphines could be proposed due to overlapping signals of the major and minor isomers. As in **5bI/II**, the substituted carbon of the allyl, in the ^{13}C{^{1}H} NMR spectrum, resonated (δ 85.5, **5cI**; δ 83.5 ppm, **5cII**) in the region normally associated with the central carbon of the allyl, while the unsubstituted carbon of was observed in the normal region (δ 64.4, **5cI**; 64.6, **5cII**).

The ambient temperature NMR spectra of **5a** (Table 3-15) was similar to that of **5b** and **5c**. However, some decomposition occurred at +27 °C over the several hours the experiments were conducted. Thus, in some cases the resolution or sensitivity suffered adverse effects. It was mentioned above that the NMR data show two isomers in solution. Indeed, the ^{31}P{^{1}H} NMR spectra show two singlets at a ratio of 2:1 but the ^{19}F NMR spectrum shows three signals with an intensity ratio of 1:0.66:0.33. It is evident that two signals are coincidence and combine to make the largest signal in the ^{19}F NMR spectrum. The pattern of signals in the ^{1}H NMR spectrum conforms to the spectral pattern demonstrated by **5b** and **5c**. However the PCH_3 signals of both **5aI** and **5aII** were well separated from the ^{t}Bu resonances and easily identified. The two resonances due to the diastereotopic ^{t}Bu groups of **5aI** were identified. In addition, one ^{t}Bu signal of the minor isomer was also identified. The allylic methyl resonances of **5aI/5aII** were not observed in the ^{1}H NMR spectrum, due to overlap, but the chemical shift was located in the COSY spectrum. The ^{13}C{^{1}H}APT data, supplemented with data from the ^{13}C{^{19}F} spectrum, of **5a** showed all of the resonances due to the major isomer but some of the minor isomer remained undetected. The spectra conformed well with the NMR data of **5bI/II** and **5cI/II**, but some observations are worth of note. Strangely, one carbonyl, δ 217.6 ppm, of **5aI** could only be detected in the $^{13}C\{^{19}F\}$ spectrum. Also, the $^{13}C\{^{1}H\}$APT spectrum helped confirm the assignment of the δ 83.8 (**5aI**) and 87.5 (**5aII**) ppm, and the δ 17.5 (**5aI**) and 16.4 (**5aII**) ppm resonances to the *C*HMe and CH*C*H$_3$ carbons, respectively.

The NMR data of **5n** (n = a, b, c) clearly indicate two isomers exist in solution. In light of the molecular structure of **5b** (Figure 3-15) it is expected that the methyl substituent occupies an *anti*-position on the allyl moiety. Indeed, the ^{1}H NMR spectrum supports this conclusion. For each isomer, one *anti*-hydrogen is observed in the region 1–3 ppm while two *syn*-hydrogens are observed in the 3-5 ppm region. The most downfield H_{syn} signal shows coupling to the protons of the allylic methyl, thus identifying this signal as the C*H*Me proton. The ^{1}H and ^{13}C NMR data confirm the expected asymmetric structure for both isomers. A reasonable conclusion is that geometric isomers coexist in solution, and that the structures are analogous to **4nI/II** (n = a, b, c). In this case both isomers must be asymmetric because of the asymmetrically substituted allyl moiety (**A** and **B** in Figure 3-21). In addition, a structure in which the methyl substituent is *trans* to the phosphine ligand (**C** in Figure 3-21) must be included as a possible isomer. Given these three possibilities, can we eliminate one based on the physical data?

The solid state molecular structure of **5b** (Figure 3-15) indicates **A** in Figure 3–21 as one definitive isomeric form. It is reasonable to conclude that this structure represents one of the isomers in solution. Of the two remaining structures in Figure 3-21, one may be excluded, based on the NMR data of the previous compounds of this type. Returning to the ^{13}C NMR data of **4nI/II** (n = a, b, c) (Tables 3-5, -8, -9) a pattern emerges concerning the $^2J_{CP}$ of the carbonyls.

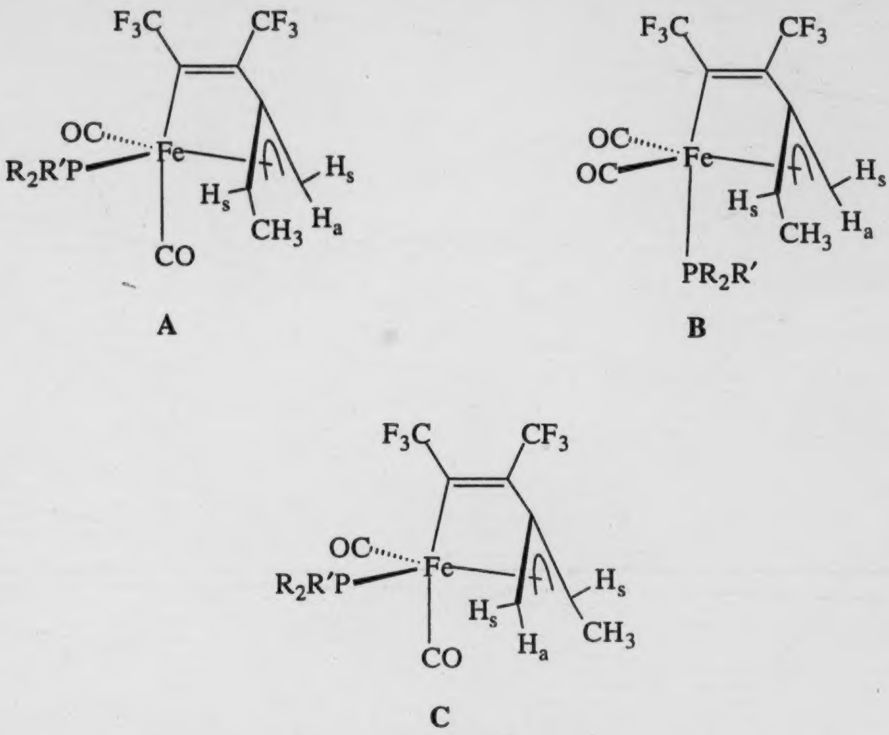

Figure 3-21 Possible Geometric Isomers of **5nI** and **5nII** (n = a, b, c).
(*enantiomers not shown*)

In the symmetrical, axial phosphine compounds **4nI** (n = a, b, c) the $^2J_{CP}$ is invariably within a narrow range, 16–19 Hz, while in the asymmetric, equatorial phosphine compounds **4nII** (n = a, b, c,) the magnitude of the $^2J_{CP}$ of one carbonyl is close to this value, in the 20-21 Hz range, but the other $^2J_{CP}$ of the second carbonyl is much smaller, in the 6-7 Hz range. This suggests that this correlation may be used as a diagnostic tool pertaining to the orientation of the carbonyls and phosphine ligand in similar structures. Consider the ^{13}C NMR data (carbonyl region) of **5nI/II** (n = b, c), the $^2J_{CP}$ values are very similar to those of **4nII**, that is, they are 4-7 Hz for one carbonyl and 20-21 Hz for the second carbonyl. We shall omit **5aII** for the time being due to poor ^{13}C NMR data regarding the carbonyls. However, **5aI** shows a

$^2J_{CP}$ = 20 Hz for one carbonyl and the second carbonyl appears as a broad singlet with a maximum width of 9 Hz. This suggests, on the basis of the correlation in **4nI/II** (n = a, b, c), that in **5nI/II** (n = b, c), **5aI**, and presumably **5aII**, the phosphine ligand is in an equatorial position and a carbonyl is in an axial position. This implies that structure **B** in Figure 3-21 is not one of the isomers in solution.

A further NMR data correlation, concerning the ^{1}H chemical shift of the protons of the methyl substituent of the phosphine ligand, in **4aI/II** and **5aI/II** can be used to exclude isomer **B**. Returning to the NMR data of **4aI/II** (Table 3-5), the PCH_3 protons in **4aI** appeared at δ 0.90 ppm, while in **4aII** the corresponding signal appeared at δ 1.43 ppm. This shows a relatively significant downfield shift in the δ of the PCH_3 protons in moving from the symmetric to asymmetric isomer. In **5aI** and **5aII** the chemical shift of the related parameter is δ 1.41 and 1.48 ppm, respectively. This is significant because it suggests, as in the ^{13}C NMR carbonyl data above, that the chemical shift of these protons could be used as an empirical diagnostic tool and would imply that in both **5aI** and **5aII** the carbonyls and phosphine ligand assume an orientation that is similar to that observed in **4aII**. On this basis, and in support of the previous conclusion, structure **B** in Figure 3-21 can be eliminated as a possible isomer for **5bI/II**. Thus for **5nI/II** (n = a, b, c) the structures of the two isomers in solution are represented by **A** and **C** in Figure 3-21.

Despite having determined the structures of the two isomers in solution, the issue of which structure in Figure 3-21 represents the major isomer and which structure represents the minor isomer is yet to be resolved. On an intuitive basis it seems reasonable to suggest that the major isomer is the one that minimizes steric interaction between the bulky phosphine ligand and the CHMe group of the allyl, **C** in Figure 3-21. In contrast, the solid state molecular structure of **5b** (Figure 3-15) suggests the counterintuitive option, **A** in Figure 3-21. However, the single crystal

X–ray structure analysis is not representative of the entire sample but rather representative of a single crystal of the sample. The implication here is that crystals of the other isomer could have been present in the sample submitted for crystallographic analysis. The ^{13}C NMR data does offer an avenue that resolves the question of the structure of the major and minor isomer. It is usually observed that through-metal two-bond ^{31}P-X (X = 1/2 spin nucleus) coupling constant ($^{2}J_{PX}$) between two ligands in a *trans*-orientation is larger than coupling between two ligands in a *cis*-orientation [39]. This phenomenon has been demonstrated in the case of $^{2}J_{PP}$ [40] and $^{2}J_{PC}$ [41]. A number of reports in the literature show that in η^3-allyl complexes with phosphorus donor ligands the ^{31}P nucleus exhibits a larger $^{2}J_{CP}$ with the *trans* terminal allyl carbon than with the *cis* terminal allyl carbon and this phenomenon can be reliably extended to η^3-allyl ligands with substitution at one terminus of the allyl [42]. In light of these precedent setting studies, the ^{13}C NMR data of **5a-c** does suggest a pattern.

Returning to the $^{13}C\{^1H\}$ NMR data of **5a-c** (Table 3-13, -14, -15) we see that in the case of the major isomer for **5a-c,** the substituted carbon appears as a doublet with $^{2}J_{CP}$ = ~10 Hz while the unsubstituted carbon appears as a singlet in **5aI** and **5cI** with a width at half height of 4-5 Hz, and a doublet in **5bI** $^{2}J_{CP}$ = 5 Hz. Evidently, the coupling between the phosphorus nuclei and the unsubstituted carbon of the allyl moiety is substantially less in these complexes. In the minor isomer of **5a** and **5c** the reverse is true and the unsubstituted carbon of the allyl now appears with the larger coupling to phosphorus ($^{1}J_{CP}$ = 9 Hz) while the substituted carbon appears as a slightly broadened singlet with a width at half height of 3-5 Hz. Comparison with the corresponding signals in **5bII** is not possible because the width at half height of the *C*HMe carbon singlet cannot be determined since the $C_{central}$ resonance of **5bII** appears as a shoulder on the *C*HMe signal. In addition, the CH_2 resonance of **5bII** appears as a doublet with one half, or one line, of the doublet as a shoulder on the larger CH_2 signal of the major isomer. However, the line shape of the signals strongly suggests a doublet multiplicity for the CH_2 signal of **5bII**, and the *minimum* $^2J_{CP}$ can be estimated to be 6 Hz. A similar pattern is observed in the ^{13}C NMR spectrum of **4aII** and **4bII**. In **4aII** one CH_2 carbon is observed as a singlet while the other is observed as a doublet with a $^2J_{CP}$ =10 Hz. In **4bII** one CH_2 carbon shows a $^2J_{CP}$ of 9 Hz while the other shows a $^2J_{CP}$ of only 4 Hz. The data for **4c** is inconclusive since the related signals are observed as broad singlets. Omitting **4c**, a pattern is exhibited by the available data and on the basis of the "trans-coupling" phenomenon it can be concluded that the carbon with the larger $^2J_{CP}$ in these complexes is *trans* to the phosphine ligand. Thus, the ^{13}C NMR data suggests a *trans* disposition between the phosphine ligand and the substituted terminus of the allyl in **5nI** (n = a, b, c) and a like disposition between the unsubstituted terminus of the allyl and the phosphine ligand in **5nII** (n = a, b, c). In Figure 3-21, **C** represents the structure of the major isomers **5nI** (n = a, b, c), while **A** represents the structures of the minor isomers, **5nII** (n = a, b, c).

3.5 Characterization of $Fe(CO)_2(PR_2R')(\eta^1,\eta^3\text{-}\{F_3CC{=}C(CF_3)C(CH_2)CMe_2\})$ (6a-c)

The molecular formulation of **6a-c** was based on the elemental microanalysis.

The IR spectrum of **6a-c** showed two terminal carbonyl stretches, the intensities indicative of a *cis*-carbonyl arrangement (Table 3-16).

Table 3-16 FT-IR Data (cm^{-1}, pentane) in the Carbonyl Region of **6a-c**

Compound	ν_{CO}
6a	2002 (s), 1951 (s)
6b	2001 (s), 1951 (s)
6c	2000 (s), 1947 (s)

Among the first data obtained for samples of **6a-c** was the solid state molecular structures of **6a** and **6b**. For reasons which will become clear later, these compounds will be labeled **6aI** and **6bI**. The characterization of these compounds will begin with these structures.

3.5.1 X-ray Crystal Structure Analysis of $Fe(CO)_2(PR_2R')(\eta^1,\eta^3\text{–}\{F_3CC{=}C(CF_3)C(CH_2)CMe_2\})$ (6aI, 6bI)

The solid state molecular structures of **6aI** and **6bI** were determined and were found to be similar. Small differences in structural parameters do, however, occur but for purposes of this thesis **6bI** serves well as a representative example.

Figure 3-22 shows the molecular structure of **6bI** (phosphine hydrogens omitted) with labeling scheme, while Table 3-17 lists selected interatomic distances and angles for both **6bI** and **6aI**. There are three molecules per asymmetric unit in the crystal of **6bI**. The three structures are similar and "molecule A" from the crystallographic analysis report will serve as a representative example. Positional disorder with respect to the three fluorines attached to C6 was observed. Two positions for each fluorine atom were calculated (*e.g.* F4A, F4B, F5A, etc.) and an occupancy of 50% was assigned to each position.

The arrangement of the ligands in **6b** is similar to those of the previous structures **4b** and **5b**. The phosphine ligand occupies an equatorial position, while a carbonyl (C2O2) occupies an axial position and the geometry around the iron is close to octahedral. The orientation of the Fe–C4 and Fe–C2 vectors with respect to the equatorial plane, and the intraequatorial angles are similar to the corresponding parameters in **4b**, and **5b**. Likewise the metrical parameters of the vinyl moiety (C3-C6) conform well to those of the previous structures. The focus of this discussion will be the 1,1–dimethylallyl moiety (C7-C11).

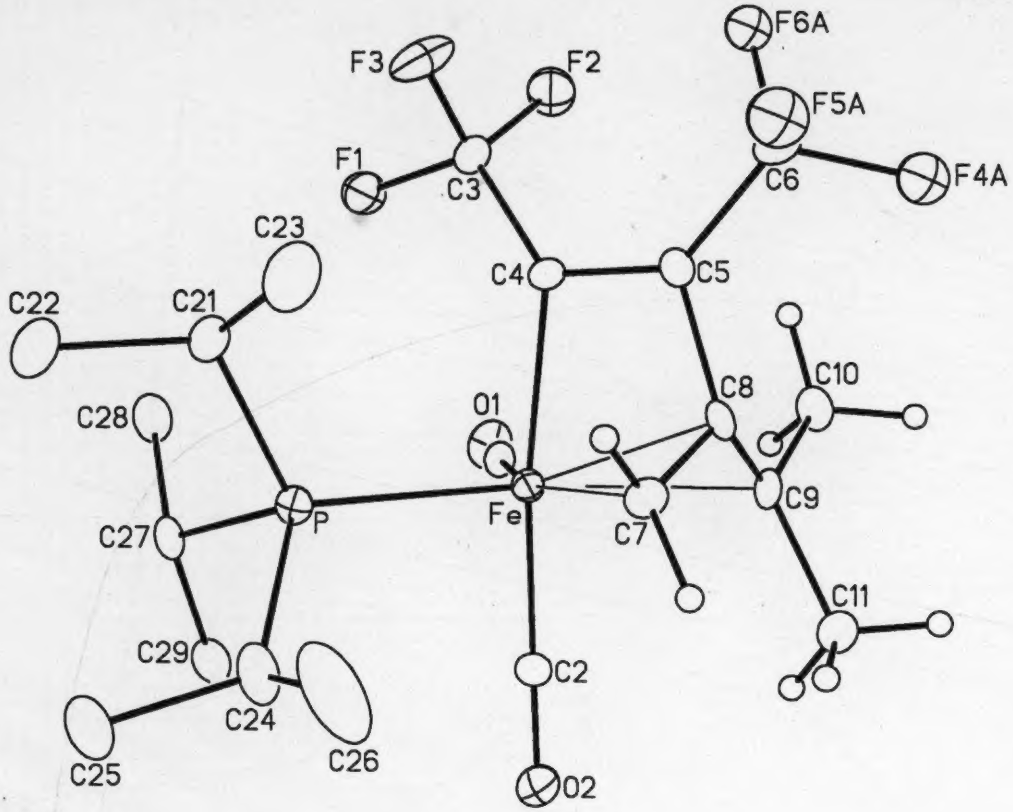
F6A
F3
F2
F5A
F1
C3
C6
F4A
C23
C4
C5
C22
C21
C10
C8
O1
C28
C9
P
Fe
C7
C27
C11
C29
C2
C24
C26
C25
O2

Figure 3-22 Solid State Molecular Structure of **6bI**.

As in **5b**, a strong asymmetry in the iron-allyl bonding is indicated. The Fe–Cn (n = 7, 9) separations of 2.145(7) and 2.287(7) Å, respectively, are greater than the Fe–C8 (2.071(7) Å) distance, but while the difference of 0.074 Å (11 esd's) between the Fe–C7/C8 separation is in the typical range, that between Fe–C8/C9 (0.216 Å, 31 esd's) is well beyond typical. Indeed the Fe–C9 separation is considerably greater than the Fe–C7 separation of 0.142 Å (20 esd's). These values are qualitatively comparable to the corresponding values in **5b,** that is, in both structures it is the substituted terminus of the allyl moiety that is farthest from the metal.

Table 3-17 Selected Interatomic Distances (Å) and Angles (deg.) in **6bI** and **6aI**.

Parameter	**6bI**	**6aI**
Fe–P	2.298(2)	2.3393(5)
Fe–C1	1.772(9)	1.771(2)
Fe–C2	1.780(7)	1.772(2)
Fe–C4	2.041(7)	2.049(2)
Fe–C7	2.145(7)	2.170(2)
Fe–C8	2.071(7)	2.063(2)
Fe–C9	2.287(7)	2.315(2)
C4–C5	1.343(10)	1.328(3)
C5–C8	1.490(10)	1.499(3)
C7–C8	1.395(10)	1.409(3)
C8–C9	1.419(10)	1.409(3)
O1–C1	1.142(9)	1.148(2)
O2–C2	1.145(8)	1.148(2)
P–Fe–C1	102.8(2)	97.8(1)
P–Fe–C2	89.1(2)	90.7(1)
P–Fe–C4	97.8(2)	98.3(5)
P–Fe–C7	97.3(2)	103.8(5)
P–Fe–C9	163.8(2)	169.1(5)
C1–Fe–C2	92.8(4)	95.2(1)
C1–Fe–C4	86.8(3)	86.3(1)
C1–Fe–C7	159.5(3)	157.9(1)
C1–Fe–C9	93.2(3)	92.4(8)
C2–Fe–C4	173.0(3)	170.7(1)
C2–Fe–C7	91.7(3)	89.6(1)
C2–Fe–C9	87.1(3)	84.5(1)
C4–Fe–C7	86.3(3)	85.7(1)
C4–Fe–C9	85.9(3)	86.2(1)
C7–Fe–C9	67.1(3)	66.5(1)
Fe–C1–O1	176.5(7)	174.6(2)
Fe–C2–O2	176.2(7)	175.6(2)

However in **6bI**, the C(9)Me_2 unit is *trans* to the phosphine ligand (P–Fe–C9 = 163.8(2)°) which is a very different arrangement to that observed in **5b**, where the CHMe unit is *cis* to the phosphine ligand. It was concluded that steric interactions between the *anti*-methyl and both the phosphine ligand and axial carbonyl (C2O2) in **5b** were the root cause of this asymmetry in the iron-$C_{terminal}$ separations. In **6bI** this asymmetry can be explained on the basis of steric interaction between both the *anti*-methyl (C11) and axial carbonyl (C2O2), and the *syn*-methyl (C10) and equatorial carbonyl (C1O1), since the C11···C2 and the C10···C1 separations of 2.879 and 3.166 Å, respectively, are decidedly within the sum of the van der Waals radii of a carbon atom and a methyl group (3.68 Å) [29, 30]. As in **5b**, and in spite of the asymmetry in the Fe–$C_{terminal}$ separations, the allylic C–C separations in **6bI** (C8–Cn, n = 7, 1.395(10) Å; n = 9, 1.419(10) Å) do not indicate a deviation from an η^3-allyl bonding mode.

In regards to the structural parameters of the CMe_2 moiety, the *anti*-methyl is positioned 41(1)° (C7–C8–C9–C11) out of the allylic plane, away from the metal. This value is close to the corresponding parameter in **5b** (44.3(3)°). The C7–C8–C9–C10 torsional angle indicates that the *syn*-methyl is positioned out of the allyl plane, toward the iron, by 11.2(7)°. Unfortunately, comparison to *syn*-methyl, or a similar simple *syn*-substituent, in known structures was not possible since relatively few structures are reported and when they are this structural parameter is not provided. However this parameter in **6bI** is within the range indicated for *syn*-hydrogens as they are found to be positioned 0-15° out of the allyl plane, toward the metal [7c, 7g, 28, 35,]. The C9–Cn (n = 10, 11) separations are equal within error of experimental measurements and not significantly different from the CH–Me distance in **5b**.

3.5.2 NMR Spectroscopic Analysis of $Fe(CO)_2(PR_2R')(\eta^1,\eta^3\text{-}\{F_3CC{=}C(CF_3)C(CH_2)CMe_2\})$ (6aI-6cI)

The NMR data of **6nI** (n = b, c, a), Tables 3-18, 3-19 and 3-20, respectively, are similar and as such the NMR spectra of **6bI** serves well as a representative example. In contrast to the previous compounds **4a-c** and **5a-c**, the $^{31}P\{^1H\}$ and ^{19}F NMR spectra indicate one compound in solution. The $^{31}P\{^1H\}$ shows one signal while the ^{19}F shows two signals at an intensity of 1:1. The familiar quartet ($^5J_{FF}$) and doublet of quartets (J_{FP} and $^5J_{FF}$) patterns are observed for the two ^{19}F signals.

The ^1H NMR spectrum also indicates the presence one compound and, as expected, exhibits characteristics of an asymmetric molecular structure. A doublet of doublets, assigned to the *syn*-hydrogen is observed at δ 3.56 ppm. The multiplicity pattern is consistent with spin-spin coupling to phosphorus, which was confirmed by decoupling the ^{31}P nuclei, and coupling to the *anti*-hydrogen located at δ 2.36 ppm. The *syn*-hydrogen and *anti*-hydrogen show a correlation in the COSY spectrum. The *anti*-hydrogen signal appears within the familiar pseudooctet of the PC*H* resonance, but the two signals can be resolved buy decoupling the ^{31}P nuclei. Two doublets appear at δ 1.78 and 1.47 ppm. Their assignment as the methyls of the allyl group is based on their relative intensity. Contrary to **5b**, the signals of the allylic methyls are well separated from the signals of the two diastereotopic methyls of the ^{i}Pr groups, which appear as doublets of doublets at δ 1.29 and 1.28 ppm.

It is reassuring, and supports our earlier assignment concerning **5nI/II** (n = a, b, c) (Section 3.4.2), that the ^1H resonance of the PCH_3 protons appears at δ 1.38 ppm in **6aI** (Table 3-20), close to the chemical shift of the corresponding resonance in **4aII** (δ 1.43 ppm). Thus, it appears that the chemical shift of this group can be used as a diagnostic; a signal in the δ 1.41-1.48 ppm region is indicative of the phosphine ligand in an equatorial position, while a chemical shift around δ 0.90 ppm is indicative of the phosphine ligand in an axial position.

Table 3-18 The $^{31}P\{^{1}H\}$, ^{19}F, ^{1}H and $^{13}C\{^{1}H\}$APT NMR Data (ppm, CD_2Cl_2, 27 °C) of **6bI**

Compound	$^{31}P\{^{1}H\}$	^{19}F	^{1}H	$^{13}C\{^{1}H\}$APT
6bI	72.9	-54.8 q $^{5}J_{FF} = 9$ Hz -66.2 dq $^{5}J_{FF} = 9$ Hz $J_{FP} = 3$ Hz	3.56 dd $^{2}J_{HH} = 2$ Hz $^{3}J_{HP} = 4$ Hz H_{syn} 2.36 br s H_{anti} 2.34 dsept $^{3}J_{HH} = 7$ Hz $^{2}J_{HP} = 7$ Hz $\mathrm{PC}\mathit{H}$ 1.78 d $^{4}J_{HP} = 1$ Hz $\mathrm{C}\mathit{C}\mathrm{H_3}$ 1.47 d $^{4}J_{HP} = 1$ Hz $\mathrm{CC}\mathit{H}_3$ 1.29 dd $^{3}J_{HP} = 14$ Hz $^{3}J_{HH} = 7$ Hz $\mathrm{PCC}\mathit{H}_3$ 1.28 dd $^{3}J_{HH} = 7$ Hz $^{3}J_{HP} = 13$ Hz $\mathrm{PCC}\mathit{H}_3$	216.8 d $^{2}J_{CP} = 4$ Hz $\mathit{C}\mathrm{O}$ 214.8 dq $^{2}J_{CP} = 21$ Hz $^{4}J_{CF} = 1$ Hz $\mathit{C}\mathrm{O}$ 156.1 dqq $^{2}J_{CF} = 32$ Hz $^{2}J_{CP} = 19$ Hz $^{3}J_{CF} = 4$ Hz $\mathit{C}_{\alpha}\mathrm{(CF_3)}$ 132.6 qq $^{2}J_{CF} = 37$ Hz $^{3}J_{CF} = 10$ Hz $\mathit{C}_{\beta}\mathrm{(CF_3)}$ 126.0 q $^{1}J_{CF} = 273$ Hz $\mathit{C}\mathrm{F_3}$ 117.5 q $^{1}J_{CF} = 274$ Hz $\mathit{C}\mathrm{F_3}$ 107.0 dq $^{2}J_{CP} = 9$ Hz $^{4}J_{CF} = 1$ Hz $\mathit{C}\mathrm{(CH_3)_2}$ 82.4 qq $^{3}J_{CF} = 3$ Hz $^{4}J_{CF} = 1$ Hz $\mathit{C}_{central}$ 59.3 dq $^{2}J_{CP} = 5$ Hz $^{4}J_{CF} = 2$ Hz $\mathit{C}\mathrm{H_2}$ 29.0 (–) d $^{1}J_{CP} = 19$ Hz PCH 24.4 (–) s $\mathrm{C}\mathit{C}\mathrm{H_3}$ 23.2 (–) s $\mathrm{C}\mathit{C}\mathrm{H_3}$ 20.1 (–) s $\mathrm{PC}\mathit{C}\mathrm{H_3}$ 18.8 (–) s $\mathrm{PC}\mathit{C}\mathrm{H_3}$

Table 3-19 The $^{31}P\{^1H\}$, ^{19}F, ^1H and $^{13}C\{^1H\}$APT NMR Data (ppm, CD_2Cl_2, 27 °C) of **6cI**

Compound	$^{31}P\{^1H\}$	^{19}F	^1H	$^{13}C\{^1H\}$APT
6cI	62.4	– 54.3 q $^5J_{FF} = 9$ Hz – 65.7 dq $^5J_{FF} = 9$ Hz $J_{FP} = 2$ Hz	3.57 dd $^2J_{HH} = 2$ Hz $^3J_{HP} = 4$ Hz H_{syn} 2.28 br s H_{anti} 1.76 d $^4J_{HP} = 1$ Hz CCH_3 1.46 d $^4J_{HP} = 1$ Hz CCH_3	217.4 d $^2J_{CP} = 3$ Hz CO 215.1 dq $^2J_{CP} = 20$ Hz $^4J_{CF} = 4$ Hz CO 156.4 dqq $^2J_{CF} = 34$ Hz $^2J_{CP} = 20$ Hz $^3J_{CF} = 4$ Hz $C_\alpha(CF_3)$ 132.6 qq $^2J_{CF} = 37$ Hz $^3J_{CF} = 10$ Hz $C_\beta(CF_3)$ 126.2 q $^1J_{CF} = 275$ Hz CF_3 117.5 q $^1J_{CF} = 274$ Hz CF_3 106.7 dq $^2J_{CP} = 9$ Hz $^4J_{CF} = 1$ Hz $C(CH_3)_2$ 82.6 qq $^3J_{CF} = 3$Hz $^4J_{CF} = 1$ Hz $C_{central}$ 58.8 dq $^2J_{CP} = 5$ Hz $^4J_{CF} = 1$ Hz CH_2 39.0 (–) d $^1J_{CP} = 17$ Hz PCH 30.2 s PC_6H_{11} 29.1 br s PC_6H_{11} 28.1 d $^2J_{CP} = 9$ Hz PC_6H_{11} 27.7 d $^2J_{CP} = 10$ Hz PC_6H_{11} 26.6 s PC_6H_{11} 24.4 (–) s CCH_3 23.1 (–) s CCH_3

Table 3-20 The $^{31}P\{^1H\}$, ^{19}F, ^1H and $^{13}C\{^1H\}$APT NMR Data (ppm, CD_2Cl_2, 27 °C) of **6aI**

Compound	$^{31}P\{^1H\}$	^{19}F	^1H	$^{13}C\{^1H\}$APT
6aI	71.8	− 53.4 q $^5J_{FF}$ = 9 Hz	3.37 dd $^2J_{HH}$ = 2 Hz $^3J_{HP}$ = 4 Hz H_{syn}	217.0 d $^2J_{CP}$ = 4 Hz $\mathit{C}\mathrm{O}$
		− 65.7 dq $^5J_{FF}$ = 9 Hz J_{FP} = 2 Hz	2.40 br s H_{anti}	216.3 dq $^2J_{CP}$ = 21 Hz $^4J_{CF}$ = 2 Hz $\mathit{C}\mathrm{O}$
			1.74 d $^4J_{HP}$ = 2 Hz $\mathrm{C}\mathit{CH}_3$	156.2 dqq $^2J_{CF}$ = 34 Hz $^2J_{CP}$ = 19 Hz $^3J_{CF}$ = 4 Hz $C_\alpha(\mathrm{CF}_3)$
			1.41 d $^4J_{HP}$ = 1 Hz $\mathrm{C}\mathit{CH}_3$	133.4 qq $^2J_{CF}$ = 37 Hz $^3J_{CF}$ = 10 Hz $C_\beta(\mathrm{CF}_3)$
			1.38 d $^2J_{HP}$ = 7 Hz $\mathrm{PC}\mathit{H}_3$	126.6 q $^1J_{CF}$ = 274 Hz $\mathit{C}\mathrm{F}_3$
			1.34 d $^3J_{HP}$ = 13 Hz $\mathrm{PC}(\mathrm{C}\mathit{H}_3)_3$	117.8 q $^1J_{CF}$ = 273 Hz $\mathit{C}\mathrm{F}_3$
			1.31 d $^3J_{HP}$ = 13 Hz $\mathrm{PC}(\mathrm{C}\mathit{H}_3)_3$	106.0 dq $^2J_{CP}$ = 10 Hz $^4J_{CF}$ = 1 Hz $\mathit{C}(\mathrm{CH}_3)_2$
				83.6 qq $^3J_{CF}$ = 1 Hz $^4J_{CF}$ = 3 Hz $C_{central}$
				61.8 dq $^2J_{CP}$ = 5 Hz $^4J_{CF}$ = 1 Hz $\mathit{C}\mathrm{H}_2$
				38.3 d $^1J_{CP}$ = 14 Hz $\mathrm{P}\mathit{C}(\mathrm{CH}_3)_3$
				38.2 d $^1J_{CP}$ = 14 Hz $\mathrm{P}\mathit{C}(\mathrm{CH}_3)_3$
				30.2 (–) d $^2J_{CP}$ = 4 Hz $\mathrm{PC}(\mathit{C}\mathrm{H}_3)_3$
				29.9 (–) d $^2J_{CP}$ = 4 Hz $\mathrm{PC}(\mathit{C}\mathrm{H}_3)_3$
				24.8 (–) s $\mathrm{C}\mathit{C}\mathrm{H}_3$
				23.7 (–) s $\mathrm{C}\mathit{C}\mathrm{H}_3$
				11.7 (–) d $^1J_{CP}$ = 19 Hz $\mathrm{P}\mathit{C}\mathrm{H}_3$

Excellent results were obtained with the $^{13}C\{^{1}H\}$APT spectrum as a result of an overnight data collection. As expected two signals of intensity 1:1 appeared in the carbonyl region. The $^{2}J_{CP}$ coupling constants exhibited by the carbonyls is indicative of a structure in which the phosphine ligand occupies an equatorial site (Section 3.4.2) and this is fully consistent with the solid state molecular structure of **6bI**. The δ 214.8 ppm signal shows long range coupling to three equivalent fluorines. This was supported in the HMBC (^{19}F-^{13}C) spectrum as the fluorine signal at δ –53.4 ppm shows a correlation with the ^{13}C NMR signal at δ 214.8 ppm. The ligating carbon of the vinyl at δ 156.1 ppm shows a multiplicity pattern that was observed previously (c.f. **5c**, Section 3.4.2). In addition, the HMBC (^{19}F–^{13}C) spectrum shows that this signal correlates with both fluorine signals and the signal appears as a doublet with $^{2}J_{CP}$ = 19 Hz upon ^{19}F decoupling. The four lines of equal intensity at δ 132.6 ppm are assigned to the β-carbon of the vinyl unit and interpreted as a quartet of quartets. Both ^{19}F signals correlate with this signal in the HMBC (^{19}F–^{13}C) spectrum thus corroborating the multiplicity. The carbons of the trifluoromethyl groups resonate within their characteristic chemical shift region and with their characteristic $^{1}J_{CF}$ coupling constant. In the HMQC (^{19}F–^{13}C) spectrum these signals at δ 126.0 and 117.5 ppm correlate with the δ –54.8 and –66.2 ppm resonances, respectively.

Surprisingly, a strong doublet (J = 9 Hz) of quartets (J = 1 Hz) appeared at δ 107.0 ppm. A resonance in this region has not been observed in the previous compounds **4n**-**5n** (n = a, b, c). Obviously, the doublet splitting is due $^{2}J_{CP}$ coupling, while the quartet splitting is due to J_{CF} coupling. The latter was confirmed by conducting $^{13}C\{^{19}F\}$ experiments. The δ 59.3 ppm signal is identified as the carbon of the unsubstituted terminus of the allyl (CH_2), through correlation with its attached protons in the HMQC spectrum; therefore, two possible assignments could be argued for the δ 107.0 ppm signal: either this signal is the central carbon of the allyl or the doubly substituted carbon of the allyl (*C*Me$_2$). Of course assignment of this signal necessarily determines the assignment of the signal at δ 82.4 ppm since this is the only other unassigned signal observed in the region in which the allylic carbons are normally found. In the ^{13}C NMR spectra of **4n-5n** (n = a, b, c) the central carbon of the allyl invariably appears in the narrow δ 84-87 ppm range and never with more than a few Hz coupling to ^{31}P, which seems to eliminate $C_{central}$ as a possible assignment to the δ 107.0 ppm signal since a $^2J_{CP}$ = 9 Hz is associated with this signal. On the other hand, assignment of the δ 107.0 ppm resonance to the doubly substituted allylic carbons looks promising. As discussed earlier, the chemical shift of the unsubstituted allylic carbon (CH$_2$) in **4nI/II** (n = a, b, c) is shifted by 19-24 ppm upon replacing a hydrogen with a methyl (CHMe) as in **5nI/II** (n = a, b, c). It is possible that this trend continues as the *C*HMe signal in **5bI/II** at δ 85.8 and 83.9 ppm is shifted 21-23 ppm downfield to 107.0 ppm in **6bI** as the second allylic hydrogen is replaced with a methyl. In addition, we have seen that if the allyl terminus, substituted or unsubstituted, is in a *trans* position with respect to the phosphine ligand, the allylic carbon shows a $^2J_{CP}$ = 9-10 Hz as in **4nII** (n = a, b) and **5nI/II** (n = a, b, c), and the carbon of the other allyl terminus shows a $^2J_{CP}$ that is typically 5Hz or less. The solid state molecular structure of **6bI** clearly shows the CMe$_2$ moiety and the phosphine ligand in a *trans* disposition. Moreover, the δ 59.3 ppm signal, which was unambiguously identified as the *C*H$_2$ resonance, exhibits a $^2J_{CP}$ = 5 Hz. Therefore, based on these observations, the resonances in the δ 106-107 ppm region in the ^{13}C NMR spectrum of **6nI** (n = a, b, c) are assigned to the doubly substituted carbon of the allyl.

Earlier, it was suggested that the downfield chemical shift of an allyl carbon is indicative of a strong olefinic character (Section 3.4.2). The δ 107.0 ppm signal is now within the chemical shift region of pure olefinic carbons ($R_2C{=}CH_2$) [43] or the γ–carbon of an η^1–allyl ligand ($M{-}C_\alpha H_2{-}C_\beta H{=}C_\gamma H_2$) [37b, 44]. The solid state molecular structure shows no indication of an increase in olenfinic character in one part of the allyl moiety since the two allylic C–C separations are within experimental error. In **5bI/II** the chemical shift of the allylic *C*HMe carbon (δ 85.8 (**5bI**) and 83.9 (**5bII**) ppm) was found near the chemical shift of the related signal (=*C*HMe) in free methylallene (δ 84.4 ppm). In **6bI** the chemical shift of the CMe_2 carbon (δ 107.0 ppm) is shifted about 13 ppm downfield of the related signal ($={C}Me_2$) in free 1,1-dimethylallene (δ 94.2 ppm). The reason for this phenomenon is not clear at this time.

With the δ 107.0 ppm signal assigned to the substituted carbon of the allyl, the δ 82.4 ppm resonance is assigned to the central carbon of the allyl, and as discussed above the δ 59.3 ppm resonance has been assigned to the CH_2 carbon. The ^{13}C NMR resonances of the phosphine ligand appear in their characteristic region. All assignments concerning these signals were confirmed using APT, HMQC and/or HMBC experiments. In particular the spectrum indicates two chemically distinct Me groups. The two methyl substituents of the allyl also appear in this region, at δ 24.4 and 23.2 ppm. They show correlation in the HMQC spectrum with the ^1H signals at δ 1.47 and 1.78 ppm, respectively.

The NMR data of **6bI** is fully consistent with the molecular structure obtained from the X-ray crystal structure analysis. Thus, in solution the phosphine ligand occupies an equatorial position, the doubly substituted terminus of the allyl (CMe_2) is *trans* to the phosphine ligand and the allyl is in an asymmetric η^3-bonding mode. With the exception of the resonances due to the phosphine ligands, the NMR data of **6cI** and

6aI are very similar in chemical shift, multiplicity, and coupling constants to the NMR data of **6bI**. In fact, so much so that they are nearly identical in many cases. It is therefore reasonable to conclude that the structures of **6aI** and **6cI** in solution are analogous to that of **6bI** (Figure 3-23).

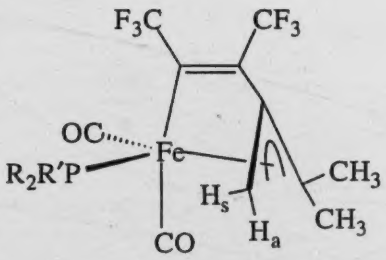

Figure 3-23 Solution and Solid State Structure of **6nI** (n = a, b, c).
(*enantiomer not shown*)

3.5.3 Variable Temperature NMR Studies of $Fe(CO)_2(PCy_3)(\eta^1,\eta^3\text{-}\{F_3CC{=}C(CF_3)C(CH_2)CMe_2\})$ (6c)

It is curious that in contrast to **4n** and **5n** (n = a, b, c) only one isomer had been detected, *via* NMR spectroscopy, in all samples of **6n** (n = a, b, c). It is clear that **6nI** is the thermodynamically preferred product as the compound is very stable in solid form and quite stable in solution for extended periods of time. Therefore it was of interest to determine if another isomeric form of **6nI** (n = a, b, c) precedes the thermodynamic product in the reaction of $Fe(CO)_2(PR_2R')(\eta^2\text{-HFB})$ and 1,1-dimethylallene. Previously, monitoring the reaction of $Fe(CO)_2(P^tBu_2Me)(\eta^2\text{-HFB})$ with allene by variable temperature NMR spectra showed that the first isomer formed at low temperature is **4aII**, the asymmetric isomer, which upon warming begins to convert into **4aI**, the symmetric isomer, and at room temperature nearly all **4aII** is quickly converted into **4aI**. In an attempt to observe the kinetic product in the reaction of $Fe(CO)_2(PR_2R')(\eta^2\text{-HFB})$ with 1,1-dimethylallene, the reaction of

$Fe(CO)_2(PCy_3)(\eta^2\text{-HFB})$ with 1,1–dimethylallene was monitored by variable temperature NMR experiments.

The procedure was performed in a manner similar to that for **4aI/II** (Section 3.3.3), with the exception that the 1,1-dimethylallene (excess) was added to a CD_2Cl_2 solution of **2c** *via* microliter syringe and the initial temperature of the NMR probe was –80 °C.

The variable temperature $^{31}P\{^1H\}$ spectra, in stacked form, are shown in Figure 3-24 . At –80 °C the spectrum exhibits two signals. One weak signal at δ 121.5 ppm (not shown in Figure 3-24) and a dominant signal at δ 55.2 ppm. The former signal is identified as belonging to unreacted starting material **2c**. The latter signal, labeled **6cII**, is not near the characteristic chemical shift of **6cI** and has not been previously observed. Upon warming the sample to –70 °C (not shown in Figure 3-24) the signal at δ 121.5 ppm disappears and no other changes are observed. Presumably, by this time the unreacted **2c** has reacted with 1,1-dimethylallene to form **6cII**, which is responsible for the resonance at δ 55.2 ppm. From –70 °C to 0 °C a spectrum is recorded every 10 °C. No changes to the spectra were observed until the sample was brought to 0 °C (Figure 3-24). At this temperature a small resonance appeared at δ 62.1 ppm, which signals the presence of small amounts of **6cI**. Upon further warming, the signal at δ 62.1 ppm increases, while the δ 55.2 ppm signal decreases. These observations are consistent with a conversion of **6cII** to **6cI** since no other signals are observed. The conversion is slow on the NMR time scale as the resonances are relatively sharp throughout the process of conversion. Once at 24 °C a spectrum is recorded after 15 minutes at this temperature (Figure 3-24). Both signals still appear in significant amounts. After 30 minutes at 24 °C the δ 55.2 signal has nearly disappeared and after 45 minutes at 24 °C only the resonance due to **6cI** is observed. Upon relowering the temperature of the sample to –80 °C, no change in the spectrum occurs, indicating that the process is not reversible.

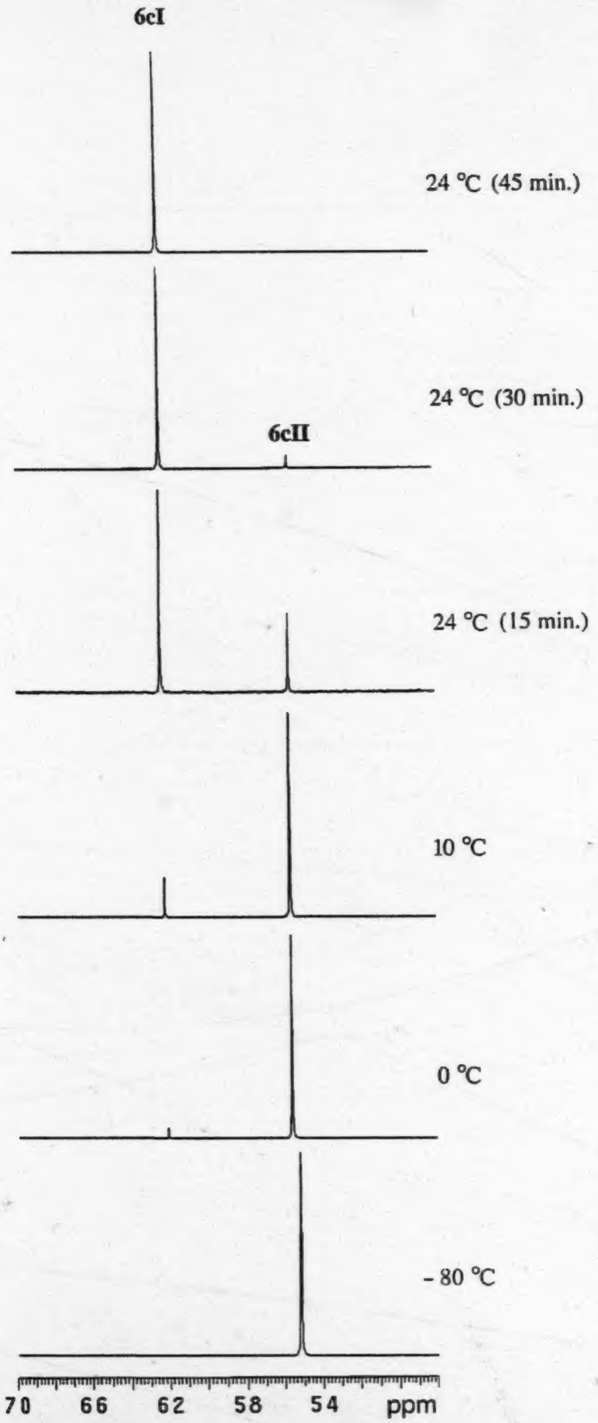

Figure 3-24 The Variable-Temperature $^{31}P\{^1H\}$ NMR (ppm, CD_2Cl_2) Spectra of the Reaction of **2c** with 1,1-Dimethylallene.

The variable temperature $^{31}P\{^1H\}$ spectra show a pattern that is indicative of a conversion of one compound to another. The conversion is reminiscent of that observed with **4aI** and **4aII** (Section 3.3.3). However, in contrast to the **4aI/4aII** system, the conversion is complete after a short period of time at ambient temperature and the initial isomer does not persist. It is suspected that **6cI** and **6cII** are geometric isomers. Since the $^{31}P\{^1H\}$ NMR spectra provide an extremely limited amount of structural information, it was of interest to obtain more data that would elucidate the structure of **6cII**. The ^{19}F, ^1H and $^{13}C\{^1H\}$ spectra were recorded at –80 °C. The results of these experiments follow.

The ^{19}F NMR spectrum of **6cII** (Table 3-21) exhibits two quartets. These resonances are similar in chemical shift and multiplicity to the two ^{19}F signals of **6cI**. This observation is consistent with two chemically inequivalent CF_3 groups similar to the vinyl moiety in the molecular structure of **6cI**.

The low temperature ^1H NMR data is listed in Table 3-21, while the variable temperature ^1H spectra (–80 °C, 0 °C, 24 °C) are shown in Figure 3-25. At –80 °C, the spectrum shows two very strong signals at δ 4.49 (septet, $^5J_{HH} = 3$ Hz) and 1.61 ppm (triplet, $^5J_{HH} = 3$ Hz). They are immediately identified as the CH_2 and CH_3 resonances, respectively, of the free $H_2C{=}C{=}C(CH_3)_2$ (labeled * in Figure 3-25). In the region normally associated with allyl hydrogens, two signals, at δ 2.85 and 2.27 ppm with an intensity ratio of 1:1, are observed. These signals are consistent with two allylic hydrogens. However, it is curious that these signals are both in a chemical shift region more associated with *anti*-hydrogens. In light of the crystal structures of **6aI** and **6bI**, it was expected that one *syn*- and one *anti*-hydrogen would be observed. Although it is not uncommon for a *syn*-hydrogen to resonate upfield of δ 3 ppm, it is a little surprising that both signals are upfield of this threshold value in **6cII,** since in all other compounds **4n**, **5n** and **6n** (n= a, b, c) the *syn*-hydrogens, without variation, resonate downfield of δ 3 ppm.

Table 3-21 The $^{31}P\{^1H\}$, ^{19}F, ^1H and $^{13}C\{^1H\}$APT NMR Data (ppm, CD_2Cl_2, –80°C) of **6cII**

Compound	$^{31}P\{^1H\}$	^{19}F	^1H	$^{13}C\{^1H\}$
6cII	55.2	– 54.2 br q $^5J_{FF}$ = 8 Hz	2.85 s H_{syn}	219.8 s *CO*
		– 63.9 br q $^5J_{FF}$ = 8 Hz	2.27 s H_{anti}	212.7 d $^2J_{CP}$ = 19 Hz *CO*
			1.69 s CCH_3	160.0 br $C_\alpha(CF_3)$
			1.23 s CCH_3	132.5 br $C_\beta(CF_3)$
				125.4 q $^1J_{CF}$ = 272 Hz CF_3
				119.9 s $C(CH_3)_2$
				116.9 q $^1J_{CF}$ = 272 Hz CF_3
				82.3 s $C_{central}$
				55.5 s CH_2
				23.8 s CCH_3
				21.8 s CCH_3

The COSY spectrum shows a strong correlation between these two signals, indicative of a $^2J_{HH}$ rather than a $^4J_{HH}$. Based on this, these signals are assigned to a *syn*-hydrogen (δ 2.85 ppm) and *anti*-hydrogen (δ 2.27 ppm) of an allyl group. Upfield of these signals, the broad resonances of the cyclohexyl substituents of the phosphine ligand appear. They appear unusually broad, probably due to slowed rotation involving the phosphine ligand. This is suspected because as the temperature is raised the signals begin to sharpen (10 °C spectrum Figure 3-25). In addition to the phosphine resonances, two relatively sharp signals appear at δ 1.69 and 1.23 ppm (labeled **6cII** in the –80 °C spectrum). The sharpness of these signals suggest that they are somewhat removed from the phosphine ligand.

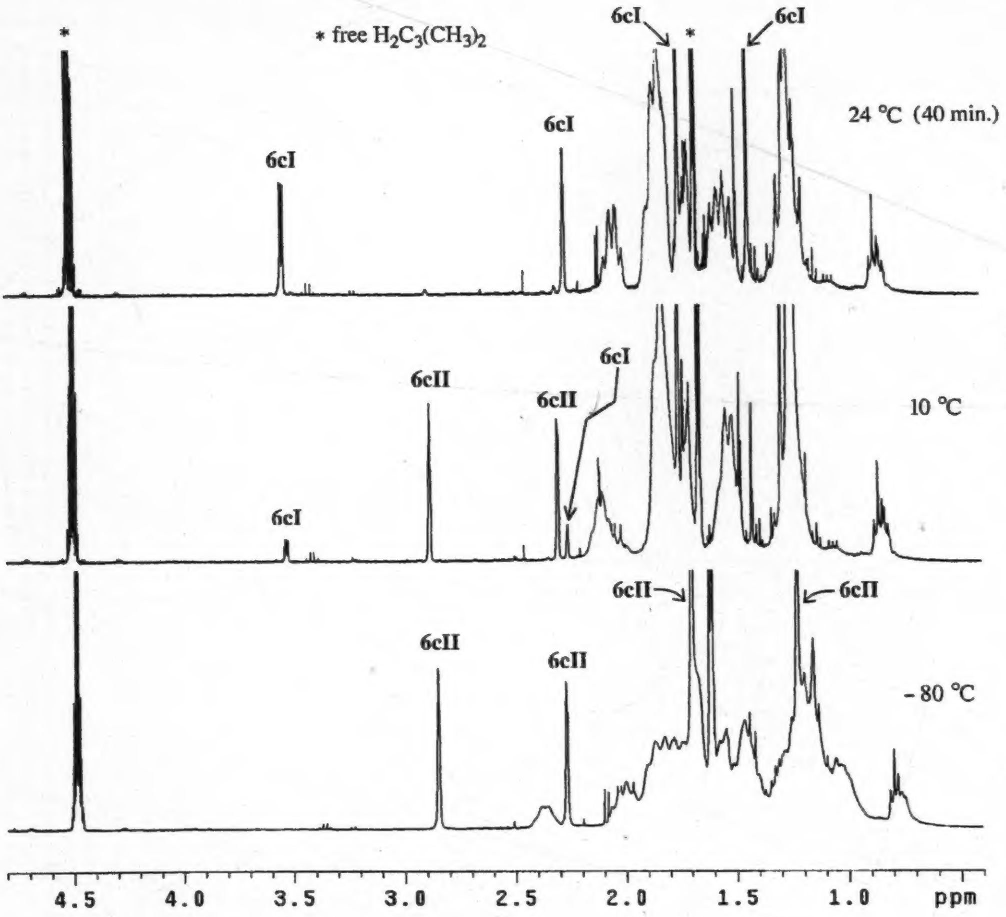

Figure 3-25 The Variable-Temperature ^1H NMR (ppm, CD_2Cl_2) Spectra of the Reaction of **2c** with 1,1-Dimethylallene.

The chemical shift of these signals are consistent with resonances of the allyl methyls. Due to the overlap with the phosphine resonances, accurate intensities could not be obtained. These signals show a correlation in the HMQC with carbon signals at δ 24.0 and 22.3 ppm and the chemical shift of these carbons resonances are very close to the chemical shift of the $C(CH_3)_2$ carbons in **6nI** (n = a, b, c). Based on these observations the signals are assigned to the hydrogens of the two allylic methyl groups.

The ^{1}H NMR spectra show a conversion from **6cII** to **6cI** upon warming the sample. At –80 °C only the resonances of **6cII** are observed. At 10 °C small amounts of **6cI** are detected. The characteristic doublet of doublets at δ 3.57 ppm and the singlet at δ 2.28 ppm indicated the presence of **6cI**. After 40 minutes at 24 °C only **6cI** is detected in significant amounts. The ^{1}H NMR data indicated the presence of a 1,1-dimethylallyl moiety in **6cII**, but it was the $^{13}C\{^1H\}$ NMR data, in conjunction with the HMQC and HMBC spectra, that confirmed these suspicions and proved very useful in determining the structure of **6cII**.

The $^{13}C\{^1H\}$ NMR spectrum (δ 50 – 230 ppm) of **6cII** at –80 °C is shown in Figure 3-26, while the data is listed in Table 3-21. The carbon resonances due to the starting material **2c** and free 1,1-dimethylallene are easily identified by comparison to a standard spectrum of each, *i.e.* isolated **2c** and 1,1-dimethylallene. Unreacted starting material is labeled **2c,** while free 1,1-dimethylallene is labeled with an asterisk (*) in Figure 3-26. The carbonyl region (*inset*) shows two resonances for **6cII**. A singlet at δ 219.8 ppm and a doublet ($^2J_{CP}$ = 19 Hz) at δ 212.7 ppm are assigned to two chemically inequivalent carbonyl groups. This pattern is reminiscent of the carbonyl resonances found in the ^{13}C NMR spectrum of **6nI** (n = a, b, c). In particular the $^2J_{CP}$ in **6cII** is close to the $^2J_{CP}$ = 20-21 Hz observed in **6nI**. The signal at δ 171.1 ppm is characteristic of the considerably deshielded alkyne carbons of the four electron donor alkyne complex **2c** (Chapter 2). The signals at δ 160.0 and 132.5 ppm are found in the characteristic C_α and C_β region, respectively, of the $FeC_\alpha(CF_3)$=$C_\beta(CF_2)$ vinyl moiety. The signals appear broad and weak in intensity, as is usually the case for the C_α and C_β signals in the previous compounds **4n**, **5n**, **6nI** (n = a, b, c).

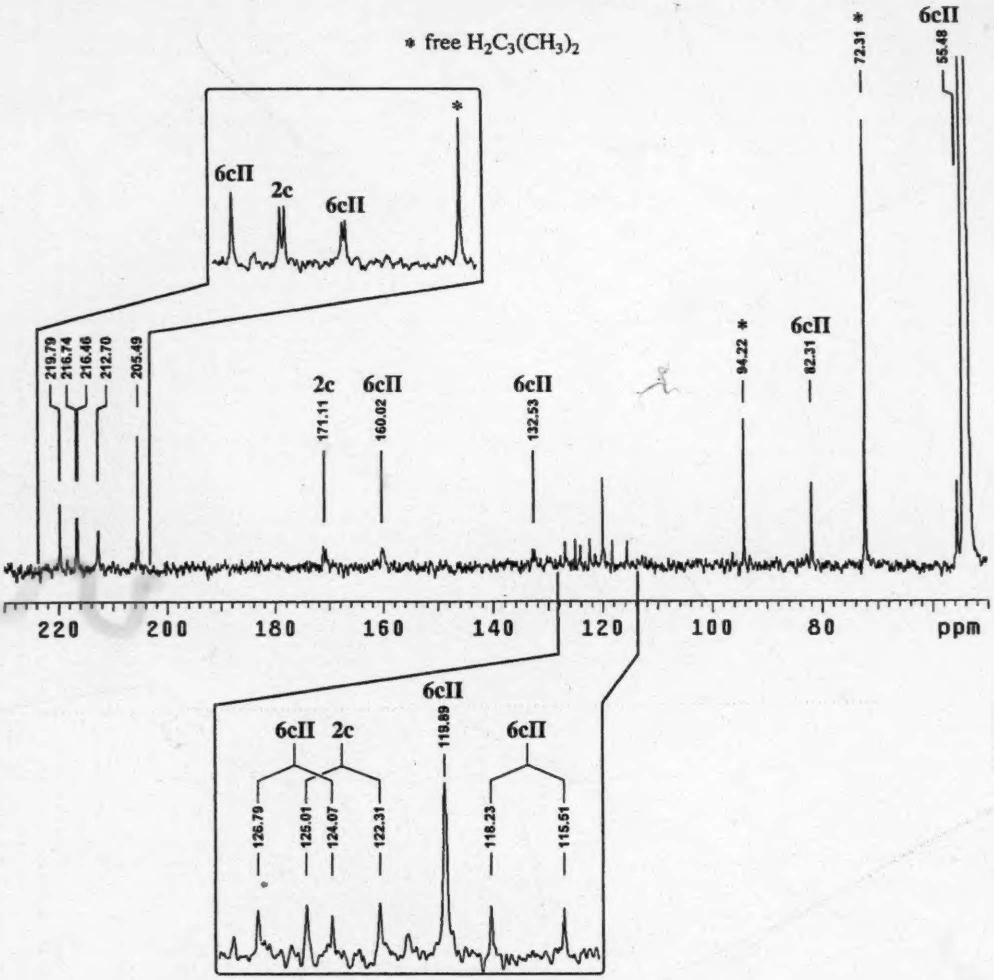

Figure 3-26 The $^{13}C\{^1H\}$ NMR (50-230 ppm, CD_2Cl_2, −80 °C) Spectrum of **6cII**.

Upon ^{19}F decoupling, these signals in **6cII** sharpen into a doublet with $^2J_{CP}$ = 19 Hz (160.0 ppm) and a singlet (132.5 ppm), again in parallel with observations of the $^{13}C\{^{19}F\}$ spectra of **4n**, **5n**, **6nI** (n = a, b, c). The δ 127-115 ppm region shows a number of resonances. The CF_3 resonances normally appear in this region as quartets, but often only the two strongest inside lines of each quartet are observed, while the smaller outside lines blend in with the baseline noise. Indeed the signal pattern in this region is consistent with two CF_3 resonances for **6cII**. The characteristic $^1J_{CF}$ = 270-275 Hz corroborates this conclusion. In addition to these signals, a relatively strong resonance at δ 119.9 ppm is also observed in this region. A signal in this region, other than the resonances due to the CF_3 carbons, has not been previously observed. This signal shows no correlation in the HMQC spectrum but does show a correlation with the *syn*-hydrogen, *anti*-hydrogen and the hydrogens of both allyl methyls $C(CH_3)$ in the HMBC spectrum, suggesting that this signal is associated with the allyl moiety. The carbon of the unsubstituted terminus of the allyl is clearly identified at δ 55.5 ppm since this ^{13}C position exhibits correlation with the *syn*- and *anti*-hydrogens in the HMQC spectrum. This spectrum also reveals the position of the two allyl methyl carbons CCH_3 at δ 23.8 and 21.8 ppm through correlation with their directly bonded hydrogens at δ 1.69 and 1.23 ppm, respectively. With these two positions unambiguously assigned, the only two unassigned carbons that remain are the doubly substituted carbon CMe_2 and the central carbon. Correspondingly, only two ^{13}C NMR resonances remain unassigned; δ 119.9 and 82.3 ppm. The chemical shift of the carbon resonance at δ 82.3 ppm is more indicative of a central carbon as judged from the previous compounds **4n**, **5n**, **6nI** (n = a, b, c). It is therefore assigned to the central carbon of the allyl. The resonance at δ 119.9 ppm, although shifted some 13-14 ppm downfield of the chemical shift of the doubled substituted carbon in **6nI** (δ 106-107 ppm) (n = a, b, c), is assigned to the CMe_2 carbon. As expected, *vide supra*, the carbon resonances of the phosphine ligand (δ 40-24 ppm) show some broadening and thus no assignments were attempted.

The NMR data of **6cII** suggests a structure that is similar to **6cI**. Clear evidence for a phosphine ligand, two chemically inequivalent carbonyls and a 2-vinyl-1,1-dimethylallyl ligand is present. However, just as clear, the structure is in some way different from that of **6cI**. Two possibilities can be envisaged; a geometric isomer in which the doubly substituted terminus of the allyl is *cis* to the phosphine ligand (**A** in

Figure 3-27), which would make the **6cI/6cII** pair analogous to the **5cI/5cII** pair, respectively, or, alternatively, a geometric isomer in which the phosphine ligand is *trans* to the α-carbon of the vinyl group (**B** in Figure 3-27), which would make the **6cI/6cII** pair analogous to the **4cII/4cI** pair, respectively. Previously, **B** in Figure 3-21 (Section 3.4.2) was excluded as a possible structure by way of an empirical correlation, based on the $^2J_{CP}$ of the carbonyls, observed with the **4nI/II** (n = a, b, c) compounds. Extending this principle to the **6nI/II** (n = a, b, c) compounds allows the exclusion of **B** in Figure 3-27 as a possible structure of **6cII**. The carbonyl signals in **6nI** (n = a, b, c) show the expected $^2J_{CP}$ constants for the phosphine ligand in an equatorial position. The crystal structures of **6aI** and **6bI** confirms this arrangement of ligands. The $^2J_{CP}$ pattern associated with the carbonyls of **6cII** is not very different from that of **6nI, 5nII** or **4nII** (n = a, b, c); one carbonyl shows a $^2J_{CP}$ = 19 Hz, while the other is observed as a singlet. If the phosphine ligand is *trans* to the alpha carbon of the vinyl one would expect both carbonyls to show a $^2J_{CP}$ = ~20 Hz as in **4nI** (n = a, b, c). Upon this basis it is tentatively conclude that the structure of **6cII** is represented by **A** in Figure 3-27. Confirmation of this supposition was needed and thus attempts to obtain crystals, suitable for X-ray crystallographic analysis, were conducted.

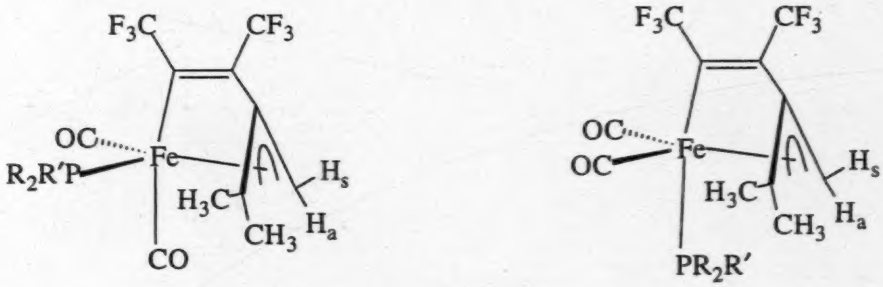

A **B**

Figure 3-27 Possible Geometric Isomers of **6nII** (n = a, b, c).
(*enantiomers not shown*)

3.5.4 X-ray Crystal Structure Analysis of the Kinetic Product $Fe(CO)_2(P^iPr_3)(\eta^1,\eta^3\text{-}\{F_3CC{=}C(CF_3)C(CH_2)CMe_2\})$ (6bII)

During the many hours spent monitoring the reaction of **2c** with 1,1-dimethylallene it became evident that the conversion of **6cII** to **6cI** is slow; conversion to **6cI** only begins at about 0°C (Figure 3-24). This led us to believe that if the reaction of **2a-c** with 1,1-dimethylallene and the workup was conducted at low temperatures one might be able to isolate crystals for X-ray crystallographic analysis of **6cII**. Indeed, reaction of $Fe(CO)_2(P^iPr_3)(\eta^2\text{-HFB})$, **2b**, with 1,1-dimethylallene at −78 °C in pentane, with subsequent concentration of solution, *in vacuo*, at −78 °C and crystallization at −80 °C produced an orange crystalline material. Quick transfer of a cold crystal to a diffractometer and subsequent data collection at −80 °C allowed us to obtain the solid state molecular structure of **6bII**.

Figure 3-28 shows the solid state molecular structure of **6bII** (phosphine hydrogens omitted) with atom labeling scheme, while Table 3-22 lists selected interatomic distances and angles.

The structure is a geometric isomer of **6bI**. Some significant differences are worthy of note. In **6bI** the doubly substituted terminus of the allyl moiety was *trans* to the phosphine ligand ($P\text{–}Fe\text{–}C(9)Me_2 = 163.8(2)°$). In **6bII** the doubly substituted terminus of the allyl is *cis* to the phosphine ligand ($P\text{–}Fe\text{–}C(7)Me_2 = 108.1(1)°$). This arrangement apparently causes significant steric interaction between the phosphine ligand and the doubly substituted terminus because the P–Fe–C(7) angle in **6bII** is 10.8° (54 esd's) larger than the corresponding angle in **6bI** (P–Fe–C7 = 97.3(2)°). As might be expected the adjacent angle C1–Fe–C9 = 86.9(1)° in **6bII** is smaller (6.3°, 21 esd's) than the corresponding angle in **6bI** (C1–Fe–C9 = 93.2(3)°).

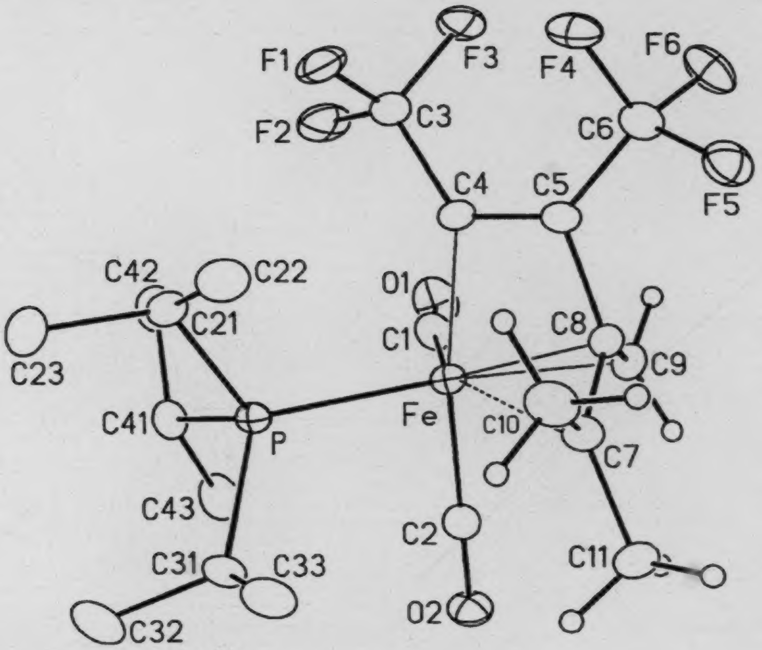
F1
F3
F4
F6
F2
C3
C6
C4
C5
F5
C42
C22
O1
C8
C21
C1
C9
C23
Fe
C41
P
C10
C7
C43
C2
C31
C33
C11
O2
C32

Figure 3-28 Solid State Molecular Structure of **6bII.**

Table 3-22 Selected Interatomic Distances (Å) and Angles (deg.) in **6bII**.

Fe–P	2.3336(7)	P–Fe–C4	98.4(1)
Fe–C1	1.752(3)	P–Fe–C7	108.1(1)
Fe–C2	1.781(3)	P–Fe–C9	171.4(1)
Fe–C4	2.021(2)	C1–Fe–C2	94.0(1)
Fe··· C7	2.518(2)	C1–Fe–C4	89.7(1)
Fe–C8	2.104(2)	C1–Fe–C7	150.8(1)
Fe–C9	2.125(2)	C1–Fe–C9	86.9(1)
C4–C5	1.326(3)	C2–Fe–C4	171.8(1)
C5–C8	1.506(3)	C2–Fe–C7	86.9(1)
C7–C8	1.394(3)	C2–Fe–C9	88.4(1)
C8–C9	1.421(3)	C4–Fe–C7	86.3(1)
O1–C1	1.152(3)	C4–Fe–C9	84.4(1)
O2–C2	1.149(3)	C7–Fe–C9	63.9(1)
P–Fe–C1	101.2(1)	Fe–C1–O1	173.2(2)
P–Fe–C2	88.2(1)	Fe–C2–O2	177.6(2)

Positioning the phosphine ligand next to the doubly substituted terminus of the allyl moiety also causes a severe asymmetry in the Fe–C_{allyl} separations. The Fe–C9 separation (2.125(2) Å) is only 0.021 Å (11 esd's) larger than the Fe–C8 separation (2.104(2) Å). Typically the M–$C_{terminal}$ distances are about 0.1 Å larger than the M–$C_{central}$ distances [16]. More interestingly, the Fe–C7 separation (2.518(2) Å) is a surprisingly 0.414 Å (201 esd's) larger than the Fe–C8 separation and 0.393 Å (197 esd's) larger than the Fe–C9 separation. The large Fe–C7 separation brings into question the validity of claiming that any meaningful bonding interaction occurs between these two atoms. In quantitative terms, this distance represents an atomic separation that is 25% greater than the sum of the covalent radii of carbon (0.77 Å) [45] and iron (1.25 Å) [46]. In relative terms, a quick survey of the Cambridge Crystallographic Data Center's structural database [47] revealed a few structures with very long Fe–C distances, up to 2.80 Å that were considered to have weak iron-carbon bonding interaction. However these differences represent the interaction between an iron atom and a semibridging carbonyl carbon and as such not directly comparable to the present case [48]. Omitting these, the next longest Fe–C separations involve η^2–olefinic type coordination of either a phenyl ring or double bond of an organic ligand. Figure 3-29 shows an example of such a compound [49]. These structures exhibit weak bonding interactions between iron and carbon with Fe–C separations of 2.40-2.47 Å. Since the Fe–C7 separation in **6bII** is significantly larger than these, on the order of 0.05 Å, it is reasonable to conclude that the bonding interaction between Fe and C7 in **6bII** is weaker than in these known examples. Differences in the allylic C–C separations were also observed. The allylic C7–C8 distance (1.394(3) Å) distance is 0.027 Å (9 esd's) shorter than the C9–C8 distance (1.421(3) Å), suggesting greater double bond character between C7 and C8 than that between C9 and C8. Also, the

^{13}C NMR resonance of the allylic carbon of the doubly substituted terminus in **6cII** was found to have a chemical shift (δ 119.9 ppm) that is in a region characteristic of a free olefin and is significantly shifted downfield from the related resonance (δ 106.7 ppm) in **6cI**.

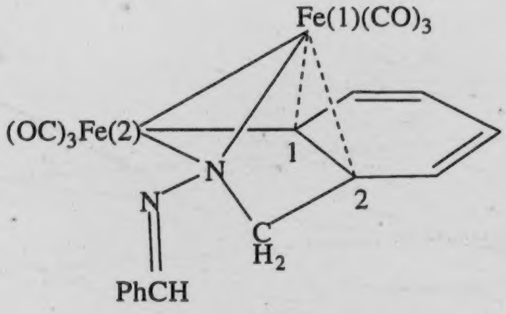

Fe1–C1 = 2.14(2) Å
Fe1–C2 = 2.47(2) Å

Figure 3-29 Structure of μ-(o-$C_6H_4CH_2NN{=}CHPh)Fe_2(CO)_6$ [49].

In valence bond terms, these observations might suggest an η^1–allyl bonding mode. However, the allyl ligand is normally positioned away from the metal in this bonding regime with both the terminal and central carbon far away from the metal [44a,b,d]. In **6bII** the central carbon (C8) is well within a Fe–C_{allyl} bonding distance. This might be a result of the geometrical constraints of the chelate but more likely an indication of Fe–C8 bonding. Moreover, the Fe–C9 and Fe–C8 separations show the expected pattern for allylic carbons; M–$C_{terminal}$ < M–$C_{central}$. These observations indicate that C9 and C8 have meaningful bonding interactions with the iron atom. These conclusions, in conjunction with the fact that the very long Fe–C7 separation suggests very weak Fe–C7 interaction, indicate the less commonly known "η^2"

bonding mode for the allyl moiety. In the η^2-allyl coordination mode only the $C_{central}$ and one $C_{terminal}$ are bonded to the metal, while the remaining $C_{terminal}$ shows no significant direct M–C bonding and is primarily sp^2 hybridized. This bonding description was first proposed in the bimetallic $Cp_2Zr(\mu\text{-}C_4H_6)(\mu\text{-}Cl)AlCl_2$ (Figure 3–30) [50]. The term "π-agostic" was used to describe this bonding mode [50].

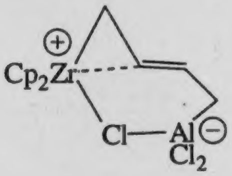

Figure 3-30 The Pictorial Representation of $Cp_2Zr(\mu\text{-}C_4H_6)(\mu\text{-}Cl)AlCl_2$ [50].

Having that been said, the C9–C8–C7–C11 torsional angle (27.9(4)°) in **6bII** shows that the *anti*-methyl is positioned well out of the allyl plane, away from the iron. This is consistent with rehybridization of the C7 carbon from sp^2 toward sp^3 and suggests some Fe–C7 bonding interaction. Thus the metal-allyl bonding in **6bII** is more accurately described as having considerable $\eta^3 \rightarrow \eta^2$ distortion and is a form of the η^1,η^2 coordination mode (Figure 3-31).

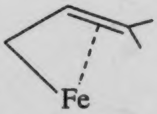

Figure 3-31 The η^1,η^2 –Allyl Bonding Mode in **6bII**.

The solid state molecular structures of **6bII** and **6bI** have unambiguously identified the kinetic and thermodynamic products in the reaction of **2n** (n = a, b, c) with 1,1-dimethylallene (Figure 3-32).

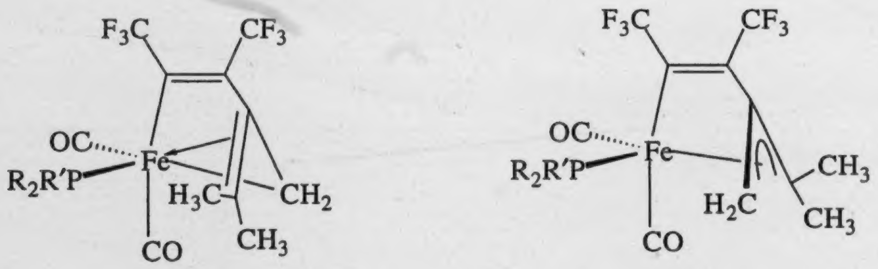

6nII **6nI**

n = a, b, c

Figure 3-32 The Kinetic Product **6nII** and Thermodynamic Product **6nI** (n = a, b, c). (*enantiomers not shown*)

It is known, through monitoring the reaction of **2c** and 1,1-dimethylalllene with variable temperature NMR spectroscopy (Section 3.5.3), that **6nII** (n = a, b, c) is the first compound to form. Over time, quickly at room temperature, **6nII** rearranges to **6nI**. The structural difference between **6nII** and **6nI** concerns the relative positioning of the allyl termini, and in the irreversible rearrangement process the positions of the allyl termini are exchanged. A number of rearrangement processes for six-coordinate complexes has been proposed in the literature [51]. Several of these can be adapted to the present case as possible rearrangement mechanisms for the conversion of **6nII** to **6nI** (n = a, b, c) [51c-f]. One such type of mechanism is the dissociative mechanism [51b]. Dissociation of a ligand from a six-coordinate octahedral complex, to give a five-coordinate intermediate, can be followed by recoordination of the ligand to form a six-coordinate octahedral molecule with a rearrangement of the ligands. The dissociative mechanism has been extended to include bidentate ligands. In this case one end of the bidentate ligand detaches from the central metal atom. The resulting intermediate is a five coordinate complex with a "dangling bidentate" ligand. Recoordination of the detached end of the dangling ligand reforms the six coordinate complex. The end result is a rearrangement of ligands. Since very few ligands of the vinyl-allyl type are reported in the literature and none are reported to act as a dangling ligand it is worth exploring the role this ligand might play in an intramolecular rearrangement mechanism.

A possible intramolecular rearrangement mechanism involving the 2-vinyl-1,1-dimethylallyl ligand could simply be a "face flip" of the allyl moiety. This mechanism is a variation on the well known π-σ-π ($\eta^3 \rightarrow \eta^1 \rightarrow \eta^3$) rearrangement mechanism proposed for the facile equilibrium of *syn* and *anti*-hydrogens in complexes with simple allyl ligands [16b]. The combination of the vinyl and allyl moieties in the vinyl allyl ligand results in an added dimension to the π-σ-π rearrangement mechanism. In the transformation of **6nII** (n = a, b, c) to **6nI**, this process requires the disubstituted terminus of the allyl to move from a position that is *cis* with respect to the phosphine ligand to a position that is *trans* with respect to the phosphine ligand. Simultaneously, the unsubstituted terminus of the allyl migrates from its position, *trans* to the phosphine ligand, to occupy the coordination site which is *cis* to the phosphine ligand. The result is an exchange of orientation of the two faces of the allyl moiety with respect to the iron. This mechanism, shown in Figure 3-33, begins with **A**, which represents **6nII** (n = a, b, c). The dimethyl terminus of the allyl swings out, away from the iron, to a position in which the allyl is coplanar with the vinyl linkage to form a five coordinate 16-electron intermediate **B** in Figure 3-33. Concomitant with this movement is a rehybridization at the iron center from six-coordinate (octahedral) to five-coordinate (trigonal bipyramidal).

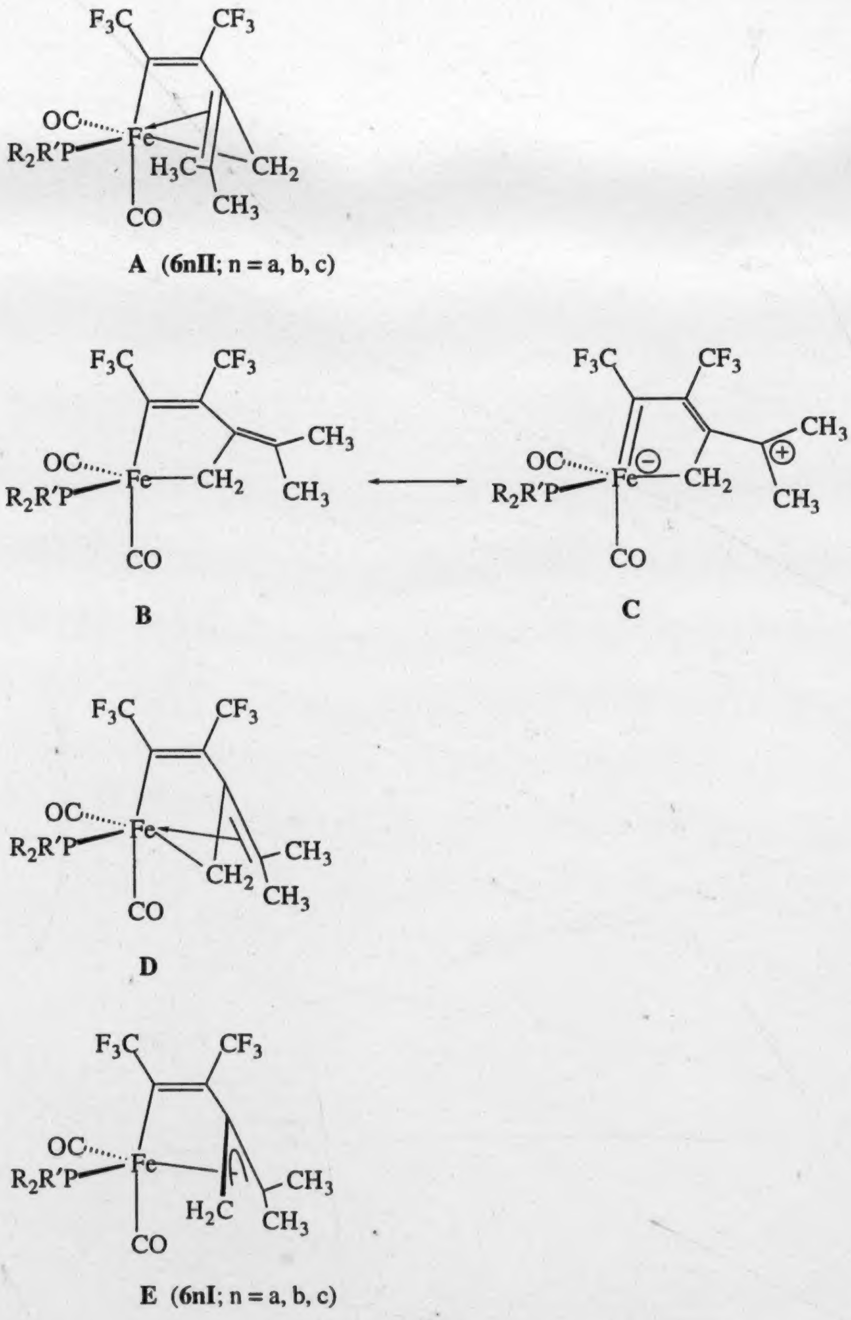
F3C
CF3
OC
Fe
R2R'P
H3C
CH2
CH3
CO
A (6nII; n = a, b, c)
F3C
CF3
CH3
OC
Fe
CH2
R2R'P
CH3
CO
B
F3C
CF3
CH3
OC
Fe
CH2
R2R'P
CH3
CO
C
F3C
CF3
OC
Fe
R2R'P
CH3
CH2
CH3
CO
D
F3C
CF3
OC
Fe
R2R'P
CH3
H2C
CH3
CO
E (6nI; n = a, b, c)

Figure 3-33 A Possible Rearrangement of **6nII** to **6nI** (n = a, b, c).

Stabilization of this intermediate occurs through charge delocalization along the conjugated π-system of the vinyl-olefinic linkage to effectively donate additional electron density to the iron center *via* the α-carbon of the vinyl, **C** in Figure 3-33. In this way the iron atom achieves a saturated electron configuration. Continuing the rearrangement, the disubstituted terminus then completes the swing motion in the direction of the equatorial carbonyl to occupy the coordination site, which opens up upon rehybridization of the iron back to six-coordinate, that is *trans* to the phosphine ligand, **D** in Figure 3-33. As discussed previously, the iron-allyl interaction in **6nI** (n = a, b, c) is more accurately described as an η^3 interaction, **E** in Figure 3-33, than the η^1,η^2 interaction show by **D** in Figure 3-33, since the allylic C–C separations in the solid state molecular structure of **6b** are not significantly different.

3.6 Conclusions

The four electron donor alkyne complexes $Fe(CO)_2(PR_2R')(\eta^2\text{-HFB})$ (**2a-c**) posses a chemoselective cross-coupling reactivity toward small unsaturated organic molecules. While being inert towards simple olefins or alkynes, these complexes show a facile reactivity toward allenic species. Reaction of **2a-c** with allene, methylallene or 1,1-dimethylallene affords products in which a rare type of chelating allyl ligand is observed. Formation of the 2-vinylallyl ligand occurs through oxidative coupling of an allene molecule and a precoordinated η^2-alkyne. A carbon–carbon bond forms between one of the ligating carbons of the alkyne and the central carbon of the allene. The vinylallyl ligand is bound to the metal through both an η^3-allyl and η^1-vinyl moiety and occupies one face of an octahedron.

An interesting dichotomy exists between the complexes containing the P^tBu_2Me ligand and the complexes containing the P^iPr_3 or PCy_3 ligands. These complexes, **4a-c**, exist in solution as two geometric isomers. The populationally preferred isomer in **4a** has C_s symmetry and the phosphine ligand in the axial position (**4aI**), while in **4b,c** the dominant isomer is asymmetric with the phosphine ligand in the equatorial position (**4nII**, n = b, c). Since it is only in **4aII** that restricted rotation of the P–C and/or C–C is observed, it is clear that the P^tBu_2Me ligand possesses a spacial profile that has greater steric interaction with the iron auxiliary in comparison to P^iPr_3 or PCy_3, in **4bII** or **4cII**, respectively. The origin of these differences stems from the difference in shape of the spacial profile of the phosphine ligands. The P^tBu_2Me ligand has an unique spacial character, two large substituents and one small substituent. It is suggested that in the molecular structure of **4aI** the P^tBu_2Me ligand has a preferred rotational orientation as a result of its unique shape. Despite **4aI** being the thermodynamically preferred isomer, it is **4aII** which forms first in the reaction of **2a** with allene. By extrapolation, we presume **4bII** or **4cII** are also the first to form in the reaction of **2b** or **2c** with allene, respectively.

As in **4a-c**, the NMR spectra of **5a-c** indicate the presence of two isomers in solution. Invariably the methyl substituent of the allyl unit occupies an *anti*-orientation and it is the *cis-/trans*-orientation of the monosubstituted terminus of the allyl, with respect to the phosphine ligand, that gives rise to the two geometric isomers. Presumably, the potential steric interaction between an axial phosphine ligand and an *anti*-methyl constrains the phosphine ligand to an equatorial position in all products. In contrast to **4a-c**, **5a-c** show a high degree of consistency with respect to the identity of the major and minor isomers, that is, in **5a-c**, **5nI** is the major isomer for n = a, b, c. This suggests that the differences between a PR_2R' and PR_3 type phosphine ligands have little effect on the products.

In contrast to the previous compounds, only one product is observed at ambient temperature in solutions of **6a-c**, but as in **5a-c** the phosphine ligand is restricted to an equatorial position. In addition, the phosphine ligand is always in a *trans*-orientation with respect to the dimethyl terminus of the allyl unit. The solid state structures of **6aI** and **6bI** are consistent with the solution NMR spectra and clearly show the doubly substituted terminus of the allyl *trans* to the phosphine ligand. A kinetic product in which the doubly substituted terminus of the allyl is *cis* to the phosphine ligand, **6bII**, was identified and shown to be the geometrical isomer of **6bI**.

The form of the major isomer in the products of the reaction of **2a-c** with allenes is determined by the type of allene and to a lesser extent by the type of phosphine ligand. In **4a-c** it was the type of phosphine ligand, PR_2R' vs. PR_3, that determined the dominant isomer in solution. Thus by choice of the type of phosphine ligand in **2a-c**, one is able to exert some measure of control over the product of the reaction. In **5a-c**, with substitution at one terminus of the allene, it is the allyl which determines the products, and we find the phosphine ligand in an equatorial position in all products and the major isomer is the one in which the substituted terminus of the allyl is *trans* to the phosphine ligand. In **6nI** (n = a, b, c), with further substitution at one terminus of the allyl, only one isomeric form is stable in solution at ambient temperature and the substituted terminus of the allyl is *trans* to the phosphine. Clearly, the steric interaction between the phosphine ligand and the allyl moiety is important in these products and the choice of allene or phosphine in the reactants can be used to control the outcome of these reactions.

3.7 Experimental

3.7.1 Solvents, Techniques and Physical Measurements

Solvents, general techniques and physical measurements were used and performed as described in Chapter 2.

3.7.2 Reagents

Allene (propadiene), methylallene (1,2-butadiene) and 1,1-dimethylallene (3-methyl-1,2-butadiene) were purchased from Sigma-Aldrich Canada Ltd. (Fluka) and used without further purification. The compounds **2a-c** were prepared as described in Chapter 2.

3.7.3 Synthetic Procedures

Synthesis of $Fe(CO)_2(PR_2R')(\eta^1,\eta^3\text{-}\{F_3CC{=}C(CF_3)C(CH_2)CR^1R^2\})$ (4a-c, 5a-c, 6a-c)

A 50 mL Schlenk tube was evacuated then back-filled with allene or methylallene to ~1 atm pressure. The Schlenk tube was taken to –78 °C at which time the allene/methylallene condensed to the bottom of the flask. The flask was back-filled with a nitrogen atmosphere. A pentane (**2a,b**) or CH_2Cl_2 (**2c**) solution of **2a-c** (90-120 mg) was prepared in a separate Schlenk flask. The solution of **2a-c** was added to the allene/methylallene *via* cannula transfer. The solution was brought to –20 °C and stirred for 30 minutes. The solvent was removed, *in vacuo,* at 0 °C. The yellow-orange residue was redissolved in a minimum amount of pentane or pentane/CH_2Cl_2 (5:1) and cannula filtered into a 50 mL Schlenk flask and crystallized at –30/–80 °C.

Regarding the reactions with 1,1-dimethylallene, the allene was simply added to a solution of **2a-c** *via* microliter syringe. The subsequent work-up was performed as describe above.

$Fe(CO)_2(P^tBu_2Me)(\eta^1,\eta^3$-$\{F_3CC=C(CF_3)C(CH_2)_2\})$ (4aI, II, II′, II″)

Elemental Analysis $C_{18}H_{25}F_6FeO_2P$; Calculated: C, 45.59%; H, 5.31%, Observed: C, 45.58%; H 5.28%.

F.W. 474.21

IR (pentane, cm^{-1}) ν_{CO} 2018(s), 1968 (s)

4aI (major isomer, CD_2Cl_2)

^1H NMR (CD_2Cl_2, 400.1 MHz, 27 °C) δ 0.90 (d, $^2J_{HP}$ = 6 Hz, PCH_3), 1.35 (d, $^3J_{HP}$ = 12 Hz $PCCH_3$), 2.25 (d, $^3J_{HP}$ = 9 Hz, H_{anti}), 3.34 (s, H_{syn})

^{19}F NMR (CD_2Cl_2, 376.4 MHz, 27 °C) δ – 58.0 (dq, $^5J_{FF}$ = 8 Hz, $^3J_{FP}$ = 3 Hz, CF_3), – 64.7 (q, $^5J_{FF}$ = 8 Hz, CF_3)

$^{31}P\{^1H\}$ NMR (CD_2Cl_2, 161.9 MHz, 27 °C) δ 68.2 (s)

$^{13}C\{^1H\}$APT NMR (CD_2Cl_2, 100.6 MHz, 27 °C) δ 217.1 (d, $^2J_{CP}$ = 16 Hz, CO), 86.6 (br, $C_{central}$), 70.9 (br s, CH_2), 36.3 (d, $^1J_{CP}$ = 14 Hz, $PC(CH_3)_3$, 29.9 (–) (d, $^2J_{CP}$ = 3 Hz, $PC(CH_3)_3$ 6.5 (–) (d, $^1J_{CP}$ = 16 Hz, PCH_3)

$^{13}C\{^{19}F\}$ NMR (CD_2Cl_2, 100.6 MHz, 27 °C) δ 217.1 (d, $^2J_{CP}$ = 16 Hz, CO), 151.9 (d, $^2J_{CP}$ = 17 Hz , $C_\alpha(CF_3)$), 135.5 (s, $C_\beta(CF_3)$), 125.4 (s, CF_3), 117.0 (s, CF_3) 86.6 (br s, $C_{central}$), 70.9 (m, CH_2), 36.3 (m, $PC(CH_3)_3$), 29.9 (m, $PC(CH_3)_3$), 6.5 (m, PCH_3).

4aI (major isomer, THF-d_8)

^1H NMR (THF-d_8, 400.1 MHz, 27 °C) δ 0.96 (d, $^2J_{HP}$ = 6 Hz PCH_3), 1.38 (d, $^3J_{HP}$ = 12 Hz $PC(CH_3)_3$), 2.34 (d, $^3J_{HP}$ = 9 Hz H_{anti}), 3.35 (s, H_{syn})

^{19}F NMR (THF-d_8, 376.4 MHz, 27 °C) δ – 58.4 (dq, $^5J_{FF}$ = 8 Hz, J_{FP}= 3 Hz, $\mathrm{C}F_3$), – 65.2 (q, $^5J_{FF}$ = 8 Hz, $\mathrm{C}F_3$)

^{31}P{^{1}H} NMR (THF-d_8, 161.9 MHz, 27 °C) δ 69.8 (s)

^{13}C{^{1}H} NMR (carbonyl region) (THF-d_8, 100.6 MHz, 27 °C) δ 218.0 (d, $^2J_{CP}$ = 16 Hz, *C*O)

4aII (minor isomer) Fast Exchange (27 °C, CD_2Cl_2)

^{1}H NMR (CD_2Cl_2, 400.1 MHz, 27 °C) δ 1.31 (d, $^3J_{HP}$ = 13 Hz, $\mathrm{PC(C}H_3)_3$), 1.35 (d, $^3J_{HP}$ = 13 Hz, $\mathrm{PC(C}H_3)_3$), 1.43 (d, $^2J_{HP}$ = 8 Hz, $\mathrm{PC}H_3$), 2.09 (s, H_{anti}), 2.37 (s, H_{anti}), 3.05 (d, $^4J_{HH}$ = 3 Hz, H_{syn}), 3.57 (dd, $^4J_{HH}$ = 3 Hz, $^3J_{HP}$ = 3 Hz, H_{syn})

^{19}F NMR (CD_2Cl_2, 376.4 MHz, 27 °C) δ – 53.5 (q, $^5J_{FF}$ = 9 Hz, $\mathrm{C}F_3$), – 65.2 (dq, $^5J_{FF}$ = 9 Hz, J_{FP} = 3 Hz, $\mathrm{C}F_3$)

^{31}P{^{1}H} NMR (CD_2Cl_2, 161.9 MHz, 27 °C) δ 71.1 (s)

^{13}C{^{1}H}APT NMR (CD_2Cl_2, 100.6 MHz, 27 °C) δ 85.4 (br s, C_{central}), 70.3 (s, $C\mathrm{H}_2$), 66.3 (d, $^2J_{CP}$ = 10 Hz, $C\mathrm{H}_2$) 30.2 (–) (d, $^2J_{CP}$ = 4 Hz, $\mathrm{PC(}C\mathrm{H_3)_3}$), 29.7 (–) (d, $^2J_{CP}$ = 4 Hz, $\mathrm{PC(}C\mathrm{H_3)_3}$) 11.6 (–) (d, $^1J_{CP}$ = 15 Hz $\mathrm{P}C\mathrm{H_3}$)

^{13}C{^{19}F} NMR (CD_2Cl_2, 100.6 MHz, 27 °C) δ 217.4 (d, $^2J_{CP}$ = 7 Hz, *C*O), 215.1 (d, $^2J_{CP}$ = 20 Hz, *C*O), 155.8 (d, $^2J_{CP}$ = 19 Hz , $C_\alpha(\mathrm{CF_3})$), 134.3 (s, $C_\beta(\mathrm{CF_3})_3$), 126.6 (s, $C\mathrm{F_3}$), 117.8 (s, $C\mathrm{F_3}$) 85.4 (br s, C_{central}), 70.3 (m, $C\mathrm{H}_2$), 66.3 (m, $C\mathrm{H}_2$), 30.2 (m, $\mathrm{PC(}C\mathrm{H_3)_3}$), 29.7 (m, $\mathrm{PC(}C\mathrm{H_3)_3}$) 11.6 (m, $\mathrm{P}C\mathrm{H_3}$)

4aII (minor isomer) Fast Exchange Spectra (27 °C, THF-d_8)

^{1}H NMR (THF-d_8, 400.1 MHz, 27 °C) δ 1.32 (d, $^3J_{HP}$ = 13 Hz, $\mathrm{PC(C}H_3)_3$), 1.37 (d, $^3J_{HP}$ = 12 Hz, $\mathrm{PC(C}H_3)_3$), 1.47 (d, $^2J_{HP}$ = 8 Hz $\mathrm{PCH_3}$), 2.14 (s, H_{anti}), 2.46 (s, H_{anti}), 3.04 (d, $^4J_{HH}$ = 3 Hz H_{syn}), 3.62 (dd, $^4J_{HH}$ = 3 Hz, $^3J_{HP}$ = 3 Hz H_{syn})

^{19}F NMR (THF-d_8, 376.4 MHz, 27 °C) δ – 53.8 (dq, $^5J_{FF}$ =9 Hz, J_{FP}= 1 Hz, $\mathrm{C}F_3$), – 65.6 (dq, $^5J_{FF}$ = 9 Hz, J_{FP} = 2 Hz, $\mathrm{C}F_3$)

$^{31}P\{^1H\}$ NMR (THF-d_8, 161.9 MHz, 27 °C) δ 71.1 (s)

$^{13}C\{^1H\}$ NMR (carbonyl region) (THF-d_8, 100.6 MHz, 27 °C) δ 218.2 (d, $^2J_{CP}$ = 8 Hz, *C*O), 215.9 (br, *C*O)

4aII (minor isomer) Fast Exchange Spectra (– 10 °C, THF-d_8)

^1H NMR (THF-d_8, 400.1 MHz, – 10 °C) δ 1.32 (d, $^3J_{HP}$ = 13 Hz, $PC(CH_3)_3$), 1.38 (d, $^3J_{HP}$ = 13 Hz, $PC(CH_3)_3$), 1.49 (d, $^2J_{HP}$ = 7 Hz PCH_3), 2.17 (s, H_{anti}), 2.47 (s, H_{anti}), 3.06 (d, $^4J_{HH}$ = 3 Hz, H_{syn}), 3.63 (dd, $^4J_{HH}$ = 3 Hz, $^3J_{HP}$ = 3 Hz H_{syn})

^{19}F NMR (THF-d_8, 376.4 MHz, – 10 °C) δ – 53.2 (s, CF_3), – 65.1 (s, CF_3)

$^{31}P\{^1H\}$ NMR (THF-d_8, 161.9 MHz, – 10 °C) δ 70.6 (s)

$^{13}C\{^1H\}$ NMR (carbonyl region) (THF-d_8, 100.6 MHz, – 10 °C) δ 218.4 (d, $^2J_{CP}$ = 7 Hz, *C*O), 215.9 (br d, $^2J_{CP}$ = 20 Hz, *C*O)

4aII′ (major conformer) Slow Exchange Spectra (–110 °C, THF-d_8)

^1H NMR (THF-d_8, 400.1 MHz, – 110 °C) δ 2.31 (br s, H_{anti}), 2.49 (br s, H_{anti}), 3.11 (br s, H_{syn}), 3.79 (br s, H_{syn})

^{19}F NMR (THF-d_8, 376.4 MHz, – 110 °C) δ – 52.9 (s, CF_3), – 65.7 (s, CF_3)

$^{31}P\{^1H\}$ NMR (THF-d_8, 161.9 MHz, – 110 °C) δ 65.9 (s)

$^{13}C\{^1H\}$ NMR (carbonyl region) (THF-d_8, 100.6 MHz, – 110 °C) δ 219.1 (br, *C*O), 215.4 (br d, $^2J_{CP}$ = 18 Hz, *C*O)

4aII″ (minor conformer) Slow Exchange Spectra (– 110 °C, THF-d_8)

^1H NMR (THF-d_8, 400.1 MHz, – 110 °C) δ 2.32 (br s, H_{anti}), 2.77 (br s, H_{anti}), 3.20 (br s, H_{syn}), 3.48 (br s, H_{syn})

^{19}F NMR (THF-d_8, 376.4 MHz, – 110 °C) δ – 53.8 (s, CF_3), – 64.1 (s, CF_3)

$^{31}P\{^1H\}$ NMR (THF-d_8, 161.9 MHz, – 110 °C) δ 75.5 (s)

$^{13}C\{^1H\}$ NMR (carbonyl region) (THF-d_8, 100.6 MHz, – 110 °C) δ 219.1 (br, *C*O), 216.4 (br d, $^2J_{CP}$ = 19 Hz, *C*O)

$Fe(CO)_2(P^iPr_3)(\eta^1,\eta^3\text{-}\{F_3CC{=}C(CF_3)C(CH_2)_2\})$ (4bI,II)

Elemental Analysis $C_{18} H_{25} F_6 Fe O_2 P$; Calculated: C, 45.59%; H, 5.31%,

Observed: C, 45.67%; H 5.09%.

F.W. 474.21

IR (pentane, cm^{-1}) ν_{CO} 2015 (s), 1964 (s)

4bI (minor isomer)

^{1}H NMR (CD_2Cl_2, 400.1 MHz, 27 °C) δ 1.30 (dd, $^3J_{HP}$ = 13 Hz, $^3J_{HH}$ = 7 Hz, PCC*H*$_3$), 2.21 (dsept, $^2J_{HP}$ = 8 Hz, $^3J_{HH}$ = 7 Hz, PC*H*), 2.51 (d, $^3J_{HP}$ = 8 Hz, *H*$_{anti}$), 3.24 (s, *H*$_{syn}$)

^{19}F NMR (CD_2Cl_2, 376.4 MHz, 27 °C) δ – 58.5 (dq, $^5J_{FF}$ = 8 Hz, J_{FP} = 3 Hz, C*F*$_3$), – 64.7 (q, $^5J_{FF}$ = 8 Hz, C*F*$_3$)

^{31}P{^{1}H} NMR (CD_2Cl_2, 161.9 MHz, 27 °C) δ 62.1 (s)

^{13}C{^{1}H} APT NMR (CD_2Cl_2, 100.6 MHz, 27 °C) δ 216.7 (d, $^2J_{CP}$ = 18 Hz, *C*O), 86.4 (br s, *C*$_{central}$), 67.7 (dq, $^2J_{CP}$ = 4 Hz, $^4J_{CF}$ = 1Hz, *C*H$_2$), 27.6 (–) (d, $^1J_{CP}$ = 17 Hz, P*C*H), 19.1(–) (br s, PC*C*H$_3$)

^{13}C{^{19}F} NMR (CD_2Cl_2, 100.6 MHz, 27 °C) δ 216.7 (d, $^2J_{CP}$ = 18 Hz, *C*O), 153.8 (d, $^2J_{CP}$ = 16 Hz, C_α(CF$_3$)), 133.9 (br, C_β(CF$_3$)), 125.2 (s, *C*F$_3$), 117.0 (s, *C*F$_3$), 86.4 (br, *C*$_{central}$), 67.7 (br, *C*H$_2$), 27.6 (br, P*C*H), 19.1 (m, PC*C*H$_3$)

4bII (major isomer)

^{1}H NMR (CD_2Cl_2, 400.1 MHz, 27 °C) δ 1.29 (dd, $^3J_{HP}$ = 13 Hz, $^3J_{HH}$ = 7 Hz, PCC*H*$_3$), 2.26 (s, *H*$_{anti}$), 2.28 (s, *H*$_{anti}$), 2.36 (dsept, $^3J_{HH}$ = 7 Hz, $^2J_{HP}$ = 8 Hz, PC*H*), 3.18 (d, $^4J_{HH}$ = 3 Hz, *H*$_{syn}$), 3.74 (dd, $^4J_{HH}$ = 3 Hz, $^3J_{HP}$ = 3 Hz, *H*$_{syn}$)

^{19}F NMR (CD_2Cl_2, 376.4 MHz, 27 °C) δ – 54.5 (q, $^5J_{FF}$ = 9 Hz, C*F*$_3$), – 65.3 (dq, $^5J_{FF}$ = 9 Hz, J_{FP} = 2 Hz, C*F*$_3$)

^{31}P{^{1}H} NMR (CD_2Cl_2, 161.9 MHz, 27 °C) δ 72.0 (s)

$^{13}C\{^{1}H\}$ APT NMR (CD_2Cl_2, 100.6 MHz, 27 °C) δ 217.5 (d, $^{2}J_{CP}$ = 7 Hz, CO), 214.0 (d, $^{2}J_{CP}$ = 21 Hz, CO), 155.5 (br, $C_{\alpha}(CF_3)$), 134.0 (br, $C_{\beta}(CF_3)$), 126.3 (q, $^{1}J_{CF}$ = 275 Hz, CF_3), 117.7 (q, $^{1}J_{CF}$ = 273 Hz, CF_3), 84.8 (dq, $^{2}J_{CP}$ = Hz, $^{3}J_{CF}$ = 1Hz, $C_{central}$) 67.4 (dq, $^{2}J_{CP}$ = 9 Hz, $^{4}J_{CF}$ = 1Hz, CH_2), 66.8 (dq, $^{2}J_{CP}$ = 5 Hz, $^{4}J_{CF}$ = 1Hz, CH_2), 29.0 (–) (d, $^{1}J_{CP}$ = 19 Hz, PCH), 20.4 (–) (s, PCCH_3), 20.0 (–) (s, PCCH_3)

$^{13}C\{^{19}F\}$ NMR (CD_2Cl_2, 100.6 MHz, 27 °C) δ 217.5 (d, $^{2}J_{CP}$ = 7 Hz, CO), 214.0 (d, $^{2}J_{CP}$ = 21 Hz, CO), 155.5 (d, $^{2}J_{CP}$ = 19 Hz, $C_{\alpha}(CF_3)$), 134.0 (br s, $C_{\beta}(CF_3)$), 126.3 (s, CF_3), 117.7 (s, CF_3), 84.8 (br s, $C_{central}$) 67.4 (br, CH_2), 66.8 (br, CH_2), 29.0 (m, PCH), 20.4 (m, PCCH_3), 20.0 (m, PCCH_3)

$Fe(CO)_2(PCy_3)(\eta^1,\eta^3\text{-}\{F_3CC{=}C(CF_3)C(CH_2)_2\})$ (4cI,II)

Elemental Analysis $C_{27}H_{37}F_6FeO_2P$; Calculated: C, 54.56%; H, 6.27%,

Observed: C, 54.28%; H 6.38%.

F.W. 594.40

IR (pentane, cm^{-1}) ν_{CO} 2011 (s), 1960 (s)

4cI (minor isomer)

^{1}H NMR (CD_2Cl_2, 400.1 MHz, 27 °C) δ 1.40-2.20 (br, PC_6H_{11}), 2.51 (d, $^{3}J_{HP}$ = 8 Hz, H_{anti}), 3.23 (s, H_{syn})

^{19}F NMR (CD_2Cl_2, 376.4 MHz, 27 °C) δ – 58.0 (dq, $^{5}J_{FF}$ = 8 Hz, J_{FP} = 3 Hz, CF_3), – 64.1 (q, $^{5}J_{FF}$ = 8 Hz, CF_3)

$^{31}P\{^{1}H\}$ NMR (CD_2Cl_2, 161.9 MHz, 27 °C) δ 53.4 (s)

$^{13}C\{^{1}H\}$ APT NMR (CD_2Cl_2, 100.6 MHz, 27 °C) δ 216.6 (d, $^{2}J_{CP}$ = 19 Hz, CO), 154.3 (br, $C_{\alpha}(CF_3)$), 125.7 (q, $^{1}J_{CF}$ = 274 Hz, CF_3), 117.1 (q, $^{1}J_{CF}$ = 271 Hz, CF_3), 86.3 (br, $C_{central}$) 67.6 (br s, CH_2)

$^{13}C\{^{19}F\}$ NMR (CD_2Cl_2, 100.6 MHz, 27 °C) δ 216.6 (d, $^2J_{CP}$ = 19 Hz, CO), 154.3 (d, $^2J_{CP}$ = 19 Hz, $C_\alpha(CF_3)$), 125.7 (s, CF_3), 117.1 (s,CF_3), 86.3 (br s, $C_{central}$) 67.6 (br s, CH_2)

4cII (major isomer)

^1H NMR (CD_2Cl_2, 400.1 MHz, 27 °C) δ 1.13-2.20 (br, PC_6H_{11}), 2.19 (s, H_{anti}), 2.23 (s, H_{anti}), 3.11 (d, $^4J_{HH}$ = 3 Hz, H_{syn}), 3.74 (dd, $^4J_{HH}$ = 3 Hz, $^3J_{HP}$ = 3 Hz H_{syn})

^{19}F NMR (CD_2Cl_2, 376.4 MHz, 27 °C) δ – 53.7 (q, $^5J_{FF}$ = 9 Hz, CF_3), – 64.6 (dq, $^5J_{FF}$ = 9 Hz, J_{FP} = 2 Hz, CF_3)

$^{31}P\{^1H\}$ NMR (CD_2Cl_2, 161.9 MHz, 27 °C) δ 60.3 (s)

$^{13}C\{^1H\}$ APT NMR (CD_2Cl_2, 100.6 MHz, 27 °C) δ 217.9 (d, $^2J_{CP}$ = 6 Hz, CO), 214.0 (d, $^2J_{CP}$ = 21 Hz, CO), 155.5 (br, $C_\alpha(CF_3)$), 133.7 (br, $C_\beta(CF_3)$), 126.1 (q, $^1J_{CF}$ = 274 Hz, CF_3), 117.7 (q, $^1J_{CF}$ = 273 Hz, CF_3), 84.4 (br s, $C_{central}$) 66.6 (br s, CH_2), 66.3 (br s, CH_2)

$^{13}C\{^{19}F\}$ NMR (CD_2Cl_2, 100.6 MHz, 27 °C) δ 217.9 (d, $^2J_{CP}$ = 6 Hz, CO), 214.0 (d, $^2J_{CP}$ = 21 Hz, CO), 155.5 (d, $^2J_{CP}$ = 19 Hz, $C_\alpha(CF_3)$), 133.7 (s, $C_\beta(CF_3)$), 126.1 (s, CF_3), 117.7 (s, CF_3), 84.4 (br s, $C_{central}$) 66.3 (br, CH_2), 66.6 (br, CH_2)

$Fe(CO)_2(P^tBu_2Me)(\eta^1,\eta^3\text{-}\{F_3CC{=}C(CF_3)C(CH_2)CHMe\})$ (5aI,II)

Elemental Analysis $C_{19}H_{27}F_6FeO_2P$; Calculated: C, 46.74%; H, 5.57%,

Observed: C, 46.70%; H 5.63%.

F.W. 488.23

IR (pentane, cm^{-1}) ν_{CO} 2010 (s), 1958 (s)

5aI (major isomer)

^{1}H NMR (CD_2Cl_2, 400.1 MHz, 27 °C) δ 1.25* ($CHC\mathit{H}_3$), 1.30 (d, $^{3}J_{HP}$ = 132 Hz $PC(C\mathit{H}_3)_3$), 1.35 (d $^{3}J_{HP}$ = 13 Hz, $PC(C\mathit{H}_3)_3$), 1.41 (d, $^{2}J_{HP}$ = 7 Hz, $PC\mathit{H}_3$), 2.65 (s, H_{anti}) 3.66 (br m, H_{syn}) 3.87 (q, $^{3}J_{HH}$ = 7 Hz $C\mathit{H}CH_3$) (* δ identified in COSY)

^{19}F NMR (CD_2Cl_2, 376.4 MHz, 27 °C) δ – 52.7 (q, $^{5}J_{FF}$ = 9 Hz, $C\mathit{F}_3$), – 64.5 (br q, $^{5}J_{FF}$ = 8 Hz, $C\mathit{F}_3$)

$^{31}P\{^{1}H\}$ NMR (CD_2Cl_2, 161.9 MHz, 27 °C) δ 68.7 (s)

$^{13}C\{^{1}H\}$ APT NMR (CD_2Cl_2, 100.6 MHz, 27 °C) δ *C*O not observed, 215.0 (d, $^{2}J_{CP}$ = 20 Hz, *C*O), 155.1 (br, $\mathit{C}_{\alpha}(CF_3)$), 135.6 (br, $\mathit{C}_{\beta}(CF_3)$), 126.4 (q, $^{1}J_{CF}$ = 273 Hz, $\mathit{C}F_3$), 117.7 (q, $^{1}J_{CF}$ = 275 Hz, $\mathit{C}F_3$), 88.3 (–) (d, $^{2}J_{CP}$ = 10 Hz, $\mathit{C}HCH_3$) 85.3 (br s, $\mathit{C}_{central}$) 67.8 (s, $\mathit{C}H_2$), 38.1 (m $P\mathit{C}CH_3/P\mathit{C}CH_3$), 30.3 (–) (s, $PC(\mathit{C}H_3)_3$), 29.8 (–) (s, $PC(\mathit{C}H_3)_3$), 17.5 (–) (s, $CH\mathit{C}H_3$), 11.8 (–) (d, $^{2}J_{CP}$ = 19 Hz, $P\mathit{C}H_3$)

$^{13}C\{^{19}F\}$ NMR (CD_2Cl_2, 100.6 MHz, 27 °C) δ 217.6 (br s *C*O), 215.0 (d, $^{2}J_{CP}$ = 20 Hz, *C*O) 155.1 (d, $^{2}J_{CP}$ = 18 Hz, $\mathit{C}_{\alpha}(CF_3)$), 135.6 (s, $\mathit{C}_{\beta}(CF_3)$), 126.4 (s, $\mathit{C}F_3$), 117.7 (s, $\mathit{C}F_3$), $\mathit{C}HCH_3$ not observed, $\mathit{C}_{central}$ not observed, $\mathit{C}H_2$ not observed, 38.1 (m $P\mathit{C}CH_3/P\mathit{C}CH_3$), 30.3 (m, $PC(\mathit{C}H_3)_3$), 29.8 (m, $PC(\mathit{C}H_3)_3$), 17.5 (m, $CH\mathit{C}H_3$), 11.8 (m, $P\mathit{C}H_3$)

5aII (minor isomer)

^{1}H NMR (CD_2Cl_2, 400.1 MHz, 27 °C) δ 1.31* ($CHC\mathit{H}_3$), 1.36 (d, $^{2}J_{CP}$ = 13 Hz, $PC(C\mathit{H}_3)_3$), 1.48 (d $^{2}J_{HP}$ = 7 Hz, $PC\mathit{H}_3$), 2.46 (s, H_{anti}) 3.12 (s, H_{syn}) 4.57 (br m, $C\mathit{H}CH_3$) (* identified in COSY)

^{19}F NMR (CD_2Cl_2, 376.4 MHz, 27 °C) δ – 52.7 (q, $^{5}J_{FF}$ = 8 Hz, $C\mathit{F}_3$), – 64.8 (br q, $^{5}J_{FF}$ = 8 Hz, $C\mathit{F}_3$)

$^{31}P\{^{1}H\}$ NMR (CD_2Cl_2, 161.9 MHz, 27 °C) δ 64.2 (s)

$^{13}C\{^1H\}$APT NMR (CD_2Cl_2, 100.6 MHz, 27 °C) δ 214.4 (d $^2J_{CP}$ = 22 Hz, *C*O), *C*O not observed, 157.5 (br, $C_\alpha(CF_3)$), $C_\beta(CF_3)$ not observed, CF_3×2 not observed, 87.5 (–) (s, *C*HCH_3) 84.2 (s, $C_{central}$) 63.3 (s, CH_2), P*C*$(CH_3)_3$ not observed, 30.0 (–) (s, $PC(CH_3)_3$), 29.4 (–) (s, $PC(CH_3)_3$), 16.4 (–) (s, $CHCH_3$), 11.6 (–) (d, $^2J_{CP}$ = 20 Hz, PCH_3)

$Fe(CO)_2(P^iPr_3)(\eta^1,\eta^3$-$\{F_3CC{=}C(CF_3)C(CH_2)CHMe\})$ (5bI,II)

Elemental Analysis $C_{19}H_{27}F_6FeO_2P$; Calculated: C, 46.74%; H, 5.57%, Observed: C, 46.73%; H 5.39%.

F.W. 488.23

IR (pentane, cm^{-1}) ν_{CO} 2008 (s), 1957 (s)

5bI (major isomer)

^1H NMR (CD_2Cl_2, 400.1 MHz, 27 °C) δ 1.29 (dd, $^3J_{HH}$ = 7 Hz, $^3J_{HP}$ = 14 Hz, PCC*H*$_3$), 1.29 (dd, $^3J_{HH}$ = 7 Hz, $^3J_{HP}$ = 14 Hz, PCC*H*$_3$), 1.34* (CHC*H*$_3$), 2.36 (dsept, $^3J_{HH}$ = 7 Hz, $^2J_{HP}$ = 7 Hz PC*H*$_3$), 2.60 (s, H_{anti}) 3.85 (m, H_{syn}) 4.06 (dq, $^3J_{HH}$ = 7 Hz, $^4J_{HH}$ = 2 Hz C*H*CH_3)

^{19}F NMR (CD_2Cl_2, 376.4 MHz, 27 °C) δ – 54.5 (q, $^5J_{FF}$ = 9 Hz, C*F*$_3$), – 65.3 (dq, $^5J_{FF}$ = 9 Hz, J_{FP} = 2 Hz C*F*$_3$)

$^{31}P\{^1H\}$ NMR (CD_2Cl_2, 161.9 MHz, 27 °C) δ 70.6 (s)

$^{13}C\{^1H\}$ NMR (CD_2Cl_2, 100.6 MHz, 27 °C) δ 217.7 (d, $^2J_{CP}$ = 4 Hz, *C*O), 214.0 (d, $^2J_{CP}$ = 20 Hz, *C*O), 154.7 (dqq, $^2J_{CF}$ = 34 Hz, $^2J_{CP}$ = 19 Hz, $^2J_{CF}$ = 4 Hz, $C_\alpha(CF_3)$), 135.4 (br, $C_\beta(CF_3)$), 126.2 (q, $^1J_{CF}$ = 274 Hz, *C*F$_3$), 117.7 (q, $^1J_{CF}$ = 274 Hz, *C*F$_3$), 85.8 (d, $^2J_{CP}$ = 5 Hz, *C*HCH_3) 84.7 (br s, $C_{central}$) 64.7 (d, $^2J_{CP}$ = 5 Hz, *C*H_2), 29.1 (d, $^2J_{CP}$ = 19 Hz, P*C*H) 20.4 (s, PC*C*H_3), 19.1 (s, PC*C*H_3), 17.5 (s, CH*C*H_3)

$^{13}C\{^{19}F\}$ NMR (CD_2Cl_2, 100.6 MHz, 27 °C) δ 217.7 (d, $^{2}J_{CP} = 4$ Hz, *C*O), 214.0 (d, $^{2}J_{CP} = 20$ Hz, *C*O), 154.8 (d, $^{2}J_{CP} = 19$ Hz, $C_{\alpha}(CF_3)$), 135.4 (s, $C_{\beta}(CF_3)$), 126.2 (s, CF_3), 117.7 (s, CF_3), 85.8 (br, *C*HCH_3) 84.7 (br s, $C_{central}$) 64.7 (m, CH_2), 29.1 (br, P*C*H) 20.4 (m, $PCCH_3$), 19.1 (m, $PCCH_3$), 17.5 (m, $CHCH_3$)

5bII (minor isomer)

^{1}H NMR (CD_2Cl_2, 400.1 MHz, 27 °C) δ 1.27* ($CHCH_3$), 2.36 (dsept, $^{3}J_{HH} = 7$ Hz, $^{2}J_{HP} = 7$ Hz PCH_3), 2.66 (br s, H_{anti}) 3.25 (br s, H_{syn}) 4.68 (m, $CHCH_3$) (* identified in COSY)

^{19}F NMR (CD_2Cl_2, 376.4 MHz, 27 °C) δ – 54.7 (q, $^{5}J_{FF} = 9$ Hz, CF_3), – 65.4 (dq, $^{5}J_{FF} = 9$ Hz, $J_{FP} = 2$ Hz CF_3)

$^{31}P\{^{1}H\}$ NMR (CD_2Cl_2, 161.9 MHz, 27 °C) δ 67.6 (s)

$^{13}C\{^{1}H\}$ NMR (CD_2Cl_2, 100.6 MHz, 27 °C) δ 218.1 (d, $^{2}J_{CP} = 7$ Hz, *C*O), 213.8 (d, $^{2}J_{CP} = 21$ Hz, *C*O), $C_{\alpha}(CF_3)$ not observed, $C_{\beta}(CF_3)$ not observed, CF_3 not observed, 117.5 (q, $^{1}J_{CF} = 274$ Hz, CF_3), 84.0 (br s, $C_{central}$), 83.9 (s, $CHCH_3$), 64.8 (d, $^{2}J_{CP} = \sim 8$ Hz CH_2), 29.4 (d, $^{2}J_{CP} = 19$ Hz, PCH), 20.3 (s, $PCCH_3$), 18.9 (s, $PCCH_3$), 16.1 (s, $CHCH_3$)

$^{13}C\{^{19}F\}$ NMR (CD_2Cl_2, 100.6 MHz, 27 °C) δ 218.1 (d, $^{2}J_{CP} = 7$ Hz, *C*O), 213.8 (d, $^{2}J_{CP} = 21$ Hz, *C*O), 156.4 (d, $^{2}J_{CP} = 20$ Hz, $C_{\alpha}(CF_3)$), 134.7 (br s, $C_{\beta}(CF_3)$), CF_3 not observed, 117.5 (s, CF_3), 84.0 (br s, $C_{central}$) 83.9 (s, $CHCH_3$), 64.8 (br, CH_2), 29.4 (m, PCH), 20.3 (m, $PCCH_3$), 18.9 (m, $PCCH_3$), 16.1 (m, $CHCH_3$)

$Fe(CO)_2(PCy_3)(\eta^1,\eta^3$-$\{F_3CC{=}C(CF_3)C(CH_2)CHMe\})$ (5cI,II)

Elemental Analysis $C_{28}H_{39}F_6FeO_2P$; Calculated: C, 55.28%; H, 6.46%, Observed: C, 54.92%; H 6.35%.

F.W. 608.43

IR (pentane, cm^{-1}) ν_{CO} 2006 (s), 1955 (s)

5cI (major isomer)

^{1}H NMR (CD$_2$Cl$_2$, 400.1 MHz, 27 °C) δ 1.30* (CHCH_3), 2.55 (s, H_{anti}) 3.87 (m, H_{syn}) 4.00 (dq, $^{3}J_{HH}$ = 8 Hz, $^{3}J_{HH}$ = 2 Hz CHCH$_3$) (* identified in COSY)

^{19}F NMR (CD$_2$Cl$_2$, 376.4 MHz, 27 °C) δ – 54.2 (q, $^{5}J_{FF}$ = 9 Hz, CF_3), – 65.1 (dq, $^{5}J_{FF}$ = 9 Hz, J_{FP} = 3 Hz CF_3)

^{31}P{^{1}H} NMR (CD$_2$Cl$_2$, 161.9 MHz, 27 °C) δ 61.2 (s)

^{13}C{^{1}H} NMR (CD$_2$Cl$_2$, 100.6 MHz, 27 °C) δ 218.1 (d, $^{2}J_{CP}$ = 5 Hz, CO), 214.1 (d, $^{2}J_{CP}$ = 21 Hz, CO), 154.7 (dqq, $^{2}J_{CF}$ = 34 Hz, $^{2}J_{CP}$ = 19 Hz, $^{2}J_{CF}$ = 4 Hz, C_α(CF$_3$)), 135.3 (qq, $^{2}J_{CF}$ = 37 Hz, $^{2}J_{CF}$ = 10 Hz, C_β(CF$_3$)), 126.2 (q, $^{1}J_{CF}$ = 274 Hz, CF$_3$), 117.7 (q, $^{1}J_{CF}$ = 274 Hz, CF$_3$), 87.0 (d, $^{2}J_{CP}$ = 9 Hz, C$_{central}$) 85.5 (d, $^{2}J_{CP}$ = 10 Hz, CHCH$_3$) 64.4 (br, CH$_2$), 17.5 (s, CHCH$_3$)

^{13}C{^{19}F} NMR (CD$_2$Cl$_2$, 100.6 MHz, 27 °C) δ 218.1 (d, $^{2}J_{CP}$ = 5 Hz, CO), 214.1 (d, $^{2}J_{CP}$ = 21 Hz, CO), 154.7 (d, $^{2}J_{CP}$ = 19 Hz, C_α(CF$_3$)), 135.3 (s, C_β(CF$_3$)), 126.2 (s, CF$_3$), 117.7 (s, CF$_3$), 87.0 (br s, C$_{central}$) 85.5 (br, CHCH$_3$) 64.4 (br, CH$_2$), 17.5 (br, CHCH$_3$)

5cII (minor isomer)

^{1}H NMR (CD$_2$Cl$_2$, 400.1 MHz, 27 °C) δ 1.21* (CHCH_3), 2.64 (s, H_{anti}) 3.19 (s, H_{syn}) 4.70 (m, CHCH$_3$) (* identified in COSY)

^{19}F NMR (CD$_2$Cl$_2$, 376.4 MHz, 27 °C) δ – 54.6 (q, $^{5}J_{FF}$ = 9 Hz, CF_3), – 65.3 (dq, $^{5}J_{FF}$ = 9 Hz, J_{FP} = 3 Hz CF_3)

^{31}P{^{1}H} NMR (CD$_2$Cl$_2$, 161.9 MHz, 27 °C) δ 56.4 (s)

^{13}C{^{1}H} NMR (CD$_2$Cl$_2$, 100.6 MHz, 27 °C) δ 218.5 (d, $^{2}J_{CP}$ = 5 Hz, CO), 213.8 (d, $^{2}J_{CP}$ = 22 Hz, CO), 156.8 (dqq, $^{2}J_{CF}$ = 34 Hz, $^{2}J_{CP}$ = 19 Hz, $^{2}J_{CF}$ = 4 Hz,

$C_{\alpha}(\mathrm{CF_3})$), 134.8 (m, $C_{\beta}(\mathrm{CF_3})$), 126.3 (q, $^{1}J_{CF}$ = 274 Hz, $C\mathrm{F_3}$), 117.6 (q, $^{1}J_{CF}$ = 274 Hz, $C\mathrm{F_3}$), 84.6 (d, $^{2}J_{CP}$ = 9 Hz, C_{central}) 83.5 (s, $C\mathrm{HCH_3}$) 64.6 (d, $^{2}J_{CP}$ = 9 Hz, $C\mathrm{H_2}$), 16.0 (s, $\mathrm{CH}C\mathrm{H_3}$)

$^{13}\mathrm{C}\{^{19}\mathrm{F}\}$ NMR ($\mathrm{CD_2Cl_2}$, 100.6 MHz, 27 °C) δ 218.5 (d, $^{2}J_{CP}$ = 5 Hz, CO), 213.8 (d, $^{2}J_{CP}$ = 22 Hz, CO), 156.5 (d, $^{2}J_{CP}$ = 19 Hz, $C_{\alpha}(\mathrm{CF_3})$), 134.8 (s, $C_{\beta}(\mathrm{CF_3})$), 126.3 (s, $C\mathrm{F_3}$), 117.6 (s, $C\mathrm{F_3}$), 84.6 (br, $\mathrm{C_{central}}$) 83.5 (br, $C\mathrm{HCH_3}$) 64.6 (br, $C\mathrm{H_2}$), 16.0 (m, $\mathrm{CH}C\mathrm{H_3}$)

$\mathbf{Fe(CO)_2(P^tBu_2Me)(\eta^1,\eta^3\text{-}\{F_3CC{=}C(CF_3)C(CH_2)CMe_2\})}$ (6aI)

Elemental Analysis $\mathrm{C_{20}\,H_{29}\,F_6\,Fe\,O_2\,P}$; Calculated: C, 47.83%; H, 5.82%,

Observed: C, 47.71%; H 6.07%.

F.W. 502.26

IR (pentane, $\mathrm{cm^{-1}}$) ν_{CO} 2002 (s), 1951 (s)

$^{1}\mathrm{H}$ NMR ($\mathrm{CD_2Cl_2}$, 400.1 MHz, 27 °C) δ 1.31 (d, $^{3}J_{HP}$ = 13 Hz, $\mathrm{PC(C}H_3)_3$), 1.34 (d, $^{3}J_{HP}$ = 13 Hz, $\mathrm{PC(C}H_3)_3$), 1.38 (d, $^{2}J_{HP}$ = 7 Hz, $\mathrm{PC}H_3$), 1.41 (d, $^{4}J_{HP}$ = 1 Hz, $\mathrm{CC}H_3$), 1.74 (d, $^{4}J_{HP}$ = 2 Hz, $\mathrm{CC}H_3$) 2.40 (br s, H_{anti}) 3.37 (dd, $^{3}J_{HP}$ = 4 Hz, $^{2}J_{HH}$ = 2 Hz H_{syn})

$^{19}\mathrm{F}$ NMR ($\mathrm{CD_2Cl_2}$, 376.4 MHz, 27 °C) δ – 53.4 (q, $^{5}J_{FF}$ = 9 Hz, $\mathrm{C}F_3$), – 65.7 (dq, $^{5}J_{FF}$ = 9 Hz, J_{FP} = 2 Hz $\mathrm{C}F_3$)

$^{31}\mathrm{P}\{^{1}\mathrm{H}\}$ NMR ($\mathrm{CD_2Cl_2}$, 161.9 MHz, 27 °C) δ 71.8 (s)

$^{13}\mathrm{C}\{^{1}\mathrm{H}\}$APT NMR ($\mathrm{CD_2Cl_2}$, 100.6 MHz, 27 °C) δ 217.0 (d, $^{2}J_{CP}$ = 4 Hz, CO), 216.3 (dq, $^{2}J_{CP}$ = 21 Hz, $^{4}J_{CF}$ = 2 Hz, CO), 156.2 (dqq, $^{2}J_{CF}$ = 34 Hz, $^{2}J_{CP}$ = 19 Hz, $^{2}J_{CF}$ = 4 Hz, $C_{\alpha}(\mathrm{CF_3})$), 133.4 (qq, $^{2}J_{CF}$ = 37, $^{3}J_{CF}$ = 10 Hz $C_{\beta}(\mathrm{CF_3})$), 126.6 (q, $^{1}J_{CF}$ = 274 Hz, $C\mathrm{F_3}$), 117.8 (q, $^{1}J_{CF}$ = 273 Hz, $C\mathrm{F_3}$), 106.0 (dq, $^{2}J_{CP}$ = 10 Hz, $^{4}J_{CF}$ = 1 Hz $C(\mathrm{CH_3})_2$), 83.6 (qq, $^{3}J_{CF}$ = 1 Hz, $^{4}J_{CF}$ = 3 Hz C_{central}), 61.8 (dq, $^{2}J_{CP}$ = 5 Hz, $^{4}J_{CF}$ = 1 Hz, $C\mathrm{H_2}$), 38.3 (d,

$^{1}J_{CP} = 14$ Hz, $PC(CH_3)_3$), 38.2 (d, $^{1}J_{CP} = 14$ Hz, $PC(CH_3)_3$), 30.2 (–) (d, $^{2}J_{CP} = 4$ Hz, $PC(CH_3)_3$), 29.9 (–) (d, $^{2}J_{CP} = 4$ Hz, $PC(CH_3)_3$), 24.8 (–) (s, CCH_3), 23.7 (–) (s, CCH_3), 11.7 (–) (d, $^{1}J_{CP} = 19$ Hz, PCH_3)

$^{13}C\{^{19}F\}$ NMR (CD_2Cl_2, 100.6 MHz, 27 °C) δ 217.0 (d, $^{2}J_{CP} = 4$ Hz, *C*O), 216.3 (d, $^{2}J_{CP} = 21$ Hz, *C*O), 156.2 (d, $^{2}J_{CP} = 19$ Hz, Fe*C*=), 133.4 (br, =CCF_3), 126.6 (s, CF_3), 117.8 (s, CF_3), 106.0 (br, $C(CH_3)_2$), 61.8 (m, CH_2)

$Fe(CO)_2(P^iPr_3)(\eta^1,\eta^3\text{-}\{F_3CC{=}C(CF_3)C(CH_2)CMe_2\})$ (6bI)

Elemental Analysis $C_{20}H_{29}F_6FeO_2P$; Calculated: C, 47.83%; H, 5.82%, Observed: C, 47.79%; H 5.80%.

F.W. 502.26

IR (pentane, cm^{-1}) ν_{CO} 2001 (s), 1951 (s)

^{1}H NMR (CD_2Cl_2, 400.1 MHz, 27 °C) δ 1.28 (dd, $^{3}J_{HH} = 7$ Hz, $^{3}J_{HP} = 13$ Hz $PCCH_3$), 1.29 (dd, $^{3}J_{HP} = 14$ Hz, $^{3}J_{HH} = 7$ Hz $PCCH_3$), 1.47 (d, $^{4}J_{HP} = 1$ Hz, CCH_3), 1.78 (d, $^{4}J_{HP} = 1$ Hz, CCH_3), 2.34 (dsept, $^{3}J_{HH} = 7$ Hz, $^{2}J_{HP} = 7$ Hz, PCH_3) 2.36 (br s, H_{anti}) 3.56 (dd, $^{3}J_{HH} = 2$ Hz, $^{3}J_{HP} = 4$ Hz H_{syn})

^{19}F NMR (CD_2Cl_2, 376.4 MHz, 27 °C) δ – 54.8 (q, $^{5}J_{FF} = 9$ Hz, CF_3), – 66.2 (dq, $^{5}J_{FF} = 9$ Hz, $J_{FP} = 3$ Hz, CF_3)

$^{31}P\{^{1}H\}$ NMR (CD_2Cl_2, 161.9 MHz, 27 °C) δ 72.9 (s)

$^{13}C\{^{1}H\}$ APT NMR (CD_2Cl_2, 100.6 MHz, 27 °C) δ 216.8 (d, $^{2}J_{CP} = 4$ Hz, *C*O), 214.8 (dq, $^{2}J_{CP} = 21$ Hz, $^{4}J_{CF} = 1$ Hz, *C*O), 156.1 (dqq, $^{2}J_{CF} = 32$ Hz, $^{2}J_{CP} = 19$ Hz, $^{3}J_{CF} = 4$ Hz, $C_\alpha(CF_3)$), 132.6 (qq, $^{2}J_{CF} = 37$ Hz, $^{3}J_{CF} = 10$ Hz, $C_\beta(CF_3)$), 126.0 (q, $^{1}J_{CF} = 273$ Hz, CF_3), 117.5 (q, $^{1}J_{CF} = 274$ Hz, CF_3), 107.0 (dq, $^{2}J_{CP} = 9$ Hz, $^{4}J_{CF} = 1$ Hz, $C(CH_3)_2$), 82.4 (qq, $^{3}J_{CF} = 3$ Hz, $^{4}J_{CF} = 1$ Hz, $C_{central}$), 59.3 (dq, $^{2}J_{CP} = 5$ Hz, $^{4}J_{CF} = 2$ Hz, CH_2), 29.0 (–) (d,

$^1J_{CP}$ = 19 Hz, P*C*H), 24.4 (–) (s, C*C*H$_3$), 23.2 (–) (s, C*C*H$_3$), 20.1 (–) (s, PC*C*H$_3$), 18.8 (–) (s, PC*C*H$_3$)

$^{13}C\{^{19}F\}$ NMR (CD$_2$Cl$_2$, 100.6 MHz, 27 °C) δ 216.8 (d, $^2J_{CP}$ = 4 Hz, *C*O), 214.8 (d, $^2J_{CP}$ = 21 Hz, *C*O), 156.1 (d, $^2J_{CP}$ = 19 Hz, C_α(CF$_3$)), 132.6 (s, C_β(CF$_3$)), 126.0 (s, *C*F$_3$), 117.5 (s, *C*F$_3$), 107.0 (br, *C*(CH$_3$)$_2$), 82.4 (br, $C_{central}$), 59.3 (m, *C*H$_2$), 29.0 (dd, $^1J_{CH}$ = 128 Hz, $^1J_{CP}$ = 18 Hz, P*C*H), 24.4 (m, C*C*H$_3$), 23.2 (m, C*C*H$_3$), 20.1 (m, PC*C*H$_3$), 18.8 (m, PC*C*H$_3$)

Fe(CO)$_2$(PCy$_3$)(η^1,η^3-{F$_3$CC=C(CF$_3$)C(CH$_2$)CMe$_2$}) (6cI)

Elemental Analysis $C_{29}H_{41}F_6FeO_2P$; Calculated: C, 55.96%; H, 6.64%, Observed: C, 55.93%; H 6.64%.

F.W. 622.45

IR (pentane, cm^{-1}) ν_{CO} 2000 (s), 1947 (s)

^1H NMR (CD$_2$Cl$_2$, 400.1 MHz, 27 °C) δ 1.46 (d, $^4J_{HP}$ = 1 Hz, CC*H*$_3$), 1.76 (d, $^4J_{HP}$ = 1 Hz, CC*H*$_3$), 2.28 (br s, H_{anti}) 3.57 (dd, $^2J_{HH}$ = 2 Hz, $^3J_{HP}$ = 4 Hz, H_{syn})

^{19}F NMR (CD$_2$Cl$_2$, 376.4 MHz, 27 °C) δ – 54.3 (q, $^5J_{FF}$ = 9 Hz, C*F*$_3$), – 65.7 (dq, $^5J_{FF}$ = 9 Hz, J_{FP} = 2 Hz, C*F*$_3$)

$^{31}P\{^1H\}$ NMR (CD$_2$Cl$_2$, 161.9 MHz, 27 °C) δ 62.4 (s)

$^{13}C\{^1H\}$APT NMR (CD$_2$Cl$_2$, 100.6 MHz, 27 °C) δ 217.4 (d, $^2J_{CP}$ = 3 Hz, *C*O), 215.1 (dq, $^2J_{CP}$ = 20 Hz, $^3J_{CF}$ = 4 Hz, *C*O), 156.4 (dqq, $^2J_{CF}$ = 34 Hz, $^2J_{CP}$ = 20 Hz, $^3J_{CF}$ = 4 Hz C_α(CF$_3$)), 132.6 (qq, $^2J_{CF}$ = 37 Hz, $^3J_{CF}$ = 10 Hz, C_β(CF$_3$)), 126.2 (q, $^1J_{CF}$ = 275 Hz, *C*F$_3$), 117.5 (q, $^1J_{CF}$ = 274 Hz, *C*F$_3$), 106.7 (dq, $^3J_{CP}$ = 9 Hz, $^4J_{CF}$ = 1 Hz *C*(CH$_3$)$_2$), 82.6 (qq, $^3J_{CF}$ = 3 Hz, $^4J_{CF}$ = 1 Hz, $C_{central}$), 58.8 (dq, $^2J_{CP}$ = 5 Hz, $^4J_{CF}$ = 1 Hz, *C*H$_2$), 39.0 (–) (d, $^1J_{CP}$ = 17 Hz, P*C*H), 30.2 (s, PC$_6$H$_{11}$), 29.1 (br s, PC$_6$H$_{11}$), 28.1 (d, $^2J_{CP}$ = 9 Hz,

PC_6H_{11}), 27.7 (d, $^2J_{CP}$ = 10 Hz, PC_6H_{11}), 26.6 (s, PC_6H_{11}), 24.4 (–) (s, CH_3), 23.1 (–) (s, CH_3)

$^{13}C\{^{19}F\}$ NMR (CD_2Cl_2, 100.6 MHz, 27 °C) δ 217.4 (d, $^2J_{CP}$ = 3 Hz, *C*O), 215.1 (d, $^2J_{CP}$ = 20 Hz, *C*O), 156.4 (d, $^2J_{CP}$ = 20 Hz, $C_\alpha(CF_3)$), 132.6 (s, $C_b(CF_3)$), 126.2 (s, CF_3), 117.5 (s, CF_3), 106.7 (br, $CCH_3)_2$), 82.6 (br s, $C_{central}$), 58.8 (m, CH_2), 39.0 (br, P*C*H), 30.2 (br, PC_6H_{11}), 29.1 (br, PC_6H_{11}), 28.1 (br, PC_6H_{11}), 27.7 (br, PC_6H_{11}), 26.6 (br, PC_6H_{11}), 24.4 (m, CH_3), 23.1 (m, CH_3)

$Fe(CO)_2(PCy_3)(\eta^1,\eta^3\text{-}\{F_3CC{=}C(CF_3)C(CH_2)CMe_2\})$ (6cII)

F.W. 622.45

^1H NMR (CD_2Cl_2, 400.1 MHz, –80 °C) δ 1.23 (s, CCH_3), 1.69 (s, CCH_3), 2.27 (s, H_{anti}) 2.85 (s, H_{syn})

^{19}F NMR (CD_2Cl_2, 376.4 MHz, –80 °C) δ – 54.2 (br q, $^5J_{FF}$ = 8 Hz, CF_3), – 63.9 (br q, $^5J_{FF}$ = 8 Hz, CF_3)

$^{31}P\{^1H\}$ NMR (CD_2Cl_2, 161.9 MHz, –80 °C) δ 55.2 (s)

$^{13}C\{^1H\}$ NMR (CD_2Cl_2, 100.6 MHz, –80 °C) δ 219.8 (s, *C*O), 212.7 (d, $^2J_{CP}$ = 19 Hz, *C*O), 160.0 (br, $C_\alpha(CF_3)$), 132.5 (br, $C_\beta(CF_3)$), 125.4 (q, $^1J_{CF}$ = 272 Hz, CF_3), 119.9 (s, $C(CH_3)_2$), 116.9 (q, $^1J_{CP}$ = 272 Hz, CF_3), 82.3 (s, $C_{central}$), 55.5 (s, CH_2), 23.8 (s, CCH_3), 21.8 (s, CCH_3)

3.7.4 X-ray Crystal Structure Determination of $Fe(CO)_2(PR_2R')(\eta^1,\eta^3\text{-}\{F_3CC{=}C(CF_3)C(CH_2)_2\})$ (4a-c)

Yellow crystals of **4a-c** were produced by several attempts of cooling a concentrated pentane solution from 0 °C to –30 °C and then from –30 °C to –80 °C. Data collection and structure refinement were performed by Dr. R McDonald of the X-ray Crystallography Laboratory, Department of Chemistry, University of Alberta. Data collection was carried out on a Bruker PLATFORM/SMART 1000 CCD (**4a,c**) or a Bruker P4/R4/SMART 1000 CCD (**4 b**) diffractometer. Programs for diffractometer operation, data collection, data reduction and absorption correction were those supplied by Bruker. Unit cell parameters were obtained from least-squares refinement of 4005 (**4a**), 5079 (**4b**) or 4544 (**4c**) centered reflections. The structure was solved using a direct methods/fragment search (*DIRDIF–96*) [52] (**4a**) or a direct methods (*SHELXS–86*) [53] (**4b,c**) method. Structure refinement was performed using a full-matrix least-squares on F^2 (*SHELXL–93*) [54] method for all three structures. All non-hydrogen atoms were located. Hydrogen atoms were place in calculated positions and geometrically constrained during final refinement. Summaries of data collection parameters are presented in Tables 3-23, **4a**; Table 3-24, **4b** and Table 3-25, **4c**. Final atomic coordinate and displacement parameters may be obtained from X-ray Crystallography Laboratory, Department of Chemistry, University of Alberta with the file identification codes TAK 9915, **4a**; TAK 0003, **4b**, TAK 9916, **4c**.

Table 3-23 Crystallographic Experimental Details for Compound **4a**

formula	$C_{18}H_{25}F_6FeO_2P$
formula weight	474.20
crystal dimensions (mm)	0.38 × 0.24 × 0.20
crystal system	monoclinic
space group	$P2_1/c$ (No.14)
unit cell parameters	
a (Å)	11.7477 (9)
b (Å)	13.7214 (11)
c (Å)	13.7026 (11)
β (deg)	107.3785 (15)
V (Å^3)	2108.0 (3)
Z	4
ρ_{calcd} (g cm^{-3})	1.494
μ (mm^{-1})	0.853
radiation (λ[Å])	graphite-monochromated Mo Kα (0.71073)
temperature (°C)	– 80
scan type	ω scans (0.3°) (30 s exposures)
data collection 2θ limit (deg)	51.50
total data collected	10295 ($-14 \le h \le 12$, $-16 \le k \le 16$, $-15 \le l \le 16$)
independent reflections	4007
number of observed reflections (*NO*)	3116 [$F_o^2 \ge 2\sigma(F_o^2)$]
absorption correction method	*SADABS*
range of transmission factors	0.8620 – 0.6633
data/restraints/parameters	4007 [$F_o^2 \ge -3\sigma(F_o^2)$] / 0 / 280
goodness of fit (S)^a	1.067 [$F_o^2 \ge -3\sigma(F_o^2)$]
final R indices^b	
R_1 [$F_o^2 \ge 2\sigma(F_o^2)$]	0.0395
wR_2 [$F_o^2 \ge -3\sigma(F_o^2)$]	0.1204
largest difference peak and hole	0.675 and – 0.433 e Å^{-3}

[a] $S = [\Sigma w(F_o^2 - F_c^2)^2/(n - p)]^{1/2}$ (n = number of data; p = number of parameters varied; $w = [\sigma^2(F_o^2)+(0.0545P)^2 + 1.7681P]^{-1}$ where $P = ([\mathrm{Max}(F_o^2, 0) + 2F_c^2]/3)$.

[b] $R_1 = \Sigma||F_o| - |F_c||/\Sigma|F_o|$; $wR_2 = [\Sigma w(F_o^2 - F_c^2)^2/\Sigma w(F_o^4)]^{1/2}$

Table 3-24 Crystallographic Experimental Details for Compound **4b**

formula	$C_{18}H_{25}F_6FeO_2P$
formula weight	474.20
crystal dimensions (mm)	0.30 × 0.14 × 0.12
crystal system	monoclinic
space group	$P2_1/c$ (No.14)
unit cell parameters	
a (Å)	8.4791 (6)
b (Å)	9.7099 (6)
c (Å)	25.5552 (18)
β (deg)	91.5899 (12)
V (Å^3)	2103.2 (2)
Z	4
ρ_{calcd} (g cm^{-3})	1.498
μ (mm^{-1})	0.855
radiation (λ[Å])	graphite-monochromated Mo Kα (0.71073)
temperature (°C)	– 80
scan type	ϕ rotations (0.3°)/ω scans (0.3°)(30 s exposures)
data collection 2θ limit (deg)	52.80
total data collected	10039 ($-10 \le h \le 10$, $-4 \le k \le 12$, $-31 \le l \le 31$)
independent reflections	4295 (R_{int} = 0.0511)
number of observed reflections (*NO*)	2833 [$F_o^2 \ge 2\sigma(F_o^2)$]
absorption correction method	empirical (*SADABS*)
range of transmission factors	0.9043 – 0.7835
data/restraints/parameters	4295 [$F_o^2 \ge -3\sigma(F_o^2)$] / 0 / 316
goodness of fit (S)[a]	0.909 [$F_o^2 \ge -3\sigma(F_o^2)$]
final R indices[b]	
R_1 [$F_o^2 \ge 2\sigma(F_o^2)$]	0.0411
wR_2 [$F_o^2 \ge -3\sigma(F_o^2)$]	0.0911
largest difference peak and hole	0.344 and – 0.308 e Å^{-3}

[a] $S = [\Sigma w(F_o^2 - F_c^2)^2/(n - p)]^{1/2}$ (n = number of data; p = number of parameters varied; $w = [\sigma^2(F_o^2)+(0.0374P)^2]^{-1}$ where $P = ([\mathrm{Max}(F_o^2, 0) + 2F_c^2]/3)$.

[b] $R_1 = \Sigma||F_o| - |F_c||/\Sigma|F_o|$; $wR_2 = [\Sigma w(F_o^2 - F_c^2)^2/\Sigma w(F_o^4)]^{1/2}$

Table 3-25 Crystallographic Experimental Details for Compound **4c**

formula	$C_{27}H_{37}F_6FeO_2P$
formula weight	594.39
crystal dimensions (mm)	0.37 × 0.20 × 0.06
crystal system	monoclinic
space group	$P2_1/n$ (a nonstandard setting of $P2_1/c$ [No.14])
unit cell parameters	
a (Å)	15.8783 (13)
b (Å)	10.8998 (9)
c (Å)	16.1692 (13)
β (deg)	94.6027 (16)
V (Å^3)	2789.4 (4)
Z	4
ρ_{calcd} (g cm^{-3})	1.415
μ (mm^{-1})	0.661
radiation (λ[Å])	graphite-monochromated Mo Kα (0.71073)
temperature (°C)	– 80
scan type	ω scans (0.3°) (30 s exposures)
data collection 2θ limit (deg)	51.50
total data collected	13620 ($-19 \le h \le 10$, $-13 \le k \le 13$, $-19 \le l \le 19$)
independent reflections	5308
number of observed reflections (*NO*)	3708 [$F_o^2 \ge 2\sigma(F_o^2)$]
absorption correction method	*SADABS*
range of transmission factors	0.9280 – 0.7154
data/restraints/parameters	5308 [$F_o^2 \ge -3\sigma(F_o^2)$] / 0 / 334
goodness of fit (S)[a]	0.962 [$F_o^2 \ge -3\sigma(F_o^2)$]
final R indices[b]	
R_1 [$F_o^2 \ge 2\sigma(F_o^2)$]	0.0446
wR_2 [$F_o^2 \ge -3\sigma(F_o^2)$]	0.1165
largest difference peak and hole	1.089 and – 0.556 e Å^{-3}

[a] $S = [\Sigma w(F_o^2 - F_c^2)^2/(n - p)]^{1/2}$ (n = number of data; p = number of parameters varied; $w = [\sigma^2(F_o^2)+(0.0645P)^2]^{-1}$ where $P = ([\mathrm{Max}(F_o^2, 0) + 2F_c^2]/3)$.

[b] $R_1 = \Sigma||F_o| - |F_c||/\Sigma|F_o|$; $wR_2 = [\Sigma w(F_o^2 - F_c^2)^2/\Sigma w(F_o^4)]^{1/2}$

3.7.5 X-ray Crystal Structure Determination of $Fe(CO)_2(P^iPr_3)(\eta^1,\eta^3\text{-}\{F_3CC{=}C(CF_3)C(CH_2)CHMe\})$ (5b)

Orange crystals of **5 b** were produced by cooling a concentrated CH_2Cl_2/pentane solution from 0 °C to –30 °C. Data collection and structure refinement were performed by Dr. R McDonald of the X-ray Crystallography Laboratory, Department of Chemistry, University of Alberta. Data collection was carried out on a Bruker P4/RA/SMART 1000 CCD diffractometer. Programs for diffractometer operation, data collection, data reduction and absorption correction were those supplied by Bruker. Unit cell parameters were obtained from least-squares refinement of 5939 centered reflections. The structure was solved using a direct methods/fragment search (*DIRDIF–96*) [52] method. Structure refinement was performed using a full-matrix least-squares on F^2 (*SHELXL–93*) [53] method. All non-hydrogen atoms were located. Hydrogen atoms were place in calculated positions and geometrically constrained during final refinement. Summary of data collection parameters are presented in Table 3-26. Final atomic coordinates and displacement parameters may be obtained from X-ray Crystallography Laboratory, Department of Chemistry, University of Alberta with the file identification code TAK 9927.

Table 3-26 Crystallographic Experimental Details for Compound **5b**

formula	$C_{19}H_{27}F_6FeO_2P$
formula weight	488.23
crystal dimensions (mm)	0.49 × 0.27 × 0.06
crystal system	monoclinic
space group	$P2_1/n$ (a nonstandard setting of $P2_1/c$ [No.14])
unit cell parameters	
a (Å)	9.4461 (6)
b (Å)	13.6254 (8)
c (Å)	16.8774 (11)
β (deg)	90.4872 (11)
V (Å^3)	2172.2 (2)
Z	4
ρ_{calcd} (g cm^{-3})	1.493
μ (mm^{-1})	0.830
radiation (λ[Å])	graphite-monochromated Mo Kα (0.71073)
temperature (°C)	– 80
scan type	ϕ rotations (0.3°)/ω (0.3°)(30 s exposures)
data collection 2θ limit (deg)	52.80
total data collected	10983 ($-11 \le h \le 11$, $-12 \le k \le 17$, $-20 \le l \le 21$)
independent reflections	4440
number of observed reflections (*NO*)	3487 [$F_o^2 \ge 2\sigma(F_o^2)$]
absorption correction method	*SADABS*
range of transmission factors	0.9622 – 0.6454
data/restraints/parameters	4440 [$F_o^2 \ge -3\sigma(F_o^2)$] / 0 / 262
goodness of fit (S)^a	1.012 [$F_o^2 \ge -3\sigma(F_o^2)$]
final R indices^b	
R_1 [$F_o^2 \ge 2\sigma(F_o^2)$]	0.0336
wR_2 [$F_o^2 \ge -3\sigma(F_o^2)$]	0.0927
largest difference peak and hole	0.422 and – 0.417 e Å^{-3}

[a] $S = [\Sigma w(F_o^2 - F_c^2)^2/(n-p)]^{1/2}$ (n = number of data; p = number of parameters varied; $w = [\sigma^2(F_o^2)+(0.0523P)^2]^{-1}$ where $P = ([\text{Max}(F_o^2, 0) + 2F_c^2]/3)$.

[b] $R_1 = \Sigma||F_o| - |F_c||/\Sigma|F_o|$; $wR_2 = [\Sigma w(F_o^2 - F_c^2)^2/\Sigma w(F_o^4)]^{1/2}$

3.7.6 X-ray Crystal Structure Determination of $Fe(CO)_2(PR_2R')(\eta^1,\eta^3\text{-}\{F_3CC{=}C(CF_3)C(CH_2)CMe_2\})$ (6aI,6bI,6bII)

Orange crystals of **6nI** (n = a, b) were produced by cooling a concentrated CH_2Cl_2/pentane solution from 0 °C to –30 °C, while orange crystals of **6bII** were produced by concentrating a pentane solution of the compound at –78°C, then crystalizing at –80 °C. Data collection and structure refinement were performed by Dr. R. McDonald (**6aI**, **6bII**) or Dr. M. J. Ferguson (**6bI**) of the X-ray Crystallography Laboratory, Department of Chemistry, University of Alberta. Data collections were carried out on a Bruker P4/RA/SMART 1000 CCD (**6aI**, **6bII**) diffractometer or a Bruker PLATFORM/SMART 1000 CCD (**6bI**) diffractometer. Programs for diffractometer operation, data collection, data reduction and absorption correction were those supplied by Bruker. Unit cell parameters were obtained from least-squares refinement of 7073, 2113 or 5178 centered reflections for **6aI**, **6bI** and **6bII**, respectively. The structure was solved using a Patterson search/structure expansion (*DIRDIF-96*) [52] (**6aI**, **6bI**) or direct methods (*SHELXS-86*) [53] method for 6bII. Structure refinement was performed using a full-matrix least-squares on F^2 (SHELXL–93) [54] method for all structures. All non-hydrogen atoms were located. Hydrogen atoms were place in calculated positions and geometrically constrained during final refinement. Summaries of data collection parameters are presented for **6aI**, **6bI** and **6bII** in Tables 3-27, 3-28 and Table 3-29, respectively. Final atomic coordinates and displacement parameters may be obtained from X-ray Crystallography Laboratory, Department of Chemistry, University of Alberta with the file identification code TAK 99281, **6aI**; TAK 0211, **6bI**; TAK 0001, **6bII**.

Table 3-27 Crystallographic Experimental Details for Compound **6aI**

formula	$C_{20}H_{29}F_6FeO_2P$
formula weight	502.25
crystal dimensions (mm)	0.44 × 0.18 × 0.16
crystal system	monoclinic
space group	$P2_1/c$ (No.14)
unit cell parameters	
a (Å)	13.6174 (12)
b (Å)	10.2918 (10)
c (Å)	16.3175 (15)
β (deg)	99.6351 (16)
V (Å^3)	2254.6 (4)
Z	4
ρ_{calcd} (g cm^{-3})	1.480
μ (mm^{-1})	0.802
radiation (λ [Å])	graphite-monochromated Mo Kα (0.71073)
temperature (°C)	– 80
scan type	ϕ rotations (0.3°)/ω (0.3°)(30 s exposures)
data collection 2θ limit (deg)	52.84
total data collected	10850 ($-17 \le h \le 5$, $-12 \le k \le 12$, $-19 \le l \le 20$)
independent reflections	4602 ($R_{int} = 0.0290$)
number of observed reflections (*NO*)	3853 [$F_o^2 \ge 2\sigma(F_o^2)$]
absorption correction method	empirical (*SADABS*)
range of transmission factors	0.8824 – 0.7191
data/restraints/parameters	4602 [$F_o^2 \ge -3\sigma(F_o^2)$] / 0 / 273
goodness of fit (S)[a]	1.025 [$F_o^2 \ge -3\sigma(F_o^2)$]
final R indices[b]	
R_1 [$F_o^2 \ge 2\sigma(F_o^2)$]	0.0311
wR_2 [$F_o^2 \ge -3\sigma(F_o^2)$]	0.0874
largest difference peak and hole	0.412 and – 0.249 e Å^{-3}

[a] $S = [\Sigma w(F_o^2 - F_c^2)^2/(n-p)]^{1/2}$ (n = number of data; p = number of parameters varied; $w = [\sigma^2(F_o^2) + (0.0512P)^2 + 0.1707P]^{-1}$ where $P = ([\mathrm{Max}(F_o^2, 0) + 2F_c^2]/3)$.

[b] $R_1 = \Sigma||F_o| - |F_c||/\Sigma|F_o|$; $wR_2 = [\Sigma w(F_o^2 - F_c^2)^2/\Sigma w(F_o^4)]^{1/2}$

Table 3-28 Crystallographic Experimental Details for Compound **6bI**

formula	$C_{20}H_{29}F_6FeO_2P$
formula weight	502.25
crystal dimensions (mm)	0.38 × 0.07 × 0.05
crystal system	monoclinic
space group	$P2_1/n$ (an alternate setting of $P2_1/c$ [No.14])
unit cell parameters	
a (Å)	10.4137 (12)
b (Å)	16.0627 (18)
c (Å)	41.277 (5)
β (deg)	94.197 (2)
V (Å^3)	6885.9 (14)
Z	12
ρ_{calcd} (g cm^{-3})	1.453
μ (mm^{-1})	0.788
radiation (λ[Å])	graphite-monochromated Mo Kα (0.71073)
temperature (°C)	– 80
scan type	ω scans (0.2°) (25 s exposures)
data collection 2θ limit (deg)	50.00
total data collected	29240 ($-12 \le h \le 12$, $-19 \le k \le 16$, $-47 \le l \le 49$)
independent reflections	12100 ($R_{int} = 0.1440$)
number of observed reflections (*NO*)	5600 [$F_o^2 \ge 2\sigma(F_o^2)$]
absorption correction method	empirical (*SADABS*)
range of transmission factors	0.9617 – 0.7539
data/restraints/parameters	12100 [$F_o^2 \ge -3\sigma(F_o^2)$] / 0 / 805
goodness of fit (S)[a]	0.993 [$F_o^2 \ge -3\sigma(F_o^2)$]
final R indices[b]	
R_1 [$F_o^2 \ge 2\sigma(F_o^2)$]	0.0818
wR_2 [$F_o^2 \ge -3\sigma(F_o^2)$]	0.1893
largest difference peak and hole	1.141 and – 0.486 e Å^{-3}

[a] $S = [\Sigma w(F_o^2 - F_c^2)^2/(n-p)]^{1/2}$ (n = number of data; p = number of parameters varied; $w = [(2(F_o^2)+(0.0708P)^2]^{-1}$ where $P = ([\mathrm{Max}(F_o^2, 0) + 2F_c^2]/3)$.

[b] $R_1 = \Sigma||F_o| - |F_c||/\Sigma|F_o|$; $wR_2 = [\Sigma w(F_o^2 - F_c^2)^2/\Sigma w(F_o^4)]^{1/2}$

Table 3-29 Crystallographic Experimental Details for Compound **6bII**

formula	$C_{20}H_{29}F_6FeO_2P$
formula weight	502.25
crystal dimensions (mm)	0.38 × 0.10 × 0.10
crystal system	monoclinic
space group	$P2_1/n$ (a nonstandard setting of $P2_1/c$ [No.14])
unit cell parameters	
a (Å)	9.3867 (7)
b (Å)	14.2026 (11)
c (Å)	17.1289 (12)
β (deg)	92.3908 (15)
V (Å^3)	2281.6 (3)
Z	4
ρ_{calcd} (g cm^{-3})	1.462
μ (mm^{-1})	0.793
radiation (λ[Å])	graphite-monochromated Mo Kα (0.71073)
temperature (°C)	– 80
scan type	ϕ rotations (0.3°)/ω (0.3°)(30 s exposures)
data collection 2θ limit (deg)	52.90
total data collected	11105 ($-11 \le h \le 11$, $-17 \le k \le 17$, $-8 \le l \le 21$)
independent reflections	4633 (R_{int} = 0.0394)
number of observed reflections (*NO*)	3186 [$F_o^2 \ge 2\sigma(F_o^2)$]
absorption correction method	empirical (*SADABS*)
range of transmission factors	0.9249 – 0.7527
data/restraints/parameters	4633 [$F_o^2 \ge -3\sigma(F_o^2)$] / 0 / 273
goodness of fit (S)[a]	0.931 [$F_o^2 \ge -3\sigma(F_o^2)$]
final R indices[b]	
R_1 [$F_o^2 \ge 2\sigma(F_o^2)$]	0.0367
wR_2 [$F_o^2 \ge -3\sigma(F_o^2)$]	0.0818
largest difference peak and hole	0.369 and – 0.227 e Å^{-3}

[a] $S = [\Sigma w(F_o^2 - F_c^2)^2/(n - p)]^{1/2}$ (n = number of data; p = number of parameters varied; $w = [\sigma^2(F_o^2)+(0.0362P)^2]^{-1}$ where $P = ([\mathrm{Max}(F_o^2, 0) + 2F_c^2]/3)$.

[b] $R_1 = \Sigma||F_o| - |F_c||/\Sigma|F_o|$; $wR_2 = [\Sigma w(F_o^2 - F_c^2)^2/\Sigma w(F_o^4)]^{1/2}$

3.8 References

1. Washington, J.; McDonald, R; Takats, J; Menashe, N.; Reshef, D.; Shvo, Y. *Organometallics* **1995**, *14*, 3996.
2. Cooke, J. Ph. D. Thesis, University of Alberta, 1998, pp 69-73.
3. Boston, J. L.; Sharp, D. W. A.; Wilkinson, G. *J. Chem. Soc.* **1962**, 3488.
4. Burt, R. B.; Cooke, M.; Green, M. *J. Chem. Soc. (A)* **1970**, 2981.
5. (a) Lukehart, C. M. *Fundamental Transition Metal Organometallic Chemistry*; Brooks/Cole: Monterey, CA, 1985; pp 162-163. (b) Collman, J. P.; Hegedus, L. S.; Norton, J. R.; Finke, R. G. *Principles and Applications of Organotransition Metal Chemistry;* University Science Books: Mill Valley, CA, 1987, pp 509-512 and 864–879. (c) Grotjahn, D. B. In *Comprehensive Organometallic Chemistry II*; Abel, E. W.; Stone, F. G. A.; Wilkinson, G.; Hegedus, L. S., Eds.; Pergamon Press: Oxford, 1995; Vol. 12; p 742. (d) Schore, N. E. *Chem. Rev.* **1988**, *88*, 1081. (e) Al-Jahdali, M.; Baker, P. K.; Lavery, A. J.; Meehan, M. M.; Muldoon, D. J. *J. Mol. Cat. (A) Chem.* **2000**, *159*, 51.
6. Lukehart, C. M. *Fundamental Transition Metal Organometallic Chemistry*; Brooks/Cole: Monterey, CA, 1985; pp 78-80.
7. (a) Asunta, T.; Rissanen, K.; Krivykh, V. V.; Rybinskaya, M. I. *J. Organomet. Chem.* **1989**, *372*, 411. (b) Tooze, R. P.; Wilkinson, G.; Motevalli, M.; Hursthouse, M. B. *J. Chem. Soc., Dalton Trans.* **1986**, 2711. (c) Goddard, R.; Krüger, C.; Mark, F. Stansfield, R.; Zhang, X. *Organometallics* **1985**, *4*, 285. (d) Brunner, H.; Weber, H.; Bernal, I.; Reisner, G. M. *Organometallics* **1984**, *3*, 163. (e) Faller, J. W.; Chodosh, D. F.; Katahira, D. *J. Organomet. Chem.* **1980**, *187*, 227. (f) Brisdon, B. J.; Edwards, D. A.; White, J. W.; Drew, M. G. B. *J. Chem. Soc. Dalton Trans.* **1980**, 2129. (g) Henc, B.; Jolly, P. W.; Salz, R.; Stobbe, S.; Wilke,

G.; Benn, R.; Mynott, R.; Seevogel, K.; Goddard, R.; Krüger, C. *J. Organomet. Chem.* **1980**, *191*, 449. (h) Deeming, A. J.; Rothwell, I. P.; Hursthouse, M. B.; Abdul Malik, K. M. *J. Chem. Soc. Dalton Trans.* **1979**, 1899. (i) Schoonover, M. W.; Kubiak, C. P. Eisenberg, R. *Inorg. Chem.* **1978**, *17*, 3050. (j) Putnik, C. F.; Welter, J. J.; Stucky, G. D.; D'Aniello, Jr., M. J.; Sosinsky, B. A.; Kirner, J. F.; Muetterties, E. L. *J. Am. Chem. Soc.* **1978**, *100*, 4107.

8. (a) Deeming, A. J. In *Comprehensive Organometallic Chemistry*; Wilkinson, G.; Stone, F. G. A.; Abel, E. W., Eds.; Pergamon: Oxford, 1982; Vol. 4; p 407-413 and 420-425. (b) Kerber, R. C. In *Comprehensive Organometallic Chemistry II*; Abel, E. W.; Stone, F. G. A.; Wilkinson, G.; Shriver, D. F.; Bruce, M. I., Eds.; Pergamon Press: Oxford, 1995; Vol. 7; p 130-133.
9. Wang, A. H. -J.; Paul, I.; Aufmann, R. *J. Organomet. Chem.* **1974**, *69*, 301.
10. Grevels, F. –W.; Feldhoff, U.; Leitich, J.; Krüger, C. *J. Organomet. Chem.* **1976**, *118*, 79.
11. (a) Becker, Y.; Eisenstadt, A.; Shivo, Y. *Tetrahedron* **1978**, *34*, 799. (b) Kerber, R. C.; Koerner von Gustoff, E. A. *J. Organomet. Chem.* **1976**, *110*, 345. (c) Churchill, M. R.; Chen, K. -N. *Inorg. Chem.* **1976**, *15*, 788. (d) Green, M.; Lewis, B.; Daly, J. J.; Sanz, F. *J. Chem. Soc., Dalton Trans.* **1975**, 1118. (e) Bond, A.; Lewis, B.; Green, M. *J. Chem. Soc., Dalton Trans.* **1975**, 1109.
12. (a) Feasey, N. D.; Knox, S. A. R.; Orpen, A. G.; Winter, M. J. *New J. Chem.* **1988**, *12*, 581. (b) Adams, R. D.; Wang, S. *Organometallics* **1987**, *6*, 45. (c) Wang, J. –L.; Ueng, C. –H.; Cheng, S. –J.; Yeh, M. –C. *Organometallics* **1994**, *13*, 4453. (d) Shibata, T.; Koga, Y.; Narasaka, K. *Bull. Chem. Soc. Jpn.* **1995**, *68*, 911.
13. Bottrill, M.; Davies, R.; Goddard, R.; Green, M.; Hughes, R. P.; Lewis, B.; Woodward, P. *J. Chem. Soc. Dalton Trans.* **1977**, 1252.

14. (a) Patel, P. P.; Welker, M. E.; Liable-Sands, L. M.; Rheingold, A. L. *Organometallics* **1997**, *16*, 4519. (b) Akita, M.; Katuta, S.; Sugimoto, S.;Terada, M.; Moro-oka, Y. *J. Chem. Soc., Chem. Comm.* **1992**, 451. (c) Akita, M.; Terada, M.; Oyama, S.; Sugimoto, S.; Moro-oka, Y. *Organometallics* **1991**, *10*, 1561. (d) Reger, D. L.; McElligott, P. J.; Charles, N. G.; Griffith, E. A. H.; Amma, E. L. *Organometallics* **1982**, *1*, 443. (e) Boland-Lussier, B. E.; Churchill, M. R.; Hughes, R. P.; Rheingold, A. L. *Organometallics* **1982**, *1*, 628.
15. Pauling, L. *The Nature of the Chemical Bond*; Cornell: Ithaca, 1960; 3rd ed., pp 230-231.
16. (a) Lukehart, C. M. *Fundamental Transition Metal Organometallic Chemistry*; Brooks/Cole: Monterey, CA, 1985; pp 167-169. (b) Clarke, H. L. *J. Organomet. Chem.* **1974**, *80*, 155.
17. Pauling, L. *The Nature of the Chemical Bond*; Cornell: Ithaca, 1960; 3rd ed., pp 290-299.
18. Janse Van Vuuren, P.; Fletterick, R. J.; Meinwald, J.;Hughes, R. E. *J. Am. Chem. Soc.* **1971**, *93*, 4394.
19. (a) Collman, J. P.; Hegedus, L. S.; Norton, J. R.; Finke, R. G. *Principles and Applications of Organotransition Metal Chemistry;* University Science Books: Mill Valley, CA, 1987, pp 175-182. (b) Green, M. L. H.; Nagy, P. L. I. *Adv. Organomet. Chem.* **1964**, 2, 325. (c) Faller, J. W.; Adams, M. A. *J. Organomet. Chem.* **1979**, *170*, 71
20. Yang, G. –M.; Su, G. –M.; Liu, R. –S. *Organometallics* **1992**, *11*, 3444.
21. Tarazano, D. L.; Bodnar, T. W.; Cutler, A. R. *J. Organomet. Chem.* **1993**, *448*, 139.

22. Nesmeyanov, A. N.; Fedorov, L. A.; Avakyan, N. P.; Petrovskii, P. V.; Fedin, E. I; Arshavskaya, E. V.; Kritskaya, I. I. *J. Organomet. Chem.* **1975**, *101*, 121.

23. (a) Bushweller, C. H.; Hoogasian, S.; English, A. D.; Miller, J. S.; Lourandos, M. Z. *Inorg. Chem.* **1981**, *20*, 3448. (b) Bushweller, C. H.; Rithner, C. D.; Butcher, D. J. *Inorg. Chem.* **1986**, *25*, 1610. (c) DiMeglio, C. M. ; Luck, L. A.; Ritner, C. D.; Rheingold, A. L.; Elcesser, W. L.; Hubbard, J. L.; Bushweller, C. H. *J. Phys. Chem.* **1990**, *94*, 6255. (d) DiMeglio, C. M.; Ahmed, K. J.; Luck, L. A.; Rheingold, A. L.; Bushweller, C. H. *J. Phys. Chem.* **1992**, *96*, 8765.

24. (a) Poulton, J. T.; Folting, K.; Streib, W. E.; Caulton, K. G. *Inorg. Chem.* **1992**, *31*, 3190. (b) Poulton, J. T.; Sigalas, M. P.; Eisenstein, O.; Caulton, K. G. *Inorg. Chem.* **1993**, *32*, 5490. (c) Notheis, J. U.; Heyn, R. H.; Caulton, K. G. *Inorg. Chim. Acta* **1995**, *229*, 187.

25. (a) Albert, J.; Bosque, R.; Cadena, M.; Delgado, S.; Granell, J. *J. Organomet. Chem.* **2001**, *634*, 83. (b) Deeming, A. J.; Speel, D. M.; Stchedroff, M. *Organometallics* **1997**, *16*, 6009. (c) Pastor, A.; Galindo, A. *J. Chem. Soc., Dalton Trans.* **1997**, 3749. (d) McFarlane, W.; Regius,C. T. *Polyhedron* **1997**, *16*, 1855. (e) Ohkita, K.; Asano, H.; Kurosawa, H.; Hirao, T.; Miyaji, Y.; Ikeda, I. *Can. J. Chem.* **1996**, *74*, 1936. (f) Notheis, J. U.; Heyn, R. H.; Caulton, K. G. *Inorg. Chim. Acta* **1995**, *229*, 187. (g) Polowin, J.; Baird, M. C. *J. Organomet. Chem.* **1994**, *478*, 45. (h) Fanizzi, F. P.; Lanfranchi, M.; Natile, G.; Tiripicchio, A. *Inorg. Chem.* **1994**, *33*, 3331. (i) Davies, S. G.; Derome, A. E.; McNally, J. P. *J. Am. Chem. Soc.* **1991**, *113*, 2854.

26. Mason, R.; Russell, D. R. *J. Chem. Soc., Chem. Comm.* **1966**, 26.

27. Lippard, S. J.; Morehouse, S. M. *J. Am. Chem. Soc.* **1969**, *91*, 2504.

28. Murrall, N. W.; Welch, A. J. *J. Organomet. Chem.* **1986**, *301*, 109.

29. Pauling, L. *The Nature of the Chemical Bond*; Cornell: Ithaca, NY, 1960; 3rd ed., p 261.

30. Carroll, F. A. *Perspectives on Structure and Mechanism in Organic Chemistry*; Brooks/Cole: Pacific Grove, CA, 1998; p 7.

31. Wang, N. -F.; Wink, D. J.; Dewan, J. C. *Organometallics* **1990**, *9*, 335.

32. Paz-Sandoval; M. A.; Powell, P.; Drew, M. G. B.; Perutz, R. N. *Organometallics* **1984**, *3*, 1026.

33. (a) Holle, S.; Jolly, P. W. *J. Organomet. Chem.* **2000**, *605*, 157. (b) Wink, D. J.; Wang, N. –F.; Springer, J. P. *Organometallics* **1989**, *8*, 259. (c) Eberhardt, U.; Mattern, G. *Chem. Ber.* **1988**, *121*, 1531. (d) Allen, S. R.; Baker, P. K.; Barnes, S. G.; Bottrill, M.; Green, M.; Orpen, A. G.; Williams, I. D.; Welch, A. J. *J. Chem. Soc., Dalton Trans.* **1983**, 927.

34. Temple, J. S.; Riediker, M.; Schwartz, J. *J. Am. Chem. Soc.* **1982**, *104*, 1310.

35. Grant, D. P.; Murrall, N. W.; Welch, A. J. *J. Organomet. Chem.* **1987**, *333*, 403.

36. Murrall, N. W.; Welch, A. J. *Acta Crystallogr., Sect. A Suppl.* **1984**, *40*, C296.

37. (a) Villanueva, L. A.; Ward, Y. D.; Lachicotte, R.; Liebeskind, L. S. *Organometallics* **1996**, *15*, 4190. (b) Trepanier, S. J.; Sterenberg, B. T.; McDonald, R.; Cowie, M *J. Am. Chem. Soc.* **1999**, *121*, 2613.

38. Levy, G. C.; Nelson, G. L. *Carbon-13 Nuclear Magnetic Resonance for Organic Chemists*; Wiley-Interscience: New York, 1972; pp 67-69.

39. Ebsworth, E. A. V.; Rankin, D. W. H.; Cradock, S. *Structural Methods in Inorganic Chemistry*; Blackwell Scientific: Oxford, 1987; pp 54-55.

40. Verkade, J. G. *Coord. Chem. Rev.* **1972**, *9*, 1.

41. (a) Bodner, G. M. *Inorg. Chem.* **1975**, *14*, 2694. (b) Bodner, G. M.; May, M. P.; McKinney, L. E. *Inorg. Chem.* **1980**, *19*, 1951. (c) Öser, Z.; Özkar, S. *Turk. J. Chem.* **1999**, *23*, 9.

42. (a) Powell, J.; Shaw, B. L. *J. Chem. Soc. A* **1967**, 1839. (b) Akermark, B.; Krakenberger, B.; Hansson, S.; Vitagliano, A. *Organometallics* **1987**, *6*, 620. (c) Baltzer, N.; Macko, L.; Schaffner, S.; Zehnder, M. *Helv. Chim. Acta* **1996**, *79*, 803. (d) Mandal, S. K.; Gowda, G. A. N.; Krishnamurthy, S. S.; Zheng, C.; Li, S.; Hosmane, N. S. *Eur. J. Inorg. Chem.* **2002**, 2047.

43. (a) Lambert, J. B.; Shurvell, H. F.; Lightner, D. A.; Cooks, R. G. *Introduction to Organic Spectroscopy*; Macmillan: New York, 1987; pp 52-62. (b) Silverstein, R. M. Spectrometeric identification of Organic Compounds; John Wiley & Sons: New York, 1998, 6th ed., pp 226-227.

44. (a) Braunstein, P.; Naud, F.; Dedieu, A.; Rohmer, M. –M.; DeCian, A.; Rettig, S. T. *Organometallics* **2001**, *20*, 2966. (b) Jenkins, H. A.; Yap, G. P. A.; Puddephatt, R. J. *Organometallics* **1997**, *16*, 1946. (c) Rülke, R.E.; Kaasjager, V. E.; Wehman, P.; Elsevier, C. J.; van Leeuwen, P. W. N M.; Vriese, K. *Organometallics* **1996**, *15*, 3022. (d) Bailey, N. A.; Kita, W. G.; McCleverty, J. A.; Murray, A. J.; Mann, B. E.; Walker, N. W. J. *J. Chem. Soc. Chem. Comm.* **1974**, 592.

45. Pauling, L. *The Nature of the Chemical Bond*; Cornell: Ithica, NY, 1960; pp 244-248.

46. Dahl, L. F.; Rodulfo de Gil, E.; Feltham, R. D. *J Am. Chem. Soc.* **1969**, *91*, 1653.

47. The search of the Cambridge Structural Database (CSD) was performed by Dr. R. McDonald of the X-ray Crystallography Laboratory, Department of Chemistry, University of Alberta. The CSD was searched through the use of the QUEST

program, provided by the Cambridge Crystallographic Data Centre: http://www.ccdc.cam.ac.uk.

48. Some representative examples of reports with a bridging carbonyl ligand include: (a) Antonova, A. B.; Johansson, A. A.; Deykhina, N. A.; Podrebnyakov, D. A.; Pavlenko, N. I.; Rubaylo, A. I.; Dolgushin, F. M.; Petrovskii, P. V.; Ginzburg, A. G. *J. Organomet. Chem.* **1999**, *577*, 238. (b) Todd, L. J.; Hickey, J. P.; Wilkinson, J. R.; Huffman, J. C.; Folting, K. *J. Organomet. Chem.* **1976**, *112*, 167. (c) Epstein, E. F.; Dahl, L. F. *J. Am. Chem. Soc.* **1970**, *92*, 493. (d) Degrève, P. Y.; Meunier-Piret, J.; van Meerssche, M.; Piret, P. *Acta Crystallogr.* **1967**, *23*, 119.

49. Nametkin, N. S.; Tyurin, V. D.; Trusov, V. V.; Nekhaev, A. I.; Batsanov, A. S.; Struchkov, Yu. T. *J. Organomet. Chem.* **1986**, *302*, 243.

50. Erker, G.; Noe, R.; Krüger, C; Werner, S. *Organometallics* **1992**, *11*, 4174.

51. (a) Mueterties, E.L. *Acc. Chem. Res.* **1970**, *3*, 266. (b) Serpone, N.; Bickley, D. G. P*rog. Inorg Chem.* **1972**, *17*, 391. (c) Bailar, J. C. *J. Nucl. Inorg. Chem.* **1958**, *8*, 165. (d) Ray, P.; Dutt, N. K. *J. Indian Chem. Soc.* **1943**, *20*, 81. (e) Burdett, J. K. *Inorg. Chem.* **1976**, *15*, 212. (f) Howell, J. M.; Rossi, A. R.; Hoffmann, R. *J. Am. Chem. Soc.* **1976**, *98*, 2484. (g) Meakin, P.; Muetterties, E. L.; Tebbe, F. N.; Jesson, J. P. *J. Am. Chem. Soc.* **1971**, *93*, 4701, and references therein.

52. Beurskens, P. T.; Beurskens, G; Bosman, W. P.; de Gelder, R.; Garcia Granda, S.; Gould, R. O.; Israel, R; Smits, J.M. *DIRDIF-96*. Program for crystal structure determination. Crystallography Laboratory, University of Nijmegen, The Netherlands, 1996.

53. Sheldrick, G. M. *Acta Crystallogr.* **1990**, *A46*, 467.

54. Sheldrick, G. M. *SHELXL-93*. Program for crystal structure determination. University of Göttingen, Germany, 1993.

Chapter 4

Reaction of $M(CO)_4(\eta^2\text{-}C_2H_2)$ (M = Fe, Os) with $(\eta^5\text{-}C_5H_5)(CO)_2W{\equiv}CC_6H_5$: Unexpected Substitution of Acetylene and Formation of $MW(\mu\text{-}CC_6H_5)(CO)_6(\eta^5\text{-}C_5H_5)$

4.1 Introduction

Chapters 1 and 3 introduced the reactivity of the $M(CO)_4(\eta^2$alkyne) (M = Fe, Ru, Os) complexes towards alkynes. Studies in the Takats laboratories have shown that these complexes are able to promote alkyne-alkyne coupling reactions [1]. In addition, these studies have shown that the $M(CO)_4(\eta^2$-alkyne) complexes are valuable building blocks for the directed synthesis of alkyne-bridged heterobimetallic complexes containing group 8 (Fe, Ru, Os) and group 9 (Co, Rh, Ir) transition metals [2]. It was logical to postulate that, on the basis of the above precedents, reaction of $M(CO)_4(\eta^2$-alkyne) compounds with a transition metal-carbyne complex (*i.e.*, an M≡CR triple bond) might result in the formation of heterobimetallic compounds bridged by hydrocarbon ligands, arising from alkyne-CR coupling with or without CO incorporation. Indeed, Stone and coworkers have exploited the isolobal analogy [3] between an alkyne (RC≡CR') and a transition metal carbyne complex ($L_nM{\equiv}CR$) to successfully prepare a variety of heterometallic transition metal cluster complexes [4]. The compounds $W({\equiv}CC_6H_4R\text{-}4)(CO)_2(\eta^5\text{-}C_5R_5)$ (R = H, Me) are the paradigm for these reactions because the $(\eta^5\text{-}C_5R_5)W(CO)_2$ fragment is isolobal to CR, and these carbyne complexes have consistently shown chemical reactivity that parallels that of organic alkynes [5].

This chapter describes the results of the reactions between $M(CO)_4(\eta^2\text{-}C_2H_2)$ (M = Fe, Os) and $W(\equiv CC_6H_5)(CO)_2(\eta^5\text{-}C_5H_5)$.

4.2 Experimental Observations

A pale yellow-colorless pentane solution of $Fe(CO)_4(\eta^2\text{-}C_2H_2)$ was mixed with a deep red pentane solution of $W(\equiv CC_6H_5)(CO)_2(\eta^5\text{-}C_5H_5)$ in an equimolar ratio at low temperature (–40 °C). Within a few minutes, and with warming (–20 °C), the IR spectrum (carbonyl region) showed the appearance of new ν_{CO} bands and a reduction in the intensity of the ν_{CO} bands of the starting materials. The end of the reaction was signaled by the complete consumption of the starting materials. Simple work-up afforded a deep brown, crystalline material (compound **7**).

4.3 Spectroscopic Characterization

Spectroscopic characterization of the compound revealed a surprising result. The IR spectrum in hexane showed six bands in the terminal carbonyl stretching region (Table 4-1). However, the ^1H NMR spectrum exhibited resonances due only to the C_6H_5 and C_5H_5 groups, no acetylenic protons were detected. Thus the reaction apparently proceeded by elimination of the acetylene ligand from $Fe(CO)_4(\eta^2\text{-}C_2H_2)$. These spectroscopic results suggested that the product was $FeW(\mu\text{-}CC_6H_5)(CO)_6(\eta^5\text{-}C_5H_5)$ (Eq. 4-1), a compound similar to one that has been previously obtained by Stone *et al.* by reacting $W(\equiv CC_6H_4Me\text{-}4)(CO)_2(\eta^5\text{-}C_5H_5)$ with $Fe_2(CO)_9$, albeit in much lower yield (10% *vs.* 62% for **7**) [6]. Further corroboration of the nature of **7** came from its $^{13}C\{^1H\}$ NMR spectrum which showed a signal at δ 332.4 ppm, close to δ 331.3 ppm reported by Stone *et al.* and assigned to the bridging carbyne carbon atom [6].

Table 4-1 The FT-IR Data in the Carbonyl Region, ^1H, and $^{13}C\{^1H\}$ NMR Data of $MW(\mu\text{-}CC_6H_5)(CO)_6(\eta^5\text{-}C_5H_5)$ (M = Fe, 7; M = Os, 8)

Compound	ν_{CO}[a]	^1H	$^{13}C\{^1H\}$
7[b]	2073 (m), 2020 (m), 1995 (s), 1988 (s), 1948 (m), 1889 (m)	7.34 m (5H) C_6H_5 5.45 s (5H) C_5H_5	332.4 s μ-*C* 221.7 s $^1J_{CW}$ = 174 Hz W-*CO* 210.3 s Fe-*CO* 162.2 s C_6H_5 128.3 s C_6H_5 127.6 s C_6H_5 125.7 s C_6H_5 93.2 s C_5H_5
8[c]	2098 (m), 2028 (s), 2010 (s), 1995 (s), 1939 (s), 1873 (m)	7.50 m (2H) C_6H_5 7.34 m (3H) C_6H_5 5.48 s (5H) C_5H_5	332.0 s μ-*C* 221.2 s $^1J_{CW}$ = 178 Hz W-*CO* 184.4 s Os-*CO* 177.1 s Os-*CO* 174.9 s Os-*CO* (×2) 164.1 s C_6H_5 129.3 s C_6H_5 128.5 s C_6H_5 127.3 s C_6H_5 92.7 s C_5H_5

[a] cm^{-1}, hexane.
[b] ^1H and $^{13}C\{^1H\}$ NMR; ppm, CD_2Cl_2, −20 °C
[c] ^1H and $^{13}C\{^1H\}$ NMR; ppm, CD_2Cl_2, 27 °C

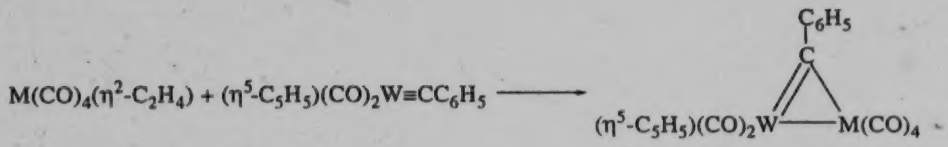
(4-1)

7 M = Fe
8 M = Os

In an attempt to suppress the loss of acetylene, $W(\equiv CC_6H_5)(CO)_2(\eta^5\text{-}C_5H_5)$ was treated with $Os(CO)_4(\eta^2\text{-}C_2H_2)$, a compound with a stronger $Os\text{-}C_2H_2$ bond [7]. The reaction also occurred readily but again proceeded by acetylene elimination to yield $OsW(\mu\text{-}CC_6H_5)(CO)_6(\eta^5\text{-}C_5H_5)$ (**8**) (Eq. 4-1).

The spectroscopic features of **8** (IR, ^1H and $^{13}C\{^1H\}$ NMR; Table 4-1) are similar to those of **7**. The presence of a two electron $\mu\text{-}CC_6H_5$ ligand is indicated by the ^{13}C NMR signal at δ 332.0 ppm, which is close to the related resonance in **7** (δ 332.4 ppm). It is interesting to note that the four high frequency ν_{CO} bands of **8** (2098, 2028, 2010 and 1995 cm^{-1}) are some 10-20 cm^{-1} higher than the corresponding bands in **7** (2073, 2020, 1995 and 1988 cm^{-1}), and hence are assigned to CO stretching vibrations localized on the $M(CO)_4$ fragment. On the other hand, the two lower frequency ν_{CO} bands of **8** (1939 and 1873 cm^{-1}) are 10-15 cm^{-1} lower than those of **7** (1948 and 1889 cm^{-1}) and this is in accord with enhanced back-bonding into the $W(CO)_2$ carbonyls in **8** due to the presence of the more electron donating osmium center [8].

In another study, Stone *et al.* reported that complexes of the type $[FeW(\mu\text{-}CC_6H_4Me\text{-}4)(CO)_6L]$ (L = $\eta^5\text{-}C_5H_5$, **A**; $HB(pz)_3$, **B**, pz = pyrazolyl-1-yl) exist in equilibrium with $[FeW(\mu\text{-}CC_6H_4Me\text{-}4)(CO)_5L]$ (L = $\eta^5\text{-}C_5H_5$, **C**; $HB(pz)_3$, **D**) [9]. In the latter compounds, the electronic unsaturation created by loss of a CO ligand is compensated by the bridging carbyne unit taking on a four electron donor role. The change from two to four electron donor $W\equiv CR$ moiety is accompanied by a marked downfield shift in the μ-CR ^{13}C NMR signal [9], in accord with the empirical correlation established by Templeton between ^{13}C NMR shifts and electron donation by alkyne ligands [10]. When solvent was removed from solutions of **7** under vacuum and the compound redissolved, the IR and NMR spectra displayed additional signals. A particularly noticeable feature in the $^{13}C\{^1H\}$ NMR spectrum was the appearance of a highly deshielded resonance at δ 392.3 ppm. The position of this resonance is virtually identical to that observed for **C**, δ 392.5 pm, and in light of these findings, it is reasonable to conclude that $FeW(\mu\text{-}CC_6H_5)(CO)_5(\eta^5\text{-}C_5H_5)$ (**9**) is the source of the extra signals in the IR and NMR spectra of **7**. The relationship between these compounds and their formulation is shown in Scheme 4-1. Compound **8** is more robust than **7** and this is reflected in the need to heat its solution to 40°C before any indication of the pentacarbonyl, $OsW(\mu\text{-}CC_6H_5)(CO)_5(\eta^5\text{-}C_5H_5)$ (**10**) (Scheme 4-1), is detected by IR spectroscopy.

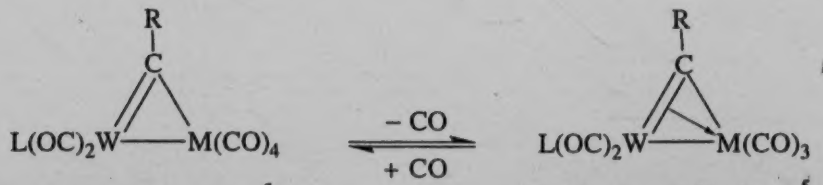

7 $M = Fe, R = C_6H_5, L = \eta^5\text{-}C_5H_5$
8 $M = Os, R = C_6H_5, L = \eta^5\text{-}C_5H_5$
A $M = Fe, R = C_6H_4Me\text{-}4, L = \eta^5\text{-}C_5H_5$
B $M = Fe, R = C_6H_4Me\text{-}4, L = HB(pz)_3$

9 $M = Fe, R = C_6H_5, L = \eta^5\text{-}C_5H_5$
10 $M = Os, R = C_6H_5, L = \eta^5\text{-}C_5H_5$
C $M = Fe, R = C_6H_5Me\text{-}4, L = \eta^5\text{-}C_5H_5$
D $M = Fe, R = C_6H_4Me\text{-}4, L = HB(pz)_3$

Scheme 4-1 Equilibrium between $MW(\mu\text{-}CR)(CO)_6L$ and $MW(\mu\text{-}CR)(CO)_5L$.

In their studies Stone *et al.* discovered that complex **A** was susceptible to further reaction with $Fe(CO)_5$ or $W(\equiv CC_6H_4Me\text{-}4)(CO)_2(\eta^5\text{-}C_5H_5)$ to give trinuclear complexes [6]. In the present case, it seems that $Fe(CO)_4(\eta^2\text{-}C_2H_2)$ provides a clean source of $Fe(CO)_4$, and further reaction with $Fe(CO)_5$ is not possible, which accounts for our higher yield (62 % *vs.* 10%). The product **7** is able to further react with $W(\equiv CC_6H_5)(CO)_2(\eta^5\text{-}C_5H_5)$ to give trinuclear species as demonstrated by Stone [6]. This side reaction was not observed in our reaction.

Previously, Stone *et al.* [9] determined the solid state structure of the $Fe(CO)_3$ containing compound, $FeW(\mu\text{-}CC_6H_4Me\text{-}4)(CO)_5(HB(pz)_3)$ (**D**) (Scheme 4-1), but not that of the $Fe(CO)_4$ species **A** or **B**. To confirm the structural predictions presented above and to provide metrical parameters for comparison with **D**, compounds **7** and **8** were subjected to single crystal X-ray structure analysis.

4.4 Molecular Structures of $MW(\mu\text{-}CC_6H_5)(CO)_6(\eta^5\text{-}C_5H_5)$ (7, 8)

The X-ray analysis showed that crystals of compound **7** contain two crystallographically independent molecules per asymmetric unit but whose metrical parameters are very similar. Structure "A" from the crystallographic analysis report provides a good representative example and the discussion will be based on this structure. The structures of **7** and **8** are shown in Figure 4-1, together with the atom numbering scheme. Selected interatomic separations and angles are listed in Table 4-2.

As argued above, and shown in Scheme 4-1, compounds **7** and **8** consist of a $M(CO)_4$ and $(\eta^5\text{-}C_5H_5)W(CO)_2$ fragments linked by a bridging carbyne ligand ($\mu\text{-}CC_6H_5$). The group 8 metals (Fe and Os) achieve their 18-electron configuration by gaining eight electrons from four terminal carbonyls and one each from the W-Fe/Os metal-metal bond and $\mu\text{-}CC_6H_5$ ligand or, its equivalent, two electrons from the $W\equiv CC_6H_5$ triple bond. The coordination geometry of Fe/Os can be described either as distorted trigonal bipyramid, with the $W\equiv CC_6H_5$ moiety occupying the normal, in-plane equatorial disposition of the alkyne ligand observed in $M(CO)_4(\eta^2\text{-alkyne})$ (M = Fe, Ru, Os) compounds [11], or distorted octahedral when considering the Fe-W-C7 core at the dimetallacyclopropene extreme. Indeed the angle between the equatorial carbonyls, C3–M–C4, (103.3(6)° in **7** and 100.5(4)° in **8**) is in between the ideal trigonal bipyramidal (120°) and octahedral (90°) values.

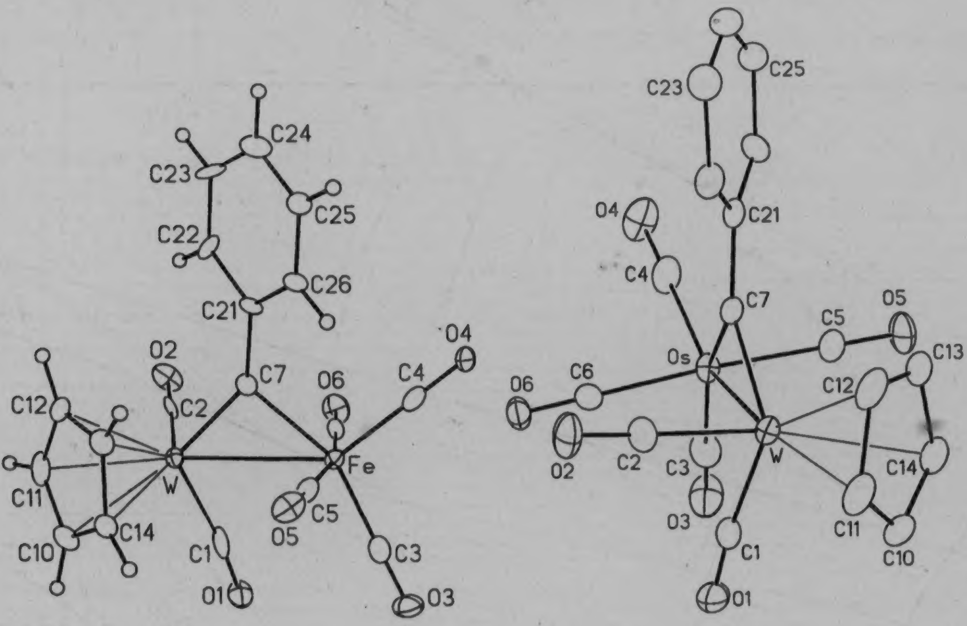
C24
C23
C25
C22
C26
C21
O4
O2
C7
O6
C4
C12
C2
Fe
C11
W
C5
C10
C14
C1
O5
C3
O1
O3
C25
C23
O4
C21
C4
C7
C5
O5
Os
C13
O6
C6
C12
W
O2
C2
C3
C14
O3
C11
C1
C10
O1

7 **8**

Figure 4-1 Solid State Molecular Structures of **7** (*left*) and **8** (*right*).

In addition, the axial carbonyls, C5O5 and C6O6, are bent towards the equatorial W–μ-C7 moiety (C5–M–C6 is 166.5(6)° in **7** and 167.5(3)° in **8**). Similar distortions have been observed in the above mentioned $M(CO)_4(\eta^2$-alkyne) compounds. In these compounds it is sometimes observed that the axial M-CO bonds are longer than the equatorial ones [11]. This is not the case in **7**. However, in **8**, the Os–C4 distance (1.892(11) Å), the bond "*trans*" to the Os–W bond, is 0.078 Å (7 esd's) shorter than the axial CO separations (Os–C5/C6 are both 1.970(8)Å). The other equatorial carbonyl (Os–C3, 1.935(9) Å) is shortened, but only marginally, and this can be ascribed to the *trans* influence of the bridging carbyne fragment [9], since C7 is opposite to it.

Table 4-2 Selected Interatomic Separations and Angles for **7** and **8**.

structural parameter	**7** (M = Fe)	**8** (M = Os)
M–W	2.833(2)	2.9141(4)
M–C3	1.80(2)	1.935(9)
M–C4	1.79(2)	1.89(1)
M–C5	1.809(14)	1.970(8)
M–C6	1.83(2)	1.970(8)
M–C7	2.015(12)	2.120(7)
W–C1	1.96(2)	1.997(9)
W–C2	1.968(14)	1.969(8)
W–C7	1.913(12)	1.955(8)
C7–C21	1.47(2)	1.460(11)
W–C1–O1	172.9(12)	170.6(9)
W–C2–O2	176.7(13)	177.0(8)
M–C3–O3	177.3(14)	178.0(9)
M–C4–O4	179.1(15)	177.2(8)
M–C5–O5	176.2(13)	177.9(7)
M–C6–O6	176.8(13)	177.8(7)
C1–W–C2	90.2(5)	90.8(4)
C1–W–C7	113.9(5)	114.9(4)
C2–W–C7	90.3(5)	88.3(3)
C3–M–C4	103.3(6)	100.5(4)
C5–M–C6	166.5(6)	167.5(3)
M–W–C1	70.1(4)	69.8(3)
M–W–C2	101.8(3)	100.4(3)
W–M–C7	42.4(3)	42.1(2)
M–W–C7	45.3(4)	46.7(2)
M–C7–W	92.3(5)	91.2(3)
W–C7–C21	141.2(9)	138.3(6)
M–C7–C21	125.9(9)	129.8(6)
W-M-C4	142.0(4)	143.1(3)
C3-M-C7	156.9(6)	158.3(4)

The tungsten center is also electronically saturated and its coordination geometry can be described as distorted octahedral with the η^5-C_5H_5 ligand occupying three facial sites and the opposite three by the two carbonyl groups and the mid-point of the M–C7 bond. The coordination geometry agrees well with several "piano stool" compounds of the form (η^5-C_5H_5)W(CO)$_2$L, where L represents a three-electron donor η^1- or η^2-bonded ligand [12]. The planar η^5-C_5H_5 ligand is bonded to tungsten by all five carbon atoms, although there are small variations in the W-C separations. Some differences can also be detected in the two tungsten carbonyl ligands. One, C2O2, is essentially linear (W–C2–O2 176.7(13)° in **7** and 177.0(8)° in **8**), while the other, C1O1, is somewhat more bent (W–C1–O1 172.9(12)° in **7** and 170.6(9)° in **8**). Similar differences were noted by Stone *et al.* in FeW(μ-CC$_6$H$_4$Me-4)(CO)$_5$(HB(pz)$_3$) (**D**) and ascribed to a semi-bridging bonding mode of the CO ligand to account for the observation of a low frequency ν_{CO} band in the IR spectrum at 1863 cm^{-1} [9]. It is tempting to postulate similar features in **7** and in particular **8**, and indeed the IR spectrum of **7** and **8** does show low frequency ν_{CO} bands at 1889 and 1873 cm^{-1}, respectively. The onset of semi-bridging CO bonding for C1O1 is further indicated by the small M–W–C1 angle (70.1(4)° in **7** and 69.8(3)° in **8**) compared to the M–W–C2 angle (101.8(3)° in **7** and 100.4(3)° in **8**).

Now we turn our attention to the most interesting part of the compounds, the three membered $\overline{\text{M}(\mu\text{-C})\text{W}}$ ring system. As anticipated, the Fe–W separation in **7** (2.833(2) Å) is much longer, 0.221 Å (110 esd's), than the corresponding parameter in the four electron μ-CR bridged compound FeW(μ-CC$_6$H$_4$Me-4)(CO)$_5$(HB(pz)$_3$) (**D**) (2.612(2) Å) [9] and longer, by 0.113 Å (57 esd's), than 2.720(1) Å found in FeW{μ-C(C$_6$H$_4$Me-4)C(Me)C(Me)}(CO)$_5$(η^5-C_5H_5) [13], a compound presumed to have an Fe–W single bond. The bridging unit in the latter compound provides a more delocalized bonding framework and probably contributes to the short Fe–W separation. There are no simple bimetallic Os-W compounds that bear similarities to **8**, but the Os–W distance of 2.9141(4) Å lies within the range (2.66-3.07 Å) observed for Os–W single bonds in saturated tri- and tetranuclear cluster compounds [14]. Interestingly, the Os–W separation in **8** is significantly shorter than the corresponding separation in the Os→W donor-acceptor bonds in $(Me_3P)(OC)_4OsW(CO)_5$ (3.0756(5) Å) or $(OC)_3(MeC(CH_2O)_3P)_2Os\text{-}Os(CO)_4W(CO)_5$ (3.039(1) Å) [15].

The Fe–μ-C7 distance of 2.015(12) Å is 0.189 Å (16 esd's) longer than the 1.826(6) Å found in **D**, the latter with significant multiple bond character [9], and is within error to the Fe–μ-C single bond separation of 1.986(3) Å found in $Fe_2(\mu\text{-CHMe})(\mu\text{-CO})(CO)_2(\eta^5\text{-}C_5H_5)$ [16]. Similarly the Os–μ-C7 distance (2.120(7) Å) is slightly longer, by 0.059 Å (7 esd's), than the Os–C(H) separation (2.061(9) Å) in $[Os_2(CO)_8(\mu\text{-}\eta^1,\eta^2\text{-CHCH}_2)][BF_4]$ [17], a compound with a σ, π-vinyl bridge, and confirms its single bond formulation. On the other hand, the W–μ-C7 distances of 1.913(12) Å in **7** and 1.955(8) Å in **8** are 0.112 Å (9 esd's) and 0.070 Å (9 esd's) shorter, respectively, than the 2.025(7) Å found in **D**, which contains a predominantly singly bonded W–μ-CR unit [9], but compares favorably with the corresponding distances in a series of similar carbyne bridged bimetallic $MW(\mu\text{-CC}_6H_4Me\text{-}4)$ (M = Co, Rh, Ti, Pt) [18] complexes (1.91-1.97 Å). These molecules have considerable W–μ-CR multiple bonding character and have been formulated as having a dimetallacyclopropene core. This is the situation in **7** and **8** also and the asymmetric ligand binding is manifest in the W–C7–C21 angles (141.2(9)° in **7** and 138.3(6)° in **8**) being some 10-15° larger than the Fe–C7–C21 angles (125.9(9)° in **7** and 129.8(6)° in **8**), as observed in the above mentioned complexes. Thus, the structural parameters of the $\overline{M(\mu\text{-C})W}$ rings nicely complement the corresponding parameters of the previously determined structure $FeW(\mu\text{-}CC_6H_4Me\text{-}4)(CO)_5\{HB(pz)_3\}$ (**D**) [9]. In **D** the Fe–W and Fe–μ-C separations indicate multiple bonding interaction. This is consistent with the alkylidyne tungsten fragment functioning as a four electron donor to the iron center (Scheme 4-1). Whereas the M–W and M–μ-C separations in **7** and **8** indicate single bonding interaction and suggests a model in which the $W{\equiv}CC_6H_5$ unit donates two electrons to the group 8 metal centers (Scheme 4-1) and functions as a non-classical two electron alkyne ligand.

4.5 Carbonyl Exchange Processes in 7 and 8

On the basis of the solid state structures the ^{13}C NMR spectrum in the carbonyl regions should exhibit six signals, four for the four different $M(CO)_4$ carbonyls and two for the $W(CO)_2$ fragment. However, the ^{13}C NMR spectrum of **7** at room temperature showed only one averaged Fe-*C*O signal at δ 210.3 ppm and one W-*C*O resonance at δ 221.7 ppm, indicating local carbonyl scrambling but no carbonyl exchange between the two metal centers. The spectrum of **8** also showed an averaged W(*C*O)$_2$ signal at δ 221.2 ppm and three distinct, but broad signals for the Os(*C*O)$_4$ moiety at δ 184.4, 177.0 and 174.9 ppm in a 1:1:2 ratio. Thus, as observed with classical $M(CO)_4(\eta^2\text{-alkyne/alkene})$ compounds [11b, 19], carbonyl scrambling at osmium is much slower than at iron. Upon lowering the temperature the Fe(*C*O)$_4$ signals decoalesce and emerge as three distinct, sharp peaks at – 90°C. It only requires – 20°C for the three osmium carbonyl peaks to sharpen up. Throughout this process the W(*C*O)$_2$ signal remains sharp. This indicates that even at the lowest temperature the static solid state structure is not achieved in solution. A rapid oscillation of the $(\eta^5\text{-}C_5H_5)W(CO)_2$ group about the M–W vector (Figure 4-1) would result in a time-averaged mirror plane of the molecule and render the two tungsten carbonyls and the two axial $M(CO)_4$ carbonyls (C5O5 and C6O6) equivalent, in accord with the low temperature ^{13}C NMR spectra of **7** and **8**.

It is interesting to note that although there is no intermetallic CO exchange between Fe and W in **7** on the NMR time-scale, when **7** was prepared from ^{13}CO enriched $Fe(CO)_4(\eta^2\text{-}C_2H_2)$ and unenriched $W(\equiv C\ C_6H_5)(CO)_2(\eta^5\text{-}C_5H_5)$, enrichment of the tungsten carbonyls also occurred, as demonstrated by $^{13}C\{^1H\}$ NMR spectroscopy. The most plausible explanation for this is slow carbonyl migration between Fe and W *via* a higher energy CO bridged intermediate [20].

4.6 Conclusions

The reaction between $W(\equiv CC_6H_5)(CO)_2(\eta^5\text{-}C_5H_5)$ and $M(CO)_4(\eta^2\text{-}C_2H_2)$ unexpectedly proceeded with elimination of the acetylene ligand and production of the carbyne bridged heterobimetallic complexes $MW(\mu\text{-}CC_6H_5)(CO)_6(\eta^5\text{-}C_5H_5)$ (M = Fe, **7**; Os, **8**), analogous to the compound obtained by Stone *et al.* [6] from the reaction of $W(\equiv CC_6H_4Me\text{-}4)(CO)_2(\eta^5\text{-}C_5H_5)$ and $Fe_2(CO)_9$. Loss of the alkyne ligand was generally not observed in the synthesis of the previously mentioned (Section 4.1) alkyne-bridged heterobimetalic complexes [2]. However, studies in our laboratories have shown another manifestation of weakened metal-alkyne bond in $M(CO)_4(\eta^2\text{-}alkyne)$ compounds, namely that of facile CO insertion and/or alkyne coupling reactions [1c, 7a]. Moreover, Cooke has reported the reaction of $Fe(CO)_4(MeC_2Me)$ with $(\eta^5\text{-}C_5Me_5)Co(CO)_2$ gives $(\eta^5\text{-}C_5Me_5)(CO)CoFe(\mu\text{-}CO)_2(CO)_3$ in good yield (68 %) [21]. Prior to this work, we have not observed loss of C_2H_2 from $M(CO)_4(\eta^2\text{-}C_2H_2)$ (M = Fe, Os) complexes.

The molecular structures of **7** and **8** show $M(CO)_4$ and $(\eta^5\text{-}C_5H_5)W(CO)_2$ fragments joined by a M–W single bond and a bridging carbyne unit (CC_6H_5). The coordination geometry around the group 8 metal can be described as a distorted trigonal bipyramid with the $(\eta^5\text{-}C_5H_5)(CO)_2W{\equiv}CC_6H_5$ pseudoalkyne moiety occupying an in-plane equatorial coordination site. Solution spectroscopy indicates an equilibrium between **7** and **9**, and **8** and **10**. The coordinatively unsaturated **9** or **10** is stabilized by additional electron donation from the W≡C group. In this role the W≡C group acts as a four electron donor to the group 8 metal.

4.7 Experimental

4.7.1 Solvents, Techniques, Physical Measurements and Reagents

Preparation of solvents, techniques and physical measurements were carried out as described in previous chapters. The compound $W({\equiv}CC_6H_5)(CO)_2(\eta^5\text{-}C_5H_5)$ [22] was prepared as described in the literature with the exception that NaC_5H_5 [23] was used in place of LiC_5H_5 and the pentane solution of the product was cold filtered (−20 °C) through a sintered glass filter instead of the chromatographic procedure described. $M(CO)_4(\eta^2\text{-}C_2H_2)$ (M = Fe [1b], Os [2b]) were prepared according to literature methods.

4.7.2 Synthetic Procedures

Synthesis of $FeW(\mu\text{-}CC_6H_5)(CO)_6(\eta^5\text{-}C_5H_5)$ (7) To a stirred 50 mL pentane solution of $Fe(CO)_4(\eta^2\text{-}C_2H_2)$ (102 mg, 0.526 mmol) was added a 20 mL pentane solution of $W({\equiv}CC_6H_5)(CO)_2(\eta^5\text{-}C_5H_5)$ (207 mg, 0.526 mmol) at –40 °C. The mixture was allowed to warm to –20 °C and stirred for one hour. The dark brown solution was then cannula filtered and the solvent removed, *in vacuo*, at –20 °C. Recrystalization from cold CH_2Cl_2/pentane gave a dark brown crystalline solid (183 mg, 62%).

F.W. 561.9

Elemental Analysis $C_{18}H_{10}FeO_6W$; Calculated: C, 38.47%; H, 1.79%,

Observed: C, 37.51%; H 1.76%.

IR (hexane, cm^{-1}) ν_{CO} 2073 (m), 2020 (m), 1995 (s), 1988 (s), 1948 (m), 1889 (m)

^1H-NMR (CD_2Cl_2, 400.1 MHz, – 20°C) δ 7.34 (m, C_6H_5), 5.45 (s, C_5H_5)

$^{13}C\{^1H\}$ NMR (CD_2Cl_2, 100.6 MHz, –20°C) δ 332.4 (μ-*C*), 221.7 (W-*C*O, $^1J_{CW}$ = 174 Hz), 210.3 (Fe-*C*O), 162.2, 128.3, 127.6, 125.7 (C_6H_5), 93.2 (C_5H_5); (CD_2Cl_2, 100.6 MHz, –90°C): 222.1 (W-*C*O), 214.7(1), 210.2(1), 207.0(2) (Fe-*C*O).

Synthesis of OsW(μ-CC_6H_5)$(CO)_6$(η^5-C_5H_5) (8) Dark brown crystals of OsW(μ-CC_6H_5)$(CO)_6$(η^5-C_5H_5) (276 mg, 40%) were obtained from $Os(CO)_4$(η^2-C_2H_2) (278 mg, 0.847 mmol) and W(≡CC_6H_5)$(CO)_2$(η^5-C_5H_5) (334 mg, 0.848 mmol) by a procedure similar to that described for **7** except that the solution was allowed to warm to 0°C and stirred at this temperature for one hour.

F.W. 696.3

Elemental Analysis $C_{18}H_{10}O_6OsW$; Calculated: C, 31.05%; H, 1.45%,

Observed: C, 31.07%; H 1.29%.

IR (hexane, cm^{-1}) ν_{CO} 2098 (m), 2028 (s), 2010 (s), 1995 (s), 1939 (s), 1873 (m)

^1H NMR (CD_2Cl_2, 27°C, ppm): δ 7.50 (m, 2H, C_6H_5), 7.34 (m, 3H, C_6H_5), 5.48 (s, 5H, C_5H_5)

$^{13}C\{^1H\}$ NMR (CD_2Cl_2, 27°C, ppm): δ 332.0 (μ-*C*), 221.2 (W-*C*O, J(WC) 178 Hz), 184.4(1), 177.0(1), 174.9(2) (Os-*C*O), 164.1, 129.3, 128.5, 127.3 (C_6H_5), 92.7 (C_5H_5).

4.7.3 X-ray Crystal Structure Determination of

MW(μ-CC$_6$H$_5$)(CO)$_6$(η^5-C$_5$H$_5$) (7, 8)

Dark crystals of **7** or **8** were obtained by cooling a CH_2Cl_2/pentane solution of the compound. Data collection and structure refinement were performed by Dr. R. McDonald of the X-ray Crystallography Laboratory, Department of Chemistry, University of Alberta. Data collection was carried out on a Siemens P4/RA (**7**) or Brüker P4/RA/SMART 1000 CCD (**8**) diffractometer. Programs for diffractometer operation, data collection data reduction and absorption correction were those supplied Siemens or Bruker. Unit cell parameters were obtained from a least squares refinement of 46 (**7**) or 5941 (**8**) centered reflections. The structure of **7** was solved using full-matrix methods (*SHELXS*-86) [24], while the structure of **8** was solved direct methods/fragment search (*DIRDIF*-96) [25]. Refinement of **7** and **8** were completed using full-matrix least-squares on F^2 (*SHELXL*-93) [26]. Two crystallographically-independent molecules with essentially identical geometries were found to exist in the asymmetric unit for **7**. Positions of the hydrogen atoms in **7** and **8** were determined from the geometries of their attached carbon atoms, while their thermal parameters were assigned a value that is 20% greater than those of the attached carbon atoms. Summary of data collection parameters are listed in Table 4-3 (**7**) and Table 4-4 (**8**). Final atomic coordinated and displacement parameters may be obtained from the X–ray Crystallography Laboratory, Department of Chemistry, University of Alberta with file identification code TAK 9842 (**7**) and TAK 9929 (**8**).

Table 4-3 Crystallographic Experimental Details for Compound **7**

formula	$C_{18}H_{10}FeO_6W$
formula weight	561.96
crystal dimensions (mm)	0.61 × 0.12 × 0.04
crystal system	monoclinic
space group	$P2_1/c$ (No.14)
unit cell parameters	
a (Å)	8.7058 (7)
b (Å)	15.0936 (13)
c (Å)	27.286 (2)
β (deg)	92.484 (7)
V (Å^3)	3582.1 (5)
Z	8
ρ_{calcd} (g cm^{-3})	2.084
μ (mm^{-1})	7.258
radiation (λ[Å])	graphite-monochromated Mo Kα (0.71073)
temperature (°C)	– 60
scan type	θ-2θ
data collection 2θ limit (deg)	50.0
total data collected	6764 ($-10 \leq h \leq 0$, $-17 \leq k \leq 0$, $-32 \leq l \leq 32$)
independent reflections	6317
number of observed reflections (*NO*)	3961 [$F_o^2 \geq 2\sigma(F_o^2)$]
absorption correction method	semiempirical (ψ scans)
range of transmission factors	0.9956 – 0.5138
data/restraints/parameters	6317 [$F_o^2 \geq -3\sigma(F_o^2)$] / 0 / 469
goodness of fit (S)[a]	1.005 [$F_o^2 \geq -3\sigma(F_o^2)$]
final R indices[b]	
R_1 [$F_o^2 \geq 2\sigma(F_o^2)$]	0.0556
wR_2 all data	0.1022
largest difference peak and hole	1.164 and – 0.956 e Å^{-3}

[a] $S = [\Sigma w(F_o^2 - F_c^2)^2/(n - p)]^{1/2}$ (n = number of data; p = number of parameters varied; $w = [\sigma^2(F_o^2)+(0.0241P)^2+ 5.8050P]^{-1}$ where $P = ([\mathrm{Max}(F_o^2, 0) + 2F_c^2]/3)$.

[b] $R_1 = \Sigma||F_o| - |F_c||/\Sigma|F_o|$; $wR_2 = [\Sigma w(F_o^2 - F_c^2)^2/\Sigma w(F_o^4)]^{1/2}$

Table 4-4 Crystallographic Experimental Details for Compound **8**

formula	$C_{18}H_{10}O_6OsW$
formula weight	696.31
crystal dimensions (mm)	0.36 × 0.10 × 0.04
crystal system	monoclinic
space group	$P2_1/c$ (No.14)
unit cell parameters	
a (Å)	15.3717 (9)
b (Å)	9.0149 (6)
c (Å)	14.6851 (10)
β (deg)	114.9520 (10)
V (Å^3)	1845.0 (2)
Z	4
ρ_{calcd} (g cm^{-3})	2.507
μ (mm^{-1})	13.14
radiation (λ[Å])	graphite-monochromated Mo Kα (0.71073)
temperature (°C)	– 80
scan type	ϕ rotations (0.3°)/ω scans (0.3°) (30 s exposures)
data collection 2θ limit (deg)	52.78
total data collected	8885 ($-19 \leq h \leq 7$, $-11 \leq k \leq 11$, $-17 \leq l \leq 18$)
independent reflections	3780
number of observed reflections (*NO*)	3145 [$F_o^2 \geq 2\sigma(F_o^2)$]
absorption correction method	SADABS
range of transmission factors	0.6028 – 0.0802
data/restraints/parameters	3780 [$F_o^2 \geq -3\sigma(F_o^2)$] / 0 / 235
goodness of fit (*S*)[a]	1.013 [$F_o^2 \geq -3\sigma(F_o^2)$]
final *R* indices[b]	
R_1 [$F_o^2 \geq 2\sigma(F_o^2)$]	0.0384
wR_2 all data	0.0952
largest difference peak and hole	1.524 and – 2.244 e Å^{-3}

[a] $S = [\Sigma w(F_o^2 - F_c^2)^2/(n-p)]^{1/2}$ (n = number of data; p = number of parameters varied; $w = [\sigma^2(F_o^2)+(0.0585P)^2]^{-1}$ where $P = ([\mathrm{Max}(F_o^2, 0) + 2F_c^2]/3)$.

[b] $R_1 = \Sigma||F_o| - |F_c||/\Sigma|F_o|$; $wR_2 = [\Sigma w(F_o^2 - F_c^2)^2/\Sigma w(F_o^4)]^{1/2}$

4.8 References

1. (a) Cooke, J. Ph. D. Thesis, University of Alberta, 1998, pp 69-73. (b) Cooke, J.; Takats, J. *J. Am. Chem. Soc.* **1997**, *119*, 11088. (c) Washington, J.; McDonald, R.; Takats, J. *Organometallics* **1995**, *14*, 3996.
2. (a) Gagné, M. R.; Takats, J. *Organometallics* **1988**, *7*, 6850. (b) Burn, M. J.; Kiel, G. -Y., Seils, F., Takats, J. *J. Am. Chem. Soc.* **1989**, *111*, 6850. (c) Takats, J. *J. Cluster Sci.* **1992**, *3*, 479., (d) Kiel, G. -Y.; Zhang, Z., Takats, J.; Jordan, R. B. *Organometallics* **2000**, *19*, 2766.
3. Hoffmann, R. *Angew. Chem. Int. Ed. Engl.* **1982**, *21*, 711.
4. Stone, F. G. A. *Pure Appl. Chem.* **1986**, *58*, 529 and references therein.
5. Stone, F. G. A. *Angew. Chem. Int. Ed. Engl.* **1984**, *23*, 89.
6. Busetto, L.; Jeffery, J. C.; Mills, R. M.; Stone, F. G. A. Went, M. J.; Woodward, P. *J. Chem. Soc., Dalton Trans.* **1983**, 101.
7. (a) Mao, T.; Zhang, Z.; Washington, J.; Takats, J.; Jordan, R. B. *Organometallics* **1999**, *18*, 2331. (b) Decker, S. A.; Klobukowski, M. *J. Am. Chem. Soc.* **1998**, *120*, 9342.
8. Angelici, R. J. *Acc. Chem. Res.* **1995**, *28*, 51.
9. Green, M.; Howard, J. A. K.; James, A. P.; N. de M. Jelfs, A.; Nunn, C. M.; Stone, F. G. A. *J. Chem. Soc., Dalton Trans.* **1986**, 1697.
10. (a) Templeton, J. L.; Ward, B. C. *J. Am. Chem. Soc.* **1980**, *102*, 3288. (b) Templeton, J. L. *Adv. Organomet. Chem.* **1989**, *29*, 1.
11. (a) Carty, A. J.; Smith, W. F.; Taylor, N.J. *J. Organomet. Chem.* **1978**, *146*, C1. (b) Ball, R. G.; Burke, M. R.; Takats, J. *Organometallics* , **1987**, *6*, 1918. (c) Marinelli, G.; Streib, W. E.; Huffman, J. C.; Caulton, K. G.; Gagné, M. R.;

Takats, J.; Dartiguenave, M.; Chardon, C.; Jackson, S. A.; Eisenstein, O. *Polyhedron* **1990,** *9,* 1867.

12. (a) Hayton, T. W.; Legzdins, P.; Sharp, W. B. *Chem. Rev.* **2002**, *102*, 935 (in particular Section 3.2.2). (b) Alt, H. G.; Thewalt, U. *J. Organomet. Chem.* **1984,** *268*, 235. (c) Hillhouse, G. L.; Haymore, B. L.; Bistram, S. A.; Herrmann, W. A. *Inorg. Chem.* **1983**, *22,* 314. (d) Hillhouse, G. L.; Haymore, B. L.; Herrmann, W. A. *Inorg. Chem.* **1979**, *18*, 2423. (e) Fischer, E. O.; Lindner, T. L.; Huttner, G.; Friedrich, P.; Kreissl, F. R.; Besenhard, J. O. *Chem. Ber.* **1977**, *110*, 3397.
13. Jeffery, J. C.; Mead, K. A.; Razay, H.; Stone, F. G. A.; Went, M. J.; Woodward, P. *J. Chem. Soc. Dalton Trans.* **1984**, 1383.
14. (a) Park, J. T.; Shapley, J. R.; Churchill, M. R.; Bueno, C. *Inorg. Chem.* **1983**, *22*, 1579. (b) Park, J. T.; Shapley, J. R.; Churchill, M. R.; Bueno, C. *J. Am. Chem. Soc.* **1983**, *105*, 6182. (c) Churchill, M. R.; Bueno, C.; Wasserman, H. J. *Inorg. Chem.* **1982**, *21*, 640. (d) Churchill, M. R.; Hollander, F. J. *Inorg. Chem.* **1979**, *18*, 161. (e) Churchill, M. R.; Hollander, F. J. *Inorg. Chem.* **1979**, *18*, 843. (f) Busetto, L.; Green, M.; Hessner B.; Howard, J. A. K.; Jeffery, J. C.; Stone, F. G. A. *J. Chem. Soc., Dalton Trans.* **1983**, 519.
15. (a) Davis, H. B.; Einstein, F. W. B.; Glavina, P. G.; Jones, T.; Pomeroy, R. K.; Rushman, P. *Organometallics* **1989**, *8*, 1030. (b) Batchelor, R. J.; Davis, H. B.; Einstein, F. W. R.; Pomeroy, R. K. *J. Am. Chem. Soc.* **1990**, *112*, 2036.
16. (a) Orpen, A. G. *J. Chem. Soc., Dalton Trans.* **1983**, 1427. (b) Meyer, B. B.; Riley, P. E.; Davis, R. E. *Inorg. Chem.* **1981**, *20*, 3024.
17. Ball, R. G.; Kiel, G. -Y.; Kiel, W. A.; Takats, J.; Grevels, F.-W. *Can. J. Chem.* **1995**, *73*, 1003.

18. (a) Abad, J. A.; Bateman, L. W.; Jeffery, J. C.; Mead, K. A.; Razay, H.; Stone, F. G. A.; Woodward, P. *J. Chem. Soc., Dalton Trans.* **1983,** 2075. (b) Ashworth, T. V.; Howard, J. A. K.; Stone, F. G. A. *J. Chem. Soc., Dalton Trans.*, **1980**, 1609.

19. Mann, B. E. In *Comprehensive Organometallic Chemistry*; Abel, E.W.; Stone, F. G. A.; Wilkinson, G., Eds.; Pergamon: Oxford, 1982; Vol. 3, Capter 20.

20. Adams, R. D.; Cotton, F. A. In *Dynamic Nuclear Magnetic Resonance Spectroscopy*; Jackman, L. M.; Cotton, F. A. Eds.; Academic Press: New York, 1975; Chapter 12.

21. Cooke, J. Ph. D. Thesis, University of Alberta, 1998, pp 293-301.

22. Fischer, E. O.; Lindner, T. L.; Kreissl, F. R. *J. Organomet. Chem.* **1976,** *112*, C27.

23. King, R. B. In *Organometallic Synthesis*, Vol. 1, Academic, New York, 1965, p. 64.

24. Sheldrick, G. M. *Acta Crystallogr.* **1990,** *A46*, 467.

25. Beurskens, P.T.; Beurskens, G.; Bosman, W. P.; de Gelder, R.; Garcia Granda, S.; Gould, R. O.; Israel, R.; Smits, J. M. M. The *DIRDIF*-96 Program system. Crystallography Laboratory, University of Nijmegen, The Netherlands, 1996.

26. Sheldrick, G. M. *SHELXL*-93. Program for crystal structure determination. University of Göttingen, Germany 1993.

Chapter 5

Reactions of $Os(CO)_4(\eta^2$-HFB) with Cyclohexylisocyanide and *Trans*–Cyclooctene: A Further Demonstration of the Reactivity of $M(CO)_4(\eta^2$-alkyne) Complexes Toward Two Electron Donor Ligands

5.1 Introduction

As discussed in Chapter 1 and demonstrated in Chapter 2, and elsewhere [1], the $M(CO)_4(\eta^2$-alkyne) (M = Fe, Ru, Os) complexes show a marked propensity to undergo ready CO exchange with free carbon monoxide and CO substitution reactions with phosphine ligands. As part of our continuing efforts to expand the boundaries of this area of chemistry, it was of interest to investigate the reactivity of these compounds with other two electron donor ligands.

One common type of two electron donor ligand are the isocyanides, or isonitriles, CNR. These ligands are similar to CO in that they are isoelectronic. However, they are poorer π-acceptors and better σ-donors [2]. In this way they are similar to phosphine ligands. They do not, however, have the considerable steric demands that many phosphine ligands posses. A growing number of reports have shown that transition metal complexes are able to promote alkyne–isocayanide coupling [3]. In particular, this chemistry has been extended to include alkyne-isocyanide coupling promoted by an osmium cluster (Eq. 5-1) [4] and alkyne-isocyanide coupling involving the HFB alkyne (Eq. 5-2) [3c, 5]. Hence, in the hopes of making a contribution to this very interesting area of chemistry cyclohexylisocyanide, CNCy, was reacted with $Os(CO)_4(\eta^2$-HFB). The results of this reaction are presented in this chapter.

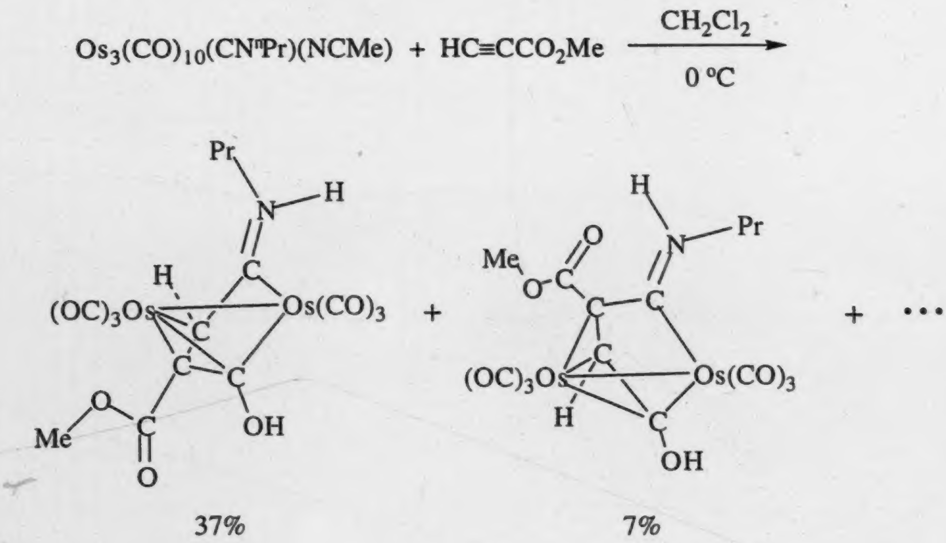
Os3(CO)10(CNnPr)(NCMe) + HC≡CCO2Me
CH2Cl2
0 °C
Pr
N
H
C
(OC)3Os
Os(CO)3
C
OH
Me
O
+
Me
O
Pr
(OC)3Os
Os(CO)3
OH
+ • • •
37%
7%

(5-1)

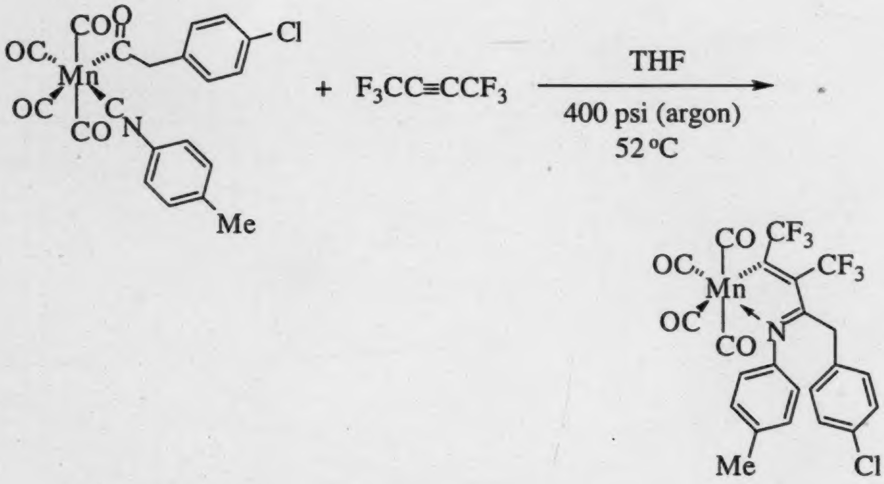
OC
CO
Mn
Cl
CO
N
Me
+ F3CC≡CCF3
THF
400 psi (argon)
52 °C
CF3
CF3
Me
Cl

(5-2)

The presence of both an olefin and an alkyne at a transition metal center is well documented [6]. However, to this date, and despite a few exploratory experiments in our laboratories, no such arrangement has been achieved with either the $Fe(CO)_2(PR_2R')(\eta^2\text{-HFB})$ (**2a-d**) or $M(CO)_4(\eta^2\text{-alkyne})$ (M = Fe, Ru, Os) systems. The significance of such an arrangement at a metal carbonyl center is demonstrated by the well-known Pauson-Khand Reaction [7]. This reaction has been carried out under many different reaction conditions and with a variety of alkenes and alkynes but the overall process is a $Co_2(CO)_8$ mediated [2 + 2 + 1] cycloaddition of an alkene, alkyne and a CO to produce a cyclopentenone ring (Eq. 5-3) [7].

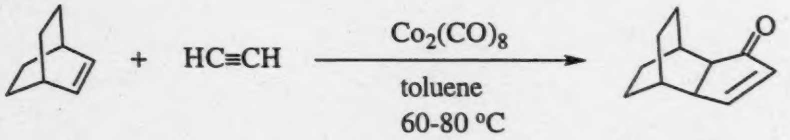

(5-3)

In light of the ability of the $M(CO)_4(\eta^2\text{-HFB})$ (M = Fe, Ru, Os) complexes to promote alkyne-alkyne coupling, it was decided that attempts to coordinate an olefin ligand to these molecules might prove fruitful and result in olefin-alkyne coupling. Having that been said, our studies suggest that substitution of CO by phosphine ligands occurs almost exclusively at axial coordination sites [1, 8], but, as discussed in Chapter 1, the coordination of an olefin in the axial site of a d^8 metal in a trigonal bipyramidal molecule is electronically disfavored [9]. However the use of a good coordinating olefin may overcome this barrier an lead to olefin coordination, which in turn may lead to olefin-alkyne coupling.

One strategy in strengthening bonding between a metal atom and an olefin is the use of strained olefins as ligands [10]. The partial $sp^2 \rightarrow sp^3$ rehybridization of an olefinic carbon upon coordination can lead to relief of geometrical stress in strained olefins, which in turn leads to greater metal-olefin interaction. One such olefin that has been successfully implemented in this way is *trans*-cyclooctene, or (*E*)-cyclooctene (*eco*) [11]. Figure 5-1 shows *eco* in its two enantiomeric forms. This olefin has been found to act as an exceptional ligand in several transition metal carbonyl compounds [12]. In view of the coordinating ability of *eco* its was decided to investigate the reaction between $Os(CO)_4(\eta^2\text{-HFB})$ and this olefin.

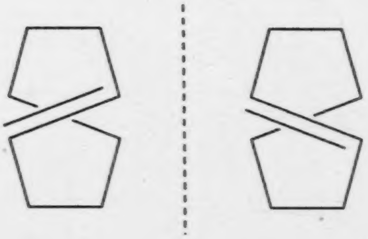

Figure 5-1 The Enantiomers of *Trans*-Cyclooctene (*eco*).

5.2 Reaction of $Os(CO)_4(\eta^2$-HFB) with Cyclohexylisocyanide

5.2.1 Experimental Observations

A pentane solution of $Os(CO)_4(\eta^2$-HFB) was treated with a slight excess (10%) molar amount of CNCy. Within 5 minutes the IR spectrum (carbonyl region) exhibited clear signs of reaction; a decrease in the intensity of the bands of the starting material and the emergence of new bands. With the help of three freeze-pump-thaw cycles the reaction was complete within 2 hours. Solvent removal at low temperature left a colorless solid which liquefied to a pale yellow viscous oil upon warming to room temperature. The oily material was redissolved in pentane and crystallized at low temperature. Pale yellow crystalline **11** was recovered in good yield.

The melting point of the crystals was determined to be 22-23 °C. Mass spectroscopic analysis ($M^+ = 547$) revealed that the formulation of **11** is consistent with $Os(CO)_3$(CNCy)(HFB).

In another experiment, a pentane solution of $Os(CO)_4(\eta^2$-HFB) was treated with ten fold excess of CNCy. Surprisingly, substitution of a second carbonyl ligand was not observed. Previously in our laboratories it was observed that two carbonyl ligands could easily be displaced from $Os(CO)_4(\eta^2$-HFB) by reaction with two equivalents of phosphine ligands [1] and, in light of this, the lack of further substitution was surprising. This reactivity pattern is however reflected in the literature as isocyanides usually replace no more than one or two carbonyl ligands in either mononuclear or cluster carbonyl compounds unless a catalyst is used [13]. The reason for the inability to CNCy to displace additional carbonyl ligands from $Os(CO)_4(\eta^2$-HFB) is not understood at this time.

5.2.2 Spectroscopic Characterization of 11

The IR spectrum (carbonyl region) of crystallized **11** exhibits a pattern indicative of a trigonal arrangement of carbonyls (Figure 5-2, Table 5-1). In addition to three strong ν_{CO} bands (2088, 2029, 2002 cm^{-1}), the IR spectrum showed two weak bands at 1790 and 2220 cm^{-1} that are consistent with the ν_{CC} of an η^2-HFB and the ν_{CN} of a coordinated CNCy ligand, respectively. The ν_{CN} stretch of the coordinated CNCy is at a significantly higher frequency than that of the free CNCy ligand (free CNCy ν_{CN} = 2136 cm^{-1}). This is in contrast to typical CO behavior but is often observed with isocyanide ligands [14]. This is because the lone pair electrons localized on the carbon atom in CNR is in a more antibonding orbital, with respect to the C≡N bond, than that of the CO ligand. Reduction of electron density in this orbital causes a strengthening in the CN bond and thus a shift of the ν_{CN} to higher frequencies and, as discussed in the introduction, isocyanide ligands are generally better σ-donors than carbonyl ligands.

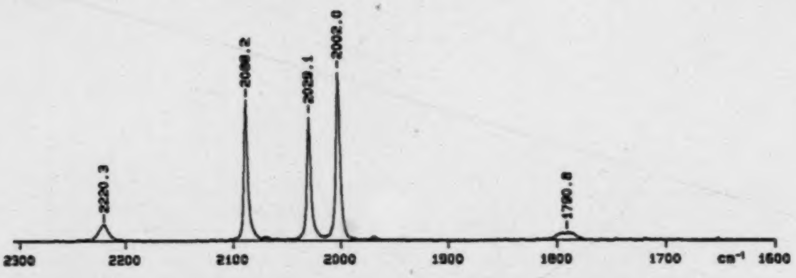

Figure 5-2 FT-IR Spectrum (carbonyl region, cm^{-1}, pentane) of **11**.

The IR and mass spectroscopic data suggests a trigonal bipyramidal structure that is shown in Figure 5-3.

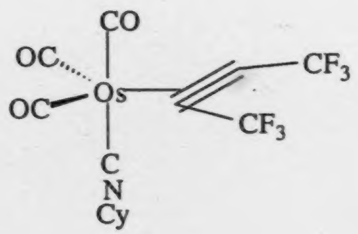

Figure 5-3 Structure of **11**.

The NMR data of **11** is listed in Table 5-1. The ^1H NMR data shows four broad signals whose integration pattern (1:2:4:4:) is consistent with the presence of a cyclohexyl ring. The ^{19}F NMR spectrum shows one signal, indicating chemical equivalence for the two CF_3 groups of the alkyne. This is consistent with the proposed structure with C_s molecular symmetry (Figure 5-3). The $^{13}C\{^1H\}$ NMR data shows two carbonyl resonances at δ 175.9 and 172.2 ppm. The lowfield resonance is assigned to the equatorial carbons because it has twice the intensity of the other resonance. Upfield of the carbonyls a resonance is observed at δ 121.6 ppm. The assignment of this signal to the CF_3 carbons is based upon the characteristic $^1J_{CF}$ coupling observed with the HFB ligand. The ligating carbons of the alkyne are observed upfield at δ 98.7 ppm with a much smaller $^2J_{CF}$ coupling. Between these signals, at δ 117.3 ppm, is a resonances which appears as a 1:1.3:1 triplet. A ligating isocyanide carbon resonance should appear as a 1:1:1 triplet which arises from ^{13}C–^{14}N spin-spin coupling (^{14}N $I = 1$), but is often observed as a broad singlet or a distorted 1:1:1 triplet with the central peak more intense than the flanking peaks [3c]. Moreover, $^1J_{CN}$ coupling are usually in the 12-30 Hz range [3c].

Table 5-1 The FT-IR (carbonyl region), ^{19}F, ^{1}H and ^{13}C{^{1}H} NMR Data of **11**.

FT-IR[a]	^{19}F[b]	^{1}H[b]	^{13}C{^{1}H}[b]
2088 (s)	– 58.0	3.87 br (1H)	175.9 s CO_{eq}
2029 (s)		1.80 br (2H)	172.2 s CO_{ax}
2002 (s) ν_{CO}		1.61 br (4H)	121.6 q $^{1}J_{\mathrm{CF}} = 267$ Hz CF_3
1791 (w) ν_{CC}		1.42 br (4H)	117.3 “t” $^{1}J_{\mathrm{CN}} = 23$ Hz CN
2220 (w) ν_{CN}			98.7 q $^{2}J_{\mathrm{CF}} = 49$ Hz CCF_3
			55.5 “t” $^{1}J_{\mathrm{CN}} = 6$ Hz $C_{\mathrm{bridgehead}}$
			32.2 s CH_2
			25.0 s $\mathrm{CH_2}$
			22.7 s $\mathrm{CH_2}$

[a] cm^{-1}, pentane, ν_{CN} (free CNCy) = 2136 cm^{-1} in pentane

[b] ppm, CD_2Cl_2, 27 °C

The δ 117.3 ppm resonance in **11** has a $^1J_{CN}$ = 23 Hz and is clearly the *C*N carbon resonance. The next resonance at δ 55.5 ppm also appears as a distorted 1:1:1 triplet ($^1J_{CN}$ = 6 Hz) with the central peak being the most intense. Thus, this signal is assigned to the bridgehead carbon of the cyclohexyl ring ($C_{\text{bridgehead}}$). The remaining carbons of the cyclohexyl ring are clearly observed at δ 32.2, 25.0 and 22.7 ppm.

High quality crystals of **11** were easily grown at low temperature and despite their low melting point an X-ray crystal structure analysis was successful. The results of the solid state structure determination are presented below.

5.2.3 X-ray Crystal Structure Analysis of $Os(CO)_3(CNCy)(\eta^2\text{-HFB})$ (11)

The results of the X-ray crystal structure analysis are presented in Figure 5-4 (omitting hydrogen atoms), with atom labeling scheme, and Table 5-2.

The results confirm the trigonal bipyramidal geometry around the osmium atom. The alkyne occupies, as usual, an equatorial coordination site with an in-plane orientation. The three carbonyl ligands occupy mutually *cis* coordination sites as predicted from the pattern of ν_{CO} in the IR spectrum. Two of the carbonyl ligands occupy equatorial coordination sites, while the third occupies an axial site. The last coordination site, axial, is occupied by the CNCy ligand.

The geometry around the osmium atom is best described as a distorted trigonal bipyramid. The most significant distortion is observed in the equatorial plane. The C2–Os–C3 angle of 95.4(2)° is considerably smaller than the ideal 120°. This is a result of the bulky alkyne ligand occupying an equatorial site with an in-plane orientation. The C2–Os–C3 angle is close to the 97.88(9)° observed for the corresponding parameter in $Fe(CO)_2(P^tBu_2Me)_2(\eta^2\text{-HFB})$ **1a** (Chapter 1) and is identical to 95.2(7)° seen in $Os(CO)_4(\eta^2\text{-HFB})$ [15].

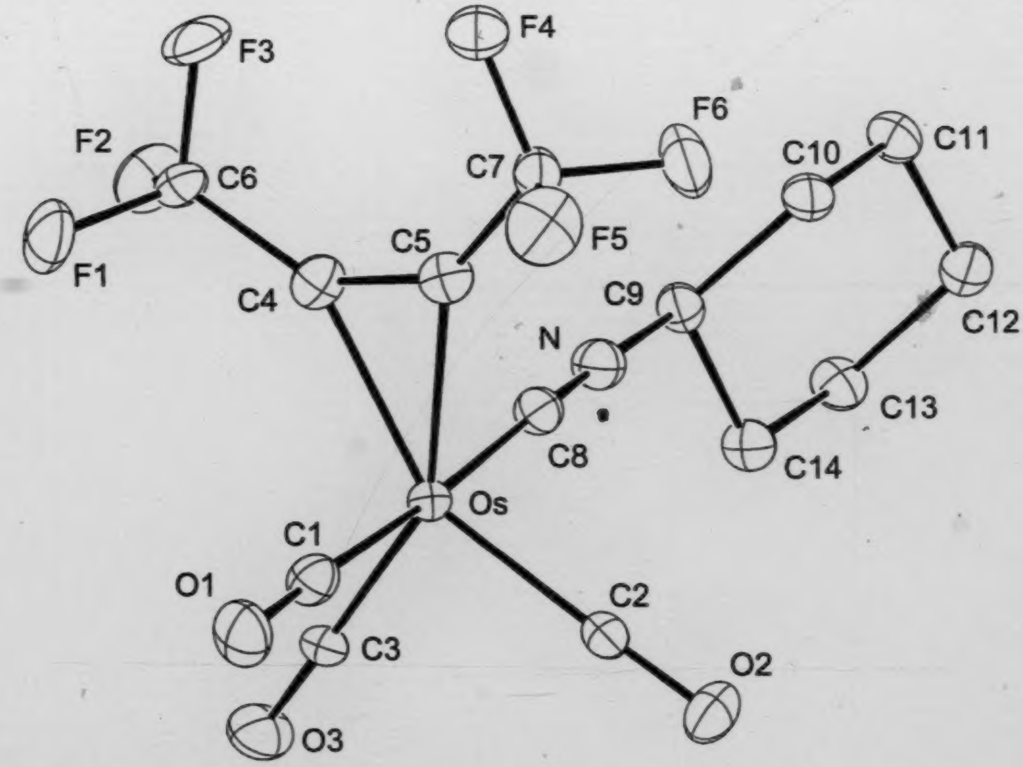
F3
F4
F6
F2
C6
C7
C10
C11
F1
C4
C5
F5
C9
C12
N
C8
C13
C14
Os
C1
O1
C2
C3
O2
O3

Figure 5-4 Solid State Molecular Structure of **11**.

Table 5-2 Selected Interatomic Distances (Å) and Angles (deg.) in **11**.

Os–C1	1.945(6)	C1–Os–C8	176.3(2)
Os–C2	1.929(6)	C2–Os–C3	95.4(2)
Os–C3	1.909(6)	C2–Os–C5	113.9(2)
Os–C4	2.132(6)	C2–Os–C8	91.9(2)
Os–C5	2.128(6)	C3–Os–C4	115.7(2)
Os–C8	2.055(6)	C3–Os–C8	89.1(2)
C4–C5	1.281(9)	C4–Os–C5	35.0(2)
C8–N	1.139(8)	C4–Os–C8	87.2(2)
C9–N	1.462(7)	C5–Os–C8	87.7(2)
C1–Os–C2	91.7(2)	C8–N–C9	177.7(6)
C1–Os–C3	89.8(3)	N–C8–Os	178.3(5)
C1–Os–C4	90.1(2)	N–C9–C10	109.0(5)
C1–Os–C5	91.6(2)	N–C9–C14	109.1(4)

The CNCy ligand in **11** is decidedly linear as both the Os–C8–N (178.3(5)°) and C8–N–C9 (177.7(6)°) angles are essentially 180°. The linear CNR linkage is the most commonly observed form in η^1-bonded CNR ligands [3c]. In terms of the valence bond description of the bonding of the M–C–N–R linkage [3c], the bent canonical form **B** in Scheme 5-1 makes no substantial contribution to the electronic structure. This would imply that no significant back donation from the metal to the π-antibonding orbitals of the CNCy ligand ($Os \rightarrow \pi^*C{\equiv}NR$) occurs and the nitrogen atom is essentially *sp* hybridized. This assertion is supported by the 84 cm^{-1} shift of the ν_{CN} to higher frequencies upon coordination. However, it has been suggested, some years ago, that the valence bond description does not adequately describe the metal-isocyanide back bonding since the $C{-}N{-}CH_3$ angle (177 ± 1.5°) in $[Co(CNCH_3)_5]^+$ is essentially linear and yet the $Co{-}CNCH_3$ separation shows a strong indication of multiple bond character [16]. It was further stated that the molecular orbital description of the MCNR bonding better represents the metal-isocyanide back donation, and that this bonding regime does not require bending in the C–N–R linkage for M-CNR back bonding to occur [16a]. The Os–C(8)NCy separation of 2.055(6)Å in **11** is significantly larger, by 0.078 Å (13 esd's), than the $Os{-}C_{sp}$ single bond separation of 1.977(4) Å in $\overline{Os(C_2CO_2Me)(CH{=}C(H)C(OMe){=}O}(CO)(P^iPr_3)_2$ [17]. This is consistent with little or no $Os \rightarrow \pi^*CN$ back donation in **11**. The C(8)–N separation (1.139(8) Å) in **11** is identical to the C≡N triple bond separation (1.141(3) Å) in the solid state molecular structure of the free 1,4-diisocyanocyclohexane ($CNC_6H_{10}NC$) ligand [18]. These observations suggest the bonding in the MCNR linkage is primarily represented by canonical form **A**, in Scheme 5-1.

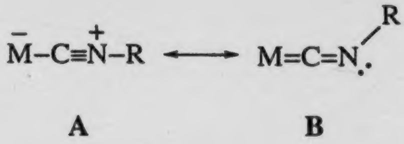

Scheme 5-1 Valence Bond Representation of MCNR Bonding.

5.3 Reaction of $Os(CO)_4(\eta^2\text{-HFB})$ with *Trans*-Cyclooctene

5.3.1 Experimental Observations

A colorless pentane solution of $Os(CO)_4(\eta^2\text{-HFB})$ was treated with an equimolar amount of *eco* at ambient temperature. After 20 minutes the FT-IR spectrum showed clear indications of a reaction; a reduction in the intensity of the bands due to the starting material and a the emergence of new bands. The reaction progressed slowly and after one hour additional *eco* (10% excess) was added to the reaction mixture. The reaction continued its slow progress and two more additions of *eco* (20% excess) and several freeze-pump-thaw cycles were needed to "coax" the reaction to go to completion. After a simple workup and crystallization, a pale yellow crystalline material (compound **12**) was obtained.

5.3.2 Spectroscopic Characterization of 12

The FT-IR (carbonyl region) of **12** is shown in Figure 5-5. The band at 1810 cm^{-1} is consistent with the retention of the η^2-alkyne ligand, *i.e.* ν_{CC}. The remaining pattern, 2025 (s) and 2113 (w), is reminiscent of a *trans*-$M(CO)_2$ arrangement with C_2 local symmetry. This would imply substitution of two carbonyl ligands, *i.e.* $Os(CO)_2(\mathit{eco})_2(\eta^2\text{-HFB})$. Strangely, the elemental analysis indicated only one *eco* ligand in the molecule, i.e. $Os(CO)_3(\mathit{eco})(\eta^2\text{-HFB})$.

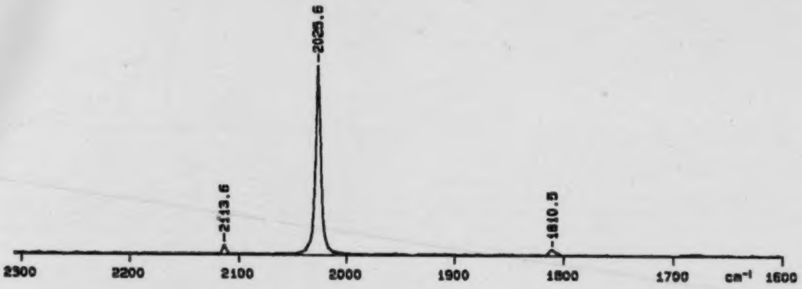

Figure 5-5 FT-IR Spectra (carbonyl region) of **12**.

This inconsistency was immediately resolved upon collecting the ^{13}C NMR spectrum (Figure 5-6, Table 5-3). It clearly exhibited three carbonyl resonances of equal intensity, indicating three chemically inequivalent carbonyl ligands. Further inspection of the $^{13}C\{^1H\}$ NMR spectrum revealed two quartets, each having a large $^1J_{CF} = 266$ Hz, at δ 122.1 and 120.8 ppm. These signals are assigned to the CF_3 carbons. The ligating carbons of the alkyne appear as a quartet of quartets at δ 93.5 and 85.0 ppm, due to coupling to both CF_3 groups ($^2J_{CF}$ and $^3J_{CF}$). Further upfield, four very intense signals, assigned to the carbons of *eco* ligand, appear at δ 63.9, 41.4, 38.1 and 28.9 ppm. The latter three signals appear in an inverted form in the DEPT (**D**istortionless **E**nhancement by **P**olarization **T**ransfer) spectrum indicating CH_2 type carbon atoms. The spectroscopic data indicate an asymmetric structure for **12**. The presence of only four carbon signals, as opposed to eight, for the *eco* ligand points to a time averaging of the two halves of the ligand, which is presumably due to rapid rotation about the Os-*eco* bond axis.

Table 5-3 The FT-IR (carbonyl region), ^{19}F, ^{1}H and $^{13}C\{^{1}H\}$ NMR Data of **12**

FT-IR^{a}	$^{19}F^{b}$	$^{1}H^{b}$	$^{13}C\{^{1}H\}^{b}$
2113 (w)	– 55.8 q $^{5}J_{FF} = 5$ Hz	4.42 m (2H)	180.7 q $^{4}J_{CF} = 2$ Hz *CO*
		2.80 m (2H)	171.4 s *CO*
2025 (vs) ν_{CO}	– 68.5 q $^{5}J_{FF} = 5$ Hz	2.11 m (4H)	171.2 s *CO*
		1.85 m (2H)	122.1 q $^{1}J_{CF} = 266$ Hz *CF*$_3$
1810 (w) ν_{CC}		1.25 m (4H)	120.8 q $^{1}J_{CF} = 266$ Hz *CF*$_3$
			93.5 qq $^{2}J_{CF} = 48$ Hz
			$^{3}J_{CF} = 8$ Hz *C*CF$_3$
			85.0 qq $^{2}J_{CF} = 46$ Hz
			$^{3}J_{CF} = 7$ Hz *C*CF$_3$
			63.9 s *C*H
			41.4 s CH$_2$
			38.1 s CH$_2$
			28.9 s CH$_2$

[a] cm^{-1}, pentane.

[b] ppm, CD_2Cl_2, 27 °C

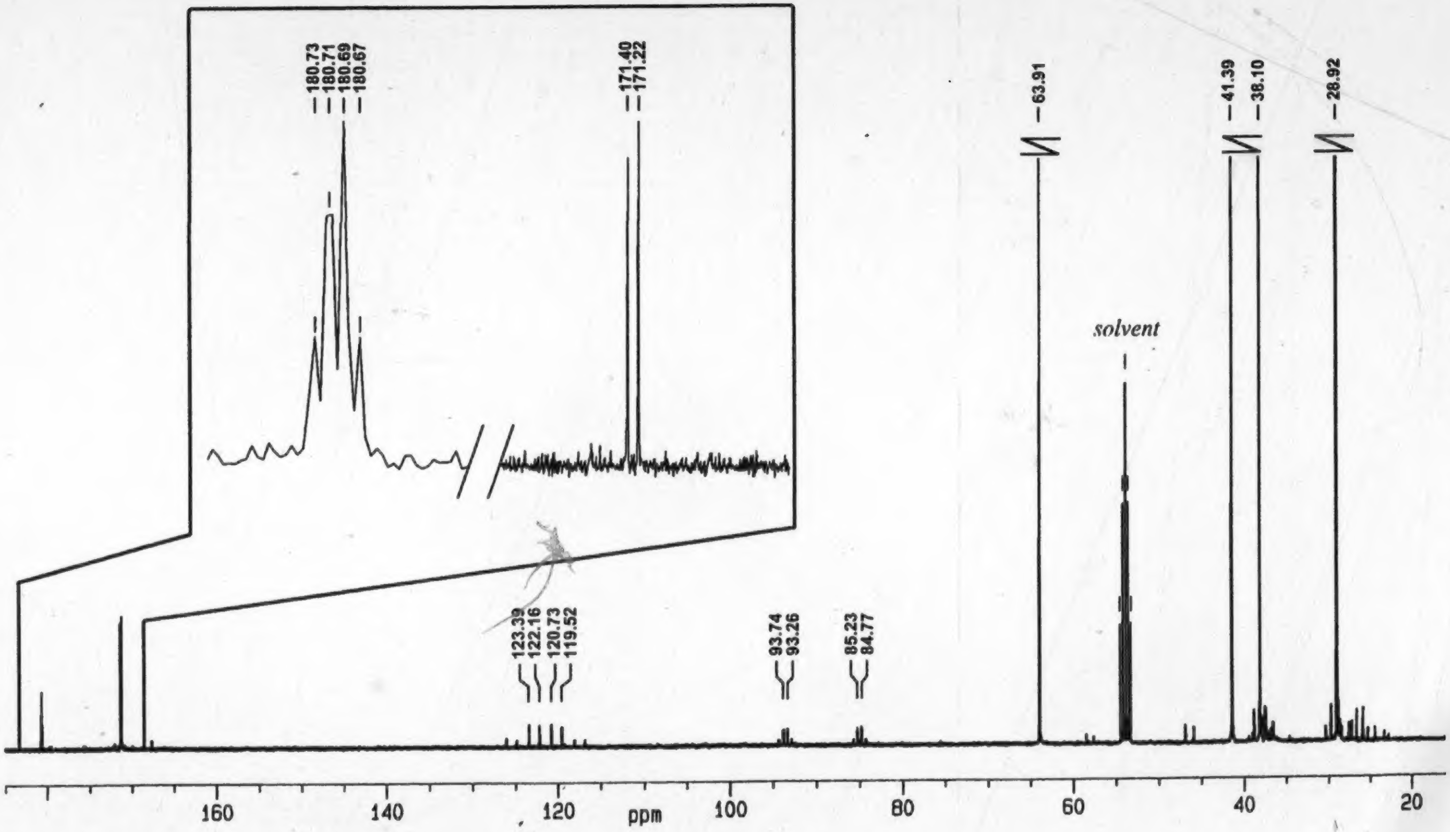

Figure 5-6 The $^{13}C\{^1H\}$ NMR (ppm, CD_2Cl_2, 27 °C) Spectrum of **12**.

Continuing with the ^1H and ^{19}F NMR spectra (Table 5-3), the ^1H NMR spectrum exhibited five broad complex multiplets in a 2:2:4:2:4 intensity ratio. Due to time averaging of the two halves of the *eco* ligand, seven signals, of equal intensity, are expected. The intensity ratio of the five observed resonances suggests two of the signals are a result of overlap. The ^{19}F NMR spectrum indicated two chemically inequivalent CF_3 groups.

With the $(Os(CO)_3(\textit{eco})(HFB)$ formulation secured and assuming the alkyne occupies an equatorial position, in a trigonal bipyramidal geometry, two structures can be envisioned; **A** and **B** in Figure 5-7. The presence of only a C_2 local symmetry in the *eco* ligand renders both structures asymmetric, by eliminating the mirror plane that would otherwise result in an equivalent equatorial **A** or axial **B** carbonyl groups. Thus both structures posses chemically inequivalent carbonyls and alkyne CCF_3 groups. Structure **A** can be eliminated since one would expect three medium-strong ν_{CO} bands in the IR spectrum (C_s $M(CO)_3$ local symmetry). Structure **B** on the other hand is more consistent with the IR spectroscopic data. In this structure, with a "T-shaped" carbonyl arrangement (C_{2v} $M(CO)_3$ local symmetry), one would also expect three ν_{CO} bands but two of them would have a medium-strong intensity, while the third would be weak. This would mean that a somewhat unusual case occurs, but one not without precedent [19], in that the two medium-strong bands are superimposed. With this superposition of the two bands the ν_{CO} pattern would then be a weak band at high frequency and a very strong band at a lower frequency similar to the observed pattern of **12**.

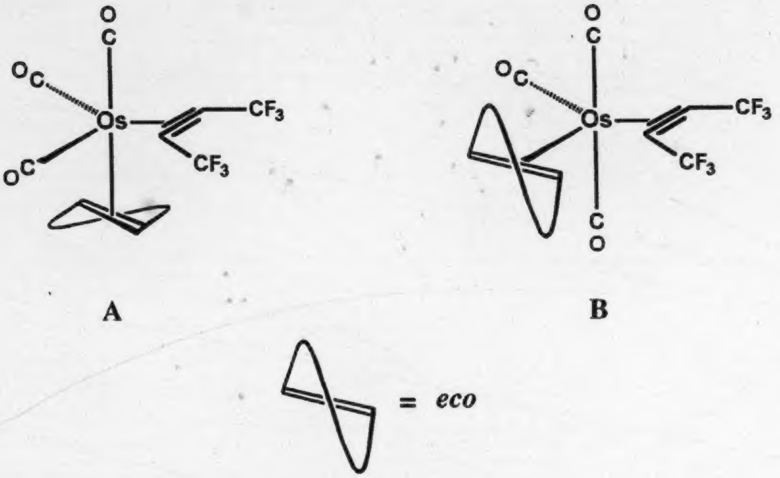

A

B

Figure 5-7 Possible Structures of **12** (*enantiomers not shown*).

To confirm the structural assignment a crystallographic structure analysis was conducted. The results are presented below.

5.3.3 X-ray Crystal Structure Analysis of Os(CO)$_3$(η^2-*eco*)(η^2-HFB) (12)

The molecular structure of Os(CO)$_3$(η^2-*eco*)(η^2-HFB) (**12**) is shown in Figure 5-8 with atom labeling scheme, while Table 5-4 lists selected interatomic distances and angles.

As predicted, the structure is represented by **B** in Figure 5-7, with the η^2-*eco* ligand (C8-C15) occupying an in-plane equatorial coordination site, while the other two equatorial sites are occupied by an η^2-HFB ligand (C4-C5), with an in-plane orientation, and a carbonyl ligand (C2O2). The axial coordination sites are occupied by the two remaining carbonyls (C1O1 and C3O3). The geometry about the osmium atom is best described as a distorted trigonal bipyramid. The axial vectors C1–Os and C3–Os are largely orthogonal with respect to the atoms of the equatorial plane. Deviations from the ideal angle of 90° are small, usually within a 5° deviation of ideal.

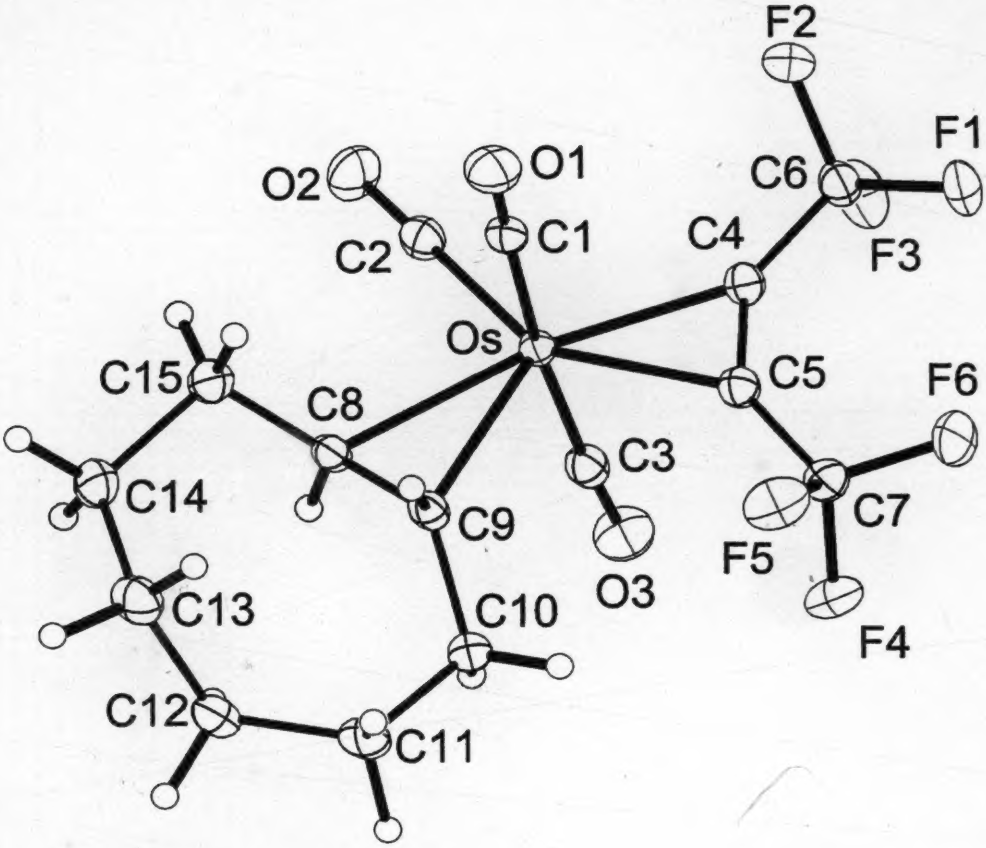
F2
F1
O2
O1
C6
C2
C1
C4
F3
Os
C15
C8
C5
F6
C3
C14
C9
C7
F5
O3
C13
C10
F4
C12
C11

Figure 5-8 Solid State Molecular Structure of **12**

Table 5-4 Selected Interatomic Distances (Å) and Angles (deg.) in **12**.

Os–C1	1.965(2)	C1–Os–C9	88.5(1)
Os–C2	1.941(2)	C2–Os–C3	93.7(1)
Os–C3	1.958(3)	C2–Os–C4	112.3(1)
Os–C4	2.123(2)	C2–Os–C5	147.3(1)
Os–C5	2.143(2)	C2–Os–C8	79.2(1)
Os–C8	2.302(2)	C2–Os–C9	115.0(1)
Os–C9	2.250(2)	C3–Os–C4	87.7(1)
C4–C5	1.281(3)	C3–Os–C5	85.8(1)
C8–C9	1.409(3)	C3–Os–C8	90.5(1)
C1–Os–C2	91.7(1)	C3–Os–C9	92.1(1)
C1–Os–C3	173.8(1)	C4–Os–C5	35.0(1)
C1–Os–C4	87.4(1)	C8–Os–C9	36.0(1)
C1–Os–C5	88.0(1)	C4–C5–C7	142.6(2)
C1–Os–C8	93.6(1)	C5–C4–C6	142.0(2)

The axial carbonyls are however slightly bent (C1–Os–C3 = 173.8(1)° in the direction between the alkyne (C5) and the olefin (C9). A similar deviation from linearity is observed in the molecular structure of $Fe(CO)_3(\eta^2\text{-}eco)_2$ (Figure 5-9) [12f], in which the corresponding C–Fe–C angle is 172.9°. In **12** significant distortions are observed in the equatorial plane. The C2–Os–C4 angle is 112.3(1)°, while the C2–Os–C8 angle is only 79.2(1)°. A similar distortion, albeit to a much less extent, was observed in $Fe(CO)_3(\eta^2\text{-}eco)_2$ [12f]. In **12** this asymmetry can be attributed to the difference in the steric demands of the alkyne and the *eco* ligand.

The geometry of the alkyne ligand in **12** is close to that observed in the previous compounds **1a-c** (Chapter 2). The C≡C separation (1.281(3) Å) is not significantly different from the corresponding value in **1a** (1.278(5)Å) or **1c** (1.267(5)Å) and is only slightly smaller (by 6 esd's) than that observed in **1b** (1.252(5)Å). The bend back angles of the CF_3 substituents in **12** (C4–C5–C7 = 142.6(2)°, C5–C4–C6 = 142.0(2)°) are slightly larger than the related parameters in **1a-c** (average = 136.4°), indicating somewhat greater metal→alkyne back donation in **12**. This is consistent with a substitution of a good π-acceptor, CO in **1a-c**, with the poorer π-acceptor *eco* in **12**.

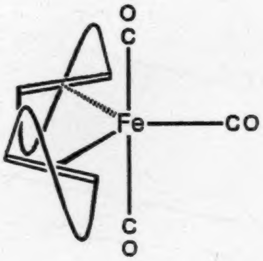

Figure 5-9 Structure of $Fe(CO)_3(\eta^2\text{-}eco)_2$ [12f].

The *eco* ligand in **12** occupies an equatorial coordination site with an in-plane orientation (C1–Os–C8–C9 = 98.2(2)°, C2–Os–C8–C9 = 173.5(3)°) much like the *eco* ligands in $Fe(CO)_3(\eta^2\text{-}eco)_2$ (Figure 5-9) [12f]. This in-plane orientation is expected in trigonal bipyramidal d^8 metal-olefin complexes (Chapter 1) [9]. The C8–C9 distance (1.409(3)Å) in **12** is appreciably longer than the C=C separation (1.341(2) Å (*neutron*); 1.330(4) Å (*X-ray*)) in the free *eco* derivative *trans*-2-cycloocten-1-yl-3,5-dinitrobenzoate (Figure 5–10) [20]. This is consistent with an elongation of the C=C double bond upon coordination and subsequent back donation from the metal into the π-antibonding orbitals of the olefin. The C=C separation in **12** is close the corresponding parameters (1.394(3) and 1.404(3) Å) in $Fe(CO)_3(\eta^2\text{-}eco)_2$ (Figure 5–9) [12f].

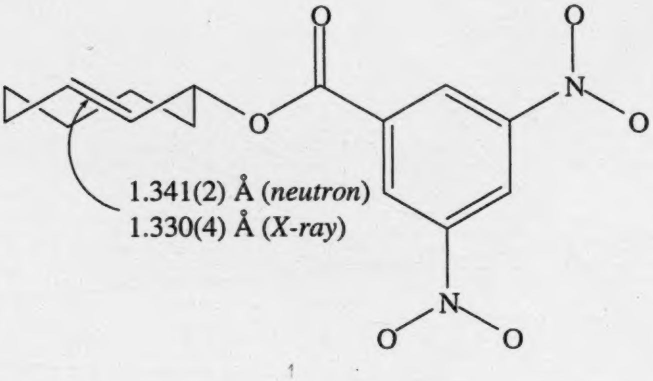

Figure 5-10 *Trans*-2-Cyclooctene-1-yl-3,5-Dinitrobenzoate [20].

Since $Os(CO)_4(\eta^2\text{-HFB})$ was reacted with racemic *eco*, one might expect that either enantiomer of *eco* would be found in the molecule. Indeed, the centrosymmetric space group of **12** ($P2_1/c$) shows that both enantiomers are present in the crystal. Figure 5-11 displays the two enantiomeric forms of **12**.

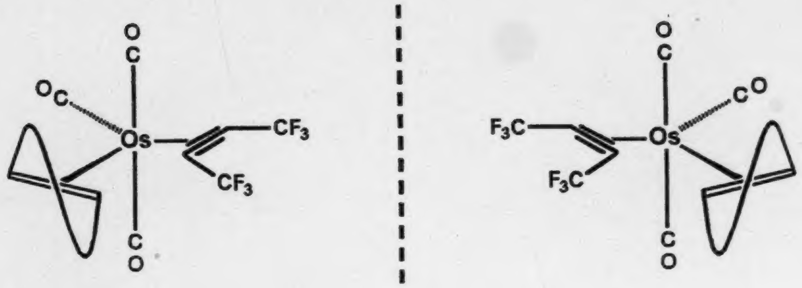

Figure 5-11 The Two Enantiomers of **12**.

5.4 Reaction of Os(CO)$_4$(η^2-HFB) with Excess *Trans*-Cyclooctene: Discovery of Alkyne-Olefin Coupling

5.4.1 Experimental Observations

The usual workup of **12** consisted of the removal of the solvent and any excess *eco*, *in vacuo*. However, during some experiments **12** was crystallized directly from the reaction solution, *i.e.* in the presence of excess *eco*. These experiments led to some very interesting results.

A small number of colorless crystals were isolated from one such reaction mixture. A melting point determination was carried out. A previous melting point determination of **12** revealed a value of 39.5 - 41.5 °C. It was therefore curious that these crystals showed no signs of melting even at 75 °C. At 94 °C the crystals began to show signs of decomposition; fracturing and darkening. Finally at 108-110 °C the crystals fully decomposed and the scent of *eco* could be detected. Clearly, these crystals were of a different compound (**13**). This conclusion was confirmed when a few crystals of **13** were dissolved in 0.2 mL of pentane and the FT-IR spectrum was recorded (Figure 5-12). A comparison of the IR spectrum of **13** and that of **12** (Figure 5-5, Section 5.3.2) clearly shows that these compounds have very different carbonyl arrangements. The IR spectrum of **13** shows the characteristic pattern for a trigonal $M(CO)_3$ arrangement of carbonyls, *cf.* Figure 5–2, Section 5.2.2. A couple of crystals of **13** were submitted for mass spectral analysis (EI-MS) and a strong molecular ion signal at *m/z* = 658 indicated an $Os(CO)_3(\mathit{eco})_2(HFB)$ formulation for **13**. Only a few crystals remained and these were submitted for X-ray crystal structure analysis. The results of that analysis are presented below.

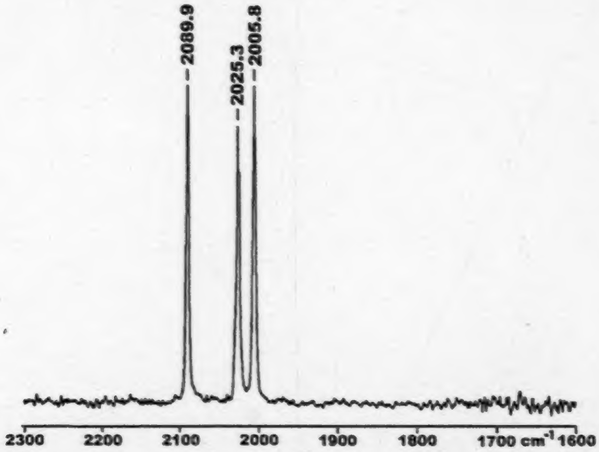

Figure 5-12 FT-IR Spectrum (carbonyl region, cm^{-1}, pentane) of **13**.

5.4.2 X-ray Crystal Structure Analysis of 13:

***fac*-$Os(CO)_3(\eta^2\text{-}\mathit{eco})(\eta^1,\eta^1\text{-}(F_3C)C{=}C(CF_3)\overline{\mathrm{CH(CH_2)_6C}}H)$**

The solid state molecular structure of **13** is shown in Figure 5-13 with atom labeling scheme, while Table 5–5 lists selected interatomic separations and angles.

The molecule consists of an osmium center surrounded by three carbonyl ligands, one intact η^2–*eco* ligand and an $\eta^1,\eta^1\text{-}(F_3C)C{=}C(CF_3)\overline{\mathrm{CH(CH_2)_6C}}H$ ligand, which arose from coupled *eco* and HFB moieties.

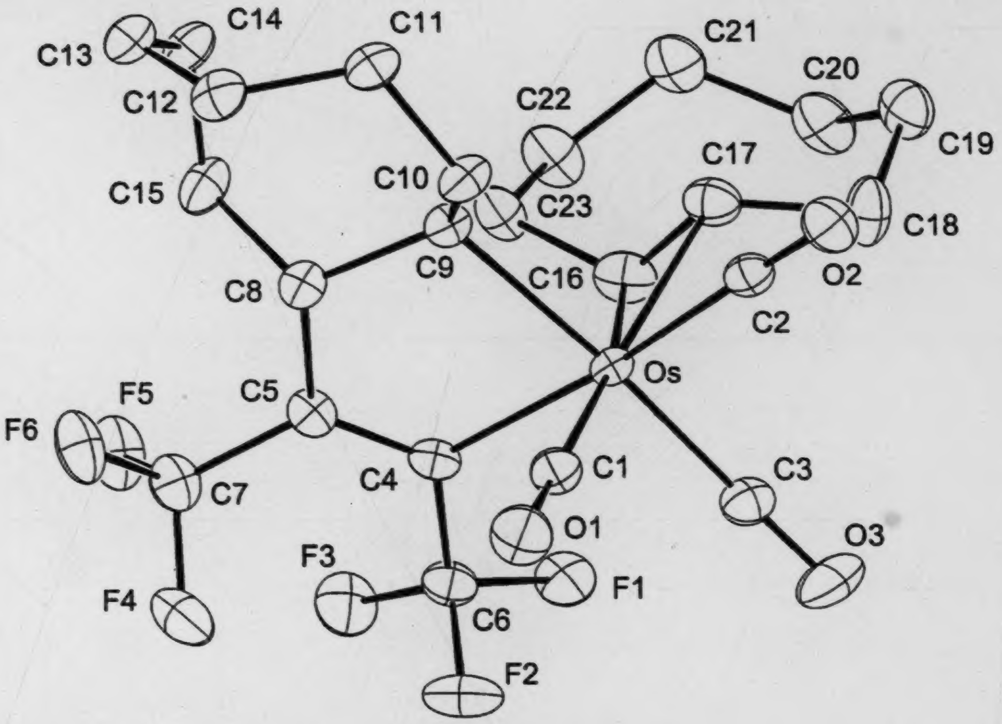
C13
C14
C11
C21
C20
C12
C22
C19
C17
C10
C15
C23
C18
C9
C16
O2
C8
C2
Os
F5
C5
F6
C1
C3
C7
C4
O1
O3
F3
F1
F4
C6
F2

Figure 5-13 Solid State Molecular Structure of **13**.

Table 5-5 Selected Interatomic Distances (Å) and Angles (deg.) in **13**.

Os–C1	1.901(4)	C1–Os–C17	164.7(2)
Os–C2	1.947(4)	C2–Os–C3	91.7(2)
Os–C3	1.959(4)	C2–Os–C9	92.1(2)
Os–C4	2.146(4)	C2–Os–C16	107.0(2)
Os–C9	2.208(4)	C2–Os–C17	73.9(2)
Os–C16	2.397(5)	C3–Os–C4	96.6(2)
Os–C17	2.416(5)	C3–Os–C16	87.1(2)
C4–C5	1.334(6)	C3–Os–C17	91.4(2)
C5–C8	1.525(6)	C4–Os–C9	79.6(2)
C8–C9	1.560(6)	C4–Os–C16	79.8(2)
C16–C17	1.379(7)	C4–Os–C17	112.0(2)
C1–Os–C2	91.2(2)	C9–Os–C16	92.2(2)
C1–Os–C3	92.7(2)	C9–Os–C17	90.1(2)
C1–Os–C4	82.2(2)	Os–C1–O1	179.2(4)
C1–Os–C9	86.8(2)	Os–C2–O2	177.4(4)
C1–Os–C16	161.8(2)	Os–C3–O3	176.2(4)

The geometry around the Os atom is best described as a distorted octahedral with one face occupied by the three carbonyl ligands C1O1, C2O2 and C3O3, while the other face is occupied by the η^2–*eco* (C16-C23) and η^1,η^1-$(F_3C)C{=}C(CF_3)\overline{\mathrm{CH(CH_2)_6C}}\mathrm{H}$ (C4-C15) ligands. The most significant deviation from ideal involves a large C3–Os–C4 (96.6(2)°) angle and the small C4–Os–C9 (79.6(2)°) angle. The deviation in the former angle is caused by the steric interaction between the CF_3 (C6F1-3) group and the C3O3 carbonyl. The CF_3 substituents of the vinyl moiety are restricted to an in-plane orientation (C6–C4–C5–C7 = 6.8(4)°) due to the sp^2 hybridization of C4 and C5. The small C4–Os–C9 angle is probably due to the geometrical constraints of the $\overline{\mathrm{Os{-}C4{=}C5{-}C8{-}C9}}$ metallacyclopentene ring. The double bond of the η^2-*eco* ligand (C16=C17) is orientated nearly eclipsed with the C2O2 carbonyl, since the C16–C17–Os–C2 dihedral angle is only 6.1(4)°. The parallel alignment of the double bond of an axial η^2-olefin ligand and an equatorial W–CO linkage, of a square planar $W(CO)_4$ moiety, has been predicted from theoretical calculations [21] and has been observed in the solid state molecular structure of $W(CO)_5(\eta^2$-*eco*) [12h]. The double bond length (C16–C17 = 1.379(7) Å) in **13** is within 4 esd's of the corresponding separation in **12** (C8–C9 = 1.409(3) Å).

The η^1,η^1-$(F_3C)C{=}C(CF_3)\overline{\mathrm{CH(CH_2)_6C}}\mathrm{H}$ ligand is the product of an *eco*-HFB coupling, and is formed through C–C bond formation between C5 and C8. The result is a bicyclic ligand with the metallacyclopentene ring ($\overline{\mathrm{Os{-}C4{=}C5{-}C8{-}C9}}$) sharing one edge (C8–C9) with the cyclooctane (C8-C15) ring. The vinyl moiety bears a striking resemblence to the vinyl moiety in **4a-c** (Chapter 3). The length of the newly formed C-C bond, C5–C8, is 1.525(6) Å, and is close to the bridiging linkage between the vinyl and the allyl moiety in **4a-c** (ave. = 1.499(5) Å, Chapter 3). The C5–C8 separation in **13** is indicative of a C_{sp^2}-C_{sp^3} (1.51 Å) single bond [22]. The C8–C9 separation (1.560(6) Å) of the metallacyclopentene ring is characteristic of a single $C_{sp}3$–$C_{sp}3$ bond (1.542 Å) [22].

Like compound **12**, compound **13** was prepared with racemic *eco*. The solid state molecular structure of **13** (Figure 5-13) shows that both enantiomers of *eco* are incorporated into the molecule; one enantiomer acts as a η^2–ligand while the other combines with HFB to give the bicyclic ligand. Since the space group of **13** is centrosymmetric ($P2_1/n$), the enantiomer of this complex is also present in the crystal. This in turn means that each enantiomer of *eco* can be found in either position in the molecule; either the η^2–ligand or as part of the bicyclic ligand. The two enantiomers of **13** are displayed in Figure 5-14.

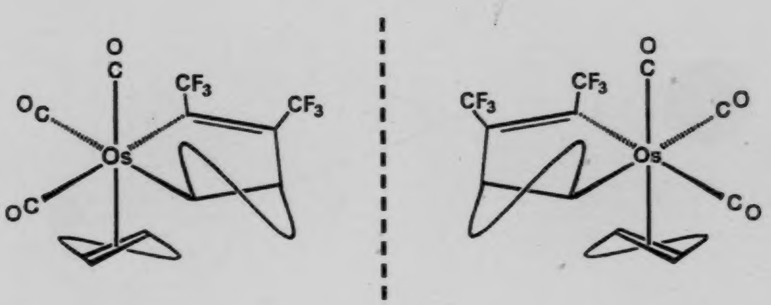

Figure 5-14 Enantiomeric Forms of **13** Containing Both Enantiomers of *Trans*-Cyclooctene.

5.4.3 Synthesis and NMR Spectroscopic Characterization of *fac*-Os(CO)$_3$(η^2-*eco*) (η^1,η^1-(F$_3$C)C=C(CF$_3$)$\overline{\text{CH(CH}_2\text{)}_6\text{C}}$H) (13)

Since all, but for a few crystals, of sample **13** were used in the initial analysis more material was needed in order to obtain suitable ^{1}H, ^{19}F and, in particular, ^{13}C NMR spectra.

The synthesis of **13** was carried out in a manner similar to that of **12**, with the exception that two equivalents of *eco* were reacted with $Os(CO)_4(\eta^2\text{-HFB})$. Consistent with previous observations, the first compound to form was **12** (FT-IR). After 25 minutes of stirring at room temperature the ν_{CO} bands of **13**, at 2089 and 2005 cm^{-1}, were detected. The ν_{CO} 2025 cm^{-1} band of **13** is coincident with the strong ν_{CO} band of **12**. The reaction progressed slowly, and with deposition of a colorless material. After 10 days, and even though significant amounts of **12** were still present in solution (FT-IR), the supernatant was separated from the precipitate. The supernatant was concentrated and taken to low temperature. The precipitate was dissolved in pentane and recrystallized. Both solutions produced crystalline material which contained a mixture of **12** and **13**. However, the product from the supernatant contained a greater proportion of **12** (FT-IR) while the product form the precipitate contained a greater proportion of **13** (FT-IR). After several weeks of repetitive fractional crystallization small amounts of **12** (7 mg, 3 % yield) and **13** (35 mg, 14 % yield) were isolated. In addition, a few small crystals of another compound (**14**) were also isolated.

The ^{19}F and $^{13}C\{^1H\}$ NMR data of **13** are listed in Table 5-6. Instead of the expected two CF_3 signals, the ^{19}F NMR spectrum showed four, the intensities of which indicated two sets of two signals each. This implies the presence of two isomers in solution. One set of signals was clearly dominant (**13**), while the second set was much weaker in intensity (**13′**). In each set a quartet and a doublet of quartets were observed. The doublet is obviously due to J_{FH} coupling and this was confirmed by the $^{19}F\{^1H\}$ NMR spectrum; all signals appear as quartets. This coupling is a result of spin-spin interaction between one of the CF_3 groups and one of the CH groups. It is not clear if this coupling occurs as a result of $^4J_{FH}$ or $^5J_{FH}$ coupling.

Table 5-6 The ^{19}F and ^{13}C{^{1}H} NMR Data of **13** and **13′**.

compound	^{19}F^a	^{13}C{^{1}H}^{a}
13	– 53.3 dq J_{FH} = 4 Hz	179.7 s *C*O
(major isomer)	$^5J_{FF}$ = 15 Hz	175.6 s *C*O
		172.4 s *C*O
	– 57.2 q $^5J_{FF}$ = 15Hz	99.9 s *C*H (η^2-*eco*)
		58.4 s *C*H
		46.8 s *C*H$_2$
		38.7 s *C*H$_2$ (η^2-*eco*)
		37.4 s *C*H$_2$ (η^2-*eco*)
		37.2 s *C*H$_2$
		30.2 s *C*H$_2$
		28.8 s *C*H$_2$ (η^2-*eco*)
		28.5 s *C*H$_2$
		27.1 s *C*H$_2$
		25.8 s *C*H
		24.4 s *C*H$_2$
13′	– 51.8 dq J_{FH} = 4 Hz	100.8 s *C*H (η^2-*eco*)
(minor isomer)	$^5J_{FF}$ = 16 Hz	57.6 s *C*H
		45.8 s *C*H$_2$
	– 57.3 q $^5J_{FF}$ = 16 Hz	37.8 s *C*H$_2$
		37.5 s *C*H$_2$
		29.6 s *C*H$_2$
		28.6 s *C*H$_2$
		27.4 s *C*H$_2$
		25.2 s *C*H$_2$

^{a} ppm, CD$_2$Cl$_2$, 27 °C

The ^{13}C{^{1}H} NMR spectrum (Figure 5-15) also indicates two isomers in solution. Considering the major isomer **13** first, the carbonyl region exhibits three signals, of equal intensity, at δ 179.7, 175.6 and 172.4 ppm, indicating three chemically inequivalent carbonyl ligands. Further upfield, a very strong signal appears at δ 99.9 ppm, while three equally strong signals at δ 38.7, 37.4 and 28.8 ppm are also observed.

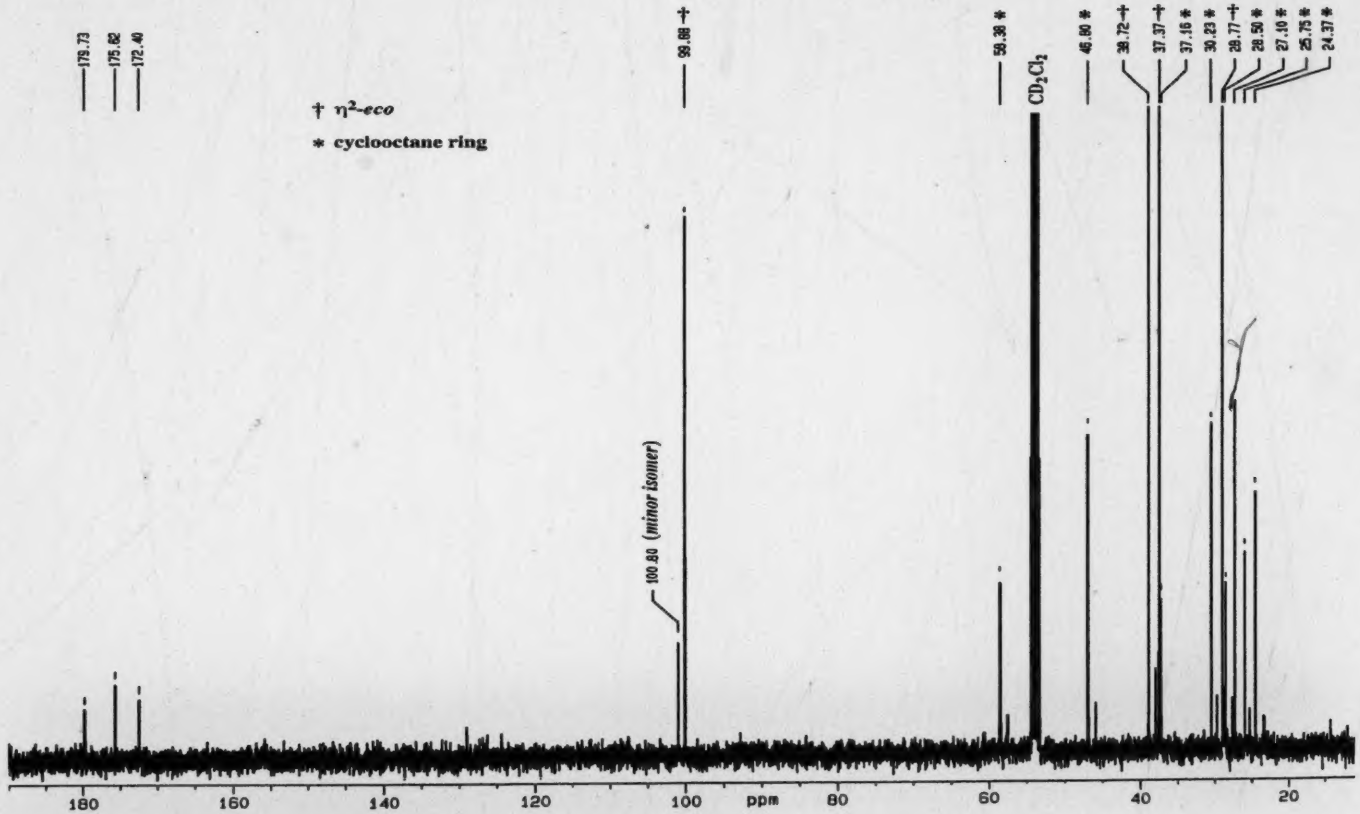

Figure 5-15 The $^{13}C\{^1H\}$ NMR (ppm, CD_2Cl_2, 27 °C) Spectrum of **13**.

The intensity of these four signals is approximately twice that of the next largest signals. The signals at δ 38.7, 37.4 and 28.8 ppm are close in chemical shift to the signals of the η^2-*eco* in **12** (δ 41.4, 38.1 and 28.9 ppm) and only the δ 99.9 ppm signal indicated a carbon of a CH group (DEPT). It is upon this basis that these four signals (labeled † in Figure 5-15) are assigned to an η^2-*eco* ligand. The next most intense signals (labeled * in Figure 5-15) are assigned to the carbons of the cyclooctane ring. As expected, eight are observed. The δ 58.4 and 25.8 ppm resonances are carbons of CH groups as indicated by the $^{13}C\{^1H\}$DEPT spectrum. The ^{13}C NMR resonances of the $(F_3C)C{=}C(CF_3)$ moiety were not observed. The ^{13}C NMR data of the major isomer is consistent with the molecular structure.

Despite its low concentration in the NMR sample many ^{13}C NMR signals of the minor isomer **13′** could be detected, these are listed in Table 5-6 but are not labeled in Figure 5-15, except for the signal at δ 100.8 ppm. No carbonyl or CCF_3 signals were observed. The signal at δ 100.8 ppm is assigned to the CH carbons of an η^2-*eco* ligand. This signal is the most intense signal of **13′** and is the carbon of a CH group as indicated by the DEPT experiment. Eight other signals were also observed (Table 5-6). Specific assignments could not be unambiguously determined. However CH and CH_2 carbons could be distinguished based on the data from the DEPT spectrum. In light of the number of signals and the similarity between the spectrums of **13** and **13′** it is reasonable to conclude that **13′** contains an η^2-*eco* and a cyclooctane moiety in the molecule.

The mass spectral analysis of **13** is consistent with an $Os(CO)_3(\eta^2$-*eco*$)$ $(\eta^1,\eta^1\text{-}(F_3C)C{=}C(CF_3)\overline{CH(CH_2)_6CH})$ formulation for both isomers. The pattern of the IR bands suggest a similar carbonyl configuration in both isomers; facial. The NMR data also suggests a similar structure for the two isomers. The solid state molecular structure clearly shows one isomer, in which both enantiomers of *eco* are contained in the molecule (Figure 5-13). Since racemic *eco* ligand was used in the synthesis, it is reasonable to assume that the other isomer is one in which the molecule contains only one enantiomer of *eco*, *i.e.* the diastereomer of the solid state molecular structure. Figure 5-14 shows the two enantiomers found in the solid state, while Figure 5-16 shows the diastereomers of these complexes. It is reasonable to conclude that the enantiomers in Figure 5-16 are responsible for the second set of signals in the ^{19}F and ^{13}C NMR spectra. The question of which pair of enantiomers is the major isomer and which pair is the minor isomer remains unanswered.

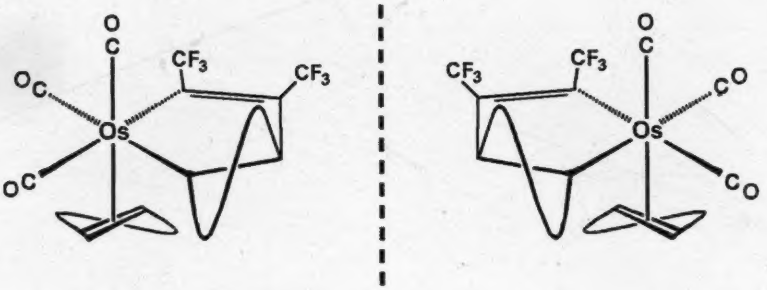

Figure 5-16 Enantiomeric Forms of **13** Containing a Single Enantiomer of *Trans*-Cyclooctene.

5.5 Discovery of *mer*-$\mathrm{Os(CO)_3(\eta^2\text{-}\mathit{eco})(\eta^1,\eta^1\text{-}(F_3C)C{=}C(CF_3)\overline{CH(CH_2)_6CH})}$ (14)

5.5.1 Experimental Observations

As mentioned previously, along with **12** and **13** a few colorless crystals of **14** were isolated from the reaction of $\mathrm{Os(CO)_4(\eta^2\text{-HFB})}$ with two equivalents of *eco*. The

FT-IR spectrum (carbonyl region) of **14** (Figure 5-17) shows the characteristic carbonyl pattern (2108 (w), 2034 (m) and 2019 (s)) for a T-shaped $M(CO)_3$ arrangement [19], *cf.* Figure 5-5, Section 5.3.2. The melting point was determined to be 149-150 °C, markedly different from **12** or **13**. The results of the mass spectroscopic analysis (m/z = 658 [M^+]) was consistent with a $Os(CO)_3$(*eco*)$_2$(HFB) formulation. The few crystals that remained were submitted for X-ray crystal structure analysis. The results are presented below.

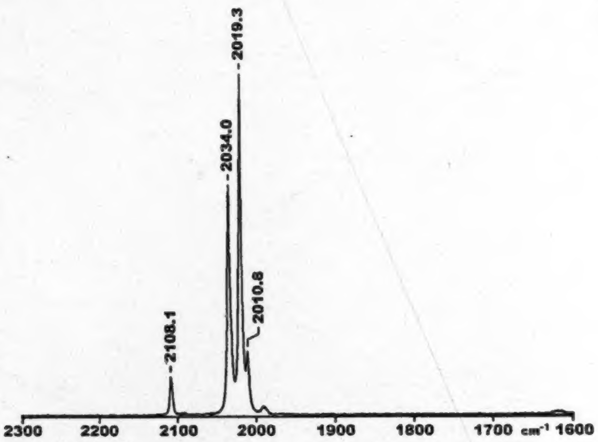

Figure 5-17 FT-IR Spectrum (carbonyl region, cm^{-1}, pentane) of **14**.

5.5.2 X-ray Crystal Structure Analysis of

mer-$Os(CO)_3(\eta^2$-*eco*$)(\eta^1,\eta^1\text{-}(F_3C)C{=}C(CF_3)\overline{CH(CH_2)_6C}H)$ (14)

The solid state molecular structure of **14** is displayed in Figure 5-18, while selected interatomic distances and angles are listed in Table 5-7.

The molecule contains the same number and type of ligands as that found in **13**. The geometry around the osmium atom is a distorted octahedral with the three carbonyls in a T-shaped orientation (C1–Os–C2 = 92.1(1)° and C1–Os–C3 = 90.7(2)°), which gives the molecule a meridional configuration.

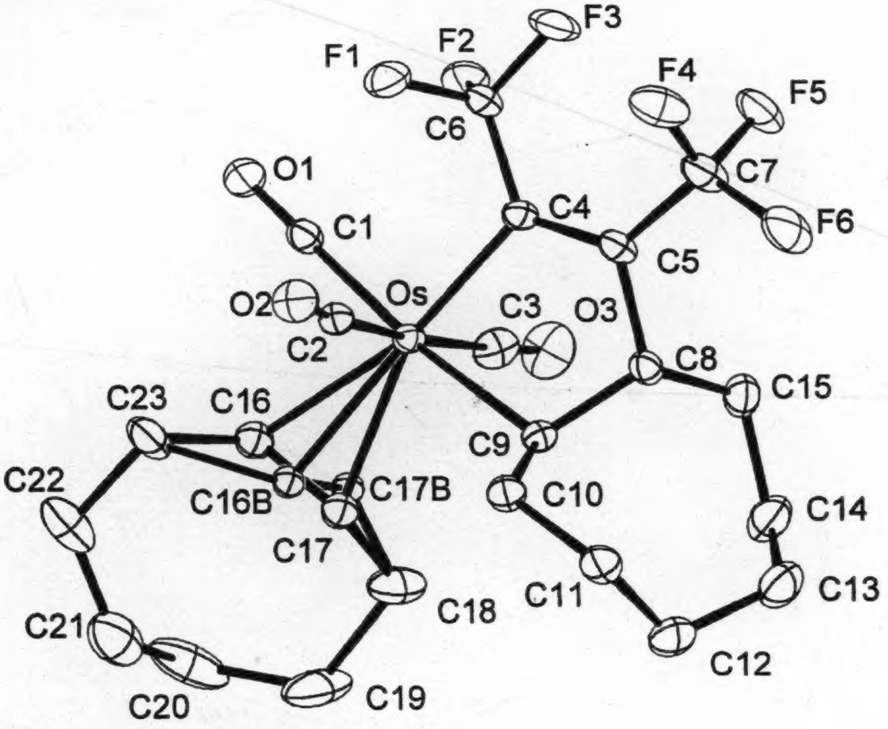
F3
F1
F2
F4
F5
C6
C7
O1
F6
C1
C4
C5
Os
O2
O3
C3
C2
C8
C15
C23
C16
C9
C22
C16B
C17B
C10
C14
C17
C13
C11
C21
C18
C12
C20
C19

Figure 5-18 Solid State Molecular Structure of **14**.

Table 5-7 Selected Interatomic Distances (Å) and Angles (deg.) in **14**.

Os–C1	1.955(3)	C1–Os–C9	172.8(1)
Os–C2	1.957(4)	C1–Os–C16	73.2(1)
Os–C3	1.942(4)	C1–Os–C17	107.3(2)
Os–C4	2.133(3)	C2–Os–C3	172.8(2)
Os–C9	2.226(3)	C2–Os–C4	85.7(1)
Os–C16	2.346(4)	C2–Os–C9	88.0(1)
Os–C17	2.297(4)	C2–Os–C16	88.9(1)
C4–C5	1.349(5)	C2–Os–C17	94.6(2)
C5–C8	1.512(5)	C3–Os–C4	87.5(1)
C8–C9	1.546(5)	C3–Os–C9	88.4(1)
C16–C17	1.3989(6)	C3–Os–C16	98.2(2)
C1–Os–C2	92.1(1)	C3–Os–C17	91.0(2)
C1–Os–C3	90.7(2)	C4–Os–C9	78.1(1)
C1–Os–C4	94.7(1)	C9–Os–C17	79.9(1)

Thus, **14** is the geometric isomer of **13**. Omitting positions C16/16B and C17/17B for the time being, the vectors C2–Os and C3–Os show good orthogonality with respect to the plane defined by the atoms C1, C4 and C9, since the Cn–Os–Cm (n = 2, 3; m = 1, 4, 9) angles are within 4° of ideal. However the C2–Os–C3 axis does show a slight bend toward C4 and C9 (C2–Os–C3 = 172.8(2)°). This *trans* OC–Os–CO bending was also observed in **12** and does not seem to be a result of inter- or intramolecular interaction since no contacts are indicated within 3 Å in either **12** or **13**.

There is positional disorder with respect to the ligating carbons of the η^2-*eco* ligand (C16-C17). Two positions were calculated for each olefinic carbon atom C16/C16B and C17/C17B. The C16 and C17 positions were assigned an occupancy of 0.8 (80%), while C16B and C17B were assigned an occupancy of 0.2 (20%). A single position, albeit with large isotropic displacement parameters (about twice that of C16/C16B and C17/C17B), for the remaining carbons (C18-C23) was calculated. The origin of this disorder is probably associated with a diastereomeric impurity of the molecule in the crystal. The best explanation is that two diastereomers of **13** exists in the crystal, with an approximate distribution of 1:4. The difference between the two diastereomers is that one diastereomer has one enantiomeric form of the *eco* ligand in the η^2-*eco* coordination site, while the other diastereomer has the other enantiomeric form of the *eco* ligand in the η^2-*eco* coordination site. The fact that one position was observed for each C18-C23 carbon atom indicates that these carbon atoms in the two diastereomers have similar positions and are not resolved in the structure. The C17–C16–Os–Cn (n = 2, –99.6(6)°; n = 3, 79.8(6)°) torsional angles show one orientation (C16 and C17) of the olefin in which the double bond vector is roughly 10° from perpendicularity with the C2–Os–C3 axis. This arrangement is displayed by **A** in

Figure 5-19 (projection along the η^2-*eco*–Os bond vector) and is a pictorial representation of the solid state molecular structure of **14**. The second orientation of the double bond (C16B and C17B) is described by the Cn–Os–C16B–C17B (n = 2, 3) torsional angles. However these angles could not be determined with a reasonable degree of accuracy, due to the large uncertainty associated with the positions of C16B and C17B, but our best estimate show the C17B–C16B–Os–C2 torsional angle to be approximately −175° while the C17B–C16B–Os–C3 torsional angle is about 5°. Thus the second orientation of the double bond appears to be roughly parallel with the C2–Os–C3 axis and is illustrated by **B** in Figure 5-19. Note that **B** has the same enantiomeric form of *eco* as does **A**. A comparison of **A** and **B** clearly shows that the general orientations of the *eco* ligands are very different, and accordingly this would make the positions of C18-C23 in **A** and **B** very different. We believe that this difference is too great to account for the single positions observed for C18-C23. However, by changing the enantiomeric form of the η^2-*eco* in **B** a diastereotopic isomer of **A** and **B** is obtained, illustrated by **C** in Figure 5-19. Of course, the C18-C23 atom positions in **A** and **C** are not coincident but clearly the position of these atoms in **C** more closely approximates the positions of the C18-C23 atoms in **A** than does the C18-C23 atoms in **B**. Upon this basis we conclude that **A** and **C** are the two molecules in the crystal, with a population distribution of about 4:1, respectively, and it is the change in the double bond orientation, with respect to the auxiliary metal moiety, coupled with the change in the enantiomeric form of the η^2-*eco* ligand that leads to the disorder in the structure of **14**.

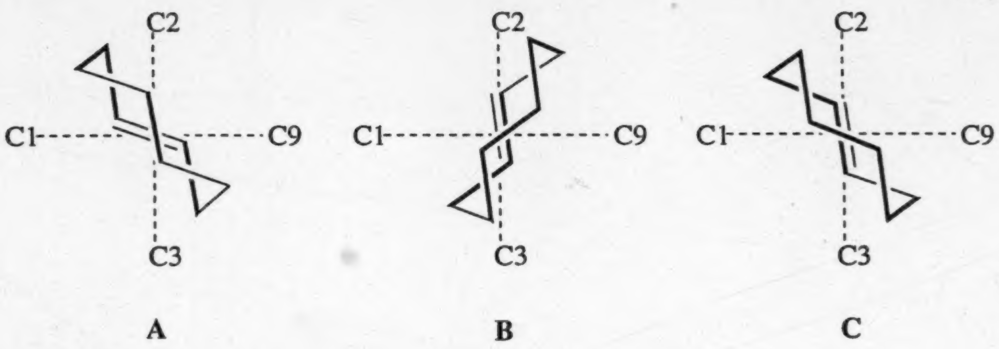

Figure 5-19 Possible Diastereomers in the Crystal of **14**.

Continuing with the analysis of the η^2-*eco* ligand, the poor resolution of the atomic positions of 16B and 17B prevents a detailed analysis involving these positions. However, the C16–C17 (1.389(6) Å) separation in **14** is identical, within error, to the corresponding parameter in **13** (1.379(7) Å). The Os–C16/C17 separations in **14** (ave. 2.322(6) Å) are smaller by 0.085 Å (14 esd's) than those observed in **13** (ave. 2.407(6) Å). This may reflect the relatively stronger *trans* influence of the axial carbonyl in **13** compared to that of the $(CF_3)C{=}C(CF_3)$ vinyl moiety in **14**. The C–C separations and C–C–C angles in **14** are very close to the corresponding parameters in **13**.

The geometric features of the η^1,η^1-$(F_3C)C{=}C(CF_3)\overline{CH(CH_2)_6CH}$ ligand are similar to the related parameters in the solid state structure of **13** and thus warrent no further discussion here.

With the ligating carbons of the η^2-*eco* in the C16 and C17 positions it is clear from Figure 5-18 that the same enantiomer of *eco* is contained within the molecule. Given the centrosymmetric space group of **14** (*P2/c*) it is certain that the enantiomer of this complex is also present in the crystal. Figure 5-20 shows a pictorial of the solid state molecular structure (C16/C17) and its enantiomer.

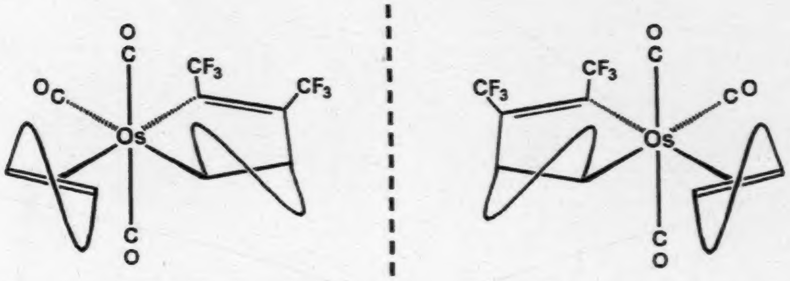

Figure 5-20 Enantiomeric Forms of **14** Containing a Single Enantiomer of *Trans*-Cyclooctene.

The solid state molecular structure of **14** also suggests, *via* atomic positions C16B and C17B, that a second molecule exists in the crystal. As discussed above, this structure contains the other enantiomer of the *eco* ligand in the η^2–*eco* position and the double bond is rotated about 90° so that it is nearly parallel with the *trans*–OC–Os–CO vector. This molecule and its enantiomer are displayed in Figure 5–21. These molecules are diastereomers of the molecules in Figure 5–20.

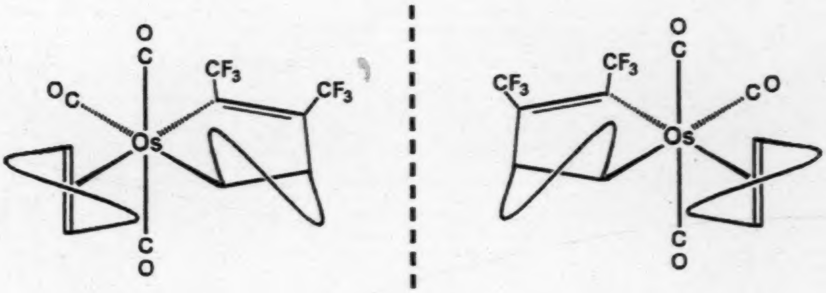

Figure 5-21 Enantiomeric Forms of **14** Containing Both Enantiomers of *Trans*-Cyclooctene.

5.5.3 Synthesis and NMR Spectroscopic Characterization of *mer*-$Os(CO)_3(\eta^2$-*eco*$)(\eta^1,\eta^1$-$(F_3C)C{=}C(CF_3)\overline{CH(CH_2)_6CH})$ (14)

Since all the crystals of **14** were used in the initial analysis more material was needed to in order to obtain suitable NMR spectra. Therefore efforts were directed toward synthesizing reasonable quantities of **14**.

The synthesis of **14** was performed in much the same way as that of **13**, except that hexane was used as a solvent to prevent solvent loss over the extended period of time needed to complete the reaction (42 days). Also, a ten fold molar excess of *eco* was used to react with $Os(CO)_4(\eta^2$-HFB). After 42 days of stirring at room temperature the FT-IR spectrum showed no further progress of the reaction and, although the IR spectrum showed the presence of significant amounts of **13**, the solvent was removed, *in vacuo*, and the resulting residue was recrystallized. Several weeks of repetitive fractional crystallization yielded 33 mg of crystals, which contained an estimated 10% (^{19}F NMR spectrum) of **13**. Thus, the isolated yield of **14** is estimated at 30 mg (10%).

The ^{19}F NMR data are listed in Table 5-8. The spectrum shows weak signals due to **13**. Ignoring these, two sets of other signals, in a ratio of 3:2, were observed. As in **13/13′** the ^{19}F NMR data of **14** indicated the presence of two isomers in solution. The major isomer (**14**) showed a doublet of quartets (J_{FH} and $^5J_{FF}$) at δ −54.9 and a quartet ($^5J_{FF}$) at δ −56.0 ppm. The minor isomer (**14′**) showed a doublet of quartets (J_{FH} and $^5J_{FF}$) at δ −55.7 ppm and a quartet ($^5J_{FF}$) at δ −56.7 ppm.

The $^{13}C\{^1H\}$ data are also listed in Table 5-8. The usefulness of the data is extremely limited. A poor signal to noise ratio and the fact that comparable amounts of **14** and **14′** exist in solution prevented unambiguous assignments of many of the resonances. As such the data for **14** and **14′** are listed together.

Table 5-8 The ^{19}F and $^{13}C\{^1H\}$ NMR Data of **14** and **14′**.

compound	$^{19}F^a$	$^{13}C\{^1H\}^a$
14	– 54.9 dq J_{FH} = 2 Hz	177.9 s CO
(major isomer)	$^5J_{FF}$ = 17 Hz	177.8 s CO
		84.6 s CH (η^2-*eco*, **14′**)
	– 56.0 q J_{FH} = 17 Hz	75.5 s CH (η^2-*eco*, **14**)
		56.2 s CH
		42.5 s CH_2
		40.7 s CH_2
14′	– 55.7 dq J_{FH} = 2 Hz	38.8 s CH_2 (η^2-*eco*, **14**)
(minor isomer)	$^5J_{FF}$ = 16 Hz	38.7 s CH_2
		38.1 s CH_2
	– 56.7 q J_{FH} = 16 Hz	37.8 s CH_2 (η^2-*eco*, **14**)
		37.6 s CH_2
		37.4 s
		34.1 s CH_2
		31.1 s CH_2
		30.2 s
		29.0 s CH_2
		28.8 s CH_2 (η^2-*eco*, **14**)
		28.7 s CH_2
		28.6 s CH_2
		28.3 s CH_2
		28.0 s CH_2
		27.8 s CH_2
		27.3 s CH_2
		17.7 s
		13.4 s

^{a} ppm, CD_2Cl_2, 27 °C

The carbonyl region showed only two signals when six are expected. It is probable that additional carbonyl resonances are masked by baseline noise. Further upfield, two strong signals appear at δ 84.6 and 75.5 ppm. Based on the intensity of these signals, they are assigned to the minor **14′** and major isomer **14**, respectively. These signals are further assigned to the *C*H carbons of an η^2-*eco* ligand, since they are clearly carbon resonances originating from a CH group (DEPT) and these resonances occur at chemical shifts that are between the chemical shifts of the corresponding group in **12** (δ 63.9 ppm) and **13**(δ 99.9 ppm)/**13′**(δ 100.8 ppm). Three other strong signals, δ 38.8, 37.8 and 28.8 ppm, are consistent with the CH_2 carbons of an η^2-*eco* of the major isomer. Assignment to CH and CH_2 groups in Table 5-8 could be made in most cases, based on the data from the DEPT experiment. Where no assignment occurs the signal was not observed in the $^{13}C\{^1H\}$DEPT spectrum. In the upfield region ($\delta \leq 100$ ppm) we expect to observe four resonances of the η^2-*eco* ligand and eight resonances of the metallacyclopentene moiety for each isomer. It is therefore reassuring that we observed twenty-four resonances in this region. This would support the conclusion that two isomers are present and that each has an η^2-*eco* ligand and a cyclooctane moiety.

The ^{19}F NMR data clearly shows two isomers in solution. The IR spectrum of the compounds is indicative of a T-shaped arrangement of carbonyl ligands for both isomers. As in **13/13′**, the proposed structures of the isomers are based on the existence of diastereomeric complexes in solution. Figure 5-20 in Section 5.5.2 shows the enantiomers in which only one enantiomer of *eco* is found, while Figure 5-21 in Section 5.5.2 shows the diastereomers of these complexes in which both enantiomers of *eco* are contained within the complex. It is reasonable to conclude that these diastereomers account for the two isomers that are observed in the NMR spectra. Also, as with **13/13′**, it cannot be determined which enantiomer represents the structure of the major isomer and which represents the minor isomer.

5.6 Conclusions

Reaction of $Os(CO)_4(\eta^2\text{-HFB})$ with CNCy produces only the carbonyl substituted product $Os(CO)_3(CNCy)(\eta^2\text{-HFB})$. The product shows no sign of alkyne-isocyanide coupling even in the presence of excess isocyanide. Furthermore the reaction stopped with a single CO substitution. Similar limited reactivity of isocyanides is observed in the literature with transition metal carbonyl compounds. This reactivity pattern is contrary to what is observed in substitution reactions of $M(CO)_4(\eta^2\text{-alkyne})$ (M = Fe, Ru, Os) and phosphine ligands. In these cases, double substitution is readily achieved. We have no explanation that would account for the limited reactivity observed with cyclohexylisocyanide.

Reaction of the *trans*-cyclooctene with $Os(CO)_4(\eta^2\text{-HFB})$ produces either the carbonyl substituted product $Os(CO)_3(\eta^2\text{-}eco)(\eta^2\text{-HFB})$ or the alkyne-*eco* coupled products *fac-/mer*-$Os(CO)_3(\eta^2\text{-}eco)(\eta^1,\eta^1\text{-}(F_3C)C{=}C(CF_3)\overline{CH(CH_2)_6CH})$, which contain a metallacyclopentene unit. A second equivalent of *eco* is needed to produce the olefin-alkyne coupled products and the reaction is slow at ambient temperature. The reaction was conducted with racemic *eco* and gives rise to enantiomeric complexes for both *fac-/mer*-geometric isomers of the alkyne-*eco* coupled products. An added dimension to this chemistry arises from the chiral nature of the *eco* ligand. Both enantiomeric forms of *eco* are found as the η^2-alkene ligand and as part of the metallacyclopentene ring. Thus, diastereomers are formed which give rise to complex NMR spectra. Similar to the reactions of $Fe(CO)_4(\eta^2\text{-HFB})$ with allene (Chapter 3), we have observed the insertion of an unsaturated hydrocarbon into the metal-alkyne bond. Both types of reactions give products that exhibit a five membered metallacycle moiety, with the alkyne invariably forming the vinyl fragment.

5.7 Experimental

As part of a long standing collaboration between the Takats Research Group, based at the Department of Chemistry, University of Alberta, and the Grevels (F. –W.) Research Group, based at the Max-Planck-Institut für Strahlenchemie (Max Planck Institute for Radiation Chemistry), Mülheim an der Ruhr, Germany, I had the opportunity of working with Dr. Grevels and the other members of his group. The experiments presented in this Chapter were conducted in Dr. Grevels laboratories at the Max-Planck-Institut für Strahlenchemie.

5.7.1 Solvents, Techniques and Physical Measurements

High purity solvents (99%, Merck), including NMR solvents (99.9%, Cambridge Isotopes Laboratories) were deoxygenated by several successive freeze-pump-thaw cycles. Experiments were conducted using Schlenk-techniques under an Argon atmosphere.

Elemental analyses were performed by Dornis and Kolbe, Mülheim an der Ruhr. FT-IR spectra (solution cell, variable path length 0.5-0.5 mm, CaF_2) were recorded on an Perkin Elmer 1600 (operating with a 2 cm^{-1} resolution). NMR data was collected on either a DRX 400, DRX 500 or AMX 300 Spectrometer. ^1H and ^{13}C NMR chemical shifts (δ) were referenced to solvent signals and are reported in ppm units relative to tetramethylsilane (TMS). ^{19}F NMR chemical shifts were referenced externally to 85% H_3PO_4. Mass spectroscopic analyses was performed by the staff at the Mass Spectroscopy Laboratory (MPI für Kohlenforschung) on a Finnigan MAT 8200 instrument.

5.7.2 Reagents

Hexafluoro-2-butyne was purchased from ABCR and Co. or Lancaster. $Os(CO)_5$ [23] and $Os(CO)_4(\eta^2\text{-HFB})$ [24] were prepared according to literature methods. *Trans*-cyclooctene (97%) was provided by Dr. Grevels. Cyclohexylisocyanide (98%) was purchased from Fluka Chemika.

5.7.3 Synthetic Procedures

Synthesis of $Os(CO)_3(CNCy)(\eta^2\text{-HFB})$ (11)

A 100 mL Schlenk flask was charged with 150 mg (0.323 mmol) of $Os(CO)_4(\eta^2\text{-HFB})$ and 50 mL of pentane added. The Schlenk flask was sealed with a rubber septum and three consecutive freeze-pump-thaw cycles were performed on the mixture. The Schlenk flask was back filled with argon to near ambient pressure. Cyclohexylisocyanide (43 μL, 0.351 mmol) was added *via* microliter syringe. The Schlenk flask was wrapped in aluminum foil. The mixture was stirred at ambient temperature for approximately 2 hours with periodic freeze-pump-thaw cycles. The solvent was removed, *in vacuo,* and the pale yellow oil redissolved in 20 mL pentane. The solution was filtered and crystallized at – 30 °C. Pale yellow crystalline **11** was recovered at –30°C. Upon bring the sample to room temperature the solid melts to a pale yellow oil (153 mg, 0.281 mmol, 87% yield).

F.W. 545.44

$C_{14}H_{11}F_6NO_3Os$

M.P. 22-23 °C

EI-MS (*m/z*): 547 [M^+] (based on Os^{192}), 519 [M^+–CO], 491[M^+–2CO]

IR (pentane, cm^{-1}) ν_{CO} 2088(s), 2029 (s), 2002 (s); ν_{CC} 1791 (w); ν_{CN} 2220

^1H NMR (CD_2Cl_2, 400.1 MHz, 27 °C) δ 3.87 (br, C_6H_{11}), 1.80 (br, C_6H_{11}), 161 (br, C_6H_{11}), 1.42 (br, C_6H_{11})

^{19}F NMR (CD_2Cl_2, 376.4 MHz, 27 °C) δ – 58.0 (s, CF_3)

$^{13}C\{^1H\}$ NMR (CD_2Cl_2, 100.6 MHz, 27 °C) δ 175.9 (s, CO_{eq}), 172.2 (s, CO_{ax}), 121.6 (q, $^1J_{CF}$ = 267 Hz, CF_3), 117.3 ("t" $^1J_{CN}$ = 23 Hz), 98.7 (q, $^2J_{CF}$ = 49 Hz, CCF_3), 55.5 ("t", $^1J_{CN}$ = 6 Hz $C_{bridgehead}$), 32.2 (s, CH_2), 25.0 (s, CH_2), 22.7 (s, CH_2)

Synthesis of $Os(CO)_3(\eta^2$-*eco*$)(\eta^2$-HFB$)$ (12)

A 80 mL Schlenk tube was charged with 200 mg (0.431 mmol) of $Os(CO)_4(\eta^2$-HFB$)$ and 50 mL of pentane added. The Schlenk tube was sealed with a rubber septum. Three consecutive freeze-pump-thaw cycles were performed on the mixture. The Schlenk tube was back filled with Argon gas to near ambient pressure. *Trans*-cyclooctene (56 µL, 0.43 mmol) was added *via* microliter syringe. The Schlenk tube was wrapped in aluminum foil. The mixture was stirred at ambient temperature for approximately 5 hours. Three freeze-pump-thaw cycles were performed. The mixture was stirred overnight (~16 hr.). A second portion of *trans*-cyclooctene (5 µL, 0.04 mmol) was added to the mixture followed by three freeze-pump-thaw cycles. The mixture was stirred for two hours and a third portion of *trans*-cyclooctene (5 µL, 0.04 mmol) was added to the mixture followed by three freeze-pump-thaw cycles. The mixture was stirred for 4 hours. The solvent was removed, *in vacuo,* the residue was redissolved in 50 mL pentane. The solution was filtered and crystallized at –30 °C overnight, then crystallized at –80 °C overnight. Pale yellow crystalline **12** (146 mg, 62% yield)was recovered.

F.W. 546.46

Elemental Analysis $C_{15}H_{14}F_6O_3Os$;

Calculated: C, 32.97%; H, 2.58%; F, 20.86; Os, 34.81.

Observed: C, 33.11%; H, 2.45%; F, 20.66; Os, 35.08.

M.P. 39.5-41.5 °C

EI-MS (*m/z*): 548 [M^+] (based on Os^{192})

IR (pentane, cm^{-1}) ν_{CO} 2025(s), 2113 (w) ν_{CC} 1810 (w)

^{1}H NMR (CD_2Cl_2, 400.1 MHz, 27 °C) δ 4.42 (m, C_8H_{14}), 2.80 (m, C_8H_{14}), 2.11 (m, C_8H_{14}), 1.85 (m, C_8H_{14}), 1.25 (m, C_8H_{14})

^{19}F NMR (CD_2Cl_2, 376.4 MHz, 27 °C) δ – 55.8 (q, $^5J_{FF}$ = 5 Hz, CF_3), – 68.5 (q, $^5J_{FF}$ = 5 Hz, CF_3)

$^{13}C\{^1H\}$ NMR (CD_2Cl_2, 100.6 MHz, 27 °C) δ 180.7 (q, $^4J_{CF}$ = 2 Hz, *C*O), 171.4 (s, *C*O), 171.2 (s, *C*O), 122.1 (q, $^1J_{CF}$ = 266 Hz, CF_3), 120.8 (q, $^1J_{CF}$ = 266 Hz, CF_3), 93.5 (qq, $^2J_{CF}$ = 48 Hz, $^3J_{CF}$ = 8 Hz, CCF_3), 85.0 (qq, $^2J_{CF}$ = 46 Hz, $^3J_{CF}$ = 7 Hz, CCF_3), 63.9 (s, CH), 41.4 (s, CH_2), 38.1 (s, CH_2), 28.9 (s, CH_2)

Synthesis of *fac*-$Os(CO)_3(\eta^2\text{-}eco)(\eta^1,\eta^1\text{-}(F_3C)C{=}C(CF_3)\overline{CH(CH_2)_6C}H)$ (13)

A 80 mL Schlenk tube was charged with 180 mg (0.388 mmol) of $Os(CO)_4(\eta^2\text{-HFB})$ and 30 mL of pentane added. The Schlenk tube was sealed with a rubber septum. Three consecutive freeze-pump-thaw cycles were performed on the mixture. The Schlenk tube was back filled with Argon to near ambient pressure. *Trans*-cyclooctene (103 µL, 0.790 mmol) was added *via* microliter syringe. The Schlenk tube was wrapped in aluminum foil. The mixture was stirred at ambient temperature for approximately 1 hour. Three freeze-pump-thaw cycles were performed. The mixture was stirred for 10 days with periodic (2-3 times per day) three freeze-pump-thaw cycles. The solvent was removed, *in vacuo,* the residue was redissolved in 15 mL pentane. Repeated fractional crystallization at low temperature (– 30 °C) produced colorless crystalline **13** (35 mg, 14 % yield) along with 7 mg of **12** (3 % yield) and 3 mg **14** (1% yield).

F.W. 656.65

Elemental Analysis $C_{23}H_{28}F_6O_3Os$;

Calculated: C, 42.07%; H, 4.30%; Os, 28.96.

Observed: C, 42.44%; H, 4.41%; Os, 28.73.

M.P. 108-110 °C (decomposition)

EI-MS (*m/z*): 658 [M^+] (based on Os^{192}), 630 [M^+–CO]

IR (pentane, cm^{-1}) ν_{CO} 2089(s), 2025 (s) 2005 (s)

major isomer (13)

^{19}F NMR (CD_2Cl_2, 376.4 MHz, 27 °C) δ – 53.3 (dq, J_{FH}= 4 Hz, $^5J_{FF}$ = 15 Hz, C*F*$_3$), – 57.2 (q, $^5J_{FF}$ = 15 Hz, C*F*$_3$)

$^{19}F\{^1H\}$ NMR (CD_2Cl_2, 282.4 MHz, 27 °C) δ – 53.3 (q, $^5J_{FF}$ = 15 Hz, C*F*$_3$), – 57.2 (q, $^5J_{FF}$ = 15 Hz, C*F*$_3$)

$^{13}C\{^1H\}$ NMR (CD_2Cl_2, 100.6 MHz, 27 °C) δ 179.7 (s, *C*O), 175.6 (s, *C*O), 172.4 (s, *C*O), 99.9 (s, *C*H), 58.4 (s, *C*H), 46.8 (s, *C*H$_2$), 38.7 (s, *C*H$_2$), 37.4 (s, *C*H$_2$), 37.2 (s, CH$_2$), 30.2 (s, *C*H$_2$), 28.8 (s, *C*H$_2$), 28.5 (s, *C*H$_2$) , 27.1 (s, *C*H$_2$) , 25.8 (s, *C*H) , 24.4 (s, *C*H$_2$).

minor isomer (13′)

^{19}F NMR (CD_2Cl_2, 376.4 MHz, 27 °C) δ – 51.8 (dq, J_{FH}= 4 Hz, $^5J_{FF}$ = 16 Hz, C*F*$_3$), – 57.3 (q, $^5J_{FF}$ = 16 Hz, C*F*$_3$)

$^{19}F\{^1H\}$ NMR (CD_2Cl_2, 282.4 MHz, 27 °C) δ – 51.8 (q, $^5J_{FF}$ = 16 Hz, C*F*$_3$), – 57.3 (q, $^5J_{FF}$ = 16 Hz, C*F*$_3$)

^{13}C{^{1}H} NMR (CD_2Cl_2, 100.6 MHz, 27 °C) δ 100.8 (s, *C*H), 57.6 (s, *C*H), 45.8 (s, *C*H$_2$), 37.8 (s, *C*H$_2$), 37.5 (s, *C*H$_2$), 29.6 (s, *C*H$_2$), 28.6 (s, *C*H$_2$), 27.4 (s, *C*H$_2$), 25.2 (s, CH$_2$).

Synthesis of *mer*-$\mathrm{Os(CO)_3(\eta^2\text{-}\mathit{eco})(\eta^1,\eta^1\text{-}(F_3C)C{=}C(CF_3)\overline{CH(CH_2)_6CH})}$ (14)

A 80 mL Schlenk tube was charged with 210 mg (0.452 mmol) of Os(CO)$_4$(η^2-HFB) and 20 mL of hexane added. The Schlenk tube was sealed with a rubber septum. Three consecutive freeze-pump-thaw cycles were performed on the mixture. The Schlenk tube was back filled with Argon to near ambient pressure. *Trans*-cyclooctene (586 μL, 4.50 mmol) was added *via* microliter syringe. The Schlenk tube was wrapped in aluminum foil. The mixture was stirred at ambient temperature for approximately 30 minutes. Three freeze-pump-thaw cycles were performed. The mixture was stirred for 42 days with periodic freeze-pump-thaw cycles. The solvent was removed, *in vacuo,* the residue was redissolved in 10 mL pentane. Repeated fractional crystallization at low temperature (– 30 °C) yielded a colorless crystalline **14** (30 mg, 10 % yield) along with 3 mg of **13** (1 % yield).

F.W. 656.65

M.P. 149.5-150.5 °C

EI-MS (*m/z*): 658 [M$^+$] (based on Os^{192}), 630 [M$^+$–CO], 602 [M$^+$–2CO]

IR (pentane, cm^{-1}) ν_{CO} 2108 (w), 2034 (s) 2019 (vs), 2010 (w)

^{19}F NMR (CD_2Cl_2, 376.4 MHz, 27 °C) **major isomer (14)** δ – 54.9 (dq, J_{FH}= 2 Hz, $^5J_{FF}$ = 17 Hz, C*F*$_3$), – 56.0 (q, $^5J_{FF}$ = 17 Hz, C*F*$_3$); **minor isomer (14′)** δ – 55.7 (dq, J_{FH} = 2 Hz, $^5J_{FF}$ = 16 Hz, C*F*$_3$), – 56.7 (q, $^5J_{FF}$ = 16 Hz, C*F*$_3$)

^{13}C{^{1}H} NMR (CD_2Cl_2, 100.6 MHz, 27 °C) δ 177.9 (s, *C*O), 177.8 (s, *C*O) 84.6 (s, *C*H, **14′**), 75.5 (s, *C*H, **14**), 56.2 (s, *C*H), 42.5 (s, *C*H$_2$), 40.7 (s, *C*H$_2$), 38.8 (s, *C*H_2, **14**), 38.7 (s, *C*H_2), 38.1 (s, *C*H_2), 37.8 (s, *C*H_2, **14**), 37.6 (s, *C*H_2), 37.4 (s), 34.1 (s, *C*H_2), 31.1 (s, *C*H_2), 30.2 (s), 29.0 (s, *C*H_2), 28.8 (s, *C*H_2, **14**), 28.7 (s, *C*H_2), 28.6 (s, *C*H_2), 28.3 (s, *C*H_2), 28.0 (s, *C*H_2), 27.8 (s, *C*H_2), 27.3 (s, *C*H_2), 17.7 (s), 13.4 (s).

5.7.4 X-ray Crystal Structure Determination of Compounds 11-14

Pale yellow crystals of **11** and **12** and colorless crystals of **13** and **14** were produced by cooling a concentrated pentane solution from room temperature to – 30 °C or – 80 °C. Data collection and structure refinement were performed by Dr. R Goddard and the staff of the X-ray Crystallography Laboratory, Max-Planck-Institut für Kohlenforschung, Mülheim an der Ruhr, Germany. Data collection was carried out on a Siemens SMART-CCD diffractometer. Programs for diffractometer operation, data collection, data reduction and absorption correction were those supplied by Siemens. Structure refinement was performed using a full-matrix least-squares on F^2 method. All non-hydrogen atoms were located. Hydrogen atoms were place in calculated positions and geometrically constrained during final refinement. Summaries of data collection parameters are presented in Tables 5-9 (**11**), 5-10 (**12**), 5-11 (**13**) and 5-12 (**14**). Final atomic coordinates and displacement parameters may be obtained from Dr. R Goddard of the X-ray Crystallography Laboratory, Max-Planck-Institut für Kohlenforschung, Mülheim an der Ruhr, Germany, with the identification codes 3638 (**11**), 3698 (**12**), 3668 (**13**) and 3840 (**14**).

Table 5-9 Crystallographic Experimental Details for Compound **11**

formula	$C_{14}H_{11}F_6NO_3Os$
formula weight	545.44
crystal dimensions (mm)	0.52 × 0.43 × 0.24
crystal system	orthorhombic
space group	$P2_12_12_1$ (No.19)
unit cell parameters	
a (Å)	10.0698 (4)
b (Å)	10.2236 (4)
c (Å)	16.2646 (6)
V (Å^3)	1674.43 (11)
Z	4
ρ_{calcd} (g cm^{-3})	2.164
μ (mm^{-1})	7.691
radiation (λ[Å])	graphite-monochromated Mo Kα (0.71073)
temperature (°C)	– 173
θ range for data collection (deg)	2.35-33.92
total data collected	18716 ($-15 \le h \le 14$, $-16 \le k \le 15$, $-8 \le l \le 25$)
independent reflections	6412 [$R_{int} = 0.1117$]
number of observed reflections (*NO*)	6041 [$F_o^2 \ge 2\sigma(F_o^2)$]
absorption correction method	*Gaussian*
range of transmission factors	0.23782 – 0.05317
data/restraints/parameters	6412 / 0 / 226
goodness of fit on F^2	1.020
final R indices	
R_1 [$F_o^2 \ge 2\sigma(F_o^2)$]	0.0426
wR_2 [$F_o^2 \ge -3\sigma(F_o^2)$]	0.1101
largest difference peak and hole	4.262 and – 2.977 e Å^{-3}

Table 5-10 Crystallographic Experimental Details for Compound **12**

formula	$C_{15}H_{14}F_6O_3Os$
formula weight	546.46
crystal dimensions (mm)	0.45 × 0.40 × 0.14
crystal system	monoclinic
space group	$P2_1/c$ (No.14)
unit cell parameters	
a (Å)	8.6979 (6)
b (Å)	12.8399 (9)
c (Å)	15.2426 (10)
β (deg)	90.036 (3)
V (Å^3)	1702.3 (2)
Z	4
ρ_{calcd} (g cm^{-3})	2.132
μ (mm^{-1})	7.563
radiation (λ[Å])	graphite-monochromated Mo Kα (0.71073)
temperature (°C)	– 173
θ range for data collection (deg)	2.07-33.14
total data collected	17802 ($-13 \leq h \leq 4$, $-18 \leq k \leq 19$, $-18 \leq l \leq 22$)
independent reflections	5837 [$R_{\text{int}} = 0.0247$]
number of observed reflections (*NO*)	5100 [$F_o^2 \geq 2\sigma(F_o^2)$]
absorption correction method	*Gaussian*
range of transmission factors	0.33462 – 0.07239
data/restraints/parameters	5837 / 0 / 226
goodness of fit on F^2	1.074
final R indices	
R_1 [$F_o^2 \geq 2\sigma(F_o^2)$]	0.0204
wR_2 [$F_o^2 \geq -3\sigma(F_o^2)$]	0.0433
largest difference peak and hole	0.930 and – 1.098 e Å^{-3}

Table 5-11 Crystallographic Experimental Details for Compound **13**

formula	$C_{23}H_{28}F_6O_3Os$
formula weight	656.65
crystal dimensions (mm)	0.60 × 0.20 × 0.18
crystal system	monoclinic
space group	$P2_1/n$ (No.14)
unit cell parameters	
a (Å)	9.9702 (3)
b (Å)	16.0984 (5)
c (Å)	14.6770 (5)
β (deg)	102.7070 (10)
V (Å^3)	2298.02 (13)
Z	4
ρ_{calcd} (g cm^{-3})	1.898
μ (mm^{-1})	5.620
radiation (λ[Å])	graphite-monochromated Mo Kα (0.71073)
temperature (°C)	– 173
θ range for data collection (deg)	1.90-33.16
total data collected	25028 ($-15 \leq h \leq 14$, $-24 \leq k \leq 21$, $-7 \leq l \leq 22$)
independent reflections	8394 [$R_{int} = 0.0737$]
number of observed reflections (*NO*)	7234 [$F_o^2 \geq 2\sigma(F_o^2)$]
absorption correction method	*Gaussian*
range of transmission factors	0.42155 – 0.04780
data/restraints/parameters	8394 / 0 / 298
goodness of fit on F^2	1.087
final R indices	
R_1 [$F_o^2 \geq 2\sigma(F_o^2)$]	0.0444
wR_2 [$F_o^2 \geq -3\sigma(F_o^2)$]	0.1127
largest difference peak and hole	3.189 and – 4.959 e Å^{-3}

Table 5-12 Crystallographic Experimental Details for Compound **14**

formula	$C_{23}H_{28}F_6O_3Os$
formula weight	656.65
crystal dimensions (mm)	0.36 × 0.22 × 0.13
crystal system	monoclinic
space group	*C2/c* (No.15)
unit cell parameters	
a (Å)	32.900 (3)
b (Å)	9.3900 (7)
c (Å)	15.6123 (12)
β (deg)	103.347 (5)
V (Å^3)	4692.9 (6)
Z	8
ρ_{calcd} (g cm^{-3})	1.859
μ (mm^{-1})	5.504
radiation (λ[Å])	graphite-monochromated Mo Kα (0.71073)
temperature (°C)	– 173
θ range for data collection (deg)	2.26-30.49
total data collected	27607 ($-46 \le h \le 45$, $-13 \le k \le 13$, $-22 \le l \le 21$)
independent reflections	6635 [$R_{int} = 0.0761$]
number of observed reflections (*NO*)	5895 [$F_o^2 \ge 2\sigma(F_o^2)$]
absorption correction method	*Gaussian*
range of transmission factors	0.52106 – 0.23552
data/restraints/parameters	6635 / 0 / 297
goodness of fit on F^2	1.080
final R indices	
R_1 [$F_o^2 \ge 2\sigma(F_o^2)$]	0.0272
wR_2 [$F_o^2 \ge -3\sigma(F_o^2)$]	0.0720
largest difference peak and hole	2.194 and – 1.263 e Å^{-3}

5.8 References

1. (a) Mao, T. –F. Zhang, Z.; Washington, J. Takats, J.; Jordan, R. B. *Organometallics* **1999**, *18*, 2331. (b) Mao, T. –F. Ph. D. Thesis, University of Alberta, 1996, Chapter 2 and 3. (c) Cooke, J. Ph. D. Thesis, University of Alberta, 1998, Chapter 4.
2. Elschenbroich, C.; Salzer, A. *Organometallics*; VCH: New York, 1989; pp 240-241.
3. (a) Kemmit, R. D. W.; Russell, D. R. In *Comprehensive Organometallic Chemistry*; Wilkinson, G; Stone, F. G. A.; Abel, E. W. , Eds.; Pergamon: New York, 1982: Vol. 5; pp 139-140. (b) Hartley, F. R. *ibid.* p 702. (c) Singleton, E; Oosthuizen, H. E. *Adv. Organomet. Chem.* **1983**, *22*, 209. (d) Adams, R. D.; Huang, M. *Organometallics* **1995**, *14*, 506. (e) Thorn, M. G.; Fanwick, P. E.; Rothwell, I. P. *Organometallics*, **1999**, *18*, 4442. (f) Adams, C. J.; Anderson, K. M.; Bartlett, I. M.; Connelly, N. G.; Orpen, A. G.; Paget, T. J. Phetmung, H.; Smith, D. W. *J. Chem. Soc., Dalton Trans.* **2001**, 1284. (g) Adams, C. J.; Anderson, K. M.; Bartlett, I. M.; Connelly, N. G.; Orpen, A. G.; Paget, T. J. *Organometallics* **2002**, *21*, 3454.
4. Huang, J. –Y.; Lin, K. –J.; Chi, K. –M.; Lu, K. –L. *J. Chem. Soc., Dalton Trans.* **1997**, 15.
5. Homrighausen, C. L.; Alexander, J. J.; Krause Bauer, J. A. *Inorg. Chim. Acta* **2002**, *334*, 419.
6. (a) Keim, W.; Behr, A.; Röper, M. In *Comprehensive Organometallic Chemistry*; Wilkinson, G; Stone, F. G. A.; Abel, E. W. , Eds.; Pergamon: New York, 1982: Vol. 8; p 426-428. (b) Jolly, P. W. *ibid.* pp 655-660. (c) Broene, R. D. In *Comprehensive Organometallic Chemistry II*; Abel, E. W.; Stone, F. G. A;

Wilkinson, G.; Hegedus, L. S., Eds.; Pergamon: Oxford, 1995: Vol. 12; p 335. (d) Harrington, P. J. *ibid.*, pp 925-926. (e) Pearson, A. J.; Dubbert, R. A. *J. Chem. Soc., Chem. Commun.* **1991**, 202. (f) Slugove, C.; Mereiter, K. ; Schmid, R.; Kirchner, K. *Organometallics* **1999**, *18*, 1011.

7. Schore, N. E. In *Comprehensive Organometallic Chemistry II*; Abel, E. W.; Stone, F. G. A; Wilkinson, G.; Hegedus, L. S., Eds.; Pergamon: Oxford, 1995: Vol. 12; Chapter 7.2.
8. Pearson, J.; Cooke, J.; Takats, J.; Jordan, R. B. *J. Am. Chem. Soc.* **1998**, *120*, 1434.
9. Albright, T. A.; Hoffmann, R.; Thilbeault, J. C.; Thorn, D. L. *J. Am. Chem. Soc.* **1979**, *101*, 3801.
10. (a) Jason, M. E.; McGinnety, J. A.; Wilberg, K. B. *J. Am. Chem. Soc.* **1974**, *96*, 6531. (b) Bly, R. S.; Hossain, M. M.; Lebioda, L. *J. Am. Chem. Soc.* **1985**, *107*, 5549. (c) Godleski, S. A.; Gundlach, K. B.; Valpey, R. S. *Organometallics* **1985**, *4*, 296. (d) Bly, R. S.; Bly, R. K.; Hossain, M. M.; Lebioda, L.; Raja, M. *J. Am. Chem. Soc.* **1988**, *110*, 7723, (e) Bly, R. S.; Silverman, G. S.; Bly, R. K. *J. Am. Chem. Soc.* **1988**, *110*, 7730.
11. Klassen, J. K.; Yang, G. K. *Organometallics* **1990**, *9*, 874.
12. (a) von Büren, M.; Hansen, H. –J.; *Helv. Chim. Acta* **1977**, *60*, 2717. (b) Grevels, F. –W.; Skibbe, V. *J. Chem. Soc., Chem. Commun.* **1984**, 681. (c) Angermund, K.; Grevels, F. –W., Krüger, C.; Skibbe, V. *Angew. Chem. Int. Ed. Engl.* **1984**, *23*, 904. (d) Ball, R. G.; Kiel, G. –Y.; Takats, J.; Krüger, C.; Raabe, E.; Grevels, F. –W.; Moser, R. *Organometallics* **1987**, *6*, 2260. (e) Grevels, F. –W.; Jacke, J.; Klotzbücher, W. E.; Özkar, S.; Skibbe, V. *Pure Appl. Chem.* **1988**, *60*, 1017. (f) Angermund, H.; Grevels, F. –W.; Moser, R. *Organometallics* **1988**, *7*, 1994. (g) Angermund, H.; Bandyopadhyay, A. K.; Grevels, F. –W.; Mark, F.

J. Am. Chem. Soc. **1989**, *111*, 4656. (h) Grevels, F. –W.; Jacke, J.; Klotzbücher, W. E.; Mark, F.; Skibbe, V.; Schaffner, K.; Angermund, K.; Krüger, C; Lehmann, C. W.; Özkar, S. *Organometallics*, **1999**, *18*, 3278. (i) Grevels, F. –W.; Kerpen, K.; Klotzbücher, W. E.; Schaffner, K. *Organometallics*, **2001**, *20*, 4775.

13. Albers, M. O.; Coville, N. J.; Singleton, E. *J. Organomet. Chem.* **1987**, *326*, 229.
14. Crabtree, R. H. *The Organometallic Chemistry of the Transition Metals*; 3rd ed.; Wiley : New York, 2001, pp 87-88.
15. Marinelli, G.; Streib, W. E.; Huffman, J.C.; Caulton, K. G.; Gagné, M. R.; Takats, J.; Dartiguenave, M.; Chardon, C.; Jackson, S. A.; Eisenstein, O. *Polyhedron* **1990**, *9*, 1867.
16. (a) Cotton, F. A.; Dunne, T. G.; Wood, J. S.; *Inorg. Chem.* **1965**, *4*, 318. (b) Cotton, F. A.; Dunne, T. G.; Wood, J. S.; *ibid*, **1964**, *3*, 1495.
17. Espuelas, J.; Esteruelas, M. A.; Lahoz, F. J.; Oro, L.A.; Valero, C. *Organometallics* **1993**, *12*, 663.
18. Lane, T. M.; Grubisha, D. S.; Hu, C.; Bennett, D. W. *J. Mol. Struct.* **1994**, *328*, 113.
19. Fleckner, H.; Grevels, F. –W.; Hess, D. *J. Am. Chem. Soc.* **1984**, *106*, 2027.
20. Ermer, O.; Mason, S. A. *Acta Crystallogr., Sect. B* **1982**, *B38*, 2200.
21. Pidun, U.; Frenking, G. *Organometallics* **1995**, *14*, 5325.
22. Pauling, L. *The Nature of the Chemical Bond*; 3rd ed.; Cornell: Ithaca, NY, 1993, pp 221-224.
23. Rushman, P; van Buuren, G, N,; Shiralian, M.; Pomeroy, R. K. *Organometallics* **1983**, *2*, 693.
24. Gagné, M. R.; Takats, J. *Organometallics* **1988**, *7*, 561.

Chapter 6

Conclusions

6.1 Conclusions

The objective of this investigation was to explore the reactivity of the $M(CO)_4(\eta^2\text{-alkyne})$ (M = Fe, Os) complexes. More specifically to investigate the carbonyl substitution patterns of these complexes with simple two electron donor ligands and small unsaturated organic molecules. Moreover, in light of the pronounced alkyne-alkyne coupling ability of these compounds, demonstrated by previous studies in the Takats laboratories [1], it was desirable to investigate the potential for alkyne-olefin coupling.

The results obtained show that $M(CO)_4(\eta^2\text{-HFB})$ (M = Fe, Os) compounds readily undergo carbonyl substitution with simple two electron donor ligands and indicate the existence of a distinct coordination site preference regime in the trigonal bipyramidal products $M(CO)_{4-n}(\eta^2\text{-HFB})L_n$ (n = 1, 2). It was demonstrated that σ donor ligands, such as phosphine (PR_2R') or isocyanide (CNR) ligands, preferentially occupy an axial coordination site, while π acceptor ligands, such as the *trans*-cyclooctene ligand and the precoordinated η^2-HFB ligand, preferentially occupy equatorial positions. These results are consistent with the site preference predictions of Hoffmann [2].

The reactions of $Fe(CO)_4(\eta^2\text{-HFB})$ with bulky phosphine ligands afforded isolation of a series of coordinatively unsaturated compounds $Fe(CO)_2(PR_2R')(\eta^2\text{–HFB})$ in which the alkyne acts as a four electron donor ligand. The complexes have been fully characterized and show the characteristic physical properties of such compounds as established by Templeton [3]. They represent realistic models for the putative intermediate, $M(CO)_3(\eta^2$-HFB), in the dissociative CO substitution reactions of the parent tetracarbonyl alkyne molecules [4].

The four electron donor alkyne compounds readily react with allenes to give $Fe(CO)_2(PR_2R')(\eta^1,\eta^3-(F_3C)C{=}C(CF_3)C(CH_2)CR^1R^2)$ products, which contain an η^1,η^3-2-vinylallyl ligand, *via* allene-alkyne coupling. In light of the reactivity of the $Fe(CO)_2(PR_2R')(\eta^2$–HFB) compounds toward two electron donor ligands, it is reasonable to assume that allene coordination occurs prior to formation of the vinylallyl ligand. A possible reaction scenario is shown in Scheme 6-1. Presumably, the alkyne in the $Fe(CO)_2(PR_2R')(\eta^2$–HFB) complex "switches" from a four electron donor ligand (**A** in Scheme 6-1) to a two electron donor ligand, thereby providing a open coordination site, which is conveniently *cis* to the alkyne ligand. Coordination of the allene ligand (**B**) and facile alkyne-allene coupling gives a coordinatively unsaturated five coordinate intermediate (**C** or **D**). Coordination of the exocyclic olefin gives the isomeric products **E** and **F**. Detection of intermediates **B-D** by low temperature NMR spectroscopy proved unsuccessful. Nevertheless, the structure of the two products are not in doubt. Clearly, facile coordination and allene-alkyne coupling occurs in these systems and they point to an extraordinary ability of the allene ligand, one which more normal olefins or alkynes do not posses.

Alkyne-olefin coupling was also shown to occur with $Os(CO)_4(\eta^2$–HFB) and *trans*-cyclooctene (*eco*). Once the CO dissociation step occurs, a potential mechanistic pathway, parallel to that shown in Scheme 6-1, can be envisioned. In this case, the precursor to the alkyne-olefin coupled product, $Os(CO)_3(\eta^2$-*eco*)$(\eta^2$-HFB) **12**, was isolated. Compound **12** clearly shows a trigonal bipyramidal geometry with both the olefin and alkyne in equatorial coordination sites, and is analogous to **B** in Scheme 6–1. In this case, formation of a metallocyclopentene ring occurs but without the exocyclic double bond as shown in the iron containing **C** or **D**. Coordination of a second molecule of *eco* is needed to achieve coordinative saturation in the product $Os(CO)_3(\eta^2\text{-eco})(\eta^1,\eta^1\text{-}(F_3C)C{=}C(CF_3)\overline{CH(CH_2)_6CH})$. This step bares resemblance to the coordination of the exocyclic double bond in **C** or **D** to form **E** and **F** in Scheme 6-1. In the osmium case, the freedom associated with the second molecule of *eco* may result in the formation of the *fac*- and *mer*- isomers. In the iron compound the tethered exocyclic double bond severely limits the choice of coordination site, since the vinylallyl ligand is geometrically constrained to occupy three mutually *cis* coordination sites. Alternatively, the *fac*- and *mer*- isomers may be a result of an isomerization process.

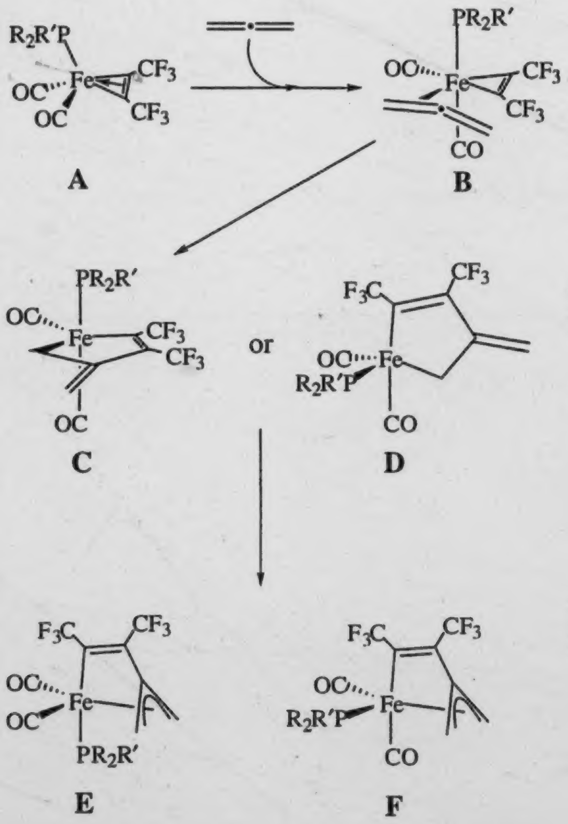
R2R'P
OC
OC
Fe
CF3
CF3
A
PR2R'
OC
Fe
CF3
CF3
CO
B
PR2R'
OC
Fe
CF3
CF3
OC
C
or
F3C
CF3
OC
Fe
R2R'P
CO
D
F3C
CF3
OC
OC
Fe
PR2R'
E
F3C
CF3
OC
R2R'P
Fe
CO
F

Scheme 6-1 Formation of $Fe(CO)_2(PR_2R')(\eta^1,\eta^3\text{-}(F_3C)C{=}C(CF_3)C(CH_2)R^1R^2)$

Although the reactivity envelope of the M$(CO)_4(\eta^2$-alkyne) (M = Fe, Os) complexes has been considerably extended as a result of the investigations reported in this thesis, many more reactivity studies can and should be explored. Since reactions of these complexes with phosphine ligands has been studied, it would be an interesting contrast, *or compliment*, to investigate the reactivity between M$(CO)_4(\eta^2$-alkyne) and aliphatic amines. These ligands are similar to phosphines in that they are good σ donors. However, they differ from phosphine ligands in that they do not posses the capacity to accept retro-dative bonding from the metal. In particular, it would be interesting to see if the four electron donor alkyne complexes, (Fe$(CO)_2(NR_3)(\eta^2$-HFB)), would form, and if so what effect the amine ligand has on the allene-alkyne coupling process. In general, reactivity studies that focus on replacing the phosphine ligand in the four electron donor complexes by other two electron donor ligands should be explored.

The reaction of the four electron donor alkyne complexes with allenes could be extended to reaction with heteroallenes. Some known heteroallenes include; CO_2, CS_2, OCNR, and RNCNR. Moreover, several metallacumulene complexes ($L_nM{=}(C{=})_nCR_2$) are known [5]. It would be interesting to see if reactions between the four electron donor alkyne complexes and metallacumulene complexes give products that are analogous to the alkyne-allene coupled products.

Trans-cyclooctene has been shown to act as an exceptional ligand due to the ring strain associated with the *trans* orientation of the ring connectivity. It is clear that the success of the reaction between Os$(CO)_4(\eta^2$-HFB) and *eco* depends on the good coordinating ability of the olefin. Therefore it would be desirable to expand on this theme and react M$(CO)_4(\eta^2$-HFB) (M = Fe, Os) or Fe$(CO)_2(PR_2R')(\eta^2$-HFB) with other strained unsaturated organic molecules [6].

6.2 References

1. (a) Mao, T. –F. Zhang, Z.; Washington, J. Takats, J.; Jordan, R. B. *Organometallics*- **1999**, *18*, 2331. (b) Mao, T. –F. Ph. D. Thesis, University of Alberta, 1996, Chapter 2 and 3. (c) Cooke, J. Ph. D. Thesis, University of Alberta, 1998, Chapter 4.
2. Albright, T. A.; Hoffmann, R.; Thibeault, J. C.; Thorn, D. Z. *J. Am. Chem. Soc.* **1979**, *101*, 3801.
3. Templeton, J. L. *Adv. Organomet. Chem.* **1989**, *29*, 1.
4. Pearson, J.; Cooke, J.; Takats, J.; Jordan, R. B. *J. Am. Chem. Soc.* **1998**, *120*, 1434.
5. Touchard, D.; Pirio, N.; Toupet, L.; Fettouhi, M.; Ouahab, L.; Dixneuf, P. H. *Organometallics* **1995**, *14*, 5263 and references therein.
6. (a) Jason, M. E.; McGinnety, J. A.; Wilberg, K. B. *J. Am. Chem. Soc.* **1974**, *96*, 6531. (b) Bly, R. S.; Hossain, M. M.; Lebioda, L. *J. Am. Chem. Soc.* **1985**, *107*, 5549. (c) Godleski, S. A.; Gundlach, K. B.; Valpey, R. S. *Organometallics* **1985**, *4*, 296. (d) Bly, R. S.; Bly, R. K.; Hossain, M. M.; Lebioda, L.; Raja, M. *J. Am. Chem. Soc.* **1988**, *110*, 7723, (e) Bly, R. S.; Silverman, G. S.; Bly, R. K. *J. Am. Chem. Soc.* **1988**, *110*, 7730.